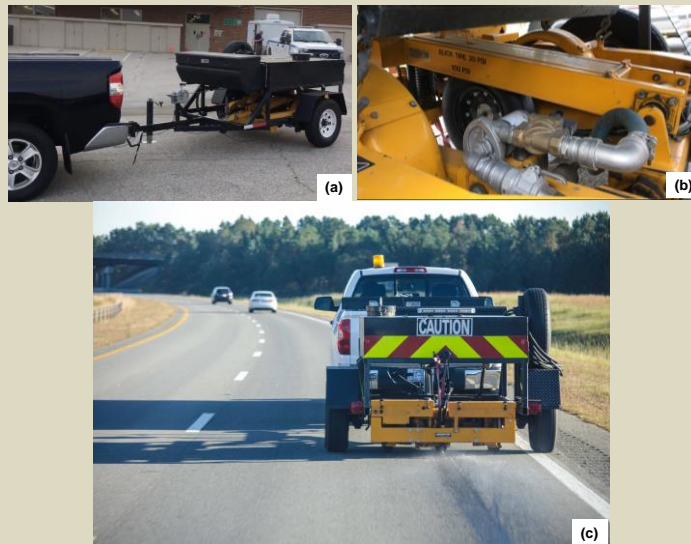# RESEARCH & DEVELOPMENT

Evolution of Pavement Friction and Macrotexture After Asphalt Overlay

(a) Moventor skiddometer BV-11 test trailer, (b) close-up photo of the test tire, and (c) tire alignment during a measurement.

B. Shane Underwood, Ph.D.
Cassie Castorena, Ph.D.
Boris Goenaga
Department of Civil, Construction, and Environmental Engineering
North Carolina State University

Paul Rogers
KPR Engineering, PLLC

NCDOT Project 2020-11

January 2022

This page is intentionally blank

Technical Documentation Page

1. Report No. FHWA/NC/2020-11	2. Government Accession No.	3. Recipient's Catalog No.
4. Title and Subtitle Evolution of Pavement Friction and Macrotexture After Asphalt Overlay	5. Report Date January 26, 2022	
	6. Performing Organization Code	
7. Author(s) B. Shane Underwood, Ph.D, Cassie Castorena, Ph.D., Boris Goenaga, Paul Rogers	8. Performing Organization Report No.	
9. Performing Organization Name and Address Civil, Construction, and Environmental Engineering, North Carolina State University 915 Partners Way Raleigh NC 27606	10. Work Unit No. (TRAIS)	
	11. Contract or Grant No.	
12. Sponsoring Agency Name and Address North Carolina Department of Transportation Research and Development Unit 104 Fayetteville Street Raleigh, North Carolina 27601	13. Type of Report and Period Covered Final Report August 1, 2019 – October 31, 2021	
	14. Sponsoring Agency Code RP2020-11	
Supplementary Notes:		

16. Abstract

A trend of observed increases in both the number and rate of total and wet crashes after resurfacing projects has become a safety concern for the NCDOT. Wet collision rates may increase due to a reduction in skid resistance under wet conditions. The precise amount of loss is dependent on many factors, but the consensus among experts is that pavement friction and macrotexture are two important factors that affect the skid resistance and the ways that this resistance changes in wet weather. Although the NCDOT actively addresses skid resistance issues as they are identified, a recent study involving a small subset of North Carolina roadways concluded that NCDOT needed to consider characterization of both friction and macrotexture as part of its pavement friction measurement and management plan. While the current studies have successfully identified the potential for issues in recently overlaid projects, they did not identify whether these effects are temporary, and if so, how long they may last. With respect to this need, this research study has set out to achieve three objectives; 1) identify whether the observations from the initial study are systemic and quantify the initial findings on a larger basis, 2) determine how long potential impacts may last after the overlay is applied and what, if any, asphalt mixture characteristics contribute to the effect and longevity, and 3) develop a strategy for how to best monitor and manage the friction and surface characteristics of NCDOT pavements. In this research, 26 sites have been selected to measure friction and texture of new overlays; in a subset of these sites, a set of field cores were extracted. It was found there is a potential to use field cores to monitor the initial field friction and texture. It was found that the binder content (Pb) and the aggregate fraction smaller than 0.075 mm (P_{200}) are mixture compositional factors that affect the initial friction and texture of overlays. There is evidence that friction increases after construction, and this increment can be as high as 50% of the initial value, the data in this study suggest it takes on average 4.0 million traffic repetitions for this increment to occur.

17. Key Words Pavement friction, macrotexture, highway safety, flexible pavements	18. Distribution Statement		
19. Security Classif. (of this report) Unclassified	20. Security Classif. (of this page) Unclassified	21. No. of Pages 218	22. Price ... ...

Form DOT F 1700.7 (8-72)   **Reproduction of completed page authorized**

TABLE OF CONTENTS

LIST OF FIGURES

LIST OF TABLES

EXECUTIVE SUMMARY

A trend of observed increases in both the number and rate of total and wet crashes after resurfacing projects has become a safety concern for the NCDOT. Wet collision rates can increase due to a reduction in skid resistance reduces under wet conditions. The precise amount of loss is dependent on many factors, but the consensus among experts is that pavement friction and macrotexture are two important factors that affect the skid resistance and changes in this resistance under wet conditions. A recent study involving a small subset of North Carolina roadways concluded that NCDOT should consider characterizing both friction and macrotexture as part of its pavement friction measurement and management plan. While the current studies have successfully identified the potential for issues in recently overlaid projects, they did not identify whether these effects are temporary, and if so, how long they may last. In addition, past studies have not been able to identify any specific causative effects that may increase or decrease the impact of overlays on skid resistance. Since the primary change after an overlay is placed is the driving surface, there is a need to better understand how the asphalt mixture composition may affect the overall skid resistance of the roadway under wet conditions.

This study investigated how overlays affect surface texture and friction characteristics of NCDOT roadways and the temporal extent of these effects. The three specific objectives of this study were to; 1) identify whether the observations from the initial study are systemic and quantify the initial findings on a larger basis, 2) determine how long potential impacts may last after the overlay is applied and what, if any, asphalt mixture characteristics contribute to the effect and longevity, and 3) develop a strategy for how to best monitor and manage the friction and surface characteristics of NCDOT pavements.

Twenty-six recently overlaid projects across the state of North Carolina were identified to monitor friction and texture right after construction. A continuous friction measurement equipment (CFME) and a high-speed laser profiler were used to characterize friction and texture, respectively. The friction and texture measurements were collected in the center of the lane (CL) as well as in the wheel path (RWP). The first measurement was obtained as closed as possible to the construction date after which sequential measurements were collected at each site over a time window that varied from half a year to almost two years. In addition, a set of field cores were acquired in ten of the monitored sites and used to evaluate different test protocols for characterizing friction and texture in the laboratory. Descriptive statistics and regression techniques were used to identify mixture compositional factors that affects the initial friction and texture values and their posterior variation.

It was found that a correlation exists between the asphalt content *(Pb)*, the gradation parameters *Cc* (coefficient of curvature), *Cu* (coefficient of uniformity), and the percent passing sieve No. 200 (P_{200}) – as reported in the Job Mix Formula (JMF) – with the initial Mean Profile Depth (*MPD*) of new overlays. This correlation was developed using data from the project, which included dense graded asphalt mixtures and ultra-thin bonded wearing course mixtures. A correlation was found between the friction and the surface parameters measured in the lab. The models developed suggest there is a potential for using field cores, such as the ones collected during construction for quality control of the in-place density, to monitor the friction and texture characteristics of the as-constructed surfaces. In the lab, friction and texture of the cores were quantified by a British Pendulum Tester and a custom laser, respectively.

Strong evidence was observed that the *MPD* reduces after an asphalt overlay and this reduction was as high as 65%; in the case of friction, evidence of a change was observed. However, in some cases friction increased whereas in others it decreased. Using the sequential set of measurements collected in each site, two sources of variation in friction were analyzed; first, a sigmoidal model was developed to describe the seasonal fluctuation; second, piecewise linear regression was applied to describe the friction variation due to repeated traffic loading. In the case of texture, only a monotonic temporal variation was observed. A power function was used to describe this process.

The mixture compositional factors that have statistically significant effects on the friction variation with traffic are the *Pb* and the P_{200}. Also, the rate at which friction increases depends on the binder content of the mixture. There is evidence that friction increases after construction, and this increment, depending on the mixture composition, can be as high as 50% of the initial value; also, the data in this study suggest it takes on average 4.0 million traffic repetitions for this increment to occur. In the case of texture, the higher the *Pb* and the P_{200}, the lower the initial texture; on the other hand, a gradation with a higher *Cc* yields a higher initial texture. The rate at which texture changes over time increase as the *Pb* and the P_{200} increase.

On the basis of these conclusions, the research team recommends that the NCDOT consider broader application of continuous friction measurements for monitoring skid resistance on its roadways. Finally, it is recommended that four equally spaced friction and texture measurements are collected during the first year of construction of new surfaces; afterwards an annual assessment can be used by collecting measurements during the summer months.

1. INTRODUCTION

1.1. Overview

Pavement friction during wet conditions is one of the safety concerns for the NCDOT. Friction is important because a critical factor affecting the safety during wet conditions is skid resistance. Skid resistance is the force that develops when a tire that is prevented from rotating (for example when brakes are applied to avoid a collision) slides along a pavement surface. When higher forces develop, e.g., when skid resistance is higher, the overall stopping distance reduces, and fewer collisions may occur. Wet conditions have a negative effect on skid resistance because the water serves to lubricate the driving surface and thereby reduce the sliding forces. This lubricating effect is dependent on many factors including the surface micro- and macro-textures, surface texture connectivity, tire characteristics, speed, and others. Historically, the NCDOT has taken an active role in identifying and correcting problematic areas by using locked-wheel skid tests and other standard and best practice methods.

Although the NCDOT has been actively addressing skid resistance issues as they are identified, a recent study involving a small subset of North Carolina roadways has suggested that wet crash rates may increase after pavements are overlaid (*1*). There are many potential causes for such occurrences, but the aforementioned study suggested that one contributing factor was the friction and macrotexture of the asphalt pavements. As important, it was shown that no single friction measurement was capable of uniquely describing the potential for traction loss on NCDOT roadways. The study's authors concluded that NCDOT should consider characterization of both friction and macrotexture as part of its pavement friction measurement and management plan.

The FHWA/NC 2017-02 project demonstrated a potential for increased crash rates after overlays, it did not identify how long after the overlay is placed any potential for increased crash rates may last or evaluate potential causative factors. The study described in this report was instigated to address this issue and build on the FHWA/NC 2017-02 findings. The specific objectives of this research are to;

1. Identify whether the observations from the initial study are systemic and quantify on a larger basis the initial findings,

2. Determine how long potential impacts may last after the overlay is applied and what, if any, asphalt mixture characteristics contribute to the effect and longevity, and

3. Develop a strategy for how to best monitor and manage the friction and surface characteristics of NCDOT pavements.

1.2. Status of the Literature

A comprehensive review of the literature pertaining to this project is presented in Appendix A, but a summary of most relevant components of this review is presented below.

1.2.1. Findings from FHWA/NC 2017-02 Study

FHWA/NC 2017-02 evaluated the use of continuous friction measurement equipment as a means of data collection to support the NCDOT pavement friction management program (*1*). Standard locked-wheel tests (LWSTs) with smooth and ribbed tires, continuous friction tests using a grip tester, and continuous friction tests combined with macrotexture measurement, Mean Profile Depth (*MPD*), using a Sideways Force Research Investigatory Machine (SCRIM) were conducted

3

on various pavement surface types and compared. The study results demonstrated that only weak correlations exist between the different friction measurements. It was also shown that no single friction measurement was capable of uniquely describing the potential for traction loss on NCDOT roadways. Standard LWST results were found to be relatively insensitive to macrotexture changes. Therefore, Flintsch et al. (*1*) proposed the use of continuous friction testing coupled with macrotexture measurements to improve the NCDOT's friction management program. Using these measurements, the study demonstrated a potential for increased crash rates after overlays are placed; however, it did not identify how long after the overlay is placed any potential for increased crash rates may last or evaluate potential causative factors.

1.2.2. Effect of Mixture Factors on Friction and Texture

Pavement friction results from the combined effects of adhesion and hysteresis. Interlocking of the vehicle tire and pavement surface upon contact results in adhesion; this bonding occurs at a small-scale and is therefore, driven by the pavement micro-texture (*2*). The microtexture of a pavement surface arises from the texture of the surface aggregate particles. Deformation of the vehicle tire upon contact with the pavement surface causes a loss in energy, termed the hysteresis component of friction. Hysteresis is affected by the macrotexture of the pavement surface, which is related to larger-scale asperities that are a function of the pavement surface layer mixture design and construction (*2*). Microtexture is most critical to pavement friction at slow speeds whereas macro-texture is most critical for pavement friction at high speeds (*3*).

Hall et al. (*2*) summarizes the effect of various factors on the macrotexture and microtexture of both asphalt and concrete pavements. These factors include aggregate size, aggregate type, gradation, air content (asphalt only), binder type (asphalt only), and texture characteristics (concrete only). With respect to the primary factors, the nominal maximum aggregate size within an asphalt concrete surface influences the dominant macrotexture wavelength because the gradation largely controls aggregate packing and thus how close or far apart the aggregates are from one another (*2, 3*). Binder viscosity and content also impact macrotexture. Low viscosity binders and/or high binder contents can lead to bleeding of asphalt on the pavement surface, resulting in a loss of macrotexture (*2*). Finally, higher air void contents increase texture and provide increased water drainage (*4*).

1.2.3. Friction Management

As part of the Highway Safety Improvement Program (HSIP), the FHWA currently requires that state agencies maintain a friction management program to minimize friction-related vehicle crashes. Friction management involves designing, constructing, and maintaining pavements with adequate friction, identifying pavement that have diminished friction and pose a safety hazard, and prioritizing resources to reduce friction-related safety hazards (*5*). While the FHWA requires that states maintain a friction management system, they do not provide specific guidance on how the management plan should be structured or specify the data collection methods and procedures that must be employed. Important considerations in the data collection to support a friction management program follow.

Frequency of Measurements

The FHWA suggests that agencies use a risk-based approach to determine the frequency and extent of friction testing (*5*). Under this approach, roadways with the highest traffic volumes, greatest likelihood of changes in friction, and the highest level of friction to safely perform braking,

steering, and acceleration are subjected to friction testing most frequently. According to the FHWA, agencies often perform friction measurements on critical portions of their network annually whereas friction measurements are performed every two to three years on lower-risk roadways (*5*).

Spatial Interval of Measurements

The LWST (*6*) is currently employed to monitor pavement skid resistance by all states except Arizona. ASTM E274 states that five determinations of skid resistance should be made at intervals of 0.5 miles or less (*5*). This approach may fail to adequately capture a network's overall skid resistance. LWST measurements cannot be made continuously without excessive tire wear (*6*). Furthermore, testing on short roadway segments and curves can produce unreliable results. Continuous friction testing using a grip tester is advantageous in that continuous measurement of skid resistance is possible, which has led the FHWA to recommend its use in practice (*5*).

Speed of Measurements

Skid resistance is known to depend on vehicle speed. Standard LWST measurements are conducted at an operating speed of 40 mph (*6*). This could pose problems for high-speed facilities because skid resistance diminishes with increasing speed. With the LWST, as the measurement speed increases, the skid number exponentially decays (*7*). Grip testers for continuous friction measurements are advantageous in that they can be operated any desired speed (*8*).

Tire Type and Location

Skid resistance measurements are mostly made in the traffic wheel path because it is expected to have the highest variation (*5*). Both ribbed and smooth tires are employed for friction testing (e.g., ASTM E274). Smooth tires are more sensitive to changes in macro-texture (i.e., *MPD*) (*8*). However, ribbed tires have been found to produce results that are less variable and less sensitive to water film thickness (*9*).

Water Film Thickness

ASTM E274 requires that 4.0 gal ± 10 percent ∕min·in. be dispensed while the vehicle is traveling at 40 mph for LWST measurements. However, skid resistance measurements are sensitive to the water film thickness during testing and thus, selection of the appropriate film thickness merits consideration. At least one study has shown that LWST results can be affected by the water film thickness, with thicker films generally leading to lower LWST skid numbers (*10*).

Parameters used to Report Friction and Texture

The mean texture depth (*MTD*) is a parameter based on a 3D representation of the macro-texture traditionally used with the sand patch or other volumetric methods of macrotexture measurement. Although the sand patch test is not suitable to characterize texture at a network level, it is still used at a project level to control construction quality. High-speed laser profilers are the most used devices because they allow users to collect continuous measurements of the texture profile. Different parameters can be computed from such profiles, like the Mean Profile Depth (*MPD*), Root Mean Squared (*RMS*), Texture-Ratio (*TR*), among others (*9*).

In the case of friction, the measurements are reported by indicating the friction value together with the measurement speed and the type of tire used. For example, if a LWST is used to measure friction at 40 mph using a smooth tire, then the operator must report the friction number as SN40S. Similarly, if a ribbed tire is used the reported value will be SN40R. In addition, because new

technologies have started to become more popular, the slip angle and slip ratio is also reported. Finally, although not reported directly with the friction value, the temperature, weather conditions at the moment of the measurement, and the water film thickness used are included as complementary information.

1.2.4. Knowledge Gaps and Applications

The recent findings from FHWA/NC 2017-02 suggest that after an asphalt concrete overlay is placed there may be a potential increase in wet crash rates. However, this project did not elucidate the asphalt mixture compositional factors that diminish safety. The literature demonstrates that asphalt pavement friction is impacted by many factors related to the material selection and volumetric design of the asphalt concrete comprising the surface layer. In addition, wet crash potential can be affected by factors not related to the asphalt concrete mixture (speed, geometry, etc.). While the literature identifies critical mixture design factors that impact friction, the relative impact of different mixture factors, their interactions, and critical limits to ensure adequate frictional characteristics remains a critical knowledge gap in the existing literature. In addition, a primary conclusion of the FHWA/NC 2017-02 research project was that continuous friction testing coupled with macrotexture measurements are necessary to understand pavement skid resistance and therefore, should be incorporated into the NCDOT's friction management program. The study did not, however, propose specific guidelines for data collection to support the improved friction management plan. Important considerations when developing a data collection plan to support friction management identified in the literature include the frequency, spatial interval, and speed of friction measurements as well as the tire type, tire location, and water film thickness used in testing.

1.3. Report Organization

This report is composed of eight primary sections and six appendices. Section 1 presents the needs, objectives, and summarizes the literature review that the research team conducted about the friction and texture surface characteristics, testing equipment and methods (see Appendix A for the full literature review). Section 2 describes the test sections and the equipment used to take the friction and texture measurements. Section 3 describes the analysis conducted to identify the mix composition factors that affects the early friction and texture development, a preliminary lab protocol to estimate field friction/texture values was evaluated, then at the end it was studied if there is a statistical relationship between friction and the different parameters used to describe the macrotexture of a pavement surface. Next, in Section 4, the friction and texture evolution are described. Here the set of sequential measurements collected in each tested site were used to analyze the friction/texture variation due to season and traffic. Subsequently, Section 5 presents the general guidelines on how to implement an effective PFM program in North Carolina. Sections 6 and 7 present the conclusions of this research and some recommendations as well as the implementation and technology transfer plan, respectively. Section 8 lists the references cited in the main body of the report. Appendices A – F provide the detailed literature review and detailed analysis and results for those who are interested.

2. FIELD FRICTION AND MACROTEXTURE MEASUREMENTS

For this research, a total of 26 sites that received a surface overlay in late 2019 and early/mid 2020 were evaluated. These sites were first identified using the dynamic Highway Maintenance Improvement Program (HMIP) plan and then supplemental information from the resident engineers, such as the actual construction schedule, coordinates, traffic control for core acquisition, etc., were used to select the sites to be tested. Table 1 summarize the information of the sites included in this study. As shown, eight of these sites are Interstates, nine are US-Routes, and the remaining nine are NC-Routes.

Table 1. Sites selected for friction and texture measurements.

Site	Route Type	ADT[a]	Mix Type	Facility Type	Overlay Date	# Observations Before	After
1	Interstate	15,000	RS9.5C	Divided	10/1/2019	-	3
2	Interstate	8,900	RS9.5C	Divided	10/1/2019	-	3
3	US	3,400	RS9.5B	Undivided	10/7/2019	-	4
4.1	Interstate	65,000	UTBWC	Divided	10/1/2019	-	4
4.2	Interstate	51,000	RS9.5D	Divided	4/10/2020	-	3
5	Interstate	37,000	UTBWC	Divided	10/1/2019	-	4
6	Interstate	65,000	RS9.5D	Divided	10/1/2019	-	6
7	Interstate	53,000	RS9.5D	Divided	8/25/2019	-	6
8	NC	4,600	RS9.5C	Undivided	4/15/2020	1	6
9	NC	3,150	RS9.5C	Undivided	10/15/2019	-	6[b]
11	NC	39,000	RS9.5C	Divided	3/20/2020	-	4
12	US	17,000	RS9.5D	Divided	10/1/2019	-	3
13	US	31,050	RS9.5C	Divided	11/1/2020	1	1
14	US	17,000	RS9.5C	Divided	10/1/2019	-	6
15	NC	1,400	RS9.5B	Undivided	10/1/2019	-	6
16	NC	1,800	RS9.5B	Undivided	10/1/2019	-	6
17	US	12,000	RS9.5C	Divided	10/1/2019	-	7
18	US	25,000	RS9.5C	Divided	10/1/2019	-	5
19	US	47,000	RS9.5C	Divided	4/1/2020	1	5
23	Interstate	10,000	RS9.5C	Divided	11/1/2019	-	4
24	NC	7,200	RS9.5C	Undivided	6/1/2020	1	2
27	US	12,000	RS9.5D	Divided	6/15/2020	-	5
28	NC	11,000	RS9.5C	Divided	3/20/2020	-	3
29	NC	11,000	RS9.5B	Undivided	8/1/2020	1	5
30	NC	13,000	RS9.5D	Divided	10/1/2020	1	2
33	US	14,000	RS9.5C	Divided	6/8/2020	1	6

[a] Average daily traffic in the design lane
[b] For site 9, after construction, five friction measurements were taken and six texture measurements were taken.

The test sites are distributed across the State of North Carolina. Once the sites were identified, the research team consulted the Highway Construction And Materials System (HiCAMS) and the NCDOT – Connect website to obtain the Job Mix Formula (JMF) and the construction dates. Using the JMF of each project, the mix volumetrics and the type of mix used was identified. Finally, the

annual traffic survey of 2019 was consulted to pull the annual average traffic volumes, these values were converted to traffic in the test lane (if applicable) using the procedure established in the NCDOT pavement design procedure.

Finally, as indicated in Table 1, seven sites received a measurement before the overlay was placed. The number of observations collected after the construction of the overlay varied from one to seven observations. Each observation consisted of measuring friction and texture; typically, both measurements were collected on the same date. If not, they were collected one day apart. The characteristics of the values collected in each observation and the analysis conducted with these observations is presented below.

2.1. Continuous Pavement Friction Measurements (CFME)

2.1.1. Overview

The equipment used to measure friction was the CFME Moventor Skiddometer BV-11. The measurements were conducted in accordance with ASTM, FHWA, and Federal Aviation Administration (FAA) recommendations. This device is approved and recommended by the International Civil Aviation Organization (ICAO) and the FAA. A view of the trailer used to transport the BV-11 is shown in Figure 1 (a) and an up close photo of the tire assemble is shown in Figure 1 (b). The BV-11 device reports friction numbers in increments of 10 m (32.8 ft). Friction was measured both in the center of the lane (CL) and right wheel path (RWP). Because the tire is centered in the trailer, the vehicle was aligned in such a way the tire was centered in the wheel path, as indicated in Figure 1 (c).
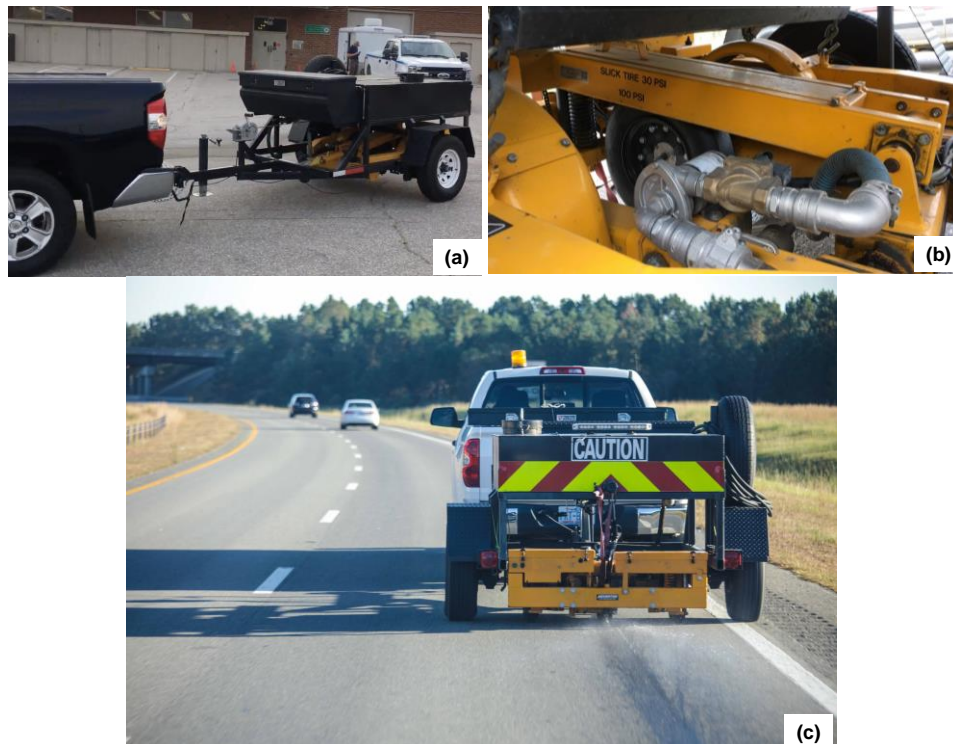
Figure 1. (a) Moventor skiddometer BV-11 test trailer, (b) close-up photo of the test tire, and (c) tire alignment during a measurement.

The friction measurements were collected in the outer most lane in the traffic flow direction, i.e., Northbound (NB), Southbound (SB), Eastbound (EB), or Westbound (WB). Also, the measurements were collected at a speed close to 60 mph (96.6 km/h). For some sites, an additional set of friction measurements were also collected at 40 mph (64.4 km/h) to evaluate the effect of vehicle speed on the friction values. The technical specifications of the BV-11 are described below.

- Mode of Braking: Continuous slip ratio of 17%.
- Tires: Two reference and one measuring tire, smooth.
- Water film thickness: A uniform water depth of 1 mm in front of measuring tire.
- Reliability: Relative error of the skiddometer in operating conditions does not exceed 5%.
- Calibration: The skiddometer does not require regular calibration before use.
- Measuring speed: Measuring speed range of 20 to 160 km/h (12.5 to 100 mph).
- Frequency of results reported: Friction averaged every 10 m (32.8 ft).

The collection dates for each site are indicated in Table B.1 of Appendix B. By comparing the information presented in Table 1 and Table B.1, one can observe that for each site the first measurement was acquired, when possible, in the first 15 to 30 days after the overlay. All of the measurements presented in this report have been collected by KPR engineering personnel.

2.1.2. CFME Data Processing

After collecting the data described above, the KPR engineers provided a ".csv" file for each measurement collected. Each file contained the following information (format of reporting in parenthesis); measurement date (dd-mm-yyyy), time of measurement (hh:ss), ambient temperature (°C), distance (in increments of 10 m), friction value (-), speed (km/h), and position (longitude and latitude coordinates, in decimal degrees).

The measurements collected at a site were reported in individual files for each measurement direction and each lateral location measured. For example, on Site 1 there are two traffic flow directions and for each traffic direction friction was collected in the RWP and CL. Therefore, for the first after construction measurement (A-1) on this site, four files were provided. Because this site received three after construction measurements, a total of twelve files needed to be processed for Site 1. In total, across all sites and measurements more than 488 ".csv" files have been processed. To facilitate this process, an Excel macro was created to copy, organize, and plot the observed values. The resulting files are included as a digital appendix of the document.

After processing all the ".csv" files, the next step consisted of matching the location of the measured friction value with the corresponding milepost of the route. The route milepost was obtained from the NCDOT PMS database. Once the milepost of the measured values was identified, the observed friction values were plotted against distance along the measurement site. Figure 2 is an example of the type of plots that were created. This figure presents the friction values collected in the RWP of Site 1. As shown in Figure 2, the overall mean was calculated and was represented by the red dashed lines; also the values were grouped into 0.1-mile increments, and for each group, the 2.5 and 97.5 percentiles value were calculated; these values are represented by the orange and purple lines, respectively, in Figure 2.

The percentiles were calculated by sorting the data, this is, first the data is arranged in ascending order; then, a percentile X is the value in the dataset where 'x' percentage of the data is less than or equal to X. For example, in the first 0.1-mile of Figure 2 (a) there were 61 observations. After arranging them in ascending order $X = 0.672$ is the friction value at which 2.5% of the 61 values

are less than or equal to 0.672. Similarly, X = 0.789 is the friction value at which 97.5% of the data are less than or equal to 0.789.

From this example, it is observed that if only the overall mean value is used to describe the whole section, one may erroneously assign a high value for a portion of the route. In the case of the A-1 observation, nearly 66% of the observed values are below the overall mean, while for the observations from A-2 and A-3, the proportion of friction values below the mean are 58% and 50%, respectively. In particular, the high friction values recorded before milepost 11 correspond to a bridge which has a portland cement concrete pavement. Because of this issue, the research team decided to use the 2.5th percentile calculated in 0.1-mile increments for further analysis.
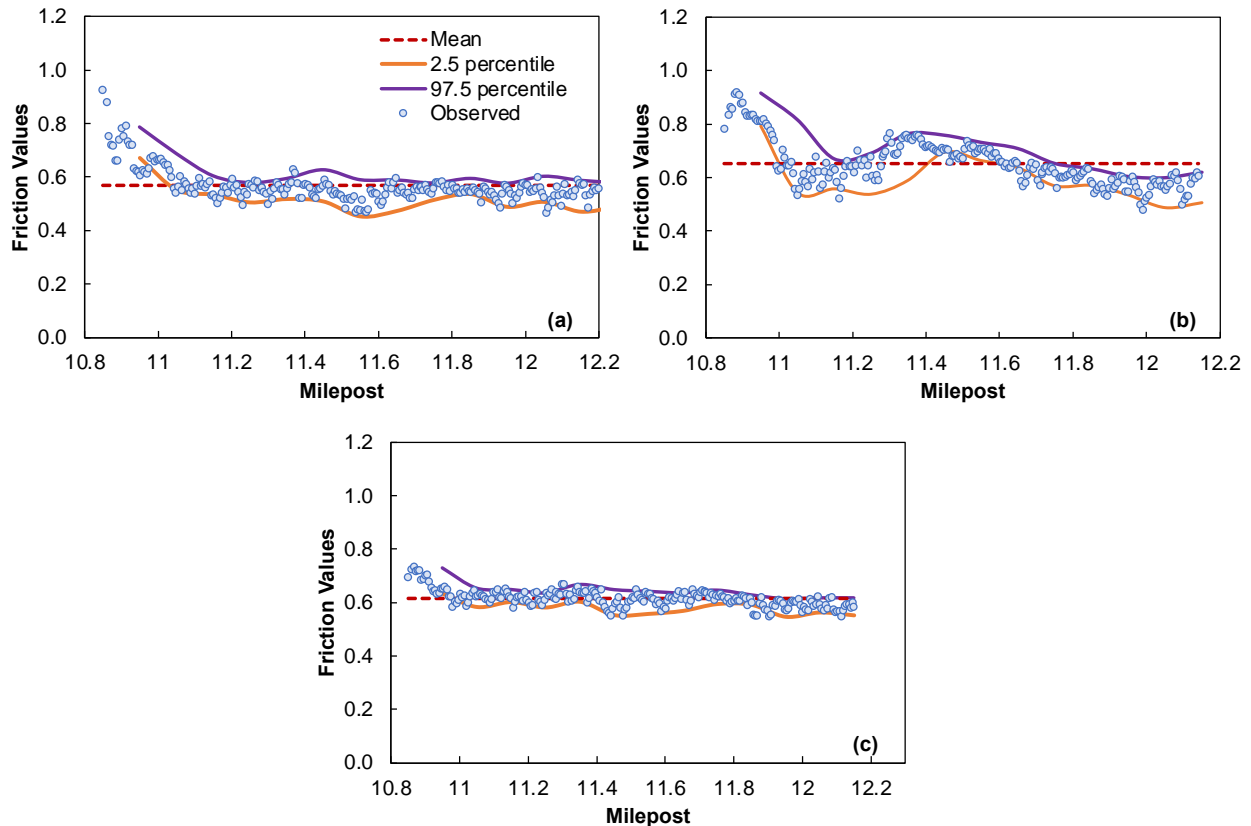
Figure 2. Example of the friction values collected for Site 1, RWP in observation (a) A-1, (b) A-2, and (c) A-3.

As shown in Figure 2, the calculated 2.5th percentile for the individual 0.1-mile segments follows the overall trend of the observed data and reduces the amount of information required to represent the entire route. Another benefit of using the 2.5 percentile to describe the friction of each route segment, is the possibility of removing possible outliers (short portion of route with high friction values) such as the presence of bridges that might affect the overall average.

A similar analysis was conducted for each route, that is, first the friction values were mile posted and then the overall mean was calculated, next the values were grouped into 0.1-mile segments and the 2.5 percentile was used to describe the friction of each segment. For each site, an Excel file was created where all the measurements were processed as explained above. All these files are included in Appendix F.

Also, a significant advantage of measuring with a CFME rather than with a LWST is that the continuous devices provide a much higher spatial testing coverage, thus reducing the chances of missing localized areas with friction deficiencies. The standard LWST test procedure results in measuring approximately 59 ft of road (at 40 mph). If the standard practice is to conduct one test every mile, the tested sample represents only 1.1 percent of the pavement surface. In contrast, the CFME measures every foot of the road, which is ideal for a proactive network-level analysis process such as the safety performance factors (SPF)-empirical Bayes (EB) method. This high resolution is particularly important to identify potential friction problems on road sections with a high friction demand, such as curves and intersections.

2.2. High-Speed Texture Measurements

2.2.1. Overview

The equipment used for macrotexture measurements is the Ames Engineering High Speed Inertial Road Profiler. This device is designed as a portable inertial profiling system that can be used on multiple vehicles and mounts onto a standard 2 in. receiver hitch (as shown in Figure 3). The specifications of the laser are described below.

- Measuring Speed: 25 to 65 mph (40 to 104 km/h)
- Resolution: Laser height sensor with a range of eight inches and a resolution of 0.002 in. The horizontal distance is measured with an optical encoder that has a resolution of 0.15 inches.
- Sampling: Pavement elevation sampling of 16,000 samples per second. The software storage 12 samples per foot.
- Profile wavelength range: 0.5 to 6400 feet
- Accelerometer resolution: 0.0001 g
- Frequency of results reported: every 3 m (9.84 ft)

Like friction, texture was measured in the CL and the RWP. The measurements were collected in the outer most lane in the traffic flow direction at the posted speed limit.

Figure 3. High Speed Inertial Road Profiler (*11*).

After collecting the texture profile, the Ames Engineering High Speed Inertial Road Profiler applies the filters indicated by ISO-13473 to remove potential outliers and then compute the following texture parameters: *MPD*, *EMTD*, *RMS*, *Ra*, *Rq*, *Rku*, and *Rsk*.

Mean Profile Depth (*MPD*)

A standard method for determining the *MPD* from the macrotexture profile of the pavement is provided in ASTM Standard E1845. The *MPD* is a 2D estimate of the 3D mean texture depth (*MTD*). To calculate the *MPD*, the measured profile of the pavement macrotexture is divided into segments for analysis purposes. The slope, if any, of each segment is suppressed by subtracting a linear regression of the segment. The segment is divided into two segments, and the highest peak in each half-segment is determined. The difference between the resulting peak level for each segment and the average level of the whole segment is referred to as mean segment depth (MSD), and these differences are averaged together (Figure 4) and reported directly as the *MPD*.
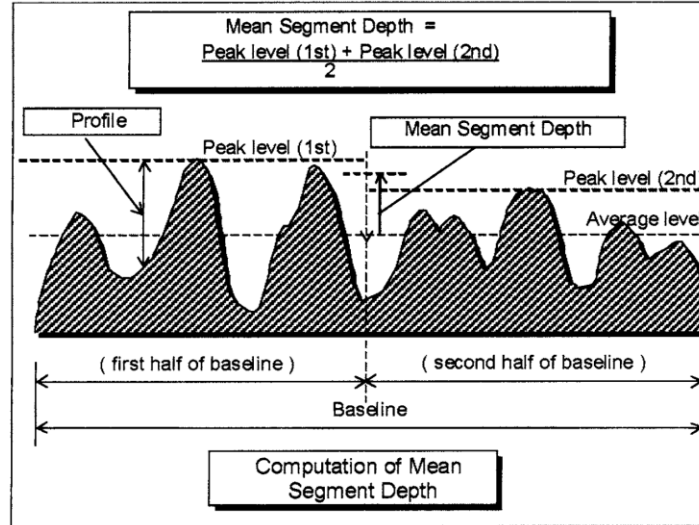
Figure 4. Procedure for Computation of Mean Segment Depth (*12*).

Estimated Mean Texture Depth (*EMTD*)

An estimated texture depth (*EMTD*) is used when the *MTD* (estimated with volumetric techniques, such as the Sand Path test) is estimated from the *MPD* using the transformative equation provided in ASTM E1845. This parameter is estimated internally using the software provided by Ames Engineering and it is reported in conjunction with the *MPD* value.

Root Mean Squared (*RMS*)

Outside of the United States, the root mean square (*RMS*) is a very common parameter used to characterize macrotexture. After removing the slope from the profile, the profile mean is set to zero and the *RMS* is the square root of the mean of the squares of a macrotexture profile as shown in Equation (1). It is a measure of the variation of measurements in a dataset. Since the calculation involves the square root of the summation of the variation, it is a standard deviation of the data. "Large variations" mean large deviations from the mean texture level. In a 2D profile, the *RMS* is equivalent to the root mean squared roughness *Rq*.

$$RMS = \sqrt{\frac{\sum_{i=1}^{n} y_i^2}{n}} \tag{1}$$

where;

L = length of segment evaluated, and

y = elevation from slope-suppressed, zero mean profile segment.

Mean Elevation (*Ra*)

The mean elevation is the average of the absolute value of the elevation from slope-suppressed, zero mean profile segment.

Kurtosis (*Rku*)

This parameter is generally used to describe the peakedness of a macrotexture profile i.e., how severe peaks and troughs are in comparison to the mean elevation. *Rku* can be calculated using Equation (2).

$$Rku = \frac{\sum_{i=1}^{n} y_i^4}{n\left(R_q^4\right)} \tag{2}$$

Skewness (*Rsk*)

This parameter is used to capture the positive or negative macrotexture behavior. Negative skewness values indicate a negative macrotexture (more throughs than peaks). *Rsk* is calculated as indicated in Equation (3).

$$Rsk = \frac{\sum_{i=1}^{n} y_i^3}{n\left(R_q^3\right)} \tag{3}$$

2.2.2. Texture Data Processing

Like the friction data, the texture measurements collected at a site were reported in individual files. In the case of texture, two separate files were generated for each measurement: one for the International Roughness Index (IRI) and other for the texture parameters. For example, for the two traffic directions of Site 1 the measurements collected in each direction consisted of four files, two for the RWP and two for the CL. Therefore, for this site a total of eight files have been provided for each measurement (A-1, A-2, etc.) performed. Because this site received three after construction measurements, a total of 24 files needed to be processed. Overall, more than 1,000 ".csv" files have been processed. Consistent with the friction data analysis, an Excel macro was created to copy, organize, and plot the observed texture information to facilitate the analysis of the raw observations. The resulting files are included as a digital appendix of the document.

For the texture records, the information extracted from the files included the date (dd-mm-yyyy), time (hh:mm), distance (in increments of 3 m), coordinates (longitude and latitude in decimal degrees), *MPD* (mm), *EMTD* (mm), *RMS* (mm), *Ra* (mm), *Rq* (mm), *Rku* (-), and *Rsk* (-). A detailed explanation of the equations used to calculate each of these parameters is provided in Appendix A. One parameter that is not included in the report provided by the Ames device is the Texture Ratio (*TR*). For *TR*, the macrotexture orientation of a pavement is estimated by taking the ratio of *MPD* to *RMS* according to Equation (4). Typically, texture ratios greater than 1.05 indicate a positive macrotexture (more asperities above the mean macrotexture level) while a ratio of less than 0.95 indicates a negative macrotexture (greater void spaces below the mean macrotexture line).

$$TR = \frac{MPD}{RMS} \tag{4}$$

Once all the information was extracted and organized, the corresponding milepost for reach observation was assigned. The dates at which texture was measured are presented in Table B.2 of Appendix B. It was noticed the texture values were collected in a longer section of the route than friction. This was a common pattern across all the sites. The coordinates of the measurements were matched with the linear referencing system of the route using QGIS, in this way each data point was associated with a given milepost.
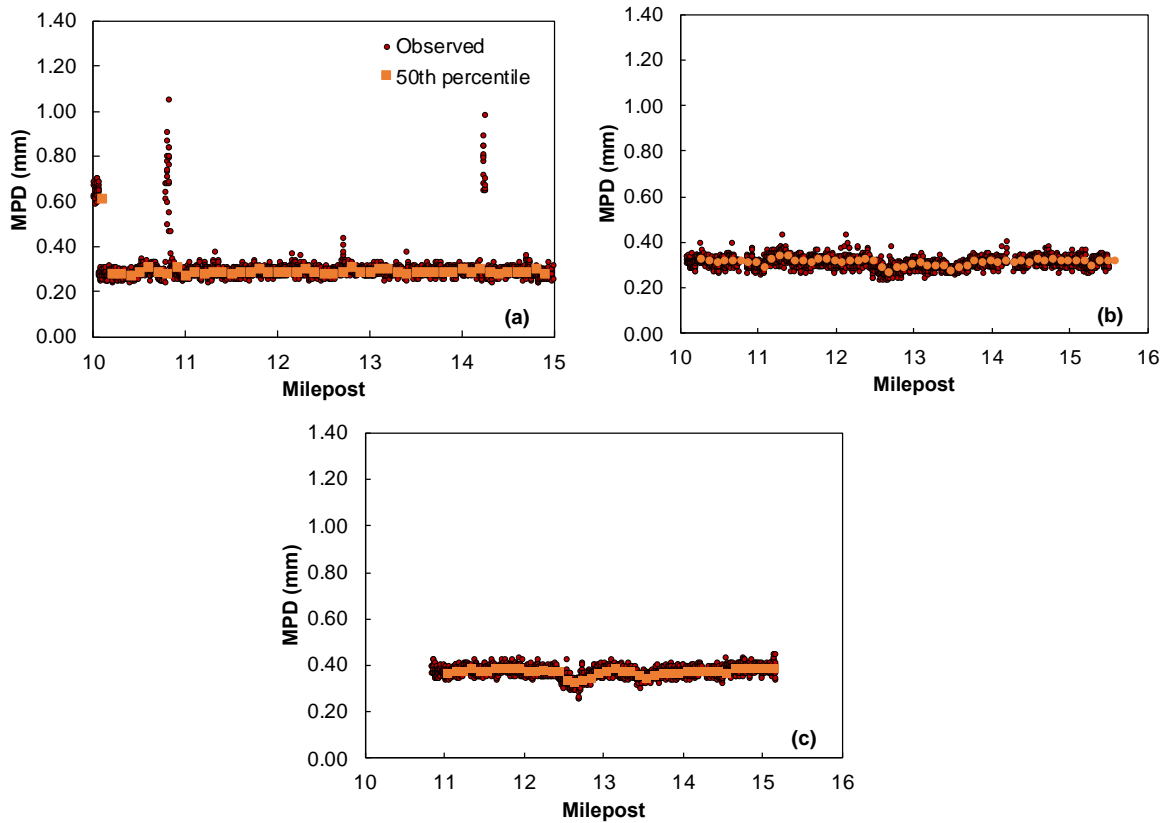
Figure 5. Example of the *MPD* values collected for Site 1 RWP in observation (a) A-1, (b) A-2, and (c) A-3.

Once the mileposts of the observations were identified, the observed texture parameter was plotted against the associated milepost. All the plots created for this research used the *MPD* as the parameter that describe texture. However, the other parameters such as *RMS*, *Ra*, *Rq*, etc. were reported in a tabular format which is also included in Appendix F.

As an example, Figure 5 shows the *MPD* values collected in Site 1 in the RWP of the SB direction. Part (a) of the figure presents the values collected during the A-1 observation, the observed values are represented by the dark red circles, and the *MPD* values were grouped into 0.1-mile increments. For each group, the 50th percentile (or median) was used as the representative value. This percentile was calculated following the same procedure used for friction, the reader can refer to the previous section for detailed explanation. The same procedure was followed with the other texture parameters. As shown in Figure 5 (a), the high-laser device can capture the different texture characteristics along the corridor. The spikes observed in mileposts 10.8 and 14.3 correspond to

portland concrete surfaces located on three bridges along the corridor, as shown in Figure 6. Although not shown in Figure 6, the spike observed in milepost 10.1 in Figure 5 (a) corresponded to a section that had some mud and miscellaneous associated materials on the pavement surface at the time of the measurement.
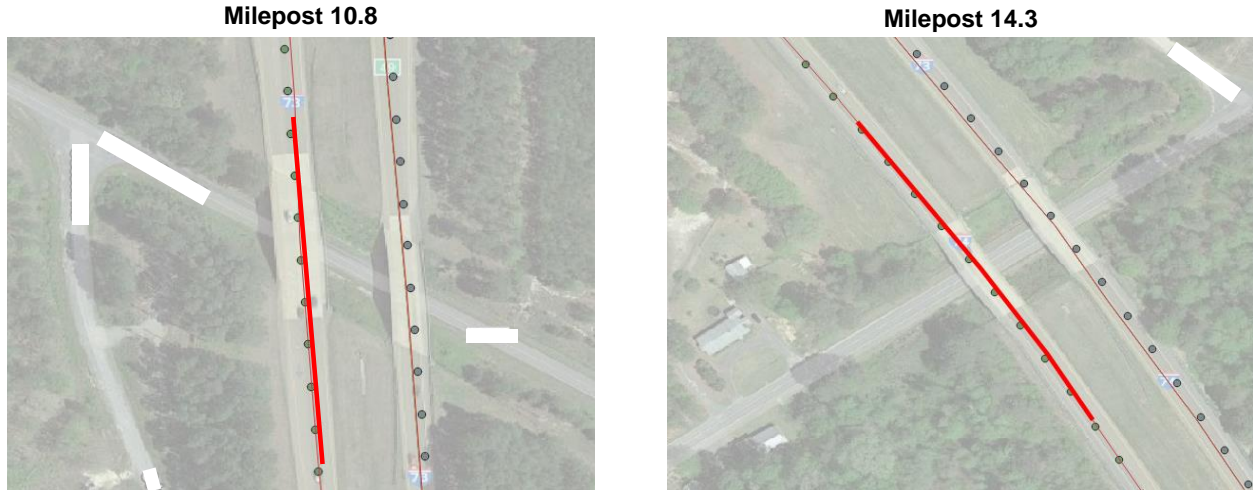
Figure 6. Location of bridges in Site 1, SB direction.

Because of these potential impacts, the median of the values grouped for each 0.1-mile have been calculated to remove the effects of outliers. Also, for the subsequent measurements, the device was calibrated in such a way that the texture was not recorded over sections with a portland concrete surface, or that were visually different from the newly overlaid material (either was an old surface, or it was contaminated with dust or disperse materials such as mud or debris from the construction site). Consequently, the spikes observed in Figure 5 (a) are not evident in Figure 5 (b) or (c) (the later measurements). A similar analysis has been conducted for all the sites, and the corresponding set of plots with the values computed in 0.1-mile increments are included in Appendix F.

This page is intentionally blank

3. FACTORS AFFECTING EARLY FRICTION AND TEXTURE

As described in the previous section, a total of 26 sites were selected to monitor the trends in friction and texture with time in the early life after overlays. For each site, the overlay date was obtained as well as complementary information such as the annual average traffic volume, road geometry, JMF, etc. In addition, for ten of these sites, a set of field cores were extracted to measure friction and texture in the laboratory. These cores were taken within a few days of the overlay placement.

Table 2 provides a summary of the information compiled from the different databases. Six sites received a RS9.5D asphalt mixture, fourteen sites received a RS9.5C mix, four received a RS9.5B, and the remaining were overlaid with an UTBWC. It is noted that the *ADT* shown in Table 2 correspond to the traffic volume in the primary travel lane, estimated using the lane distribution factors from the NCDOT pavement design manual.

Table 2. Characteristics of the tested sites.

Site	Route	*ADT*	Mix	*Pb*	*VFA*	*VMA*	*Cc*	*P_{200}*
1	Interstate	15,000	RS9.5C	6.40	75.70	17.30	0.53	6.30
2	Interstate	8,900	RS9.5C	6.30	77.20	18.20	0.62	7.50
3	US	3,400	RS9.5B	6.30	78.50	18.30	1.12	5.90
4.1	Interstate	65,000	UTBWC	5.20	60.10	17.80	5.95	4.10
4.2	Interstate	51,000	RS9.5D	6.00	76.50	17.30	0.75	5.80
5	Interstate	37,000	UTBWC	5.50	34.57	15.44	1.99	3.50
6	Interstate	65,000	RS9.5D	5.60	76.50	16.70	0.80	5.80
7	Interstate	53,000	RS9.5D	5.70	76.00	16.70	0.76	6.50
8	NC	4,600	RS9.5C	5.70	77.80	16.90	1.25	5.80
9	NC	6,300	RS9.5C	6.40	77.80	18.40	0.97	6.70
11	NC	39,000	RS9.5C	6.00	76.90	17.30	0.66	7.20
12	US	17,000	RS9.5D	5.40	75.30	16.20	0.73	6.20
13	US	69,000	RS9.5C	6.50	77.50	17.90	0.76	7.20
14	US	17,000	RS9.5C	6.20	76.90	17.30	0.60	7.30
15	NC	1,400	RS9.5B	6.20	78.50	17.90	0.61	6.90
16	NC	1,800	RS9.5B	6.80	78.80	18.90	0.66	7.00
17	US	12,000	RS9.5C	5.70	74.10	17.40	0.49	5.90
18	US	25,000	RS9.5C	5.70	75.50	16.50	0.60	6.10
19	US	47,000	RS9.5C	6.00	76.90	17.30	0.76	7.20
23	Interstate	10,000	RS9.5C	6.00	76.60	17.10	0.87	7.00
24	NC	7,200	RS9.5C	5.80	76.60	17.50	1.34	5.90
27	US	12,000	RS9.5D	5.50	73.10	16.00	1.10	6.40
28	NC	11,000	RS9.5C	6.60	77.70	18.70	0.82	7.80
29	NC	11,000	RS9.5B	6.30	79.60	19.50	0.75	7.00
30	NC	13,000	RS9.5D	5.30	75.30	16.20	1.02	6.40
33	US	14,000	RS9.5C	5.60	75.50	16.60	0.62	6.70

Note: Sites where field cores were extracted are highlighted in gray.

The individual JMF of the mix used in each site is summarized in Appendix F. Across all sites, the asphalt content (*Pb*) ranged from 5.2% to 6.8%, the percent voids filled with asphalt (*VFA*), percent voids in mineral aggregate (*VMA*), and P_{200} varied from 34.57% to 79.60%, 15.44% to 19.50%,

and 3.50% to 7.80%, respectively. It is important to notice that all of the volumetric properties shown here are those reported in the JMF; therefore, values in the field might be slightly different from the ones reported in Table 2.

The gradation of each mix is summarized using the coefficient of curvature, *Cc*, and coefficient of uniformity, *Cu*, defined in Equations (5) and (6), respectively. Both parameters are widely used to describe gradation shape and aggregate size distribution (*13*). For the gradation to be well graded, the value *Cc* must range between one and three, and for a single sized gradation both *Cc* and *Cu* are equal to one. In addition, a *Cu* greater than six indicates a densely graded material with a considerable range of particle size, while a *Cu* less than four indicates a uniformly graded material. The *Cc* parameter varied among sites from 0.49 to 5.95. The *Cu* parameter varied from 8.56 to 30.16. It is not included in Table 2, but is shown in Appendix F.

$$Cc = \frac{D_{30}^2}{D_{10} \times D_{60}} \tag{5}$$

$$Cu = \frac{D_{60}}{D_{10}} \tag{6}$$

where;

D_{60} = particle size at 60% finer,
D_{30} = particle size at 30% finer, and
D_{10} = particle size at 10% finer.

3.1. Lab Measurements

Laboratory characterization of the field cores was performed using the sand patch test (SPT), a custom-built bench scale laser scanner, and the British Pendulum Tester (BPT). The average height and diameter of the cores was 8-10 in. (20-25 cm) and 6-8 in. (15-20 cm), respectively. In the field, the cores were collected in the center of the RWP, and their precise location were estimated using a GPS receiver. The NCDOT personnel evenly spaced the cores along the section surveyed with the CFME device and the Ames laser scanner. Three cores were extracted from each site, except for Site 24 where four cores were extracted.

Once the cores were collected, they were transported to the lab for testing. There, the cores were cut to an approximate height of 4 in. (10 cm) so that they would fit underneath the laser profiler and inside the BPT testing jig. In the case of friction, the BPT measurements were carried out according to ASTM E303-93. The research team developed a support and mounting base for the BPT and to hold the field cores steady and keep the surface leveled, as shown in Figure 7 (a).

A SPT was first conducted on each core following ASTM E965-15 to measure the *MTD*. Then, the benchtop laser was used to scan the surface of the cores. This laser was capable of collecting surface elevation with a spatial frequency of 0.3 mm and with a vertical resolution of 0.01 mm. The laser measurements were processed according to the ISO 13473. Three parameters were extracted from the scanned surface, the estimated mean texture depth (*EMTD*), the average *peak* height, and the average *valley* depth. The *peak* height is the positive difference between the surface elevation and the mean plane, while the *valley* depth is the negative difference between the surface elevation and the surface mean plane.
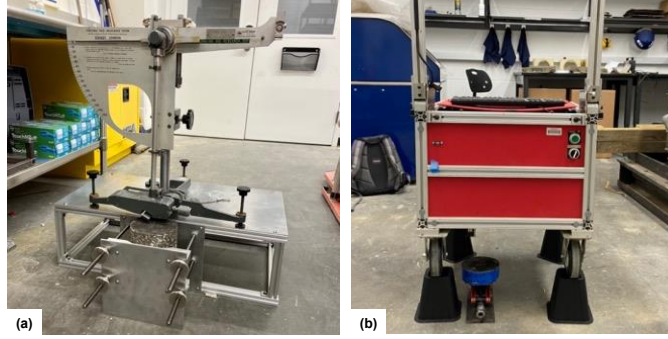
Figure 7. (a) Support base for the BPT and (b) proprietary laser used to scan the surface of field cores.

To compare the lab results against the field observations the average of the continuous friction and texture measurements in the vicinity of each core was determined. The window for this determination was set at ± 250 ft (76 m) around the core location. An example of this procedure is illustrated in Figure 8, where the continuous texture and friction profiles are plotted, the yellow dots indicate the location where the cores were extracted, the label next to the points are the mean value of the texture and friction, respectively, in the vicinity of the core location. The results of the field and lab measurements are summarized in Table 3. Columns 4 to 8 contain the result of the lab measurements, while columns 9 and 10 refer to the field measurements results.
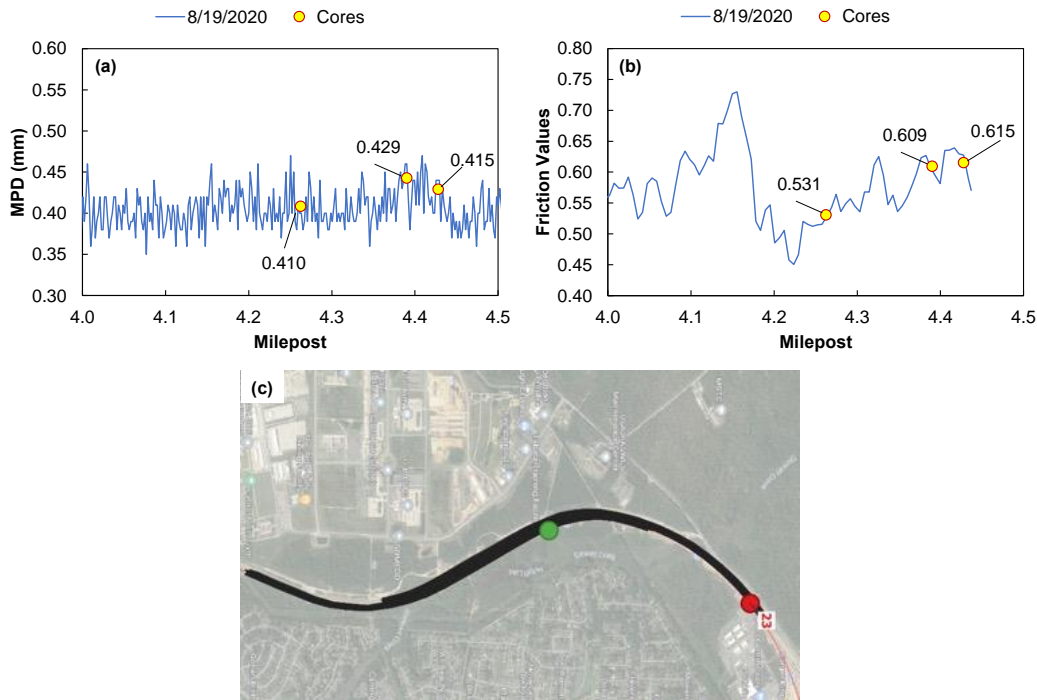
Figure 8. Field measurements and core locations for site 23: (a) *MPD*, (b) friction value, and (c) location of the core along the tested site.

As indicated in Table 3, the friction measured with the BPT was in the range of 47 to 70 *BPN* units, with a standard deviation of 1 to 2 units. As a point of reference, the average friction value measured with the CFME in the core locations varied from 0.43 to 0.76. In the lab, similar texture values were obtained with the SPT test and the laser scanner; the *MTD* estimated with the SPT

ranged from 0.34 to 0.49 mm (0.013 to 0.020 in.), while the *EMTD* calculated with the scanned surface of the cores varied from 0.26 to 0.54 mm (0.010 to 0.021 in.). The *peak* and *valley* depths were in the range of 0.08 to 0.16 mm (0.003 to 0.006 in.) and 0.1 to 0.23 mm (0.004 to 0.009 in.), respectively; these values suggest that on average, the surface has deeper valleys, or negative texture, than height in peaks, or positive texture. In general, surfaces where the positive macrotexture is higher than the negative macrotexture are desired.

Table 3. Summary of the lab and field friction/texture measurements.

(1) Site No.	(2) Route Type	(3) Core	(4) BPN[a]	(5) *MTD* (mm)	(6) *EMTD* (mm)	(7) *Peak* (mm)	(8) *Valley* (mm)	(9) Mean[b] *MPD* (mm)	(10) Mean[b] Friction
8	NC	1	54.00	0.49	0.45	0.14	0.17	0.39	0.76
		2	56.25	0.44	0.46	0.15	0.23	0.42	0.74
		3	57.00	0.48	0.42	0.15	0.22	0.38	0.65
13	US	1	73.50	0.34	0.35	0.09	0.10	0.31	0.46
		2	52.50	0.35	0.34	0.10	0.10	0.30	0.47
		3	55.00	0.35	0.32	0.10	0.11	0.30	0.43
14	US	1	69.25	0.38	0.36	0.10	0.13	0.41	0.53
		2	62.25	0.35	0.34	0.10	0.13	0.40	0.53
		3	64.00	0.38	0.32	0.09	0.10	0.39	0.53
17	US	1	55.75	0.47	0.47	0.16	0.22	0.38	0.62
		2	52.00	0.48	0.54	0.16	0.21	0.40	0.60
		3	56.50	0.43	0.43	0.14	0.19	0.38	0.56
23	Interstate	1	58.50	0.41	0.41	0.13	0.17	0.41	0.53
		2	59.75	0.40	0.44	0.13	0.18	0.43	0.61
		3	56.00	0.40	0.43	0.12	0.15	0.41	0.62
24	NC	1	54.25	0.34	0.31	0.10	0.12	0.33	0.68
		2	55.50	0.37	0.33	0.12	0.17	0.33	0.67
		3	60.50	0.37	0.34	0.11	0.13	0.34	0.65
		4	60.00	0.39	0.40	0.12	0.16	0.36	0.68
27	Interstate	1	62.50	0.41	0.31	0.11	0.20	0.37	0.73
		2	60.00	0.39	0.28	0.10	0.16	0.35	0.63
		3	65.50	0.36	0.30	0.10	0.18	0.36	0.59
28	NC	1	52.00	0.35	0.28	0.09	0.14	0.31	0.50
		2	49.75	0.35	0.40	0.14	0.23	0.33	0.50
		3	50.50	0.36	0.26	0.08	0.13	0.30	0.53
30	NC	1	60.25	0.44	0.41	0.14	0.23	0.38	0.62
		2	50.50	0.40	0.30	0.11	0.17	0.37	0.63
		3	47.50	0.37	0.31	0.12	0.20	0.36	0.64
33	US	1	54.75	0.38	0.33	0.10	0.16	0.35	0.51
		2	49.75	0.39	0.36	0.11	0.15	0.37	0.55
		3	60.00	0.34	0.31	0.11	0.17	0.35	0.56

[a] average of four measurements
[b] averaged over a window of +/- 76 m (250 ft)

Surface Type   RS9.5C   RS9.5D

Figure 9 shows a graphical comparison of the average friction and texture values obtained in the laboratory with the average friction and texture values measured in the field in each site. As illustrated, there is not a clear correlation between the two quantities; however, based on the figure it is possible to see some proportionality between the two. As indicated in Figure 9, there is not a marked difference between the values observed in the RS9.5C and RS9.5D sites. Of particular interest is Site 14 (enclosed with the red-dashed circle in Figure 9) because this site has the highest *BPN* value observed among the sites, *BPN* = 65, but a field friction of only 0.53. On the other hand, the texture for this site is in the upper side of the measured values with a field *MPD* of 0.4 mm and *EMTD* of 0.34 mm. At this point, there is not a plausible explanation for this situation, other than variability in the test values. To provide more insight in the friction mechanism and the relationship between friction and texture it is necessary to account for the aggregate polishing resistance characteristics (e.g., using the Polished Stone Value test – PSV), because the aggregate characteristics affects the laboratory measurements more than the field measurements due to the low speed of the BPT measurements.
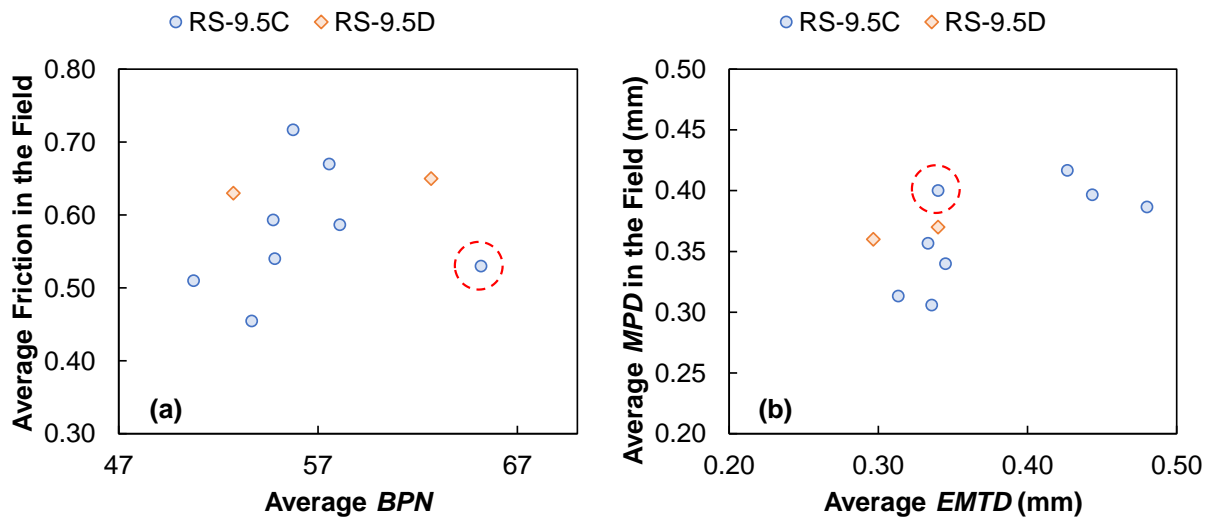
Figure 9. (a) Comparison of the friction measured with the BPT and the CFME, and (b) comparison of the *EMTD* measured in the lab with the field *MPD*.

3.2. Analysis

The data described above was used in three different analyses.

- The relationship between the laboratory and field friction/texture values was characterized by using data from the ten sites where cores were taken after construction. In total, there were 31 cores, for a total of 31 field/lab pairs of observations.
- A model was calibrated to relate the average friction/texture values in the field with the mix volumetric parameters using measurements from all 26 sites. For this purpose, the first after construction measurement was used; each site has two observations, one per direction (except for Site 27 where the overlay was applied only in the WB direction), for a total of 51 observations.
- The correlation between friction and the different texture parameters was evaluated using data from all 26 sites, again the observations collected in the first after construction

measurements were used. As stated in the previous bullet point, there are 51 observations available.

3.2.1. Field-Lab Relationships

In the first analysis, correlation coefficients between the various texture/friction variables measured in the laboratory (using the field cores) and the ones collected in the field were obtained. As shown in Table 3, a total of 31 field cores were acquired during this project and all were used to evaluate the correlations and ultimately develop the predictive model. The results from the initial correlation analysis are summarized in Table 4. As noticed, the surface average *peak*, average *valley*, and *Cc* variables have the highest positive correlation with friction. In the case of texture, the highest positive correlation is obtained with the *EMTD* (estimated with the surface laser scanned), average *peak*, and average *valley* depth. On the other hand, the parameters with the highest negative correlation with friction and texture are *Pb*, *VMA*, and P_{200}. It is worth noting that the second least correlated variable to field friction was the *BPN*.

Table 4. Correlation coefficient of the lab measurement quantities and the field mean texture and friction.

Parameter	MPD_{field}[a]	$Friction_{field}$[b]
BPN	0.18	0.10
EMTD	0.63	0.27
Peak	0.55	0.44
Valley	0.41	0.50
Pb	-0.21	-0.54
VFA	-0.01	-0.08
VMA	-0.37	-0.38
Cc	-0.20	0.74
P_{200}	-0.17	-0.77

[a] *MPD* measured using a high-speed laser profiler
[b] friction value collected with a CFME.

Based on these correlation coefficients, multivariate regression using different combination of the parameters were performed. Through this process, the functional form of Equation (7) was determined as the one that best related the combined effects of the highly correlated variables to field friction. In the case of Equation (7), all coefficients were found to be significant at a 95% confidence level and the adjusted R^2 of the model was 0.76. The model prediction accuracy is shown in Figure 10. The significance of Equation (7) is as a means to predict the in-service friction on the basis of mixture composition (*Pb* and P_{200} as reported in the JMF) as well as the surface texture, which could be measured directly in the field or based on QA field cores.

$$Friction = 0.645 + 0.141 \times (Cc + Peak + Valley) - 0.00548 \times (Pb \times P_{200}) \tag{7}$$

where;

Cc = gradation coefficient of curvature, see Equation (5),
Peak = average surface peak height,
Valley = average surface valley depth,
Pb = asphalt content by weight, and
P_{200} = aggregate fraction passing the No. 200 sieve.
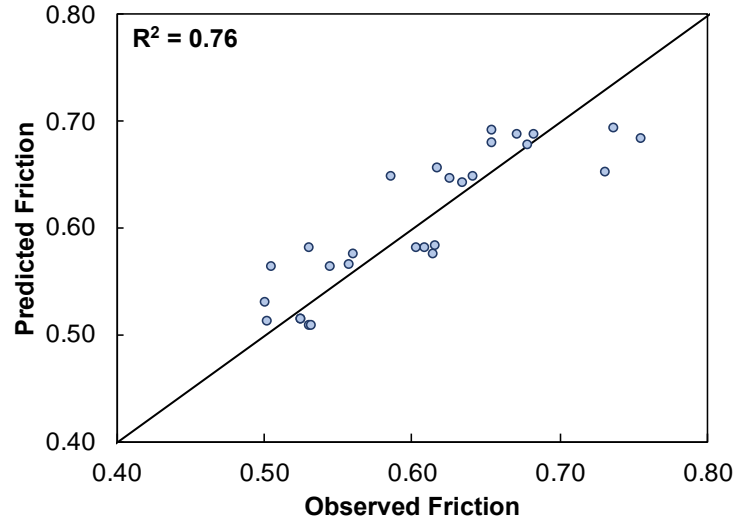
Figure 10. Friction model prediction check.

Similar multiple linear regression analysis was conducted to relate field texture measurements to laboratory measurements. Equation (8) was the most promising model identified, but the overall R^2 of the model was only 0.39. As shown, this model can predict only 39% of the data variability, indicating more observations are needed to establish a more robust prediction of field texture using laboratory measurements.

$$MPD = 0.243 + 0.331 \times EMTD \tag{8}$$

where;

MPD	=	mean texture depth measured with a high-speed laser profiler, and
EMTD	=	estimated mean texture depth calculated using a field core laser scanned surface.

3.2.2. Effect of Mix Volumetrics on Friction and Texture Values

Models that relate mixture composition to either texture or friction were developed to understand the factors that contribute to texture/friction and their relative importance. Data from all 26 sites were used, but for this purpose, only the A-1 measurements were included. Each site received a measurement per traffic direction, except for Site 27 were friction and texture were measured only in the WB direction. Hence, a total of 51 observations were available for the analysis. The response variable was set as the average texture or friction and the predictors were the mix volumetrics. The variables used and their respective range of values are specified in Table 5 and Table 6, respectively.

For this analysis, variables were filtered out in terms of importance by first calculating the correlation coefficient of each predictor with the response. The correlation coefficient, *r*, is calculated using the expression shown in Equation (9), and the results for each pair of variables is summarized in Table 5. As shown, the friction shows some proportionality with a few of the variables but does not seem to correlate at a high level with any of them. Though not individually very strong, the analysis suggests that friction reduces with the total *Pb* content, *VFA*, *VMA*, and P_{200}. On the other hand, texture seems to correlate with *VFA*, *Pb* Virgin Ratio, *VTM*, *Cc*, and P_{200}. Although the total volume of air in the mix (*VTM*) is highly correlated with texture, this value was not used as a predictor because this is the air void target during the mix design, hence most of the

values reported in the JMFs are equal to four. Owing to the poor overall correlation, multivariate regression was not performed for friction.

Table 5. Variables used in the model.

Variable	Description	Role
MPD	Mean value of the 50th percentile *MPD* reported every 0.1-mile	Response
Friction	Mean value of the 2.5th-percentile friction reported every 0.1-mile	
Total *Pb*	Total asphalt binder in the mix	
VFA	Percent of voids filled with asphalt	
Pb Virgin Ratio	Ratio of the virgin binder added in the mix to the total binder in the mix	
Virgin *Pb*	Total virgin asphalt binder added to the mix	Predictor
VMA	Void in mineral aggregates	
VTM	Total volume of air	
Cc	Coefficient of curvature	
Cu	Coefficient of uniformity	
P_{200}	Percent of the gradation passing the sieve No.200	

Table 6. Variables range of value.

Variable	Low	Median	Average	High
Total *Pb*	5.20	5.90	5.92	6.80
VFA	34.57	76.60	74.15	79.60
Pb Virgin Ratio	60.00	75.00	76.46	100.00
Virgin *Pb*	3.60	4.60	4.63	5.60
VMA	15.44	17.30	17.32	19.50
VTM	4.00	4.00	4.40	10.10
Cc	0.49	0.76	1.06	5.95
Cu	8.56	18.69	18.17	30.16
P_{200}	3.50	6.40	6.35	7.80
Friction	0.29	0.55	0.55	0.71
MPD	0.24	0.34	0.41	1.47

$$r = \frac{\sum_{i=1}^{N}(x_i - \bar{x})(y_i - \bar{y})}{\sqrt{\sum_{i=1}^{N}(x_i - \bar{x})^2 \sum_{i=1}^{N}(y_i - \bar{y})^2}} \tag{9}$$

where;

r = correlation coefficient,
x_i = values of the x-variable in the sample,
$\bar{x}$ = mean of the values of the x-variable,
y_i = values of the y-variable in the sample, and
$\bar{y}$ = mean of the values of the y-variable.

Table 7. Correlation coefficient between the mix volumetrics and average friction and texture for Analysis 2.

Variable	Average MPD[a]	Average Friction[b]
Total Pb	-0.49	-0.42
VFA	-0.78	-0.19
Pb Virgin Ratio	0.70	0.38
Virgin Pb Content	0.42	0.07
VMA	-0.19	-0.29
VTM	0.83	0.17
Cc	0.92	0.17
Cu	0.08	0.11
P_{200}	-0.76	-0.45
Friction	0.13	1.00
MPD	1.00	0.13

[a] average of the MPD 50-percentile, measured with a high-speed inertial profiler, calculated every 0.1 mile.
[b] average of the friction 2.5-percentile, collected with a CFME, calculated every 0.1-mile.

Though the measurements could not be used to directly characterize a predictive model for in-service pavement friction, it was possible to calibrate a model for texture. As in Section 3.2.1, multivariate regression was performed by starting with the variables showing the greatest correlation in Table 7. The model structure was assumed linear and different combinations of the parameters were evaluated (including each variable individually or as a combination of variables, addition, and multiplication of variables, etc.). The final functional form identified through this process is shown in Equation (10). All parameters were statistically significant at a 95% confidence level and the R^2 of the model was equal to 0.93.

$$MPD = 0.674 + 0.150 \times Cc - 0.00088 \times P_{200} \times VFA \tag{10}$$

where;

MPD	=	mean value of the 50-percentile MPD reported every 0.1-mile,
VFA	=	percent of voids filled with asphalt,
P_{200}	=	percent of gradation passing the sieve No. 200, and
Cc	=	coefficient of curvature, calculated using Equation (5).

The resulting model was contrasted against the NCHRP 441 model (*13*) (see Equation (49) in Appendix A). This comparison is illustrated in Figure 11. In part (a), the comparison includes all 26 sites, while in part (b), only the sites with dense graded asphalt surfaces are shown. The UTBWC sites in part (a) are those that have a MPD higher than 0.5 mm (0.02 in.), and represent around 10% of the data used to calibrate Equation (10). As indicated in part (a) of Figure 11, the R^2 of the model, with respect to the line of equality, is equal to 0.93. However, if one focuses only on the dense graded mixes and computes the R^2 of the model, it reduces to 0.72 and produces results like those predicted from the NCHRP 441 model (though it appears to correct some slight bias in the NCHRP 441 model

The previous results partially explain why the relationship evaluated between the texture measured in the lab and in the field, i.e., Equation (8), yielded a low R^2. Recall that this model showed a relatively low R^2 (0.39), but it only included the dense graded mixtures. Also, it is necessary to collect more measurements in the texture range of 0.5 mm to 2.0 mm to improve the accuracy and more robustly establish the statistical significance of the models of Equation (8) and (10).
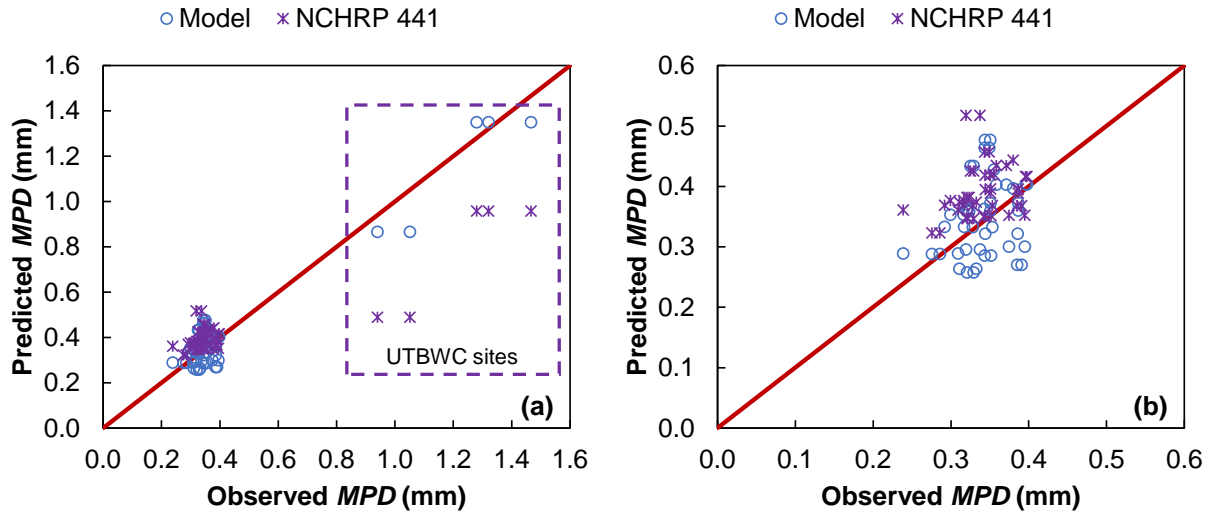
Figure 11. Comparison of the prediction texture model of Equation with the NCHRP 441 model: (a) comparison including all 26 sites, and (b) comparison by using only the Superpave dense mixes.

3.2.3. Relationship between Friction and Texture Parameters

As mentioned in the previous section, efforts were made to establish a friction prediction model similar to the one shown in Equation (10); however, because of the lack of any strong correlation between friction and the independent variables, it was not possible to obtain a model that predicts friction as a function of the mix volumetric properties. This may be a consequence of insufficient data available within this study. Development of such a model for friction may be possible if more observations are incorporated into the dataset that provide additional insight into the effect of the mixture properties on field friction.

Correlation between friction and texture parameters reported by the AMES laser profiler were investigated because it is widely accepted that the hysteresis mechanism is one of the most important friction components, especially under wet conditions. Most of these parameters, except by the *MPD* and *RMS*, are not widely used by stage highway agencies to monitor texture; therefore, the relationships derived here are preliminary and are used mainly to identify a possible proportionality of these parameters with friction. The correlation coefficients between friction and the texture parameters are shown in Table 8.

Table 8. Correlation coefficient between friction and texture parameters.

Variable	r
MPD	0.17
RMS	0.21
Rku	0.36
Rks	-0.58
TR	-0.51
# Observations	51

As presented, the *MPD* and the *RMS* have similar correlation with friction, but as indicated in the previous sections, the *RMS* is an indicator of the profile variability while the *MPD* is an indicator

26

of the mean peaks in a profile. Thus, the *MPD* is still regarded as more informative than the *RMS*, but both parameters should be reported to get a better insight of the overall pavement texture characteristics.

The *Rku* parameter has a positive correlation with friction and this correlation is stronger than the one observed with the *MPD* and *RMS*. This finding suggests the friction values are more affected by how large the peaks are with respect to the mean value (i.e., the severity of the peaks), which are represented by the *Rku*, rather than the peaks themselves. In the case of the *Rks*, a negative correlation exists with friction, because for all the sites, the *Rks* is negative which indicates the negative macrotexture prevails over the positive macrotexture, i.e., there are more voids than peaks. Thus, the results match intuition; friction increases when the size of the peaks increases, and friction reduces when the number of voids respect the number of peaks increase.

The *TR* shows a negative correlation with friction because the parameter decreases as the gradation becomes coarser (increases in D_{60} and *Cc*), as indicated in Figure 12. Recall that the *TR* is the ratio of the *MPD* to *RMS*, and thus it increases either because the *MPD* increases or because the profile elevation variability reduces. As indicated, the lowest *TR* correspond to the UTBWC surfaces, which might indicate that coarser gradations produce a more heterogeneous texture profile in which the *MPD* is close to the *RMS*, i.e., the variance is almost the same as the mean and the proportion of peaks is equivalent to the proportion of valleys. Conversely, finer gradations have a more homogeneous distribution because the *RMS* is smaller (low variation) than the *MPD* indicating there might be more peaks or more voids.
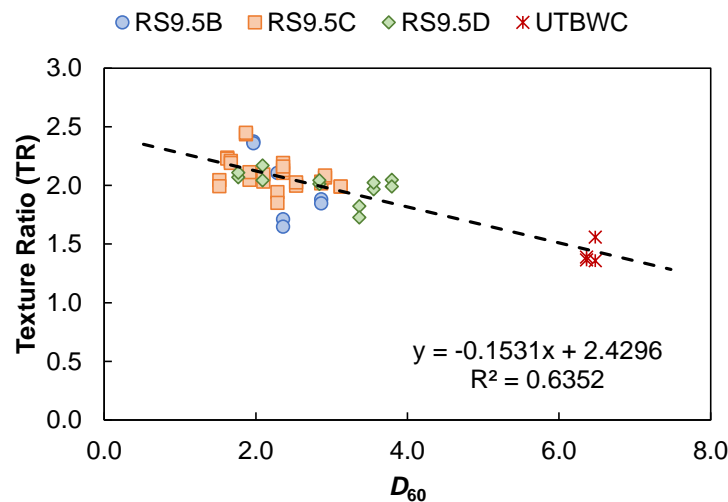
Figure 12. Variation of the *TR* as a function of gradation D_{60}.

Finally, each texture parameter was used as an independent variable in a regression model, one for each parameter, to predict friction to further evaluate relationships. The resulting models are presented in Figure 13. As indicated, the lowest R^2 is obtained when the predictor is the *MPD*. Also, both the *MPD* and the *RMS* can distinguish the texture characteristics of the UTBWC. The use of *Rks* and *TR* parameters to predict friction produces the highest R^2. Because the *TR* incorporates both the *MPD* and the *RMS*, this parameter is of greatest interest for incorporation in a future model to predict friction.
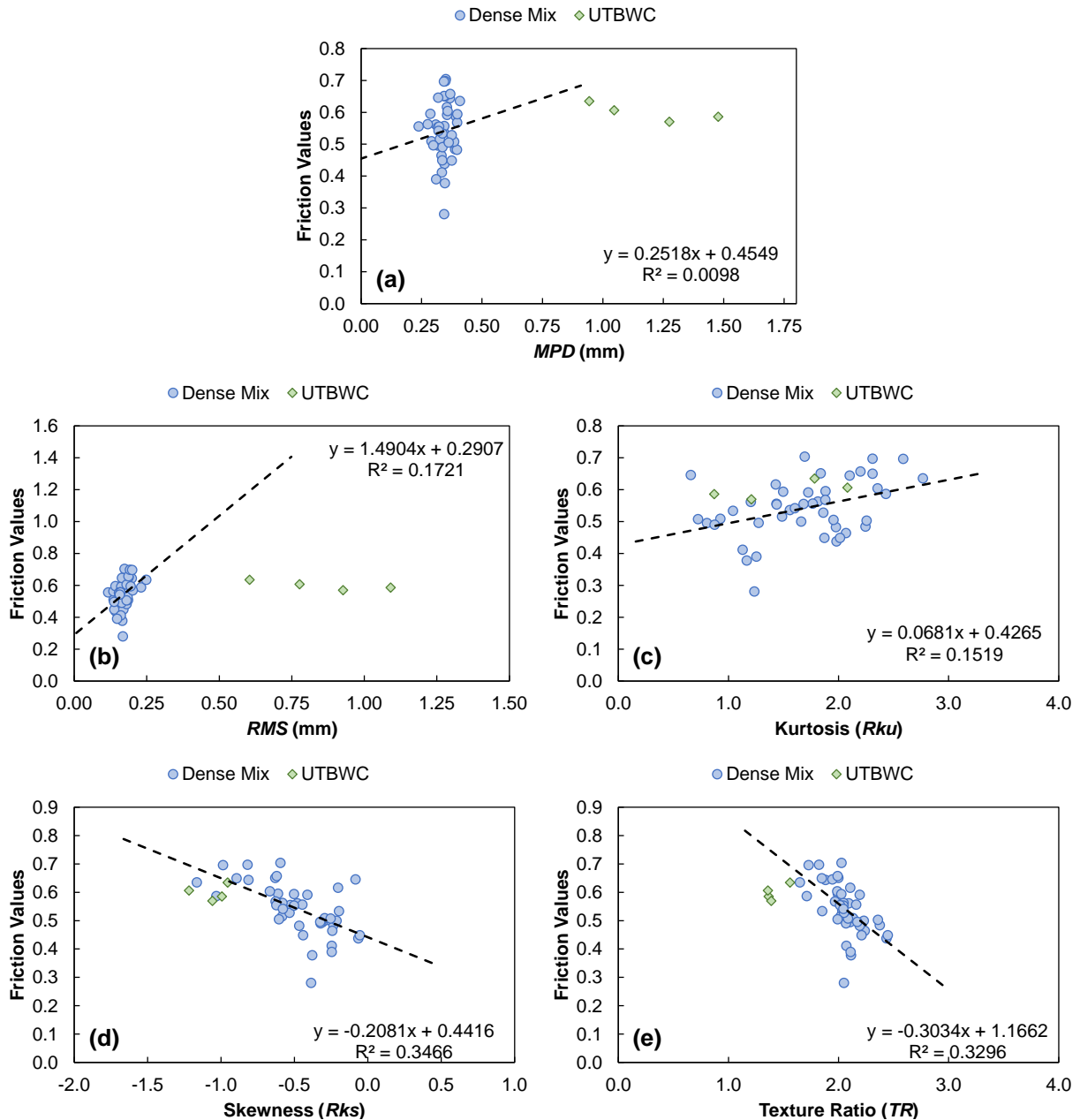
Figure 13. Regression model between friction and texture parameters: (a) *MPD***, (b)** *RMS***, (c)** *Rku***, (d)** *Rks***, and (e)** *TR***.**

3.3. Summary of Analysis

In this section, the effect of the mix volumetric properties in the early friction and texture have been analyzed. The primary takeaway findings are that predictive equations are capable of estimating the in-service friction/texture with varying degrees of accuracy. The highest predictive capabilities are obtained by measuring properties of field extracted cores of the roadways and suggest there is a potential for using field cores, such as the ones collected during construction quality control of the in-place density, to verify the friction and texture characteristics of the as-constructed surfaces. In the lab, a BPT and a custom laser, respectively quantified friction, and

texture. However, in theory, the methodology can be applied with other type of devices that measures friction and texture. The other equations developed from the measured data had less predictive power, but essentially showed that correlations with friction/texture exist between the asphalt content, the gradation parameters *Cc* and *Cu*, and P_{200}. The correlation between field friction and texture values was highest using the *Rku*, Rsk, and *TR* parameters. The *TR* parameter is of particular interest because it simultaneously incorporates two of the most accepted texture parameters in the US, i.e., *MPD* and *RMS*.

This page is intentionally blank

4. FRICTION AND TEXTURE EVOLUTION

4.1. Overview

In this section, the effects of pavement overlays on the friction and texture are presented and discussed. Recall that the friction and texture values for each site are summarized using the 2.5-percentile and 50-percentile, respectively (see Section 2). Based on the literature review included in the appendices of this document, there are two sources of variation in friction and texture values for a given pavement surface: a seasonal fluctuation associated to the weather effect and a variation induced by traffic. To isolate the effect of traffic, analysis must first be conducted to account for the seasonal effects and then measurements should be corrected to the same condition. Finally, the change in friction/texture over time due to time or traffic can be modeled.

Because the analysis presented in this section focuses on determining the trend in friction and texture with time after construction, only the sites that have at least three after construction measurements were evaluated. Accordingly, Table 9 presents the list of sites used to calibrate the seasonal variation and traffic effects models. As shown, four sites are RS9.5B, twelve are RS9.5C, four are RS9.5D, and two are UTBWC.

Table 9. Sites used in the seasonal effect analysis.

Surface	Site No.	Route Type	AADT[a]	Facility Type	Traffic in Design Lane[b]
RS9.5B	15	NC	1,400	Undivided	700
	16	NC	1,800	Undivided	900
	3	US	3,400	Undivided	1,700
	29	NC	11,000	Undivided	5,500
RS9.5C	8	NC	4,600	Undivided	2,300
	9	NC	6,300	Undivided	3,150
	2	Interstate	8,900	Divided	4,005
	23	Interstate	10,000	Divided	4,500
	28	NC	11,000	Divided	4,950
	17	US	12,000	Divided	5,400
	33	US	14,000	Divided	6,300
	1	Interstate	15,000	Divided	6,750
	14	US	17,000	Divided	7,650
	18	US	25,000	Divided	11,250
	11	NC	39,000	Divided	17,550
	19	US	47,000	Divided	21,150
RS9.5D	27	US	12,000	Divided	5,400
	12	US	17,000	Divided	7,650
	7	Interstate	53,000	Divided	23,850
	6	Interstate	65,000	Divided	29,250
UTBWC	5	Interstate	37,000	Divided	16,650
	4.1	Interstate	65,000	Divided	29,250

[a] Bidirectional Average Annual Daily Traffic (AADT).
[b] Daily traffic after including the directional and lane distribution factor.

Two main assumptions are made to model seasonal effects. The first is that the variation in the CL measurements is strictly weather related. The second assumption is that the RWP also experiences the same seasonal effect as the CL and thus the effect can be estimated based on the model developed to describe the seasonal variation in the CL measurements. The variables considered in the analysis of seasonal effects were the average temperature in the 7-days before the measurement and the number of cumulative dry-days at the location up to the day of the measurement. These variables were selected based on the work of Cenek et al. (*14*), and Jayawickrama and Thomas (*15*), who developed similar models for New Zealand and Texas, respectively. The weather information was acquired from the MERRA-2 weather dataset for the period of January 1, 2019, to April 30, 2021 (*16*). This dataset contains many different climatologic variables. However, for this research, two variables were of particular interest: the air temperature at 2 meters above the surface and the total daily precipitation. The information is reported with a spatial resolution of 0.5° by 0.625° for 128 separate coordinates across North Carolina. A map of North Carolina showing the different climate regions and the weather data grid is depicted in Figure 14.

To obtain the most accurate values of the temperature and precipitation at the tested sites, interpolation using the nearest four grids was conducted based on the inverse distance from the center point of the grid to the project site. Ultimately, the temperature profile was defined for each site and the monthly variation was obtained. The summary of these results is presented in Figure 15, where the sites are grouped by region. For each region, the mean, maximum and minimum temperature profile is identified. As shown, in Figure 15(d), all the regions exhibit their maximum temperatures in Month 7 (July), and the lowest records are observed in Months 1 and 12 (January and December, respectively).
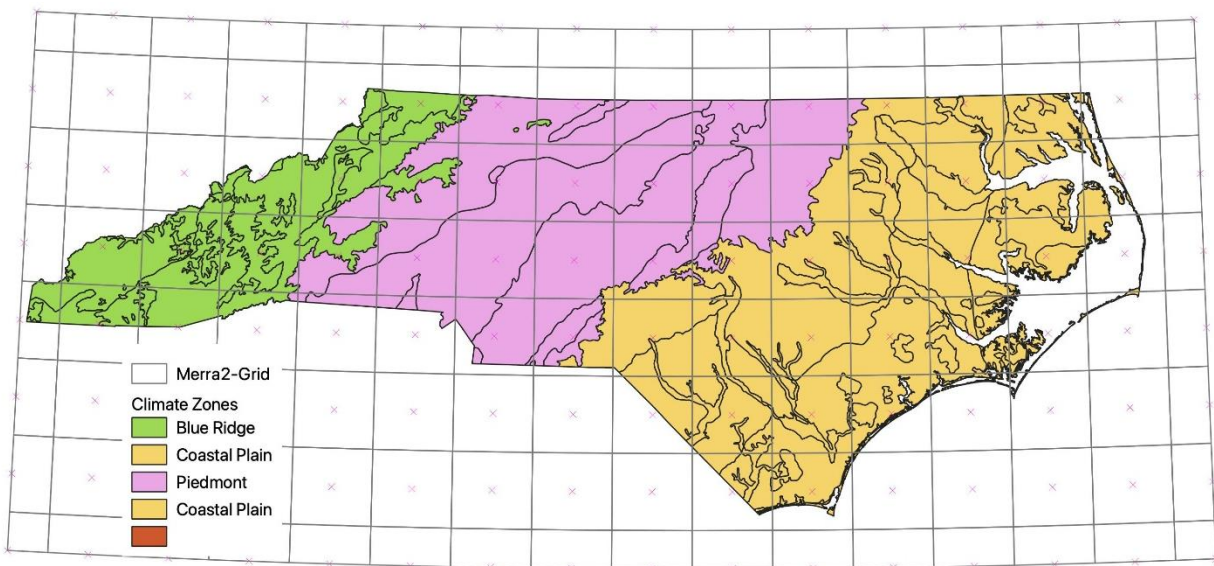
Figure 14. North Carolina climate zones and MERRA-2 information grid.

To estimate the cumulative number of dry-days prior to a measurement, the daily cumulative precipitation was first extracted and plotted. Then, a day was defined as 'dry' or 'wet' based on whether the amount of precipitation was less than 2.5 mm (0.1 inch) (dry) or more than 2.5 mm (wet). An example of this calculation is shown in Figure 16 for Site 7. The red line in Figure 16 (a) indicates the limit of 2.5 mm. In this example, the first rain event greater than 2.5 mm occurred on January 4 and the next one registered on January 12. Thus, there were a total of eight dry days

between them. Proceeding in this way it is possible to create the incremental number of dry days as a function of time shown in Figure 16 (b). Similar to the data presented in Figure 15 for temperature, the monthly variation in the average number of dry days is presented in Figure 17.
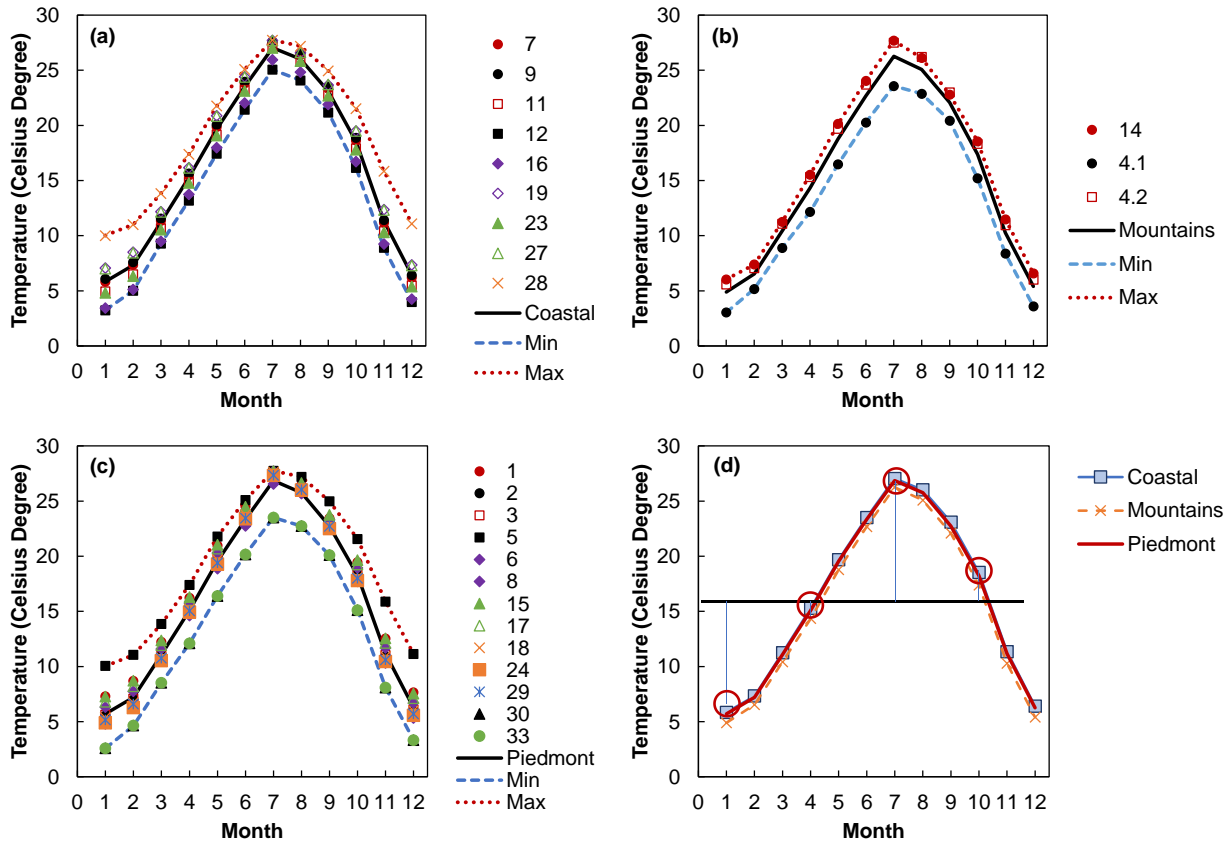
Figure 15. Monthly average temperature variation at each site located in the: (a) coastal region, (b) mountain region, (c) piedmont region, and (d) average per region.
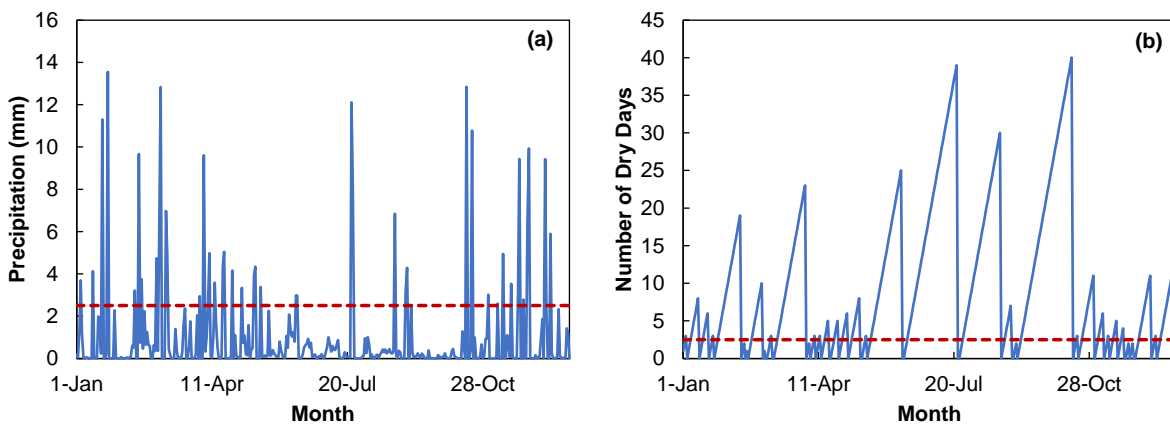
Figure 16. Calculation of the number of dry days for Site 7: (a) daily precipitation and (b) number of dry days.
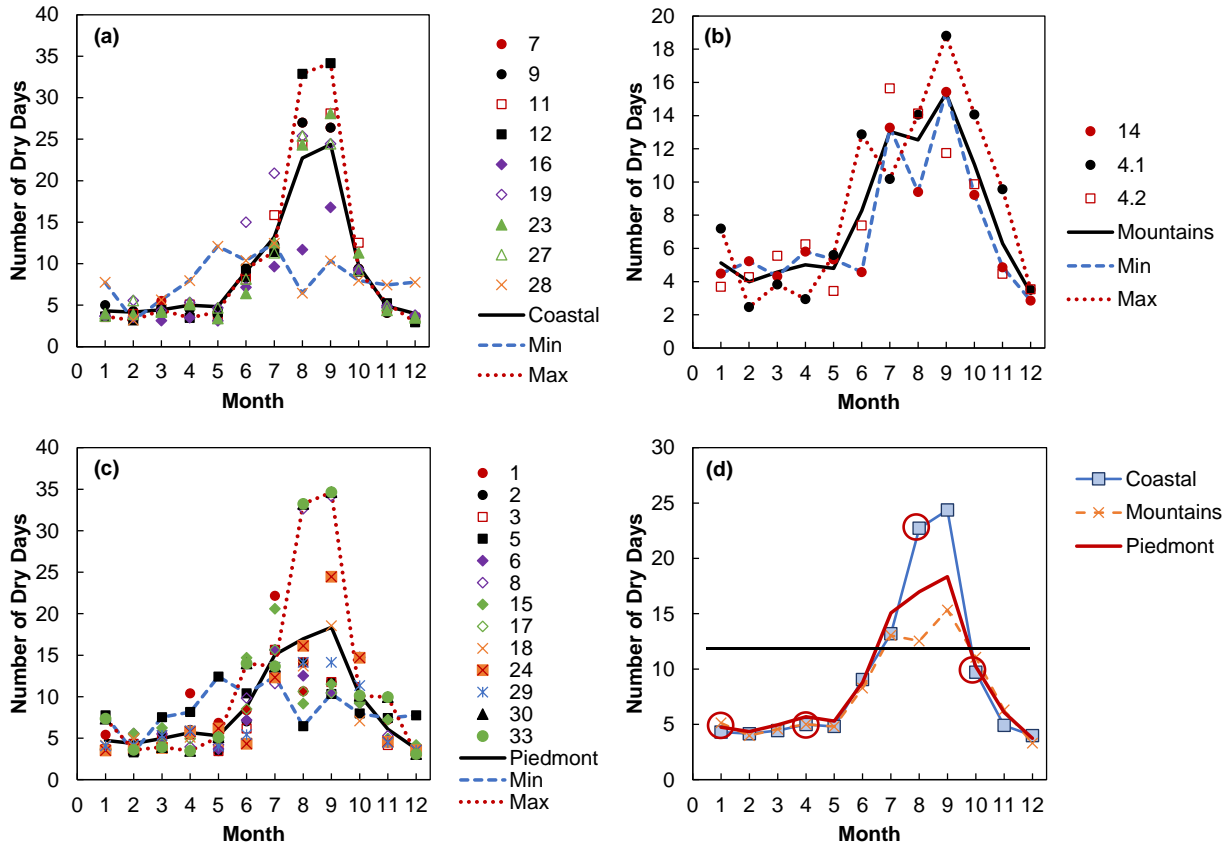
Figure 17. Number of dry days monthly variation in each site located in: (a) coastal region, (b) mountain region, (c) piedmont region, and (d) average per region.

Monitoring friction using a 3-month frequency yields a total of four measurements per year. According to the literature, the lowest friction values are expected during the high temperature months and during prolonged periods without rain. Based on the trend depicted in the figures above, the lowest friction is expected to occur around Month 7 and 8 while the greatest friction is expected to occur around January and December (barring weather events like freezing temperatures and rain). To capture the combined effects of both variables on the friction/texture, a measurement schedule like the one shown in Figure 15 (d) and Figure 17 (d) could be used (the red circles indicate the time to collect a measurement, i.e., January, April, July, and October). A more in-depth discussion of this issue is provided in Section 5.

4.2. Observed Variation in Friction and Texture after an Overlay

As indicated in Table 1, there are seven sites (8, 13, 19, 24, 29, 30, and 33) that received a pre-construction friction and texture measurement. After inspecting these observations, it was observed that the asphalt overlay induced two main effects in the friction values. In some sites, the friction increased after the overlay and in others the friction reduced. However, in the case of texture, all sites showed a reduction in *MPD*, except for Site 19 where an increase in *MPD* was observed. Figure 18 (Site 8) and Figure 19 (Site 33) provide examples of these trends. In these figures, parts (a) and (b) shows the friction variation in the RWP and CL, respectively, whereas parts (c) and (d) shows the *MPD* variation in the RWP and CL, respectively.
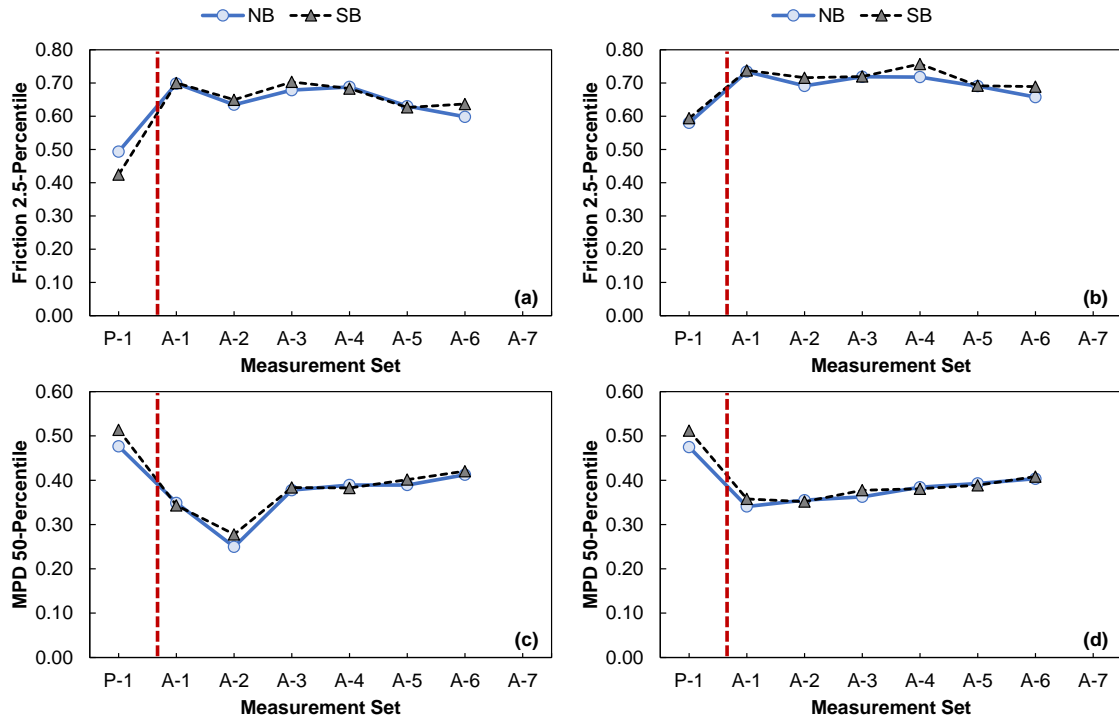
Figure 18. Effect of asphalt overlay in Site 8 for friction: (a) RWP and (b) CL, and for *MPD* (c) RWP and (d) CL.
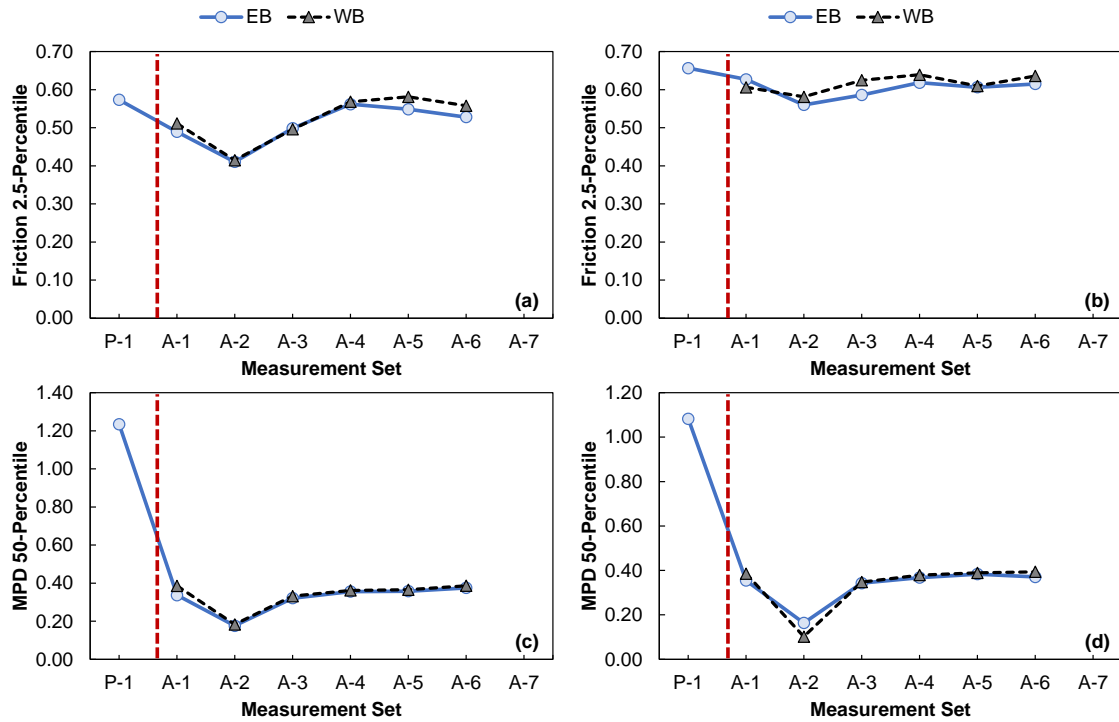
Figure 19. Effect of asphalt overlay in Site 33 for friction: (a) RWP and (b) CL, and for *MPD* (c) RWP and (d) CL.

Figure 18 shows that in the NB approach of Site 8, friction increased 41.5% and 26.5% in the RWP and CL, respectively, whereas in the SB approach friction increased 64.9% and 24.2% in the RWP and CL, respectively. An opposite trend was observed in Figure 19 for Site 33 in the EB approach, where friction reduced 14.6% and 4.5% in the RWP and CL, respectively (the WB approach was not tested in the pre-construction condition in Site 33). In the case of texture, a reduction of 26.8%, 28.2%, 33.2%, and 30.1% was observed in Site 8 in the NB-RWP, NB-CL, SB-RWP, and SB-CL, respectively. Conversely, Site 33 showed a reduction of 72.7% and 67.3% in the EB-RWP and EB-CL, respectively. A summary of the changes identified in each site is provided in Table 10. This table shows that across the sites, the amount of change registered in the RWP is, in general, higher than those observed in the CL. Also, this difference is often greater in the case of friction than texture.

Table 10. Friction and texture percent change caused by the asphalt overlay.

Site	Approach	Percent Change			
		Friction RWP	Friction CL	Texture RWP	Texture CL
8	NB	41.5	26.5	-26.8	-28.2
	SB	64.9	24.2	-33.2	-30.1
13	EB	-16.0	n.c.[a]	-53.6	-69.0
	WB	-19.0	n.c.	-52.9	-53.9
19	NB	12.5	-1.6	8.3	8.0
	SB	20.0	23.9	6.5	13.8
24	NB	-1.3	0.2	-57.2	-56.7
	SB	23.3	9.9	-60.7	-62.7
29	EB	-1.6	6.6	-66.4	-54.0
	WB	-17.9	1.2	-64.1	-48.3
30	NB	-16.1	-10.8	-63.5	-50.7
	SB	-3.1	-7.3	-49.7	-35.9
33	EB	-14.6	-4.5	-72.7	-67.3
	WB	n.c.	n.c.	n.c.	n.c.

[a] measurement not collected

4.3. Friction Modeling

4.3.1. Seasonal Variation

For this model, the friction 2.5-percentile reported in 0.1-mile increments was used. The first step of the analysis consisted of determining the mean value of the observations collected. To illustrate this process, the observations collected in Site 17 are used, because in this site a total of seven after construction observations were obtained. Figure 20 (a) and (b) show the measurements taken in the NB and SB, respectively. It is important to remember that these measurements were taken in the CL.

For each site, the overall mean friction value collected during the period of analysis was calculated. For example, in Site 17, the mean of the seven friction measurements collected in the NB and SB were 0.59 and 0.63, respectively. These mean values are identified with the red lines in Figure 20 (a) and (b); this mean was used as the basis for interpreting seasonal fluctuations as deviations from the mean.

The seasonal factor is defined as the ratio of the observed friction value to the friction mean. For example, in Figure 20 (c) the average friction of the 0.1-mile segments observed in the NB direction of Site 17 is represented by the blue dots, while the individual 0.1-mile observations are represented by the gray dots. For this section of the route, the average friction value in the first after construction measurement (November 2019) is 0.55 while the friction mean without adjustment for seasonal effects is equal to 0.59; therefore, the seasonal factor is equal to 0.55/0.59 = 0.93. Similarly, the friction seasonal factors for the remaining observations are 1.00, 0.95, 1.06, 1.06, 1.06, and 0.94. A similar plot is obtained for the SB direction, as presented in Figure 20 (d).
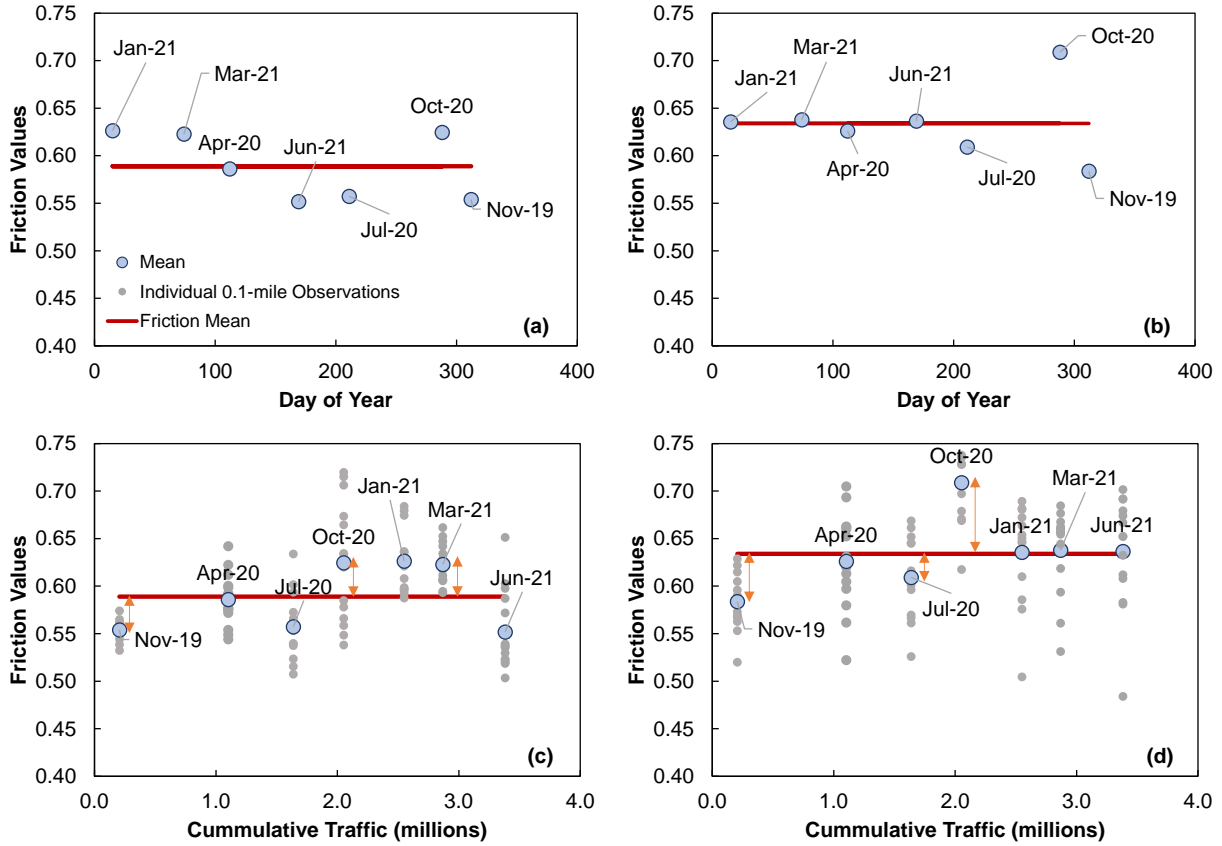
Figure 20. Example of the friction seasonal factor calculation for Site 17: friction mean in the (a) NB and (b) SB; and friction seasonal factor in the (c) NB and (d) SB.

This procedure was applied in all the sites, then the sites were grouped by surface type as indicated in Table 9. The proposed model is shown in Equation (11). The form of this model was defined based on the work of Cenek et al. (*14*), and Jayawickrama and Thomas (*15*). As mentioned, this model was calibrated using the friction values measured in the CL. Because the site temperature and precipitation are inputs of Equation (11) the most recent information available in the MERRA-2 database was used to obtain the most up to date data.

$$SF = \frac{Friction_{Sesonal}}{Friction_{Mean}} = a_0 + a_1 \times \sin\left(\frac{2\pi \times DoY}{365} + a_2\right) + a_3 \times Temp + a_4 \times DD \qquad (11)$$

where;

SF = friction seasonal factor,

Friction$_{Seasonal}$ =	friction recorded at any given day of the year,
Friction$_{Mean}$ =	mean value of the friction without seasonal effect,
a$_0$ to *a$_4$* =	coefficients to be calibrated,
DoY =	Julian calendar days,
Temp =	average 7-day mean temperature, Celsius degrees, and
DD =	number of dry days.

The models were calibrated by minimizing the sum of square errors using Solver in Excel. The coefficients of the model that were obtained after the optimization process are shown in Table 11. During the calibration process, the datasets for each surface type have been divided as follows:

- RS9.5B sites: Sites15 and 16 used for calibration; Sites 3 and 29 used for verification.
- RS9.5C sites: Sites 9, 14, 17, 18, 19, 23, 28, 33 used for calibration; Sites 1, 2, 8, and 11 user for verification.
- RS9.5D sites: Sites 6, 7, and 12 used for calibration; Sites 27 and 39 used for verification.
- UTBWC sites: Sites 4.1 and 5 used for calibration.

Table 11. Coefficients of the friction seasonal model.

Surface Type	*a$_0$*	*a$_1$*	*a$_2$*	*a$_3$*	*a$_4$*
RS9.5B	1.0742	-0.0292	1.5182	-0.0053	-0.0010
RS9.5C	1.0930	-0.0456	1.3219	-0.0058	-0.0033
RS9.5D	1.0128	-0.0453	1.2005	-0.0015	-0.0009
UTBWC	0.8247	0.8575	0.9816	0.0059	0.0442

Also, an additional verification step was included in some of the sites by not including the friction observations collected during the months of June/July of 2021 in the calibration of the seasonal effects model, but using these data to verify the model accuracy. The verification process consisted of predicting the seasonal factor, and then using the friction mean without seasonality to determine the actual friction value as $Friction_{Mean} \times SF$. Afterwards, the observed friction was plotted against the predicted value to evaluate the model accuracy. The R^2 for both the calibration and verification set with respect the line of equality was calculated.

Figure 21 shows the verification plot for the four friction seasonal models, one per surface type; as indicated, the models have a good prediction capability, except for Site 29, which was used for verification in the model derived for the RS9.5B sites as shown in Figure 21 (a). The model fails to predict the observations in April and June of 2021 in Site 29. However, the MERRA-2 database was only available up to April 29 of 2021, and therefore, the previous year temperature and precipitation were used to make the predictions. It is possible that the temperature and precipitation on the day the measurement was collected was different from the previous year. Finally, individual verification plots were created for each site and are included in Appendix C.
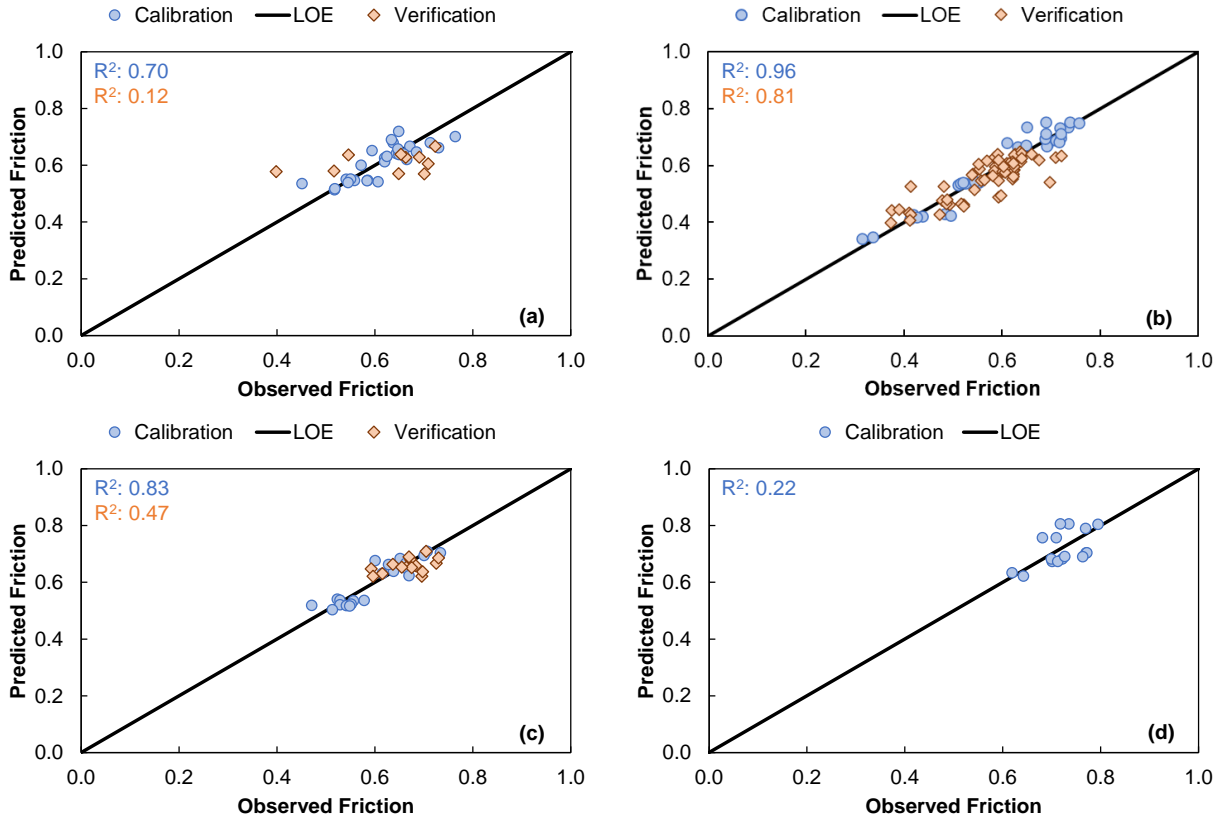
Figure 21. Friction seasonal model verification plot for sites with mix: (a) RS9.5B, (b) RS9.5C, (c) RS9.5D, and (d) UTBWC.

4.3.2. Traffic Effect

Only the RWP measurements were used to evaluate how traffic affects pavement friction. The process of calibration first involved correcting the measured data for any seasonal effects by using Equation (12) in combination with Equation (11).

$$Friction_{corrected,i} = \frac{Friction_i}{SF_i} \tag{12}$$

An example of the outcomes of this correction is presented in Figure 22, where the average friction values for Site 4.1 are represented by the black 'x' point series and the corrected values by red squares. In this figure, the measurements collected in both traffic flow directions, EB and WB, are plotted together. The seasonal factor on each measurement date is first predicted using Equation (11) and then the correction of the measured data is made using Equation (12). Figure 22 also shows the measured and corrected values in a tabular form as well as the percent difference between the corrected and uncorrected values. As seen, for this site the seasonal correction produces a percent difference less than 12%.
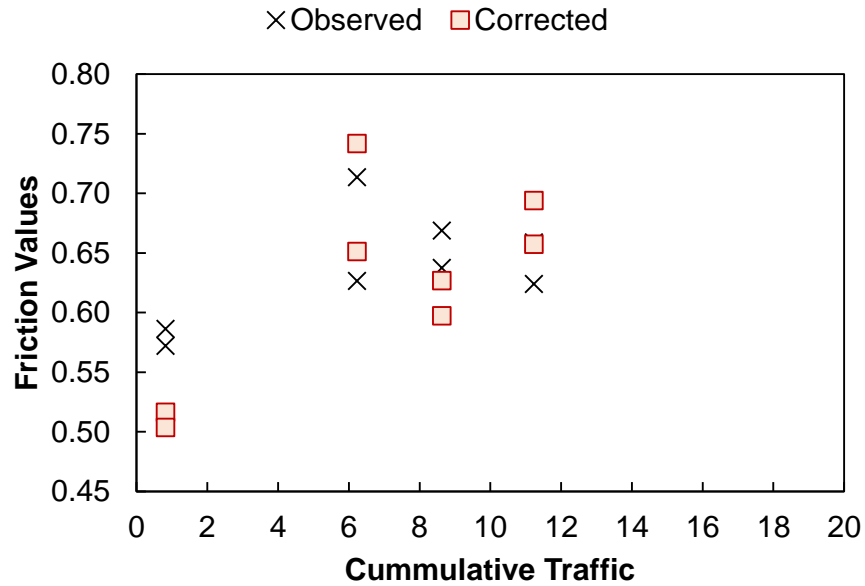
| Date | Approach | Cumulative Mix Traffic (Millions) | Friction | | %Difference |
			F_i	$F_{corrected}$	
10/29/19	EB	0.82	0.586	0.516	-11.97
5/1/20	EB	6.23	0.714	0.742	3.95
7/22/20	EB	8.63	0.669	0.627	-6.31
10/19/20	EB	11.23	0.659	0.694	5.32
10/29/19	WB	0.82	0.572	0.503	-11.97
5/1/20	WB	6.23	0.626	0.651	3.95
7/22/20	WB	8.63	0.637	0.597	-6.31
10/19/20	WB	11.23	0.624	0.657	5.32

Figure 22. Friction values correction by removing the seasonal effect, example with Site 4.1.

After removing the seasonal effects from each site and plotting the resultant friction with respect to both time and traffic levels, sites were found to show one of three distinct trends, which are shown in Figure 23. In all trends, there is first initial friction, F_{ini}, which changes over time. Sites exhibiting Trend 1 show a consistent increase in friction with time at a constant rate, m_1. Based on the literature review, friction increases because the traffic repetitions help to remove the binder from the surface, thereby exposing the underlying aggregate and causing an increase in the friction microtexture component (*17–20*). Sites that exhibited Trend 2 show an increase in friction from the F_{ini} at a rate of m_1 until they reach a maximum value F_{max}. The amount of traffic required to reach F_{max} is labeled as T_1. After the maximum value is reached, friction starts to decrease at a rate of m_2. This trend is observed because once the binder has been removed from the aggregates, the traffic action begins to polish the aggregates and therefore reduces the available microtexture friction.

The measurements taken during the current project did not directly evaluate microtexture, rather the effects of microtexture are indirectly observed through changes in the friction values. These changes are not easy to interpret and understanding them at a fundamental level is beyond the scope of this project. The microtexture depends on the mineralogy and shape of the aggregates; it is important because at this scale there exist molecular interactions between the aggregate particles

and the tire rubber that results in adhesion. According to the literature, the microtexture friction component is present at any vehicle speed but gains more relevance at lower speeds. The most popular speed used to capture the microtexture friction component is around 20 km/h (13 mph). In this project, most measurements were taken at 60 mph and some were taken at 40 mph. Although the microtexture component was captured in the friction measurements collected at these speeds, this component was not isolated, i.e., the observed friction values incorporate both the adhesion (microtexture) and hysteresis (macrotexture) components.

In parallel with the traffic polishing effect, the whole asphalt layer might experience a densification caused by the traffic repetitions. If this densification occurs, then the surface macrotexture will reduce and thereby reduce frictional resistance. Trend 2 was the most common trend observed in the sites. Finally, sites that exhibited Trend 3 start from F_{ini}, but immediately begin to show a reduction in friction (assumed to be a linear reduction at a constant rate of m_2). This trend might occur if the densification process described above prevails or is more significant than the aggregates exposure caused by the binder wearing. It is noted that this trend was only observed in three of the sites.
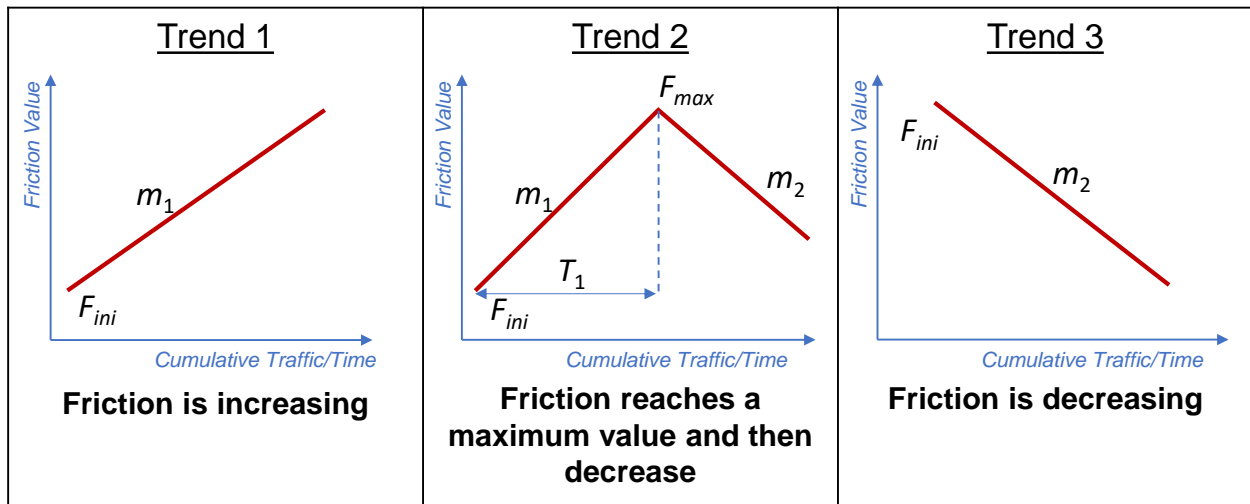
Figure 23. Trends observed in the database.

Table 12 summarizes the type of trend that was observed for each site, the F_{ini}, and the m_1 and m_2 values (as applicable). Mixture compositional factors, including the Pb, Cc, and P_{200} values, have also been included in Table 12 so that the effect of composition on the observed trends can be explored. Initially, all sites have were plotted together to identify the general effect of the mixture compositional factors on F_{ini} and m_1, as shown in Figure 24 and Figure 25. As shown in these figures there are two sites that stand out from the rest, Sites 4.1 and 11, which have an UTBWC and RS9.5B surface layer, respectively. Both sites were not included in the regression analysis. At this moment there is not a clear explanation for why Site 11 has the lowest initial friction, an aspect that was not evaluated in this research is the aggregate polishing resistance. It is possible that the aggregate source used in this mix might have low polishing resistance. More research is needed to evaluate the effect of the aggregate characteristic on the initial friction values.

- Based on Figure 24, the initial friction reduces when the Pb and the P_{200} fraction increases, while the initial friction increases when the coefficient of curvature increases. This finding match what it was reported in Section 3.

- Similarly, Figure 25 indicates that the rate at which friction increases after construction, represented by the parameter m_1, is weakly correlated with the mixture compositional factors; however, the regression models suggest that higher m_1 values are obtained when the binder content and the P_{200} fraction increases; whereas m_1 reduces when Cc increases, though this is the regression model with the lowest R^2.
- Finally, to identify if there is a distinct effect of the mixture compositional factor in F_{ini} and m_1 by mix type, Figure 26 and Figure 27 are shown. Because of the limited sample size is not possible to make a statistically significant inference; however, except for RS9.5B, in general the trend described above for all the sites applies to each individual mix type category.

Table 12. Observed trend in each of the sites.

Site No.	Route Type	Surface Type	Traffic	*Pb*	*Cc*	*P*$_{200}$	Trend	*F*$_{ini}$	*m*$_1$	*m*$_2$
16	NC	RS9.5B	900	6.80	0.66	7.00	1	0.59	0.05	-
15	NC	RS9.5B	700	6.20	0.61	6.90	2	0.56	0.12	-
3	US	RS9.5B	1,700	6.30	1.12	5.90	2	0.61	0.34	-
29	NC	RS9.5B	5,500	6.30	0.75	7.00	2	0.61	0.04	-
9	NC	RS9.5C	3,150	6.40	0.97	6.70	1	0.44	0.05	-
2	Interstate	RS9.5C	4,005	6.30	0.62	7.50	1	0.47	0.03	-
23	Interstate	RS9.5C	4,500	6.00	0.87	7.00	1	0.56	0.03	-
28	NC	RS9.5C	4,950	6.60	0.82	7.80	1	0.35	0.15	-
1	Interstate	RS9.5C	6,750	6.40	0.53	6.30	1	0.50	0.03	-
14	US	RS9.5C	7,650	6.20	0.60	7.30	1	0.47	0.02	-
11	NC	RS9.5C	17,550	6.00	0.66	7.20	1	0.21	0.05	-
17	US	RS9.5C	5,400	5.70	0.49	5.90	2	0.52	0.04	-
33	US	RS9.5C	6,300	5.60	0.62	6.70	2	0.47	0.07	-
18	US	RS9.5C	11,250	5.70	0.60	6.10	2	0.52	0.03	-
19	US	RS9.5C	21,150	6.00	0.76	7.20	2	0.47	0.02	-
8	NC	RS9.5C	2,300	5.70	1.25	5.80	3	0.71	-	-0.070
27	US	RS9.5D	5,400	5.50	1.10	6.40	1	0.59	0.02	-
7	Interstate	RS9.5D	23,850	5.70	0.76	6.50	2	0.50	0.02	-
6	Interstate	RS9.5D	29,250	5.60	0.80	5.80	2	0.58	0.01	-
12	US	RS9.5D	7,650	5.40	0.73	6.20	3	0.67	-	-0.008
4.1	Interstate	UTBWC	29,250	5.20	5.95	4.10	2	0.48	0.03	-
5	Interstate	UTBWC	16,650	5.50	1.99	3.50	3	0.72	-	-0.003
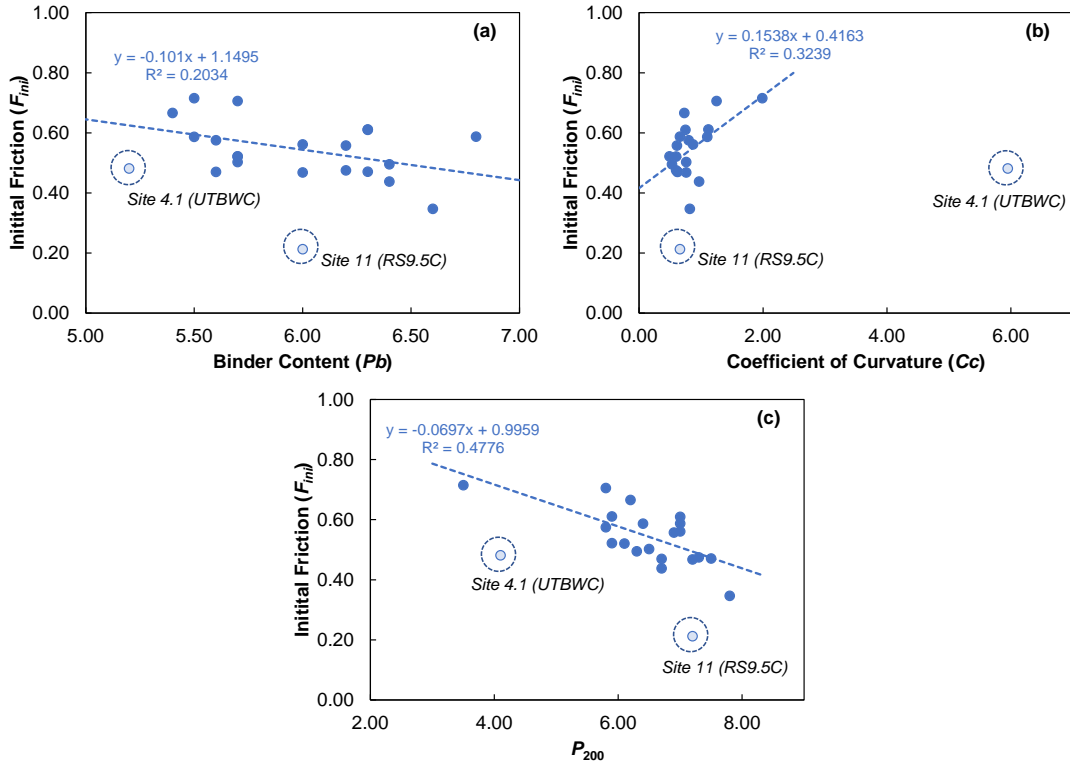
Figure 24. Effect of mix volumetrics in the initial friction (F_{ini}): (a) Pb, (b) Cc, and (c) P_{200}.
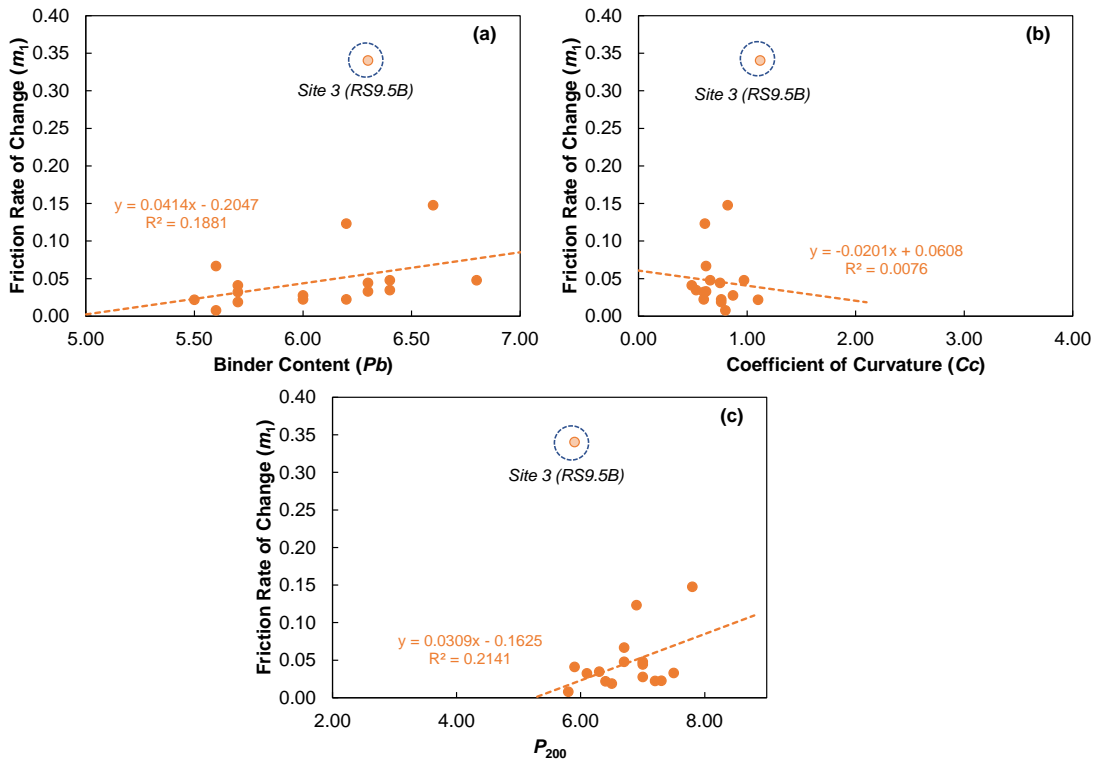
Figure 25. Effect of mix volumetrics in the friction rate of change (m_1): (a) Pb, (b) Cc, and (c) P_{200}.
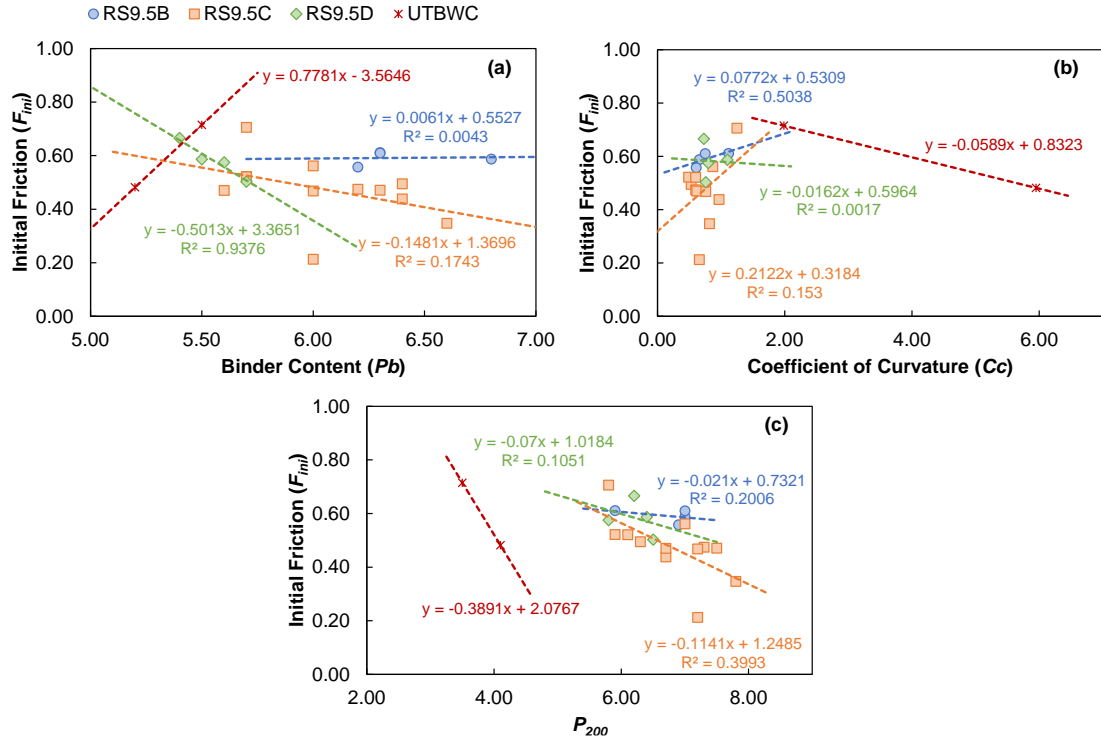
Figure 26. Effect of mix volumetrics in the initial friction (F_{ini}) segregated by mix type for: (a) Pb, (b) Cc, and (c) P_{200}.
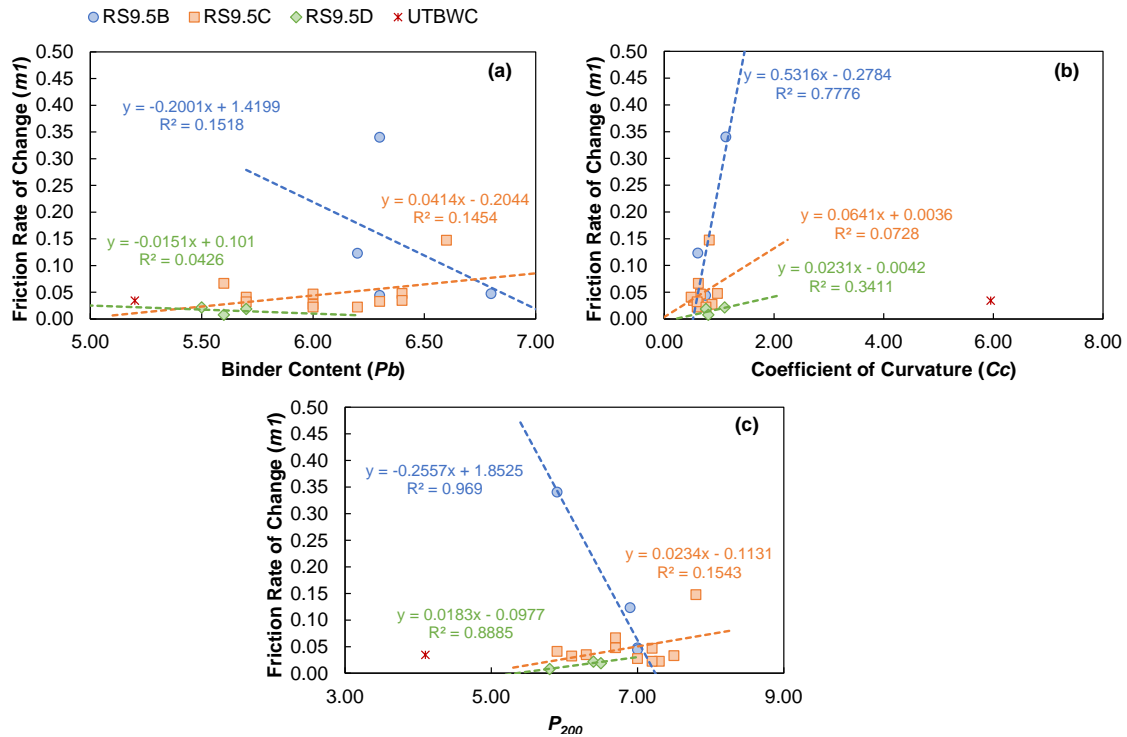
Figure 27. Effect of mix volumetrics in the initial rate of change (m_1) segregated by mix type for: (a) Pb, (b) Cc, and (c) P_{200}.

Table 13 provides some additional information for those sites exhibiting Trend 2. As indicated in Table 13, higher traffic intensity lowers the number of months to reach the maximum friction. The data suggests it requires between 5.5 to 18 months to reach the maximum friction value and the traffic required to reach the maximum friction was in the range of 0.3 to 15 million repetitions. The rate of decrease in friction after the point of maximum friction m_2, was calculated only when the site had at least two observations after F_{max}. As shown in Table 13, only two sites meet this criterion, Sites 7 and 4.1. Also included in Table 13 are the percent increment from F_{ini} to F_{max}.

Table 13. Additional information for sites with Trend 2.

Site No.	Route Type	Surface Type	F_{ini}	m_1	T_1[a]	t_1[b]	F_{max}	% Increment	m_2
15	NC	RS9.5B	0.56	0.12	0.22	10.30	0.57	5.0	-
3	US	RS9.5B	0.61	0.34	0.33	6.57	0.72	18.7	-
29	NC	RS9.5B	0.61	0.04	0.90	5.43	0.62	6.6	-
17	US	RS9.5C	0.52	0.04	2.87	17.70	0.61	19.4	-
33	US	RS9.5C	0.47	0.07	1.76	9.33	0.58	25.8	-
18	US	RS9.5C	0.52	0.03	3.48	10.30	0.67	22.7	-
19	US	RS9.5C	0.47	0.02	4.91	7.73	0.57	25.0	-
7	Interstate	RS9.5D	0.50	0.02	8.59	12.00	0.71	32.1	-0.03
6	Interstate	RS9.5D	0.58	0.01	14.51	16.53	0.69	25.8	-
4.1	Interstate	UTBWC	0.48	0.03	6.23	7.10	0.66	44.6	-0.01

[a] cumulative traffic in millions for maximum friction; [b] number of months for maximum friction

It is believed that the sites exhibiting Trend 1 will eventually show behavior like that in Trend 2, i.e., sites in Trend 1 will eventually reach a maximum value (F_{max}) after which friction will start decaying. Thus, to estimate how long the pavements in Trend 1 will take to reach F_{max}, a model was developed to predict the expected percentage friction increase from the initial value after construction to maximum value, termed the *%Increment* herein, and defined in Equation (13). There are ten sites that showed Trend 2, and the correlation coefficient between the friction percent increment and all the parameters summarized in Table 12 and Table 13 was calculated. It was found that the highest predictability of the friction *%Increment* occurred when the average daily traffic and the initial friction; hence, these variables were used as predictors as presented in Equation (14).

$$\% Increment = \frac{F_{max} - F_{ini}}{F_{ini}} \times 100 \tag{13}$$

$$\% Increment = 11.3 + 5.53 \times Log(ADT) - 72.3 \times F_{ini} \tag{14}$$

Equation (14) has an adjusted R^2 of 0.59, and all the parameters were significant at a 95% confidence level. The comparison between observed and predicted values is included in Figure 28. Using this model, it was possible to estimate the friction percent increment of the nine sites with Trend 1 (see Table 12), afterwards the expected maximum friction, F_{max}, the cumulative traffic for F_{max}, T_1, and the time to reach F_{max}, t_1, were approximated as well. These calculation results are presented in Table 14.

As summarized in Table 14, the model of Equation (14) produces an erroneous prediction of the friction *%Increment* for Site 11 and 28. The predicted *%Increment* is 50.0% and 33.3%, respectively, based on these values the traffic needed to reach this increment is 2.27 and 0.78

million repetitions. However, when the last measurement was collected, the cumulative traffic was already 5.60 and 1.21 million repetitions for Site 11 and 28, respectively. This underprediction occurred because both sites have one of the lowest initial friction values of 0.21 and 0.35, respectively, and these values are outside the range of values used to calibrate the model as presented in Table 13. Nevertheless, the model properly estimates the *%Increment* for the remaining seven sites, based on these predictions the traffic required the reach the maximum friction ranged between 0.79 to 5.56 million repetitions. On the other hand, the time to reach the maximum friction varied from 17 months to up to 29.3 months. The last column of Table 14 shows the difference between the number of months required to reach the maximum friction, t_1, and the number of months elapsed since construction until the last measurement collected, t. Based on the differences in these times, the additional time required to reach the maximum friction for those sites exhibiting Trend 1 is estimated to fall between 8 to 19 months.

Table 14. Prediction of F_{max} and T_1 for those sites that showed Trend 1.

Site No.	Surface Type	Observed						Predicted			
		F_{ini}	ADT	m_1	T	t	%Inc.	F_{max}	T_1[a]	t_1[b]	$t_1 - t$
16	RS9.5B	0.59	900	0.05	0.37	13.8	6.5	0.63	0.79	29.34	15.51
9	RS9.5C	0.44	3,150	0.05	1.50	15.9	24.2	0.54	2.21	23.37	7.50
2	RS9.5C	0.47	4,005	0.03	1.05	8.7	23.1	0.58	3.30	27.45	18.75
23	RS9.5C	0.56	4,500	0.03	2.22	16.5	17.2	0.66	3.50	25.92	9.45
28	RS9.5C	0.35	4,950	0.15	1.21	8.2	33.3	0.46	0.78	5.26	-2.91
1	RS9.5C	0.50	6,750	0.03	1.76	8.7	24.3	0.62	3.45	17.05	8.35
14	RS9.5C	0.47	7,650	0.02	3.71	16.2	26.4	0.60	5.56	24.25	8.08
11	RS9.5C	0.21	17,550	0.05	5.60	10.6	50.0	0.32	2.27	4.30	-6.33
27	RS9.5D	0.59	5,400	0.02	1.25	7.7	16.4	0.68	4.40	27.18	19.44

T: cumulative traffic until last measurement collected
t: time elapsed since construction until the last measurement collected, in months
T_1: cumulative traffic required to reach maximum friction
t_1: time required to reach maximum friction, in months

Finally, using the information compiled in Table 13 and Table 14, as well as the predictions made with Equation (14), it is possible to plot the variation of the *%Increment* as a function of the different volumetric properties as shown in Figure 29. Based on this figure one can conclude the following:

- The lowest percent increment was observed in the RS9.5B mixes.
- The *Cc* has a minor effect on the *%Increment*.
- A higher *Pb* results in a lower *%Increment*.
- A higher P_{200} results in a lower *%Increment*.
- It seems the variable that affects the most the *%Increment* is the binder content, the model that uses *Pb* as the predictor has the highest R^2.
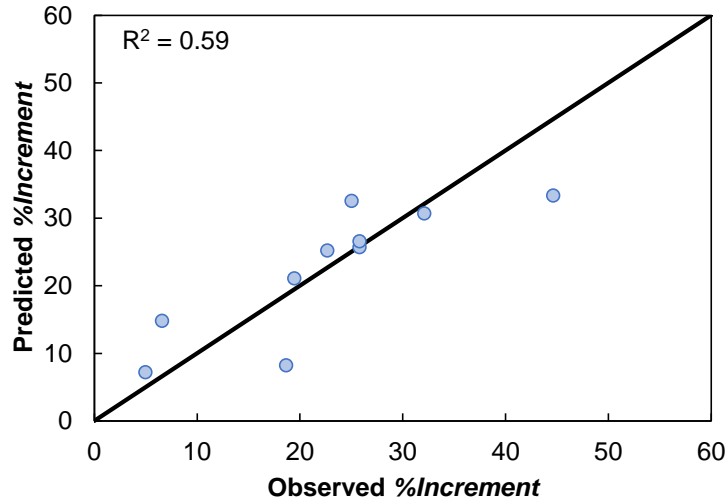
Figure 28. Prediction checks of the friction *%Increment* model.
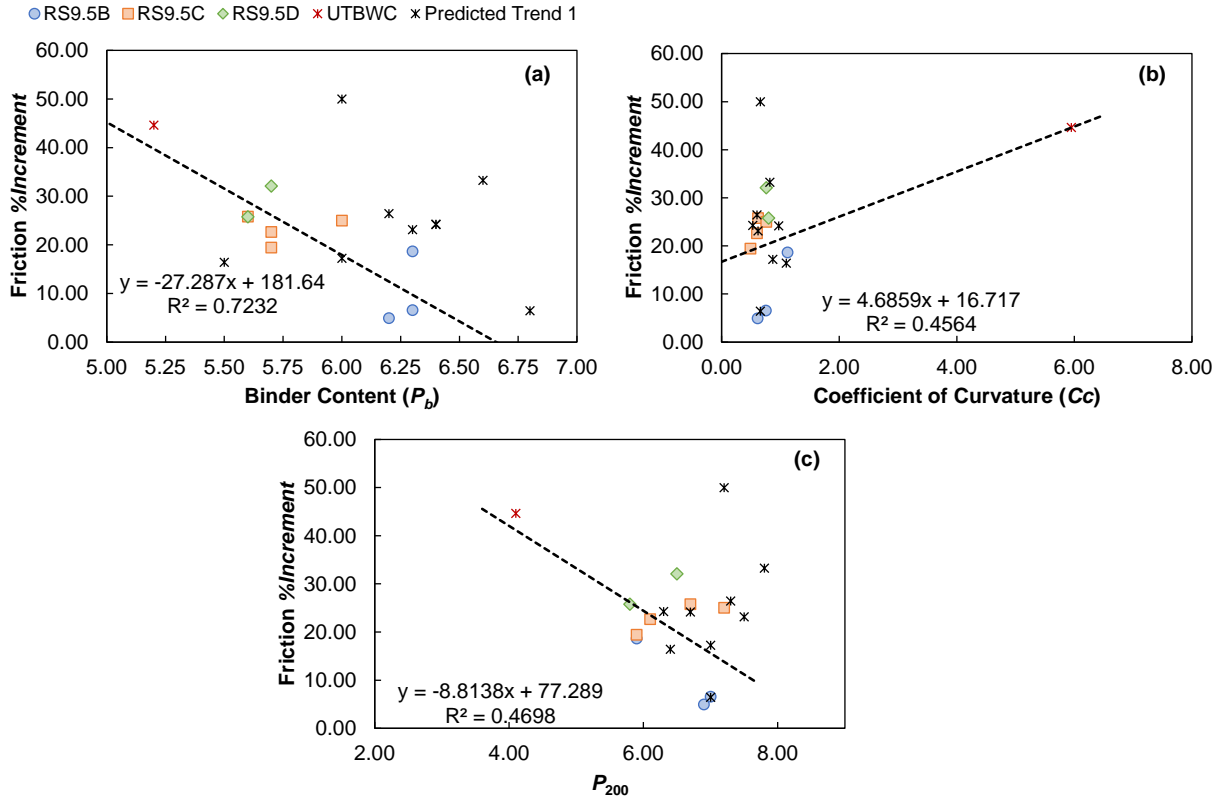
Figure 29. Effect of mix volumetrics in friction *%Increment*: (a) *Pb*, (b) *Cc*, and (c) *P₂₀₀*.

4.4. Macrotexture Modeling

In the case of texture, the measurements collected in the CL and RWP were plotted as a function of the time elapsed since the overlay. In this analysis, the representative value reported in 0.1-mile increments, i.e., the *MPD* 50-percentile, was used. An example of these plots is presented in Figure 30 using data from Site 7. Figure 30 (a) and (b) shows the variation of the *MPD* values collected

47

in the CL of the NB and SB, respectively; while Figure 30 (c) and (d) show the variation of the *MPD* values observed in the RWP of the NB and SB, respectively.
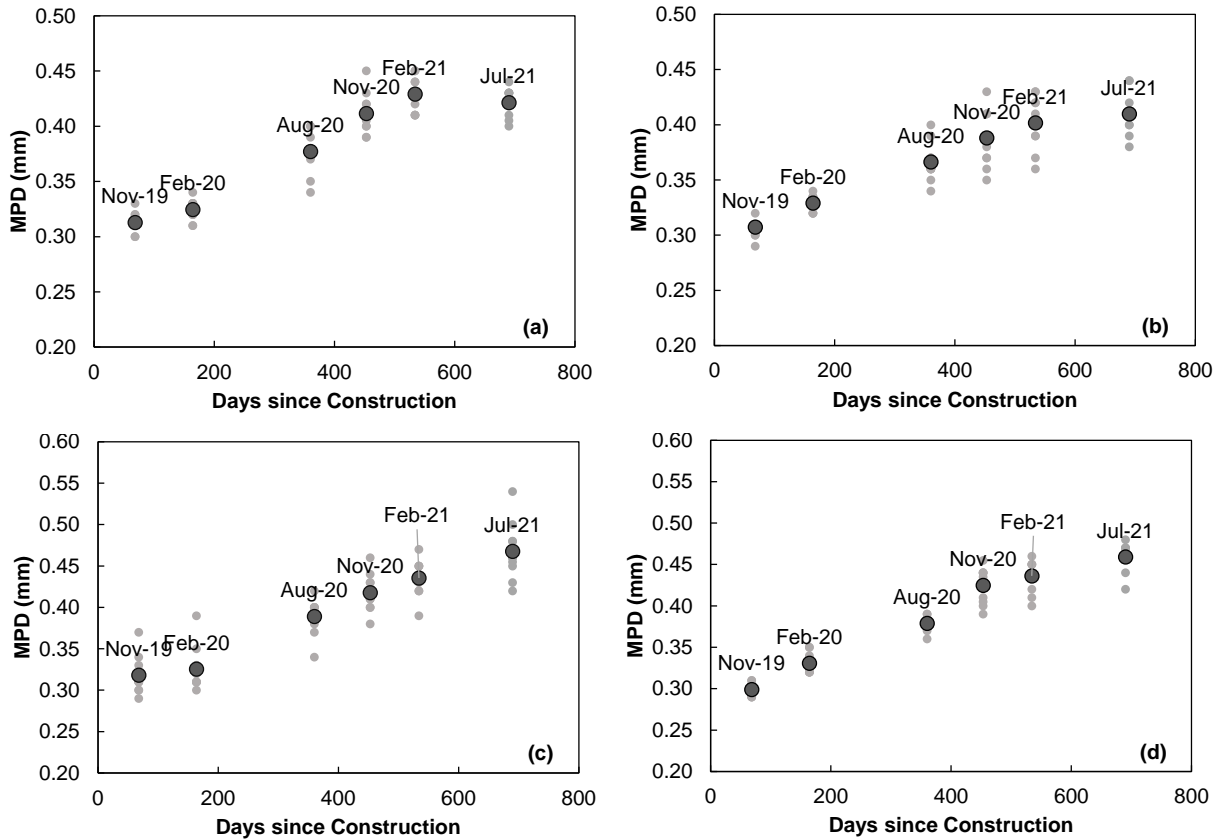
Figure 30. *MPD* **in Site 7 for measurements collected in the: (a) CL-NB and (b) CL-SB; (c) RWP-NB and (d) RWP-SB.**

At Site 7, it was observed that the CL and RWP observations followed a similar pattern of an increase in macrotexture with time following a power law. This finding suggests neither the texture CL nor the RWP seem to have seasonal fluctuations in macrotexture. After inspecting a similar set of plots for each site, the same conclusion was reached; as a consequence, it was decided that the team would omit the seasonal model for texture. Thus, the temporal variation was studied as follows:

- First, the CL observations were used to calibrate the model shown in Equation (15). The observations collected in the different traffic directions were used together to calibrate this model.
- Second, once calibrated, the resulting model was used to predict the texture values in the RWP, letting the RWP serve as a verification of the hypothesis that there is no a traffic effect in the texture variation and time can be used as the independent variable to model texture evolution.

$$MPD = a + b \times (t)^c \qquad (15)$$

where;

t	=	time since construction, in days,							
a	=	parameter of the model representing the initial *MPD* in mm, and							
b, c	=	parameters of the model representing the *MPD* rate of change.							

The coefficients of the model described in Equation (15) are summarized in Table 15. The effect of the mix volumetric factors – Pb, Cc, and P_{200} – on the texture coefficients is shown in Figure 31 to Figure 33. As shown in these figures, the mixture composition factors do not seem to correlate with the model parameters. It seems though that the coefficient of curvature relates with the initial *MPD*, parameter a of the model, because as shown in Figure 31 (b) if one fits a linear model using the information of all the sites together there is a strong linear trend; however, this trend is induced mainly by the UTBWC sites orange dots in Figure 31 (b).

Table 15. Summary of the parameters of the texture model.

Mix Type	Site No.	Route Type	Traffic	a	$b \times 10^{-6}$	c	Pb	Cc	P_{200}	Region
RS9.5B	15	NC	700	0.281	0.448	1.915	6.2	0.61	6.9	Piedmont
RS9.5B	16	NC	900	0.254	1,577	0.679	6.8	0.66	7.0	Coastal
RS9.5B	3	US	1,700	0.365	19	1.373	6.3	1.12	5.9	Piedmont
RS9.5B	29	NC	5,500	0.235	120,372	0.082	6.3	0.75	7.0	Piedmont
RS9.5C	8	NC	2,300	0.343	159	0.982	5.7	1.25	5.8	Piedmont
RS9.5C	9	NC	3,150	0.306	2,201	0.634	6.4	0.97	6.7	Coastal
RS9.5C	2	Interstate	4,005	0.318	13	1.547	6.3	0.62	7.5	Piedmont
RS9.5C	23	Interstate	4,500	0.300	12,332	0.413	6.0	0.87	7.0	Coastal
RS9.5C	28	NC	4,950	0.270	3,251	0.649	6.6	0.82	7.8	Coastal
RS9.5C	17	US	5,400	0.195	42,615	0.242	5.7	0.49	5.9	Piedmont
RS9.5C	33	US	6,300	0.202	51,116	0.222	5.6	0.62	6.7	Piedmont
RS9.5C	1	Interstate	6,750	0.290	0.001	3.177	6.4	0.53	6.3	Piedmont
RS9.5C	14	US	7,650	0.322	40,432	0.136	6.2	0.60	7.3	Mountains
RS9.5C	18	US	11,250	0.282	511	0.885	5.7	0.60	6.1	Piedmont
RS9.5C	11	NC	17,550	0.290	880	0.877	6.0	0.66	7.2	Coastal
RS9.5C	19	US	21,150	0.303	68,622	0.085	6.0	0.76	7.2	Coastal
RS9.5D	27	US	5,400	0.210	45,323	0.294	5.5	1.10	6.4	Coastal
RS9.5D	12	US	7,650	0.350	22,753	0.222	5.4	0.73	6.2	Coastal
RS9.5D	7	Interstate	23,850	0.287	417	0.911	5.7	0.76	6.5	Coastal
RS9.5D	6	Interstate	29,250	0.382	655	0.833	5.6	0.8	5.8	Piedmont
UTBWC	5	Interstate	16,650	0.890	84,559	0.161	5.5	1.99	3.5	Piedmont
UTBWC	4.1	Interstate	29,250	1.174	27,895	0.137	5.2	5.95	4.1	Mountains
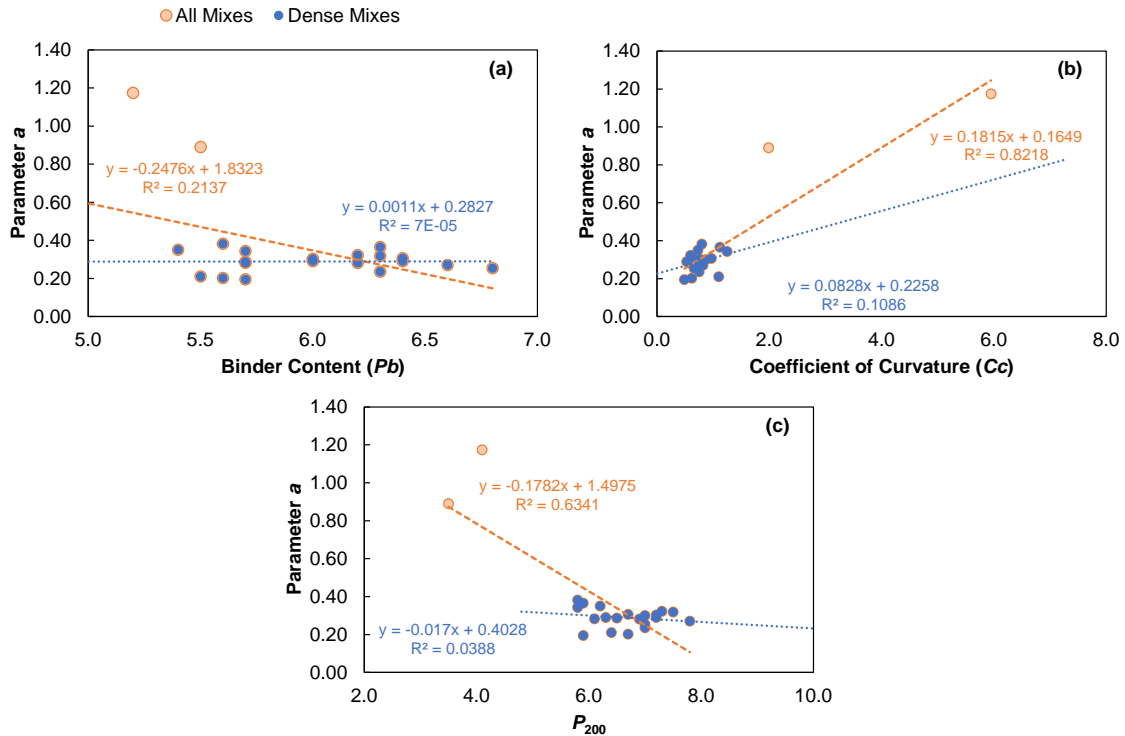
Figure 31. Effect of the mixture volumetric in parameter *a*: (a) *Pb*, (b) *Cc*, and (c) *P*₂₀₀.
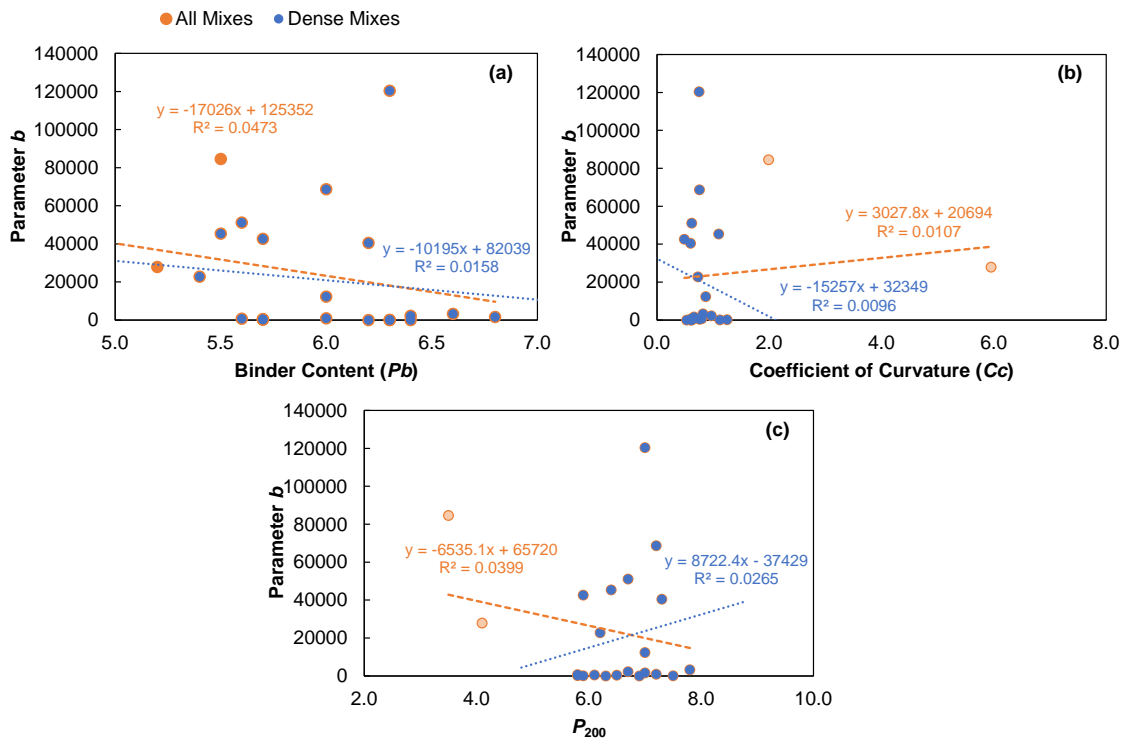
Figure 32. Effect of the mixture volumetric in parameter *b*: (a) *Pb*, (b) *Cc*, and (c) *P*₂₀₀.
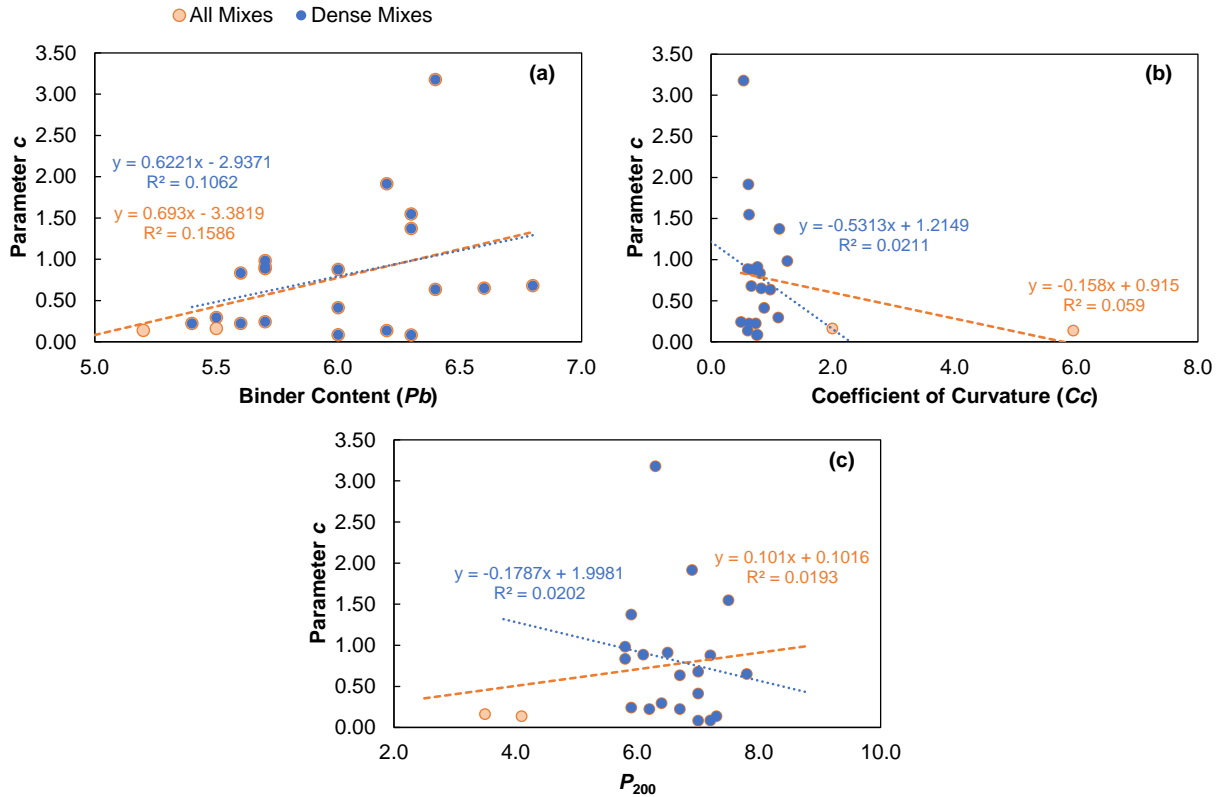
Figure 33. Effect of the mixture volumetric in parameter *c*: (a) *Pb*, (b) *Cc*, and (c) *P*₂₀₀.

As stated, in general the relation between the model parameters and the mixture compositional factors is weak and more observations are needed to get a better picture of the texture evolution and its relationship with the mixture volumetrics. However, as shown in the figures, the parameters of the UTBWC sites stand out from those of the dense-graded mixes, which suggests the texture performance of these two mix types are distinct.

4.5. Effect of Asphalt Overlaid in Crash Frequencies

A preliminary analysis has been conducted in this study to compare the crash rates and the average vehicle speeds 'before' and 'after' an overlay. This analysis is documented in detail in Appendix D. In the case of crashes, a naïve before-after study was conducted, and it was observed that the number of crashes per month were in general higher in the 'after' period than in the 'before' period. Also, the UTBWC seems to provide better safety performance than dense-graded mixtures because this surface type had the lowest crash rate change post overlay. In the case of vehicle speeds, the results suggested the speeds in the 'after' period were on average 1.80% higher than those observed in the 'before' period.

It is strongly emphasized that the amount of data collected after the overlay is very limited so definitive conclusions, supported by standard statistical measures, regarding the effects of the overlay on safety cannot be reached. More observations are required to evaluate the statistical significance of the calculated changes in crash rates. Finally, it is important to point out that COVID-19 related traffic impacts affected many of the 'after' periods in this database. Based on the method of calculating crash frequencies (non-adjusted for traffic volumes), not accounting for this effect may mean that the impacts of the overlays are understated.

51

4.6. Summary of Analysis

In this section, the effect of weather seasonality, traffic, and time on friction and texture variation was evaluated. Strong evidence was observed that the *MPD* of roadways reduces after an asphalt overlay and that this reduction could be as high as 65%. Likewise, in the case of friction, evidence exists of an immediate reduction in frictional resistance after an overlay. In most cases, this reduction in friction was followed by a steady increase to a maximum value, but in some cases, the friction continued to decrease after the overlay was placed. It is believed that one factor, which dictates the prevalence of one trend over the other is the relative amount of fine and coarse fractions in the mixture. The asphalt content and amount of aggregate filler also play a role. None of these factors could single handedly explain the changes. The main conclusions from the friction data shown in this section include:

- Three trends in friction evolution due to traffic were observed among the sites. Trend 1, where friction is still increasing after construction (9 sites); Trend 2, where friction increased up to a maximum value and then started to decrease (10 sites); and Trend 3, where friction decreased after construction (3 sites).
- Linear regression models suggested the initial friction reduces when the *Pb* and the P_{200} fraction increases, while the initial friction increases when the coefficient of curvature increases. Though promising, more data is needed to improve the model accuracy.
- The rate at which friction increases after construction, represented by the parameter m_1, is weakly correlated with the mixture compositional factors; while the predictive capability of the models is relatively weak, the regression models suggest that higher m_1 values are obtained when the *Pb* and the P_{200} fraction increases, whereas m_1 reduces when *Cc* increases.
- The percent increase in friction from the initial value after construction to the maximum value observed in Trend 2 cases, termed the *%Increment*, is affected by the *Pb* and P_{200} based on the results in this study. Higher *%Increment* values occurred for lower *Pb* and P_{200} values. The *Cc* value does not seem to affect the friction percent increase.
- A model was developed to predict the expected friction *%Increment*. The best combination of variables was obtained using the initial friction and average daily traffic as the independent variables. Only sites that exhibited Trend 2 were used for the model calibration. Therefore, the model should be refined by including friction observations on mixtures with a wider range of texture, because most of the current sites have similar texture vales. Eight of the ten sites that exhibited Trend 2 were dense mixes with similar macrotexture.

In the case of texture, the main conclusions are:

- A power function was used to describe the texture evolution. No seasonal variation in texture was observed.
- More observations are needed to understand texture evolution and its relationship with the mixture volumetrics.
- The power law parameters of the site-specific models are distinct for UTBWC compared to dense-graded mixes. This suggest the texture performance in this type of mixes might be different from the dense mixes; however, more UTBWC and/or OGFC needs to be included in the analysis to gain stronger conclusions because only two UTBWC had enough observations to calibrate a texture model.

5. PAVEMENT FRICTION MANAGEMENT RECOMMENDATIONS

In this section a set of recommendations are provided for the implementation of a pavement friction management program (PFMP) in North Carolina roadways. These recommendations are grounded on the literature review, the conclusions drawn from the observations that were collected, the experience of the research team and knowledge gained from discussions with members of the steering and implementation committee. The recommendations provided herein focus on seven different elements: 1) frequency of measurement, 2) spatial resolution, 3) speed of measurements, 4) equipment, 5) performance indices, 6) friction demand, and 7) investigatory thresholds.

5.1. Frequency of Measurements

Section 4 discussed friction and texture evolution and showed that a seasonal effect in friction measurements exists for North Carolina roadways. It is therefore best to measure friction in multiple seasons to calibrate or consider how these seasonal effects align with any critical traffic volumes (i.e., to balance the risks). However, in the absence of these measurements and predictive capabilities, it is suggested that friction be measured during the summer months (preferably in July) when friction is expected to be the lowest. Calibration of a seasonal model requires one measurement every three months, starting in mid-January if possible. For newly constructed pavements, it is recommended to collect four equally spaced measurements during the first year of construction and then afterwards that any new measurements can be collected in the summer. More research and observations are needed to understand both the early friction development and the long-term performance.

For texture, it was observed that time has a major impact on texture measurements. It is recommended that texture measurements be collected during the summer, and for newly constructed surfaces texture measurements should be made at least three times in the first year after construction. Although there is no evidence that the number of dry-days prior to the measurement affects the resulting texture value based on the results in this study, it is recommended to avoid collecting friction or texture values in sites with more than 20 consecutive dry-days, because there are more chances that the presence of dust and contaminants could affect the measurements.

5.2. Spatial Resolution

Both friction and texture have been analyzed in 0.1-mile increments in this study. However, both variables were recorded in a finer scale. In the case of friction, the values were reported every 10 m (around 30 ft) while the texture values were reported every 3 m (around 10 ft). As indicated in Section 2.1 and 2.2, the representative friction and texture value analyzed for every 0.1-mile segment was set as the 2.5-percentile and 50-percentile, respectively.

Because of the considerable amount of information generated when measuring friction and texture, one important aspect to consider when implementing a PFMP at a network level is the storage capacity of the database. The effect of varying the spatial frequency used to calculate the representative friction and texture values is analyzed as shown in Figure 34 using data from the Northbound RWP of Site 8. The standard way of analyzing the data using approximately 30 feet (friction) or 10 ft (texture) is shown along with the observed data in parts (a) and (b) of this figure. Then, three additional frequencies are considered for friction (60 ft, 90 ft, and 120 ft) and four additional frequencies for texture (20 ft, 30 ft, 40 ft, and 60 ft). By only using the observations

collected at these frequencies the friction 2.5-percentile and *MPD* 50-percentile were calculated every 0.1-mile as indicated in Figure 34 (c) and (d), respectively.

In the case of friction, changing the spatial frequency to 90 ft or 120 ft produces a deviation from the line of equality and thus the resulting friction 2.5-percentile at 90 or 120 ft is different from the calculated at 30 ft (the original spatial frequency). In the case of texture, the spatial frequency does not have an effect because the *MPD* 50-percentile calculated at any of these frequencies lies on the line of equality. Therefore, it is recommended to report friction and *MPD* every 60 ft.
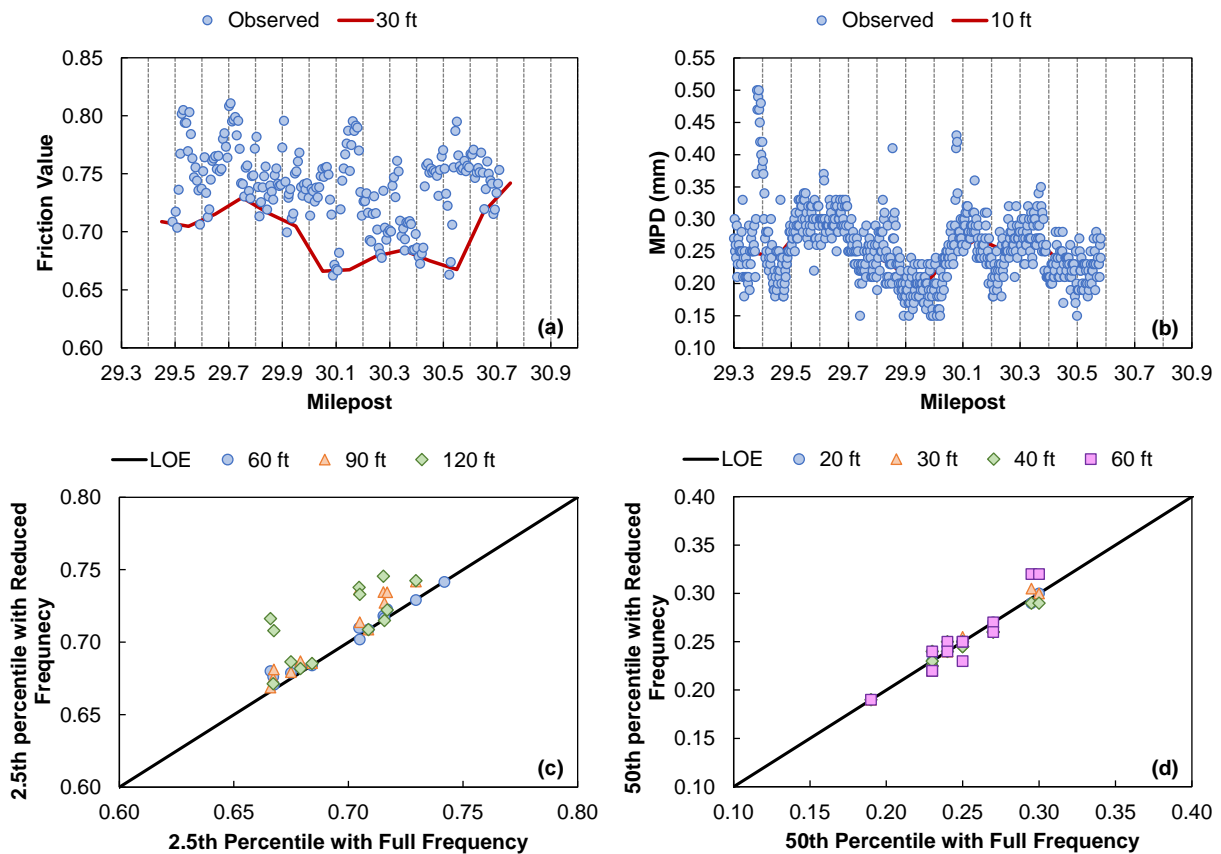
Figure 34. Variation of friction and texture values with data spatial resolution for Site 8 NB RWP: (a) friction, (b) *MPD*, (c) comparison of representative friction values at different spatial resolution, and (d) comparison of representative texture values at different spatial resolution.

5.3. Speed of Measurements

According to several studies, friction values vary exponentially with vehicle speed as (*1, 21–23*). In this research, friction measurements were acquired at both 40 mph and 60 mph in seventeen sites to understand the effect of measurement speed in friction values. In some of these sites, friction at 40 mph was collected in two different set of measurements, i.e., in two different dates; therefore, a total of 58 different pairs of values were available. These 58 paired observations are plotted in Figure 35. In general, the results show that friction increases when speed reduces, but this trend is not consistent. In fact, some sites showed a higher friction at 60 mph in one measurement, but in the next measurement set the friction at 40 mph was higher. Appendix E includes the results from individual t-tests to evaluate the statistical difference between the friction

values measured at different speeds. The statistical test indicated that nearly 60% of the tested sites had a friction value at 40 mph that is both higher and statistically different than the friction measured at 60 mph.

There is not a clear explanation of why friction might increase in some cases and reduce in others. The IFI model suggests that friction variation as a function of vehicle speed should be related to the surface macrotexture (*2*, *24*). Although a relationship between the surface texture and the friction difference at 40 mph and 60 mph was evaluated, in this dataset there were no evidence of a texture dependence in the friction variation with vehicle speed.
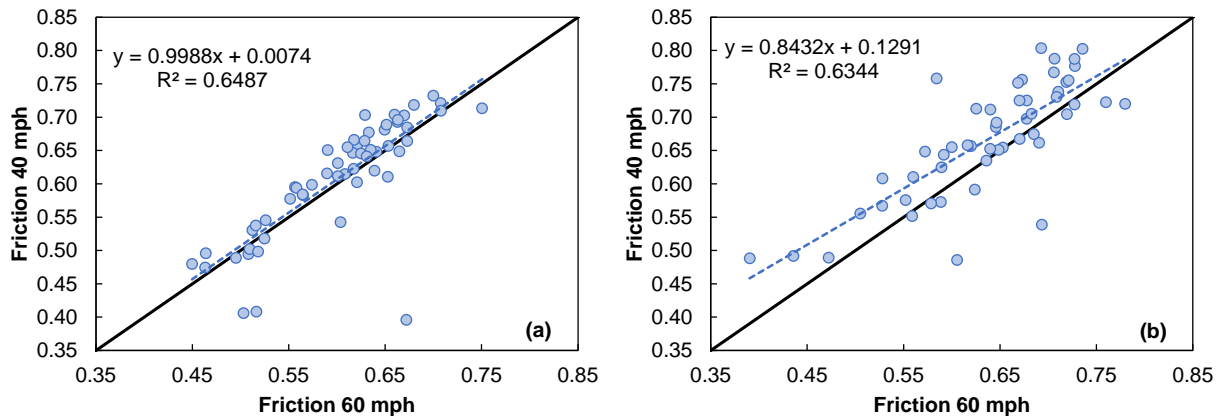
Figure 35. Variation of friction values with measurement speed for (a) RWP and (b) CL.

For this reason, it is necessary to add more information to this dataset to fully understand the variables that affects friction variation. Based on the measurements collected, it is recommended that friction is monitored at both at 40-mph and 60-mph to gather enough information that allows to describe the friction-speed-macrotexture variation. However, if it is possible to only measure at a single speed, then the speed that is most consistent with the data in this report is 60-mph and that is the suggested speed that should be measured. It is noted that the most common value from practice and the literature (largely stemming from LWST) is 40-mph.

5.4. Equipment

5.4.1. Continuous Pavement Friction Measurement Device

An important part of the pavement friction management (PFM) process is the selection of the most appropriate friction measuring equipment. In this project, the capabilities of the Moventor Skiddometer BV-11, a type of continuous friction measurement (CFME) device, and its ability to provide information to support PFMP were evaluated based on comprehensive field data collection. The device can capture the friction variation due to speed and surface type. Therefore, it is recommended to continue using this or a similar fixed slip device that can monitor friction continuously. Different authors have reported the advantages of using a CFME over a LWST. The primary factor for selecting a CFME to monitor friction at a network level is the potential of relating friction at a fine scale, such as 0.1-mile increments, with crash numbers.

Though the Moventor Skiddometer BV-11 provides a geo-referenced measurement, it is important to identify, the closest mile marker in the road and the distance between the beginning of the measurement and the marker at the point of measurement. This is quite important to keep consistency between the PFMP and the PMS database. Finally, it is necessary to define/build a

calibration section and to establish a calibration protocol that guarantees consistency between measurements made with different devices.

5.4.2. High-Speed Texture Measurement Device

Equally important is the selection of the device for monitoring macrotexture at a network level. For this research, the device used for macrotexture measurements was the Ames Engineering High Speed Inertial Road Profiler. This equipment could characterize the macrotexture of different road surfaces and differentiating texture variations due to a change in the surface type, like changing from dense graded asphalt mixes to portland concrete pavements. In general, this device allows for monitoring texture at a network level and can be used at the road operational speed.

Like friction, it is important to define a calibration/verification protocol to verify the accuracy of the devices. The use of commercially available walking macrotexture measuring equipment with a line laser appears to be the most practical method to collect reference profiles to verify and/or certify high-speed macrotexture measuring devices. Engineered surfaces with can and probably should be used to test the accuracy of line-laser-equipped reference walking devices. The surfaces can be scanned with a high-resolution laser texture beam to determine the reference measurements.

Finally, although most of the high-speed inertial road profilers can geo-reference the measurements, it is necessary to annotate/associate the section to be measured with the available closest route referencing marker in order to facilitate the analysis of the results and expedite the communication with the PMS.

5.5. Performance Indices

5.5.1. Friction

Each CFME reports a measure of friction. For example, the Grid Number (GN) is reported by the grid tester and the Scrim Number (SN) is reported by the SCRIM. Other variants like the International Friction Index (IFI), defined as established in the ASTM 1960-07, are used to standardize friction measurements, and facilitate the comparison between different equipment and measuring speed. The Moventor Skiddometer does not have a predefined parameter, though like the other devices, it reports the friction value in conjunction with the measuring speed.

In this research, the 2.5-percentile was used to represent the lowest friction 'envelope' in the route. Based on the results presented in this document, using the 2.5-percentile allows to account for the most unfavorable friction condition along the whole route, but also allows to separate any possible outlier from the trend observed in the data. It is recommended to continue using this index as the representative value of a 0.1-mile section; however, it is encouraged to compute other statistics that describe central position (like mean, median, etc.) and dispersion (standard deviation) because a relationship between friction and texture is still missing, and these statistics might be good candidates for developing such a relationship.

5.5.2. Texture

In the case of texture, the research team used the 50-percentile as the representative value of each 0.1-mile road segment. This value was selected because friction already considers the lowest 'envelope' of the route. Currently, the most commonly reported parameters to represent macrotexture at a network level are the *MPD* and the *RMS* (*25*); however, as indicated in Section 2.2, there are other parameters that provides a better correlation with friction. It is recommended to continue collecting the *Rku* (kurtosis), *Rks* (skewness), and Texture Ratio (*TR*); it is also

recommended to include a measure of dispersion for each parameter (standard deviation). Also, whenever is possible, a static texture measurement needs to be collected along the route to check the accuracy of the device.

5.6. Friction Demand

According to the NCHRP 109 (*2*), friction demand categories are defined by grouping road segments by: i) road category, ii) traffic, iii) climate, and iv) geometry (number of lanes or degree of curvature). Once grouped, the friction demand is quantified by using two criteria included in the AASHTO geometry design manual (*26*):

- The side force friction demand experienced in curves defined in Equation (16), and
- The stopping-sight distance defined in Equation (17).

$$F_s = \frac{V^2}{15 \times R} - e \tag{16}$$

where;

F_s = side-force friction demand in lb,
e = super-elevation rate, ft/ft,
V = speed, mi/hr, and
R = curve radius, ft.

$$SSD = (1.47 \times v \times t) + \frac{v^2}{30(\mu \pm G)} \tag{17}$$

where;

SSD = stopping-sight distance,
t = driver reaction time, in seconds,
G = longitudinal grade, in percent, and
V = vehicle speed, mi/hr.

One challenge in implementing these equations is the need for obtaining the degree of curvature and longitudinal grade for the whole road network. These are inputs in Equation (16) and (17), respectively. Friction demand categories are fundamental to control measurement frequencies and are the base for establishing a relationship between surface friction and crash risk.

5.7. Investigatory Thresholds

Currently, there is no widely accepted specification on friction or pavement texture within the U.S., while some countries have such a requirement to maintain proper performance. A summary of the up-to-date research and specifications for both friction and texture are provided in Appendix A. In addition, no CFME criteria has been officially established in within the US. However, the Moventor Skidometer have been included in the Advisory Circular No. 150/5320-12D of the Federal Aviation Administration (FAA) (*27*). This Advisory Circular contains guidelines and procedures for pavement evaluation with friction measurement equipment, and maintenance of high skid-resistance pavements. This AC identifies recommended minimum friction value for the different equipment evaluated by the FAA. The values for the Moventor Skiddometer BV-11 are indicated in Table 16.

Table 16. Friction level classification for the Movement Skiddometer BV-11.

Measurement Speed	Action Level	Planning Level	New Construction
40 mph (65 km/h)	0.50	0.60	0.82
60 mph (95 km/h)	0.34	0.47	0.74

Similarly, there is no widely accepted specification for pavement texture within the U.S. Some countries do have such specifications in an effort to maintain proper performance. The FAA recommends a minimum *MPD* of 0.76 mm (0.03 in.) for new asphalt or PCC surfaces (*27*). Based on the findings of the research project FHWA/NC 2017-02 (*1*) and the thresholds used in United Kingdom and New Zealand (*2*, *28*, *29*), the preliminary minimum *MPD* requirements for asphalt concrete pavement are proposed in Table 17.

Table 17. Minimum Mean Profile Depth (*MPD* in mm).

Speed Limit	Asphalt Concrete		
	Planning Level	Action Level	New Construction
Less than 70 km/h	0.70	0.50	1.20
More than 70 km/h	0.90	0.50	1.60

This research has not studied the viability of these threshold limits for North Carolina roadways and therefore cannot make any recommendations pertaining to the required investigatory or intervention levels at this time.

6. CONCLUSIONS AND RECOMMENDATIONS

This chapter presents some of the major conclusions derived from the reviews of the friction/texture–crash relationship studies and pavement safety programs, and the results of the experimental program that surveyed more than twenty recently overlaid asphalt pavements in North Carolina. It also presents key recommendations regarding the proposed implementation of a PFM program for NCDOT.

6.1. Conclusions

- The maximum spatial frequency at which friction and texture should be reported is 60 ft.
- From the parameters typically used to describe macrotexture, the *Rks* (Skewness) and Texture Ratio (*TR*) were the ones that showed the most promising correlation with friction.
- By using the friction 2.5-percentile and the texture 50-percentile of a given roadway segment, it is possible to remove potential outliers; in the case of friction, it also allows for accounting for the envelope of the lowest friction value across the road segment.
- Individual relationships for friction and texture were evaluated and it was found that field cores, like the ones collected to control in-place densities, can be used to identify average friction and *MPD* values in the field.
- Higher binder (*Pb*) and fines (P_{200}) contents result in lower initial friction values; the initial friction of an asphalt surface increases as the gradation coarseness increases, as measured by the coefficient of curvature (*Cc*).
- The initial texture of an asphalt surface reduces with the increase in the fines content in the mix (higher P_{200}), and the binder content; coarser gradations provide higher texture.
- It is necessary to account for the friction seasonal variation when interpreting trends in friction with respect to time and traffic. In general, friction can vary up to 12% due to temperature and precipitation.
- After removing the seasonal effect, it was observed that in 19 of the 22 sites used, friction increased after construction; in ten of these sites, friction reached a maximum value after which friction started to decrease. In terms of time, it required between 5.5 to 18 months to reach that maximum friction. In terms of traffic, it required between 0.3 and 15 million vehicle passes to reach the maximum friction.
- The rate at which friction increases after construction is weakly correlated with the mixture compositional factors; however, the regression models suggest that higher rates occur when the *Pb* and the P_{200} fraction increases.
- The observed percent increase in friction from the initial value after construction to the maximum observed value was as high as 50% of the initial value. It was found that the friction increase to the maximum can be predicted using the average daily traffic and the initial friction. This model was applied to those sites that have not reached the maximum friction yet, and it was estimated that those sites will require another 7.5 to 20 months for friction to continue to develop prior to reaching the maximum value.
- For texture, it was observed that time has a major impact on texture measurements. No seasonal fluctuations were observed. It was found the most suitable functional form to describe the texture temporal variation was a power function.
- The mixture compositional factors were not correlated with the texture model parameters. However, the parameters of the UTBWC sites are distinct from those of the dense-graded

mixes, suggesting the texture performance in this type of mixes might be different from those achieved with the dense-graded mixes.

- Although a relationship between the surface texture and the friction difference at 40 mph and 60 mph was evaluated, there was no evidence of a texture dependence on the friction variation with vehicle speed.
- The naïve before-after study and the speed analysis indicate the overlay had an effect, the number of crashes per month were in general higher in the 'after' period than in the 'before' period.

6.2. Recommendations

Based on the aforementioned conclusions, the research team makes the following recommendations.

- The NCDOT should consider broader application of continuous friction measurements for monitoring skid resistance on its roadways. Continuous friction measurement capabilities are important because friction along a given segment can vary substantially and alternatives (i.e., LWST) may miss these critical areas.
- For the development and calibration of a seasonal effects model, a subset of newly constructed pavements should have friction and texture measurements taken for four equally spaced time periods during the first year after construction. The model calibration recommendation may need to be integrated into the friction and texture management processes once friction and texture threshold values have been established. These thresholds may need to be developed for various mix designs and pavement types.
- Once friction and texture threshold values have been established for various mix designs and pavement types and a friction and texture management process has been established, JMF's should be screened for potential friction/macrotexture issues using the formulae developed in this research. For surface mixtures that have a higher potential for friction/macrotexture issues, cores should be extracted and evaluated. Density quality assurance cores may be used for this purpose, if available.
- The dataset collected in this research should be expanded and supplemented with crash data, surface characteristics, mixture design details, and geometric factors to; 1) improve the models developed in this study, 2) identify friction demand, and 3) establish investigatory and intervention threshold values for friction/macrotexture measurements.
- According to the literature reviewed, the friction adhesion mechanism (friction microtexture) is present at any vehicle speed; however, this mechanism is more important at lower speeds. The high-speed measurements, including those collected in this project, primarily reflect the hysteresis mechanism. In other words, more research is needed to fully understand the friction microtexture component. To fully characterize friction microtexture, the characteristics of the aggregates such as mineralogy, shape, and abrasion resistance must be accounted for. The adhesion friction component depends on the aggregates microtexture; therefore, it is suggested to start cataloging the aggregate characteristics and evaluate their friction properties in the lab.

7. IMPLEMENTATION AND TECHNOLOGY TRANSFER PLAN

The Traffic Safety Unit and Materials and Tests Unit of the NCDOT are the primary users of the outcomes of this research. The friction and macrotexture models developed in this project can be used by the NCDOT to preliminarily screen or evaluate their mix designs for potential issues and/or to leverage quality assurance field cores to do similar screening. In addition, the measurement guidelines developed in this project can be used to establish testing and reporting requirements for continuous friction measurements and continuous macrotexture measurements. Although the research project did not identify investigatory and intervention threshold limits, (which was beyond the scope of work), the results of the study can still be used by the NCDOT to identify situations where pavement overlays may result in reduced friction and macrotexture. The findings from this study are being communicated to the NCDOT in the form of this report, the appendices, and a closeout meeting with the project panel.

For follow-up activities, the research team believes that the NCDOT could consider the following activities:

- allocating resources to evaluate a larger set of sites, both newly overlaid and aged pavements, to improve the accuracy of the friction/macrotexture performance models;
- allocating resources to simultaneously evaluate crash rates, travel speeds, geometric details, and other contributing factors on the same routes in order to establish preliminary investigatory and intervention thresholds; and
- testing field cores taken as part of quality assurance activities using the surface texture scanning method identified in this study to identify sites that may have the potential for low macrotexture and low initial friction following an overlay.

8. REFERENCES

1. Flintsch, G. W., D. Ph, and F. Street. Evaluation of Methods for Pavement Surface Friction , Testing on Non- Tangent Roadways and Segments. No. August, 2017.

2. Hall, J. W., K. L. Smith, L. Titus-Glover, A. R. A. Inc., and I. Champaign. *NCHRP Document 108: Guide for Pavement Friction*. 2009.

3. Henry, J. J. *NCHRP Synthesis 291: Evaluation of Pavement Friction Characteristics*. 2000.

4. Sandburg, U., and J. A. Ejsmont. *Tyre/Road Noise Reference Book*. Kisa, Sweden, 2002.

5. FHWA. Pavement Friction Management: Technical Advisory. https://www.fhwa.dot.gov/pavement/t504038.cfm. Accessed Jul. 20, 2021.

6. ASTM E274/E274M -15. *Standard Test Method for Skid Resistance of Paved Surfaces Using a Full-Scale Tire*. 2015.

7. Fwa, T. F. Skid Resistance Determination for Pavement Management and Wet-Weather Road Safety. *International Journal of Transportation Science and Technology*, Vol. 6, No. 3, 2017, pp. 217–227.

8. McCarthy, R., E. de León Izeppi, G. Flintsch, and K. K. McGhee. Comparison of Locked Wheel and Continuous Friction Measurement Equipment. 2018.

9. Meyer, W. E., and T. D. Gillespied. *Locked-Wheel Pavement Skid Tester Correlation and Calibration Techniques*. 1974.

10. Wang, H., and Z. Wang. Evaluation of Pavement Surface Friction Subject to Various Pavement Preservation Treatments. *Construction and Building Materials*, Vol. 48, 2013, pp. 194–202.

11. Ames Engineering. High-Speed Inertial Profiler. https://amesengineering.com/products/8300-high-speed-profiler/. Accessed Jun. 6, 2020.

12. ASTM E1845 -01. *Standard Practice for Calculating Pavement Macrotexture Mean Profile Depth*. 2001.

13. Stroup-Gardiner, M., and E. R. Brown. *NCHRP Report 441*. 2000.

14. Cenek, P. D., D. J. Alabaster, and R. B. Davie. *Seasonal and Weather Normalisation of Skid Resistance Measurements. Transfund New Zealand Research Report No. 139*. 1999.

15. Jayawickrama, P. W., and B. Thomas. Correction of Field Skid Measurements for Seasonal Variations in Texas. *Transportation Research Record*, No. 1639, 1998, pp. 147–154.

16. GES Disc. Merra-2 Database: The Second Modern-Era Retrospective Analysis for Research and Applications. https://disc.gsfc.nasa.gov/datasets/M2SDNXSLV_5.12.4/summary.

17. Masad, E., A. Rezaei, A. Chowdhury, and T. Freeman. *Field Evaluation of Asphalt Mixture Skid Resistance and Its Relationship to Aggregate Characteristics*. 2010.

18. Masad, E., A. Rezaei, A. Chowdhury, and P. Harris. *Predicting Asphalt Mixture Skid Resistance Based on Aggregate Characteristics*. 2009.

19. Pomoni, M., C. Plati, A. Loizos, and G. Yannis. Investigation of Pavement Skid Resistance and Macrotexture on a Long-Term Basis. *International Journal of Pavement Engineering*,

2020, pp. 1–10.

20. Wu, Z., and C. Abadie. Laboratory and Field Evaluation of Asphalt Pavement Surface Friction Resistance. *Frontiers of Structural and Civil Engineering*, Vol. 12, No. 3, 2018, pp. 372–381.

21. Fisher, N. I., and P. Hall. Bootstrap Confidence Regions for Directional Data. *Journal of the American Statistical Association*, Vol. 84, No. 408, 1989, pp. 996–1002.

22. Flintsch, G. W., K. K. Mcghee, E. D. L. Izeppi, and S. Najafi. *The Little Book of Tire Pavement Friction*. 2012.

23. Cerezo, V., M. T. Do, D. Prevost, and M. Bouteldja. Friction/Water Depth Relationship - In Situ Observations and Its Integration in Tire/Road Friction Models. *Proceedings of the Institution of Mechanical Engineers, Part J: Journal of Engineering Tribology*, Vol. 228, No. 11, 2014, pp. 1285–1297.

24. ASTM E1960 -07 (Reapproved). Standard Practice for Calculating International Friction Index of a Pavement. *Astm*, Vol. i, No. October 2003, 2015, pp. 1–5. https://doi.org/10.1520/E1960-07.2.

25. Flintsch, G. W., E. de León Izeppi, V. Bongioanni, S. W. Katicha, K. Meager, E. Fernando, R. Perera, and K. K. McGhee. *Protocols for Network-Level Macrotexture Measurement*. Washingtion, D.C., 2021.

26. AASHTO. *A Policy on Geometric Design of Highways and Streets*. 2018.

27. Federal Aviation Administration (FAA). *AC NO:150/5320-12D: Measurement and Maintenance of Skid-Resistant Airport Pavement Surfaces*. 2005.

28. Transport Agency, N. *T10:2002 New Zealand Specification for State Highway Skid Resistance Management*. 2012.

29. Viner, A. H. E., R. Sinhal, and A. R. Parry. Linking Road Traffic Accidents With Skid Resistance – Recent UK Developments, TRL Paper Reference PA/INF4520/05. *Highways*, No. August 2004, 2005, pp. 1–13.

30. Hauer, E. *Observational Before-After Studies in Road Safety. Estimating the Effect of Highway and Traffic Engineering Measures on Road Safety*. 1997.

31. Hauer, E. Identification of Sites with Promise. *Transportation Research Record*, No. 1542, 1996, pp. 54–60.

32. Hauer, E., and B. N. P. Problem of Identifying Hazardous Locations Using Accident Data. *Journal of Transportation Research Record*, 1994, pp. 531–540.

This page is intentionally blank

APPENDIX A: DETAILED LITERATURE REVIEW

Pavement Friction and Surface Texture

Definition

The friction developed at the tire-pavement interface is one of the most important factors that contributes to the safety performance of a given road because a driver's control of their vehicle is directly proportional to the amount of friction that can be reached between the tire and the pavement. Normally, the friction force that develops between the tire and the pavement is referred as Skid Resistance (F_R) (*1*). From this definition, it follows that the skid resistance is the result of the interaction between the tire and the pavement, hence it is not a property of the tire or the road surface itself but rather is defined as a combination of the two.

Although poor skid resistance is rarely the first cause of a crash, a potential exists whenever the vehicle friction demand exceeds the maximum friction coefficient that can be achieved between the tires and the road (whether wet or dry). If the vehicle friction demand surpasses the maximum available friction in a particular location, the tire will start slipping, which can cause the vehicle to spin out of control, rollover, or depart the road/lane (*2*). The friction force developed at the tire-pavement interface is characterized by the coefficient of friction (μ), which is the ratio of the tangential force (F_R) at the contact interface to the normal force on the wheel (N). Since both forces have the same unit, μ is a dimensionless quantity. The friction forces developed in the tire-pavement contact area depend on both the vehicle speed and the road texture, the latter is the more important component and can be subdivided in two parts, the micro- and the macrotexture.

Flitsch et al. (2012) (*2*) presented a detailed literature review on the frictional properties of pavements and discussed the different wavelengths of the road profile that contribute to the friction coefficients (see Figure A.1). They concluded that the microtexture (i.e., dimensions below 0.5 mm) of the aggregate particles play an important role in the friction development at the tire-pavement interface. Further they concluded that this role was important at any speed but more so at low speed. The microtexture is important because at this scale there exist molecular interactions between the aggregate particles and the tire rubber that result in adhesion.

Figure A.1 also shows that there is a second wavelength component of relevance, the macrotexture, which is linked to the shape and size of the coarse aggregate or to the grooves cut in the surface (like the ones that are made on the portland cement concrete pavements). The macrotexture scale varies from 0.5 mm to almost 10 mm. As stated before, the microtexture plays an important role at any speed; however, for wet conditions it is believed that the macrotexture is the more important component of friction especially at high speeds. For example, in 2009 Hall et al. (*3*) concluded that for speeds above 56 mph (90 km/h) on wet pavements, the macrotexture surface component is responsible for a large portion of the friction, regardless of the slip speed.
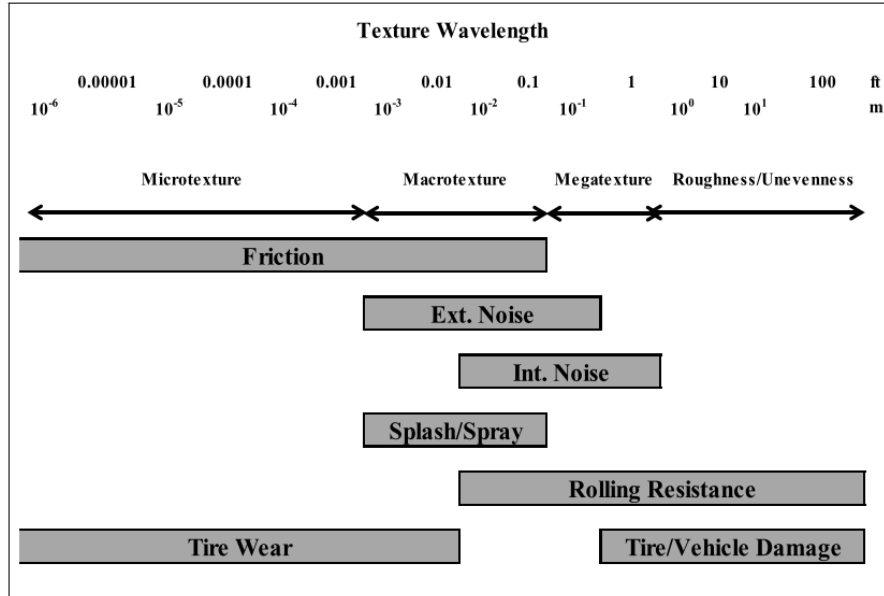
Figure A.1. Influence of texture wavelength on tire pavement interaction (*2*).

Friction Mechanism

A tire is a type of elastomer that defoRMS under the action of external forces. When a tire interacts with a pavement there will be different interaction components depending on the amount of deformation and the properties of the contact interface. Normally three components are defined as shown in Equation (18):

$$\mu_{overall} = \mu_{adhesion} + \mu_{hysteresis} + \mu_{cohesion} \tag{18}$$

where $\mu_{overall}$ is the net available friction coefficient, $\mu_{adhesion}$ is the resulting friction from the molecular interaction in the tire-pavement contact interface, $\mu_{hysteresis}$ is the friction component related to the hysteresis resulting from the energy loss due to the tire deformation, and $\mu_{cohesion}$ associated with the friction produced by the tire wear (*4*).

The three friction mechanisms are shown in Figure A.2, as can be seen from the schematic, each mechanism is associated with a roughness profile. Adhesion determines the friction characteristics and is the component that produces the grip under smooth and dry road surface conditions, Figure A.2 (a), or under icy or snowy road surfaces. The hysteresis is the most important friction component under wet conditions, providing most of the grip necessary for good wet braking performance. When a tire compresses and defoRMS due to the surface irregularities, energy is stored that is later released while the tire relaxes. Part of this energy is recovered, but a fraction is lost as heat (hysteresis), which adds to the net frictional force that contributes to stopping any forward motion. The hysteresis compound is higher for rough surfaces, Figure A.2 (b). Cohesion is associated with the tire wear product of the abrasion process that occurs at rough or sharp surfaces. However, the influence of the friction coefficient by cohesion over the total friction coefficient is generally slight to negligible compared to adhesion or hysteresis terms (*3*, *4*).

(a) Smooth surface   (b) Rough surface   (c) Sharpened surface
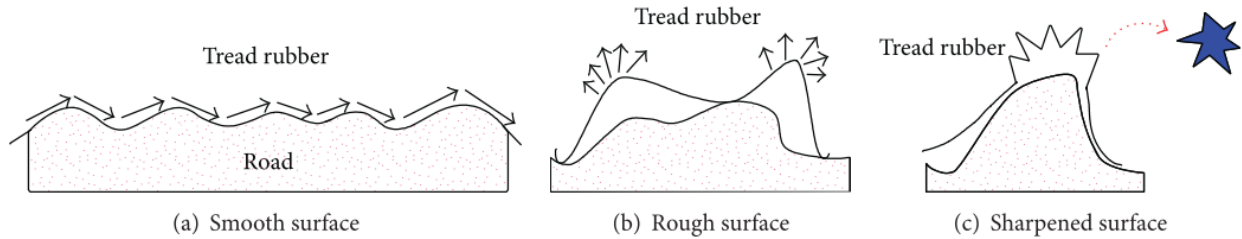
Figure A.2. Variation of the friction mechanism by road roughness (*4*).

Friction Components

The frictional properties of the tire-pavement interface are a key input for a pavement friction management program, highway design (minimum stopping distance, horizontal and vertical alignments, and maximum super-elevation on curves), and for identifying mitigation measures that need to be applied in case of high crash rates. In general, the amount of friction that can be developed between the tires and the pavement have a direct effect on the control the driver has over his vehicle. Accelerating, braking, or cornering a vehicle may include two friction vectors, a longitudinal vector that is the product of the tangential forces parallel to the movement direction and a lateral or side-friction vector that is perpendicular to the movement direction as shown in Figure A.3, these friction components depend on the tire yaw angle. When the tire yaw angle is zero, the side-friction is negligible, and the only force component is the longitudinal one.
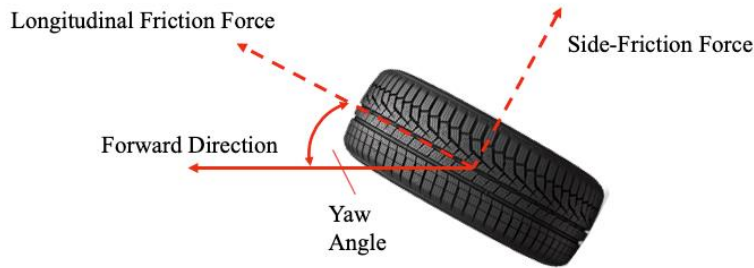
Figure A.3. Friction force vectors.

<u>Longitudinal Friction Forces</u>

When a vehicle is moving in a free rolling resistance mode (no braking) and following a straight line, the contact path of its wheel is constant. Hence, only a small amount of friction is developed at the tire/road interface. Of course, due to the surface profile irregularities, and by the adhesion and cohesion friction mechanism, there always will be a small rolling resistance component (*2*, *3*, *5*). Figure A.4 (a) illustrates the force diagram of a free-rolling tire (no braking). The vehicle engine produces a torque that translates into a tire rotation and the weight of the vehicle (F_W) produces a contact pressure between the tire and the pavement. Then, because of the tire deformation, the ground force (F_G) that is the resultant reaction in the contact area, is out of center by a distance *a*. This offset causes a counter-momentum that tries to reduce the vehicle momentum, and the required force to overcome this opposition is the so-called rolling resistance force (F_R) (*3*).
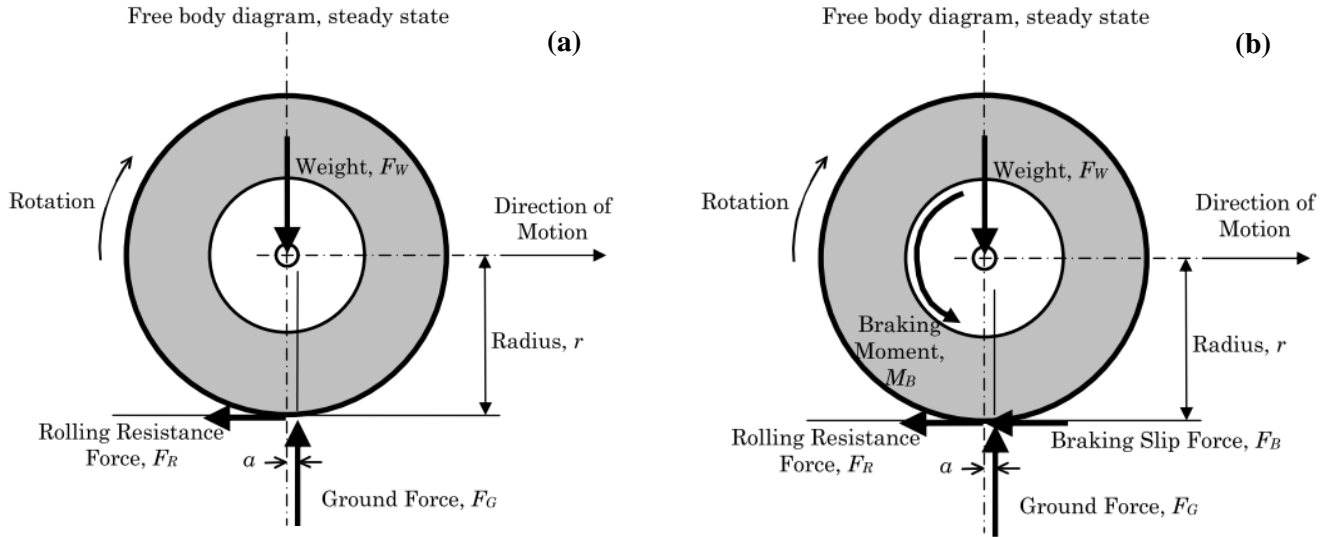
Figure A.4. Forces and moments at: (a) free rolling tire, and (b) constant-braked wheel (*3*).

In the free-rolling mode, the relative speed between the pavement and the tire perimeter, referred to as the slip speed, is zero (*4*), and the rolling resistance is negligible. However, as soon as the driver starts applying the brakes or accelerating, i.e., a maneuver that involves changing either the speed or the movement direction, the slip speed, and the distance *a* start increasing, which results in a higher counter-momentum and ultimately a higher rolling resistance. In the case of a braking maneuver, see Figure A.4 (b), the brakes apply an additional counter-momentum, the braking momentum (M_B) produces an additional resistance force, braking slip force (F_B) that adds to the rolling resistance force.

During the braking process, the rotational speed of the tire starts decreasing at a higher rate than the vehicle speed; therefore, the slip speed, which is zero when the vehicle is at a free rolling mode, will increase until it reaches the maximum value of the vehicle speed. Equation (19) shows the relationship between the vehicle speed (*V*) in mi/h and the slip speed (*S*), where ω is the angular velocity of the tire in rad/s, *r* is the tire radius in ft and V_P is the average peripheral speed of the tire in mi/h. If the vehicle is at rolling-free mode V_P is nearly equal to *V*, and the slip speed will be zero (*2, 3*).

$$S = V - V_p = V - (0.68 \times \omega \times r) \tag{19}$$

As soon as the braking maneuver starts, V_P begin decreasing and *S* increases until the slip ratio (*SR*), that varies between 0 and 100%, reaches the critical value ($S_{critical}$, typically 20-30%) at which point a peak in the value of the coefficient of friction (μ_{peak}) occurs, see Figure A.5. This friction is the maximum value that can be produced between the tire and the pavement while the wheel has not been fully locked. After the $S_{critical}$ the coefficient of friction start reducing until it reaches a constant value (μ_{slip}) that is maintained when the wheel is fully locked (*6*).

$$SR = \frac{S}{V} \times 100 \tag{20}$$
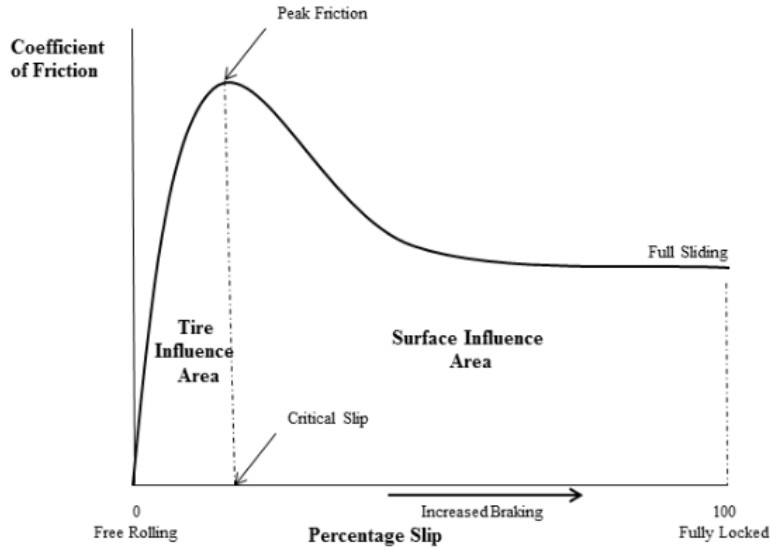
Figure A.5. Friction vs slip ratio (5).

During dry conditions, there is not much difference between μ_{slip} and μ_{peak} and further, the values will not change by much as the vehicle speed changes. However, under wet conditions μ_{peak} reduces considerably and both friction values decrease with increasing speed. A similar situation occurs during acceleration, even though the contact path may remain constant, an excessive demand for acceleration can surpass the μ_{peak} available and the wheel will start to slip, or in the worst-case scenario, to spin with little or no acceleration at all (5).

Lateral Friction Forces

In the case of cornering, lateral friction forces are generated to maintain a vehicle inside its path while it is traveling around a curve. When the combination of a radius of curvature (influenced by the horizontal and vertical alignment, as well as with the super-elevation and steering angle, see Figure A.6) and forward speed result in a friction demand that exceeds the maximum the road can provide, the wheel may slip sideways. In the case the demand is higher than the peak friction, the wheel may slide sideways causing the vehicle to yaw, in this case large differences between the peak and sliding friction may translate into a rapid loss of control (3). A more complex scenario occurs when braking and cornering occur simultaneously. In this case the available friction must be shared by two mechanisms. In a curve, if μ_{peak} is surpassed, the side friction force goes to zero and the driver will be unable to steer, ultimately losing control of their vehicle.

69
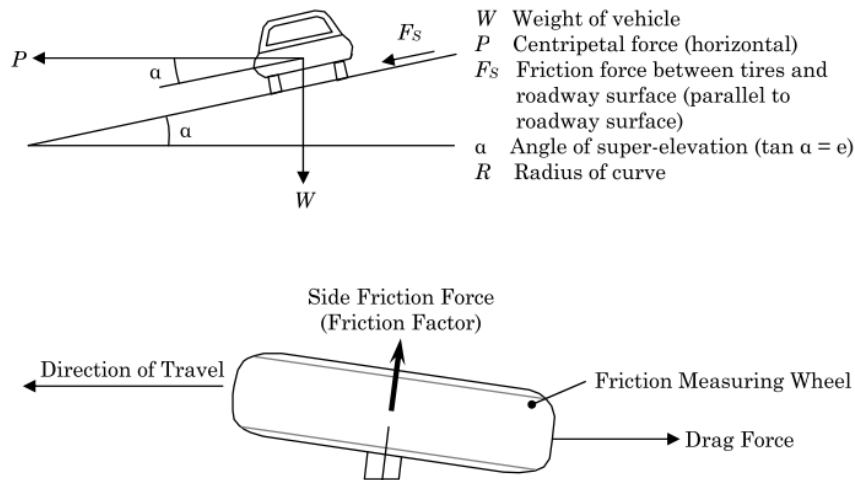
Figure A.6. Vehicle dynamics traveling around a curve (*2, 3*).

Pavement Friction Related Variables

The variables that affect the friction properties at the tire-pavement interface can be categorized into four groups: pavement surface characteristics, vehicle operating characteristics, tire properties, and environmental conditions, as summarized in Table A.1. As can be seen in Table A.1, each of these variables play an important role in the amount of friction that can be developed. Since each of these factors affects friction, friction is often referred to as a process rather than a property of the pavement.

Table A.1. Factors affecting available pavement friction (*2, 3, 7*).

Pavement Surface Characteristics	Vehicle Operating Parameters	Tire Properties	Environment
-Microtexture -Macrotexture -Unevenness -Material properties -Temperature	**Slip Speed** -Vehicle speed -Braking action **Driving Maneuver** -Turning -Overtaking	-Footprint -Tread design/Condition -Rubber comp. and hardness -Inflation pressure -Load -Temperature	**Climate** -Wind -Temperature -Water (rainfall, condensation) -Snow and ice **Contaminants** -Dirt, mud, debris, salt

Effect of Mixture Factors on Pavement Friction and Texture

As stated in Section 0, several factors affect the coefficient of friction at the tire-pavement interface. The microtexture is important at any speed but has a greater effect at low speed and the macrotexture claims a more important role under wet conditions contributing to the hysteresis friction mechanism and to water drainage. Figure A.5 showed the variation of the coefficient of friction against the slip ratio. It is important to notice that when friction measurements occur on the left side of the peak they are mostly influenced by the characteristics of the tire, but when they are made on the right side of the peak, they are mostly influenced by the surface properties (micro and macrotexture) (*3*).

70

Aggregate Texture Characterization

Different researchers (*2*, *3*, *5*, *6*) have agreed that the most important aggregate properties that affect friction are hardness and mineralogy, polish resistance, abrasion/wear resistance, macroscopic morphology, and soundness. The role of each of these properties are described below.

Hardness and Mineralogy

It has been found that aggregates with a more compact crystal structure and composed of hard minerals embedded in a matrix of softer minerals have the best friction properties for longer periods of time (*5*). Harder aggregates have better wear resistance against the abrasion forces applied by the traffic. However, an equilibrium is needed because while aggregates that are composed of only hard minerals will resist wear, they may be prone to polishing under traffic load. On the other hand, if the aggregates are made mostly of moderately soft minerals alone, and thus resist polishing, they will wear quickly when subjected to traffic. The hardness of the aggregates is normally determined by the Scratch hardness test (Mohs Test); however, using a petrographic analysis, ASTM-C295 (*8*), it is possible to determine both the mineralogy composition and the hardness of each aggregate type.

Polish Resistance

The aggregate's ability to retain its microtexture during the grinding, mixing, construction and operation under traffic loads is known as its polish resistance. This property is measured using two widely accepted procedures: the acid insoluble residue test (*AIR*) and the polished stone value (*PSV*). While the *PSV* is the most common method, new developments at the National Center for Asphalt Technology (*NCAT)* have resulted in refinement to the Three Wheel Polishing Device (*TWPD*), and it is gaining in popularity (*9*). Regardless of the measurement method though, polishing resistance is important because when an aggregate becomes smooth, it will not contribute to the friction performance and will become slippery especially at wet conditions.

Abrasion/Wear Resistance

Good friction performance requires higher abrasion resistance. The abrasion/wear resistance can be measured by two different tests (*3*): the Micro-Deval test for fine and coarse aggregates and the Los Angeles (LA) abrasion test. Both test procedures measure the aggregate resistance to a mechanical degradation produced by a set of standardized balls.

The Micro-Deval test can be used to test either fine (*10*) or coarse aggregates (*11*) used for either a portland cement concrete or asphalt concrete surfacing. On the other hand, the LA abrasion test can be applied only to coarse aggregates used in a new (conventional or innovative) portland cement concrete or asphalt concrete surfacing (*12*). Of these two procedures the more common is the LA abrasion test.

Shape, Texture and Angularity

Aggregate macromorphology is described in terms of the particle's shape, texture, and angularity. All three properties are important for defining both the micro- and macrotexture properties of an asphalt pavement. With respect to shape, flat and elongated particles are not desired because they have low interlock potential, and when they are used in a blend tend to be horizontally oriented, which translates in lower macrotexture depth. In contrast, sharp and elongated particles will produce a more variable structure with a higher interlock between particles translating into higher macrotexture depth. Aggregate morphological properties are typically measured as part of the mix

design process, i.e., the angularity (AASHTO T 304 for fine particles and the ASTM D5821 for coarse particles), and the shape (roundness and flat-elongate ratio by ASTM D4791).

Soundness

The soundness is defined as the percent loss of materials from an aggregate blend due to the degradation caused by climatic/environmental effects such as wetting, thawing, freezing, drying, etc. The test procedure is described in AASHTO T 104/ASTM C88 and consists of submerging a sample of aggregates and then drying it in an oven over five consecutive cycles. The total mass loss is reported. The desired outcome is a low percent loss results because this will mean that the aggregates have a higher resistance to the weather-related degradation.

Pavement Surface Measurements

From the last section it follows that the shape, angularity, and texture of the aggregate particles are extremely important for the friction properties of a pavement. In the case of asphalt concrete or portland cement concrete, several methods exist to quantify and describe the relevant properties that affect the resulting skid resistance. While many methods exist, only the most common are discussed herein.

First, is important to point out that there is no direct way to measure the microtexture of a pavement in the field. Even in the laboratory, the process is highly complicated. For this reason, many different studies have tried to obtain surrogate measures that indicate microtexture, including ASTM E303-93 (*13*), which uses the British Pendulum Tester (BPT). However, recent researchers (*1*, *6*) have shown that the underlying assumptions used in these surrogate approaches are not always correct. The prevailing knowledge today suggests that measurements of microtexture friction contribution using a BPT may also reflect part of the macrotexture friction component.

In contrast, several methods are available to measure the macrotexture as shown in Figure A.7. These methods can be largely classified into two groups: static measures (used at a project level) or dynamic measures (used at a network level). The most common static or contact method is the sand patch and volumetric technique test (*14*). Nowadays the most common dynamic or non-contact methods uses a laser profiler that measures, at high frequencies, the texture elevation profile of the pavement. This data is processed to estimate the average texture depth.

In the past decades several surface characterization techniques have been proposed for various application and are grouped into two categories: scale-dependent and scale-independent. A scale-independent parameter indicate texture characterization results are independent of the measurement scales or data resolution. Then, it follows that a scale-dependent parameter means that texture characterization results are dependent on the measurement scales or the frequency at which the data are collected. In other words, the analysis results might be quite different when different measurement scales are used. The scale-dependent parameters are the most common texture characterization quantities (*15*) and are summarized in Figure A.8.

Amplitude Parameters

The amplitude parameters are descriptors of the pavement surface deviation from a theoretical flat surface. They are calculated on a given baseline segment and describe either the magnitude of the deviations or the distribution of these deviations along the baseline segment. As shown in Figure A.8 there are five amplitude parameters that can be used to describe surface texture namely Mean Texture Depth (*MTD*), Mean Profile Depth (*MPD*), Root Mean Square (*RMS*), Skewness (*Rks*),

72

and Kurtosis (*Rku*). Currently the amplitude parameters are the most common indices used to describe pavement texture (*15*).
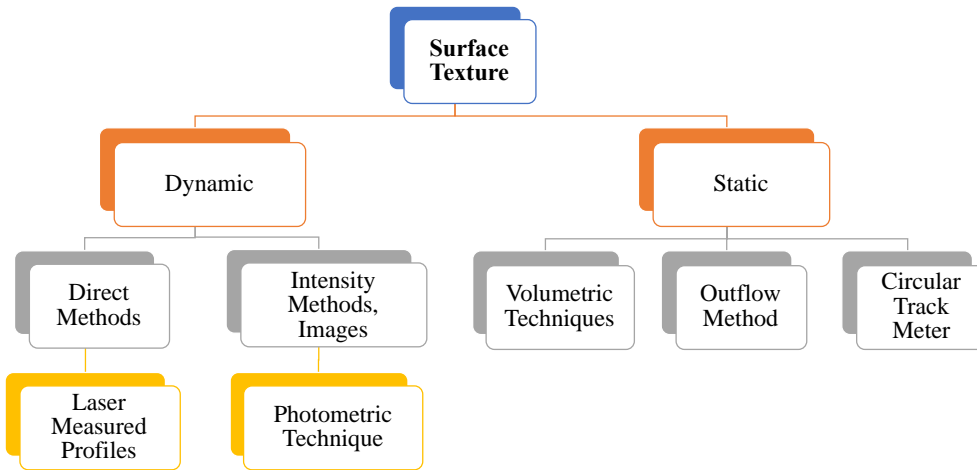
Figure A.7. Pavement macrotexture measuring methods.
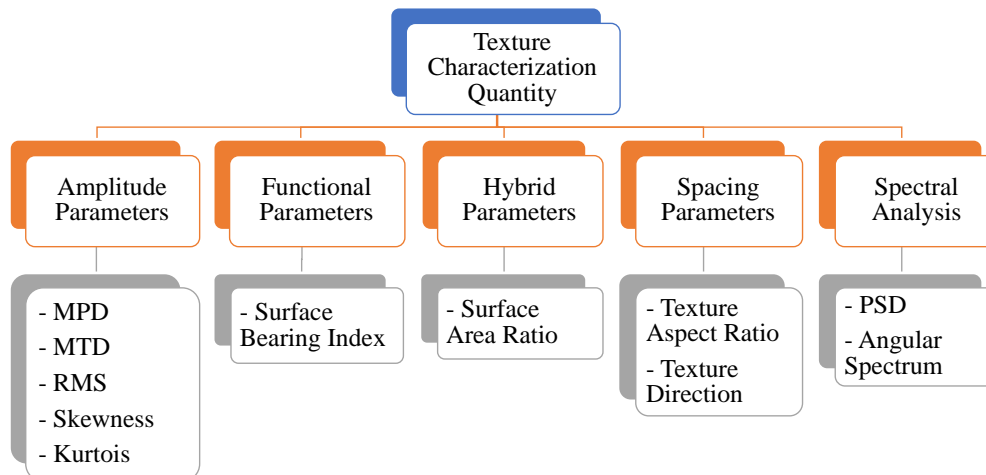
Figure A.8. Schematic diagram of pavement surface characterization technique (*15*).

Mean Texture Depth

Pavement macrotexture is the deviation of a pavement surface from a true planar surface with the characteristic dimensions of wavelength and amplitude from 0.5 mm up to those that no longer affect tire-pavement interaction (see Figure A.9). The mean texture depth (*MTD*) is the average difference or average height between the actual pavement surface and the true planar surface (*16*) and is calculated using static methods, such as volumetric techniques or the Circular Test Meter (see Figure A.7).

Mean Profile Depth (MPD)

While the MTD is obtained by static methods, the mean profile depth (*MPD*) is obtained from laser measured profiles, which is one of the dynamic methods presented in Figure A.7. Typically, these profiles are collected using a laser equipment that take measurements at continuous intervals. Once the profile is obtained, the standard for calculating the *MPD* is ASTM E1845-01. The measured profile is divided, for analysis purposes, into segments each having a base length of 100

mm (3.9 in.). The slope, if any, of each segment is suppressed by subtracting a linear regression of the segment. The segment is further divided in half and the height of the highest peak in each half segment is determined. The difference between that height and the average level of the segment is calculated. The average value of these differences for all segments making up the measured profile is reported as the *MPD*, as can be seen in Figure A.9.
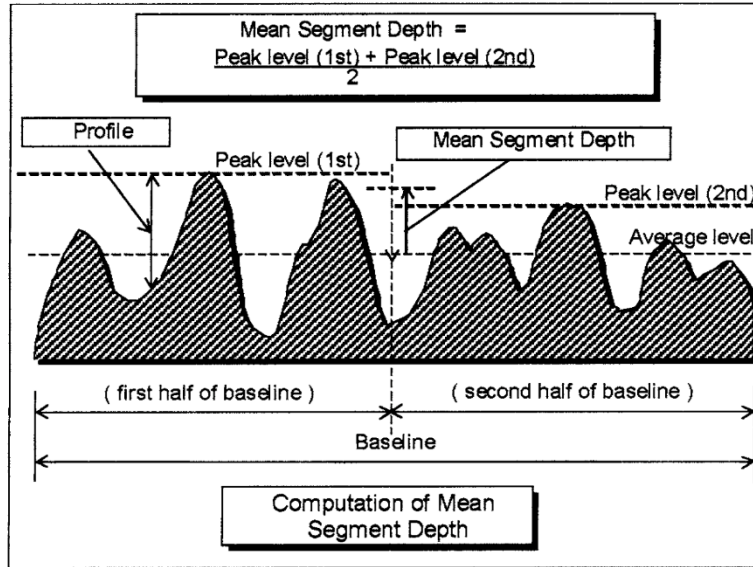
Figure A.9. Procedure for computation of mean segment depth (*17*).

MPD values measured using a laser profilometers are not the same as *MTD* values measured using volumetric techniques (sand patch test). However, *MPD* can be converted to *EMTD* (Equivalent to *MTD* of volumetric method) to indicate macrotexture (*3*) using one of the following equations:

$$EMTD = 0.8 \times MPD + 0.008 \text{ (units for MPD and EMTD are in.)}$$
$$EMTD = 0.8 \times MPD + 0.2 \text{ (units for MPD and EMTD are mm.)}$$

(21)

Root Mean Square (RMS)

The *RMS* is a parameter obtained from laser measured profile and represents a general measurement of the surface texture deviation property. A larger *RMS* indicates that there is a significant deviation in surface texture characteristics. The *RMS* calculation is described by Equation (22):

$$RMS = \sqrt{\frac{\sum_{x=1}^{N}\sum_{y=1}^{M} z(x, y)^2}{M \times N}}$$

(22)

where *M* is the number of points per profile, *N* is the number of profiles, *z(x,y)* is the elevation difference between point (*x,y*) and the mean plane, and *RMS* is the mean root square of the surface (*15*).

Skewness and Kurtosis

Similarly, the Skewness and Kurtosis parameters are calculated using a laser measured profile and are used to represent the three-dimensional surface texture height distribution properties. A

histogram of the heights of all measured points is computed and then the symmetry and deviation from an ideal normal distribution is represented by skewness, *Rks*, and kurtosis, *Rku*. The mathematical descriptions of these variables are given by Equation (23) and Equation (24).

$$Rks = \frac{\sum_{x=1}^{N}\sum_{y=1}^{M} z(x, y)^3}{M \times N \times RMS^3} \tag{23}$$

$$Rku = \frac{\sum_{x=1}^{N}\sum_{y=1}^{M} z(x, y)^4}{M \times N \times RMS^4} \tag{24}$$

Where *M* is the number of points per profile, *N* is the number of profiles, *z(x,y)* is the elevation difference between point (*x,y*) and the mean plane, and *RMS* is the mean root square of the surface.

The *Rks* represents the degree of symmetry of surface heights with respect the mean plane. The sign of *Rks* indicates the predominance of peaks (*Rks* > 0) or valley structures (*Rks* < 0) comprising the surface. *Rku* indicates the presence of the inordinately high peaks/deep valleys (*Rku* > 3) making up the texture. If surface heights are normally distributed, then *Rks* is 0.00 and *Rku* is 3. Similarly, surface heights are positively skewed (*Rks*>0) or negatively skewed (*Rks* < 0). Surface height distributions can be considered as the slow variation (*Rks*<3) or extreme peaks or valleys (*Rku*> 3). The less the *Rku* is, the smaller the height variation is. The larger the *Rku* is, the larger the height variation is (*15*).

Spacing Parameters

Texture on the pavement surface may have anisotropic or isotropic patterns (*15*), like the ones shown in Figure A.10. An anisotropic surface is one where the dominant texture components are oriented in one direction, an isotropic surface is one where the texture components are equally distributed in all directions. The Autocorrelation Function (*ACF*) is one of the most effective and robust approaches for texture pattern recognition, it is used to obtain a measure of the correlation between points separated by various time lags (or by distance increments) (*18*).

The *ACF* is obtained by taking a duplicate surface *z((x-Δx), (y-Δy))* of the measured surface *z(x,y)*, where Δ*x* and Δ*y* are a small increment in the *x* and *y* direction respectively, and then mathematically multiplying the two surfaces. Subsequently, the resulting function is integrated and normalized to yield a measure of the degree of overlap between the two functions.

Generally, the *ACF* of the anisotropic pavement surface has the fastest decay along the direction perpendicular to the predominant texture direction and the slowest decay along the texture direction, as shown in Figure A.10 (a). The *ACF* of an isotropic pavement surface has similar texture aspects in all directions, so it is difficult to determine the fastest and slowest decay of the test sample, as shown in Figure A.10 (b).
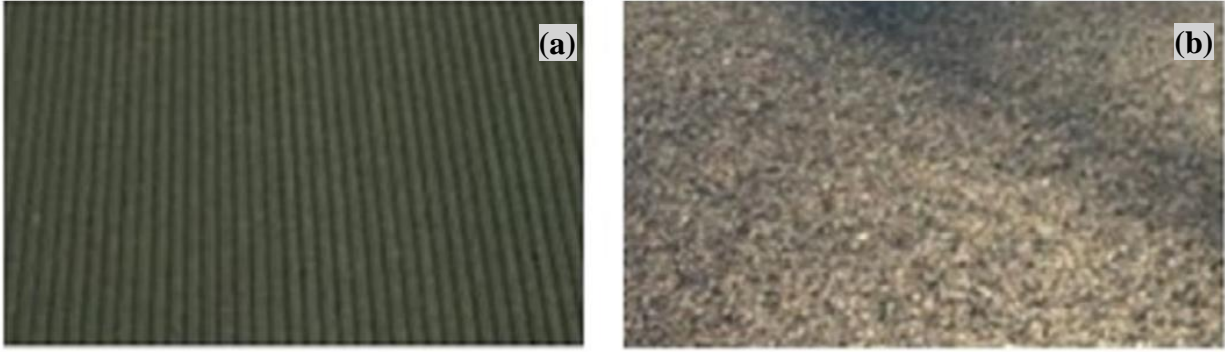
Figure A.10. (a) Anisotropic pavement surface, like the one found in a portland concrete pavement; (b) Isotropic pavement surface like the one found in a new asphalt concrete pavement (*15*).

Texture Aspect Ratio

Texture Aspect Ratio (*TAR*) is a measure of the spatial isotropy or directionality of the surface texture. The length of fastest decay is defined as the distance over the surface such that the new location $z((x-\Delta x), (y-\Delta y))$ will have a minimum correlation with the original location $z(x,y)$, i.e. when the obtained *ACF* is lower than 0.2. In contrast, the length of slowest decay is defined as the distance over the surface such that the new location $z((x-\Delta x), (y-\Delta y))$ will have a maximum correlation with the original location $z(x,y)$, i.e. the longest distance in any direction before reaching an *ACF* lower than 0.2.

$$TAR = \frac{Distance\ that\ normalize\ ACF\ has\ the\ fastest\ decay\ to\ 0.2\ in.\ in\ any\ possible\ direction}{Distance\ that\ normalize\ ACF\ has\ the\ slowest\ decay\ to\ 0.2\ in.\ any\ possible\ direction} \quad (25)$$

In principle, the *TAR* has a value between 0 and 1. Larger values, say *TAR* > 0.5, indicate stronger isotropic or uniform texture aspects in all directions, whereas the smaller values, say *TAR* < 0.3, indicate the stronger periodic texture properties (*15*).

Hybrid Parameters

Hybrid parameters are used to overcome the limitations of the amplitude parameters (these only consider a general description of amplitudes and distributions) and the spatial parameters (these only consider changes of macrotexture in different directions and also do not take into account the amplitude distribution). One of the most used hybrid parameters is the Surface Area Ratio (*SAR*) (*15*), which is defined as the ratio of the interfacial area to the total sampling area as shown in Equation (26).

To calculate the interfacial area is necessary to divide the total sampling area into smaller units as show in Figure A.11. Take for example the quadrilateral ABCD, because the vertices of this quadrilateral may not be in the same plane, the interfacial area A_{ij} of this quadrilateral is calculated using Equation (27).

$$SAR = \frac{Interfacial\ area\text{-}Total\ surface\ area}{Total\ surface\ area} \quad (26)$$

76

$$A_{ij} = \frac{\left(\left|\overrightarrow{AB}\right| + \left|\overrightarrow{CD}\right|\right)}{2} \times \frac{\left(\left|\overrightarrow{AD}\right| + \left|\overrightarrow{BC}\right|\right)}{2} \tag{27}$$

Then, the total interfacial area of the whole surface is calculated using the Equation (28).

$$A = \sum_{j=1}^{N-1} \sum_{i=1}^{M-1} A_{ij} \tag{28}$$

where M and N are the number of vertices in the X and Y direction respectively. So, the *SAR* can be written as shown in Equation (29).

$$SAR = \frac{A - (M-1) \times (N-1) \times \Delta x \times \Delta y}{(M-1) \times (N-1) \times \Delta x \times \Delta y} \tag{29}$$
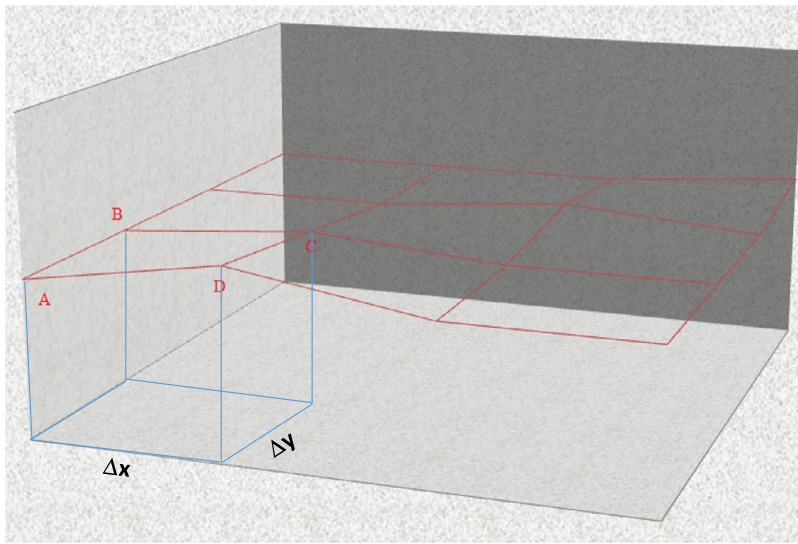
Figure A.11. Schematic diagram of the interfacial area (*15*).

The developed interfacial area ratio reveals the hybrid property of surfaces. A large value indicates the significance of either the amplitude or the spacing or both (*15*).

Functional Parameters

For a long time, the automotive industry has tried to find ways for optimizing and defining parameters that allow functional characterization of a surface texture (in the automotive industry surface is understood as the contact area between two different bodies), in order to make them more effective and to improve their correlation with functional parameters. In this sense, the Surface Bearing Ratio (*SBR*) parameter was defined for describing the functional characteristics of the pavement surface that may affect the wearing or friction of the tires (*15*).

This parameter is associated to the distribution of heights and its cumulated curve, related with the areal material ratio curve. The areal ratio (*AR*) represents the proportion of the total area that has a surface height equal to the surface height *H*, the vertical axis is ordered in a way that represents the cumulative distribution of the height values in a given area (*19*).
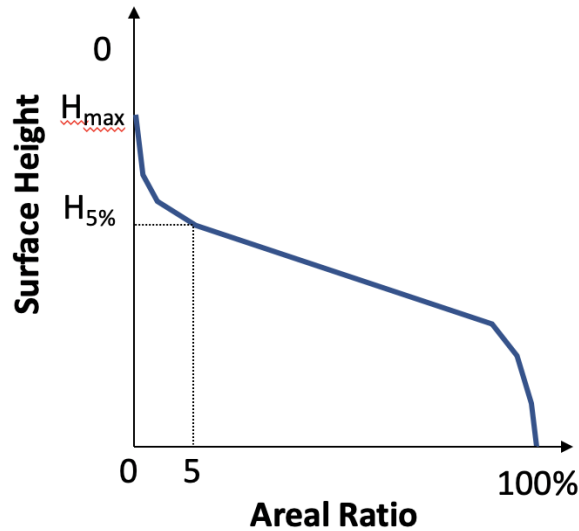
Figure A.12. Areal material ratio curve (*20*).

The *SBR* for pavements can be written as the ratio of the root mean square of the surface height (*RMS*) to the surface height corresponding to 5% bearing area (*H5%* in Figure A.12):

$$SBR = \frac{RMS}{H_{5\%}} \tag{30}$$

Spectral Analysis

The spectral analysis method consists of evaluating the texture spectrum of a given surface profile, typically the texture spectrum is described by a Power Spectral Density (PSD) function, that represents the frequency distribution of the different wave lengths components of the profile. The ISO 13473-2:2019 defines the different bandpass filters that must be applied to the profile to separate the wavelength components that describe the micro-texture, macro-texture, and mega-texture.

Surface Texture Measurement Methods

<u>*Static or Contact Methods*</u>

Volumetric Techniques

According to Figure A.7 the sand patch test or the volumetric technique procedure to measure *MTD* is a static method that involves spreading a known volume of material on a clean and dry pavement surface, measuring the area covered, and subsequently calculating the average depth between the bottom of the pavement surface voids and the tops of surface aggregate particles. This measurement of pavement surface texture depth reflects the pavement macrotexture characteristics. The standard for this test is the ASTM E965-15. This procedure is designed to provide an average depth value of only the pavement macrotexture and is considered insensitive to microtexture characteristics.

This test method is not considered suitable for use on grooved surfaces or pavements with large (≥1.0 in. (25 mm)) surface voids. However, the test is useful for improving pavement finishing practices or for defining maintenance schedules. Also, when used in conjunction with other

physical tests, the macrotexture depth values derived from this test method may be used to determine the pavement skid resistance capability and the suitability of paving materials or finishing techniques. The apparatus used in the field during the test are presented in Figure A.13.
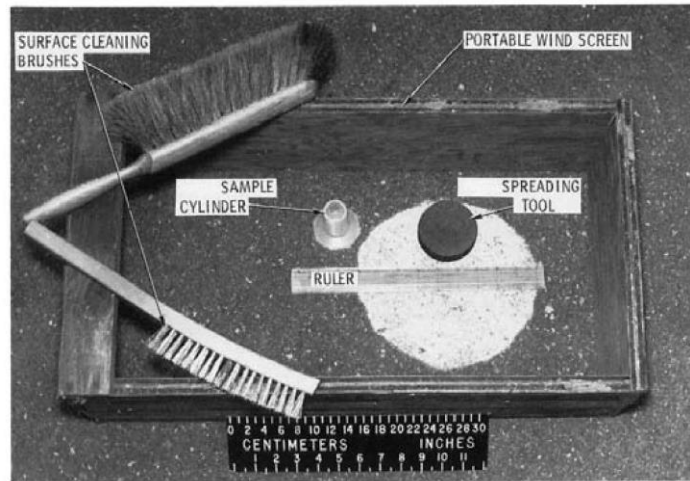
Figure A.13. Apparatus for measuring surface macrotexture depth (*16*).

Outflow Method

This test is a static method, as shown in Figure A.7, that is suitable as a field test to evaluate the surface drainage, and in some cases, the internal drainage of the surface coarse of a pavement. When used with other tests, the outflow time may be used to evaluate the texture produced by an asphalt concrete mix, a finishing method used on portland cement concrete pavement, and refinishing operations on old pavement surfaces. Research has shown that outflow meter tests correlate with other methods such as the *CTMeter*, *MPD*, and *MTD* (*3*, *21*).

The outflow meter device consists of a timer, a cylinder filled with water, and two float switches (one for activating a timer and the other for deactivating it). The outflow time (*OFT*) is the time required for the water level in the cylinder to fall from the level of the upper float switch to the level of the lower float switch, the blue dash region presented in the Figure A.14 (a). A lower *OFT* indicates a thinner water film may exist between the tire and the pavement, which means that lower water pressure will be developed under the tire and hence a lower likelihood for hydroplaning.

It is possible to identify a threshold *OFT* through comparison of *OFT* on pavements with and without hydroplaning issues. However, these thresholds may be very specific to other factors inherent to the pavements (pavement type, aggregate type, etc.). The standard procedure for this test is ASTM E2380/E2380M-15. The following equation can be used to estimate the *MTD* from *OFT*:

$$MTD = 3.114 / OFT + 0.636 \tag{31}$$
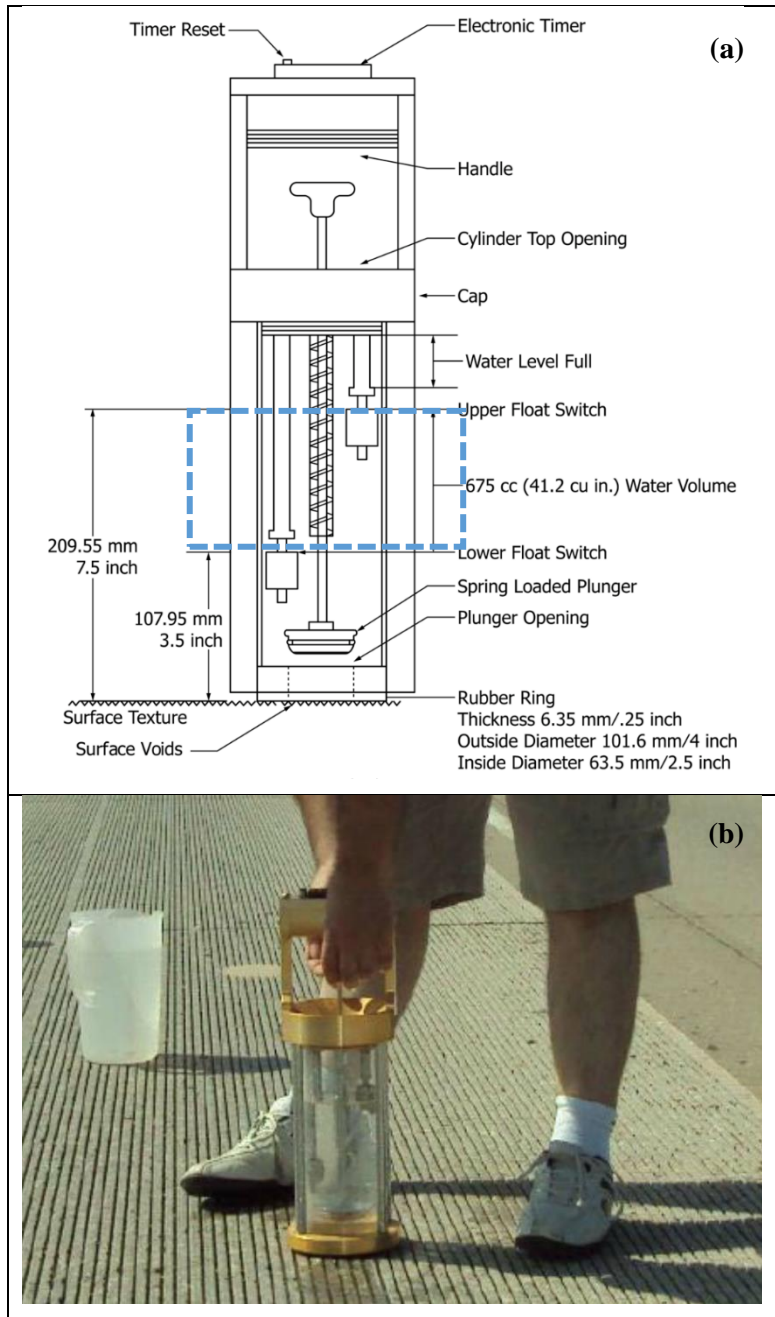
Figure A.14. (a) Flow meter device scheme (*22*), and (b) flow meter used in the field (*23*).

Circular Track Meter (CTM)

The Circular Track Meter (CTM) is a static method that is used to determine the *MPD* and the MTD, see Figure A.7 and Figure A.8. The standard procedure for the *CTM* test is ASTM E2157-15. The test itself uses a displacement sensor that is mounted on an arm that rotates clockwise at a fixed elevation from the surface being measured. The sensor is attached to the arm at a radius of 142 mm. The sensor measures vertical macrotexture depth and does not account for concave recesses in the pavement surface. The device is controlled by a notebook computer that saves and

process the data. During a test, the device takes eight measurements in a circular path (see Figure A.15), which constitute a profile for which both the *MPD* and the *RMS* is calculated.

The ASTM E2157-15 standard includes the Equation (32) that allows correlating the *MPD* obtained with a *CTMeter* with the Mean Texture Depth (*MTD*) obtained from volumetric procedures. In this Equation both the *MPD* and the *MTD* are in millimeters.
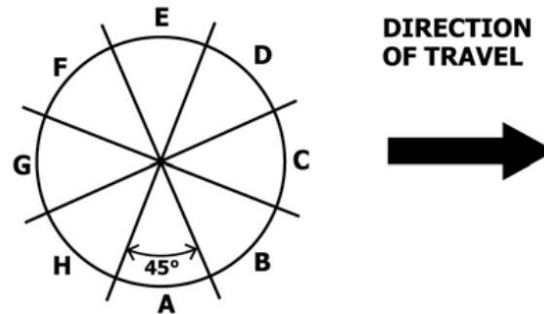
Figure A.15. Segments of the circular track profile (*24*).

$$MTD = 0.947 \times MPD + 0.069 \tag{32}$$

<u>*Dynamic or Non-Contact Methods*</u>

Laser-Measured Profiles

The main disadvantages of the static methods are the amount of information that can be collected per test, and the necessity of closing lanes for its application. This is one of the main reasons for which static methods are not used at a network level. As an alternative, high-speed methods for characterizing pavement surface texture are typically based on non-contact surface profiling techniques, like laser texture scanners (*LTS*). A *LTS* can measure surface elevations at intervals <0.25 mm. More recent *LTS* are capable of measuring texture profiles with wavelengths down to 0.05 mm and can be used at a network level (*6*).

Photometric Technique

This method consists of developing a three-dimensional model of the pavement surface based on the photometric stereoscopic method, in which the pavement surface is lit from different directions, while a still camera registers the intensity images of the pavement surface (see Figure A.16). Alternatively, the camera can be moved while the lighting is fixed. The three-dimensional model allows a more comprehensive analysis of the pavement surface, as it is possible to evaluate specific features on a three-dimensional area. This method allows an evaluation of the texture nature with statistical indicators (*18*). However, according to Sun and Wang (2017), this method has a disadvantage that it is not able to fully capture the microtexture details. This is a laboratory procedure in the case where the camera is fixed and the light source position changes but can be used in a field setting if a fixed light source (the sun) is used and the camera moved.
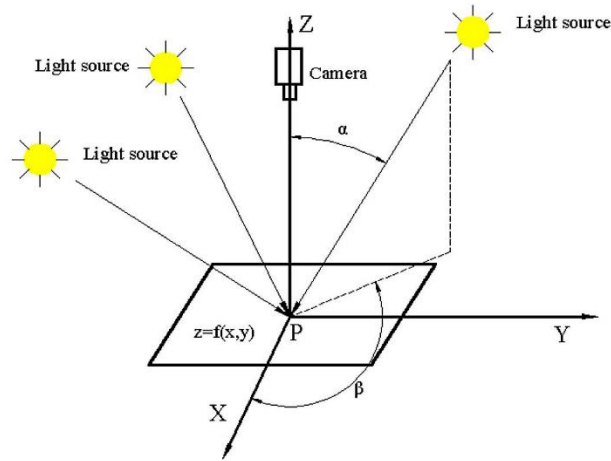
Figure A.16. Schematic diagram of the photometric technique (*18*).

Pavement Friction Measurements

The common methods currently used for measuring friction either in the lab and the field are summarized in Figure A.17.
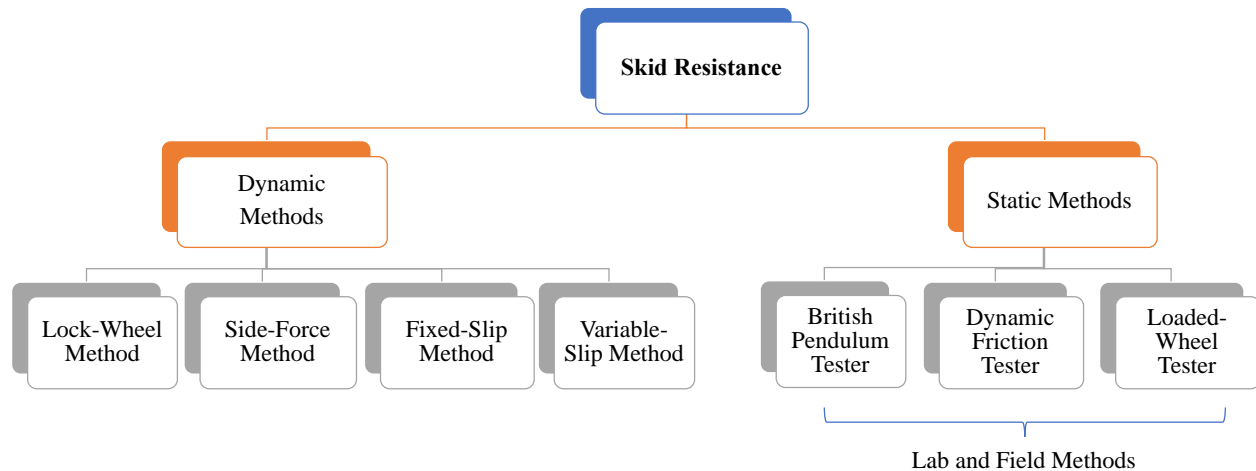
Figure A.17. Pavement friction measuring methods.

British Pendulum Test

The standard procedure for the British Pendulum Test is ASTM E303-93 (reapproved 2018). For the experiment, the surface is first cleaned and wetted. Then, the pendulum slider, Figure A.18, is positioned so that the rubber slider barely contacts the test surface at its lowest position. The pendulum is then raised to a locked position and released. As the pendulum swings past the surface the slider comes in contact with the test surface and slows. A drag pointer indicates the British Pendulum Number (*BPN*), which is an indication of the energy lost as the rubber slider passed over the surface. The greater the friction between the slider and the test surface, the more the swing is retarded (more energy is loss), and the larger the *BPN* reading. The test is repeated four times in order to record a final test value.
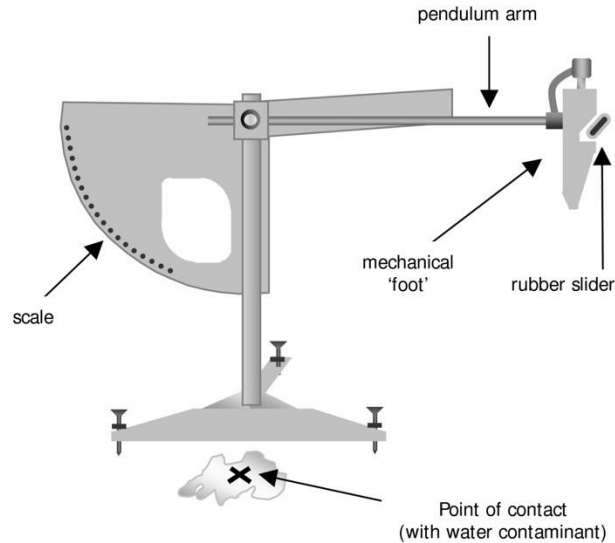
Figure A.18. Schematic diagram of the British Pendulum Tester (*25*).

The resulting *BPN* varies from a 0 (no friction) to 150 (highest value) scale. It is important to ensure a minimum contact path of 125 ± 1.6 mm for flat surfaces and $76 - 78$ mm for polishing wheel specimens. This test has been used to measure the frictional properties provided by the microtexture component of the asphalt mix. It is believed that the *BPN* represents the low-speed pavement wet friction component, although recent researchers have found that the microtexture component is present at any speed. The test method can be used to determine the relative effect of various polishing process on materials or material combination and can be applied to any flat surface either in the lab or in the field

Dynamic Friction Tester

The Dynamic Friction Tester (DFT), Figure A.19, consists of a horizontal spinning disk fitted with three spring loaded rubber sliders which contact the paved surface. The spinning disk contacts the surface and as it does so its rotational speed decreases due to the friction generated between the sliders and the paved surface. A water supply unit delivers water to the paved surface being tested. The torque generated by the slider forces measured during the spin down is then used to calculate the friction as a function of speed. The DFT can be used for laboratory investigations and in the field on actual paved surfaces.

The DFT can provide a maximum tangential velocity of 90 km/h (55 mph). The torque signal is reduced to a measurement of friction by converting the torque to the force on the sliders and dividing by the weight of the disk and motor assembly. The friction at 20, 40, 60, and 80 km/h (12, 24, 36, and 48 mph) is recorded and the friction-speed relationship may be plotted. The DFT is used more and more around the world as a replacement of the BPT. The standard for this test is ASTM E1911-09a.
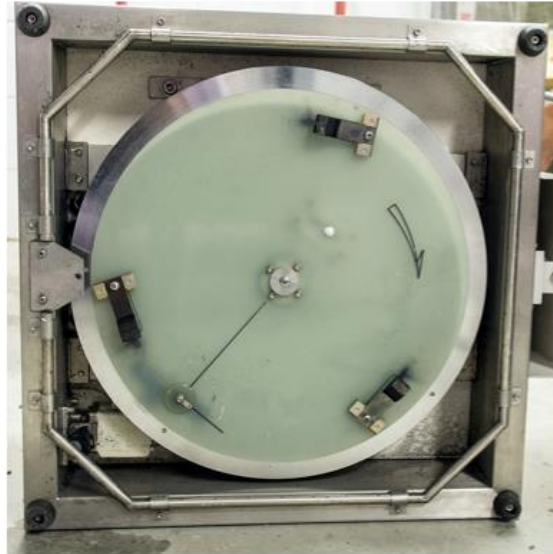
Figure A.19. Example setup of a Dynamic Friction Tester (*26*).

Loaded Wheel Tester

The loaded wheel tester was originally designed to test the rutting potential of paving materials. Jafari, and Toufig (*27*), modified the device to evaluate wear by attaching a studded steel roller. In this case, the studded steel wheel is moved along the top of the pavement at a frequency of 1 cycle per second. The steel studs are 10 mm in diameter and 5 mm in height, as depicted in Figure A.20. The load weight used to measure abrasion resistance was 890 N. After each 100 cycles, surfaces of the specimens were cleaned, and weighed. The weight loss percentage was measured and reported at each step up to 2,000 cycles.
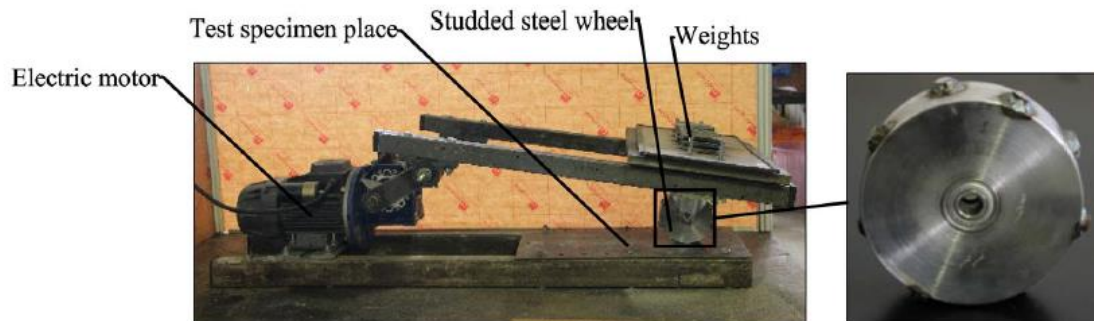
Figure A.20. Loaded wheel tester scheme (*27*).

Dynamic Methods

Field measurements of pavement friction are made using a vehicle with a mounted trailer housing a wheel. The roll mode of the wheels in the trailer varies depending on the specific technique and can include locked-wheel, side-force, fixed-slip, or variable slip.

Locked-wheel method

The standard for locked-wheel skid testing is ASTM E274. This method uses a wheel that is completely locked and oriented in such a way that the major plane is parallel to the vehicle motion

direction. During the measurements, a controlled flow of water is added at the tire-pavement interface to simulate wet breaking performance in the results. The results are summarized by the Friction Number (*FN*) or Skid Number (*SN*), which is calculated as shown in Equation (33):

$$SN(v) = 100 \times \mu = 100 \times \frac{F}{W} \tag{33}$$

where v is the velocity of the test tire (normally in the range of 40 to 60 mi/h), μ is the coefficient of friction, F is the tractive horizontal force applied to the tire (lb) and W is the vertical load applied to the tire (lb).

Figure A.21 shows a common lock-wheel test trailer setup this device consists of a trailer that is attach to a truck and a computer in the truck cabin controls the mechanism that locks the wheel, the device can use a smooth tire or a ribbed tire. More discussion on this issue is provide in Section 0 below.

Figure A.21. Lock-Wheel test trailer (*28*).

Currently, the LWST are the most used devices for measuring friction in the US (see section 0); however, despite its popularity this device has certain limitations:

- Is not capable of taking continuous measurements.
- The water tank capacity of the trailer is limited, reducing the efficiency in the number of measurements that can be made per day.
- The friction is measured only in the forward direction.
- The slip ratio cannot be varied.
- The friction values measured in a curve are not reliable because it cannot capture the whole lateral friction component.

Side-force method

The side-force method is standardized in ASTM E670. The test is like the locked-wheel test because it also uses a trailer mounted in a vehicle (although newer devices are assembled in a whole truck that can carry more water for a higher mileage measurements), but the wheel orientation with respect the motion direction is varied, in order to simulate the friction demand exerted by a vehicle when transiting over a curve. The side-force coefficient (*SFC*) is calculated as indicated in Equation (34).

$$SFC(v, \alpha) = 100 \times \frac{F_s}{W} \tag{34}$$

where v is the slip velocity of the test tire (typically low slip velocities, below 20 mi/h), α is the yaw angle (normally between 7.5° and 20°), F_s is the force perpendicular to the plane of rotation (lb) and W is the vertical load applied to the tire (lb).

Fixed-slip method

This type of measurements tries to capture the maximum friction coefficient between a tire and the pavement. To achieve these measurements, the system uses an anti-lock braking system (ABS) that allows the experimentalist to control the slip ratio. The typical values for this slip ratio are between 10 to 20 percent (see Figure A.5). These measurements are more representative of the real braking system of modern vehicles. Currently, there are several options of fixed-slip devices like roadway and runway friction testers (RFTs), airport surface friction tester (ASFT), Saab friction tester (SFT), Griptester, Road Analyzer and Recorder (ROAR), and the SCRIM. The current technology allows this equipment to perform continuous friction measurements and the test procedure is established in ASTM E2340/E2340M with the tire specifications for the test given in ASTM E1551.

According to the ASTM E2340/E2340M standard, routine testing is usually carried out on the left wheel track of each lane. The length of the test may be as little as 100 m [300 ft] or as much as 50 km [30 miles]. Standard test speeds as low as 20 km/h [12 mph] and as high as 80 km/h [50 mph] have been established for particular types of continuous friction measurement equipment (CFME) and particular applications. Standard nominal water film thicknesses are typically 0.25, 0.50, and 1.00 mm [0.01, 0.02, and 0.04 in.] according to the type of CFME and the application.

During the test, the frictional force parallel to the vehicle motion direction is recorded, which is necessary to compute the slip ratio, defined as shown in Equation (35):

$$P = \frac{(v - r \times \omega)}{v} \times 100 \tag{35}$$

where, r and ω are the radius and angular velocity of the test tire, respectively.

Variable-slip method

The ASTM E1859 is the standard that defines the test method that covers the measurement of the longitudinal friction coefficient with a measurement device that imposes braking-slip between a tire and a surface for the full range of braking-slip speed values.

This test method utilizes a series of incremental single measurements of friction force on a braked test wheel as it is pulled over a wetted or contaminated pavement surface. The rotational velocity of the braked wheel is feedback controlled in order to give a predetermined variable slip ratio gradient in accordance with set program parameters. The test wheel is kept under a constant static normal load and at a constant longitudinal speed of travel. Its major plane is perpendicular to the road plane and parallel to its direction of motion.
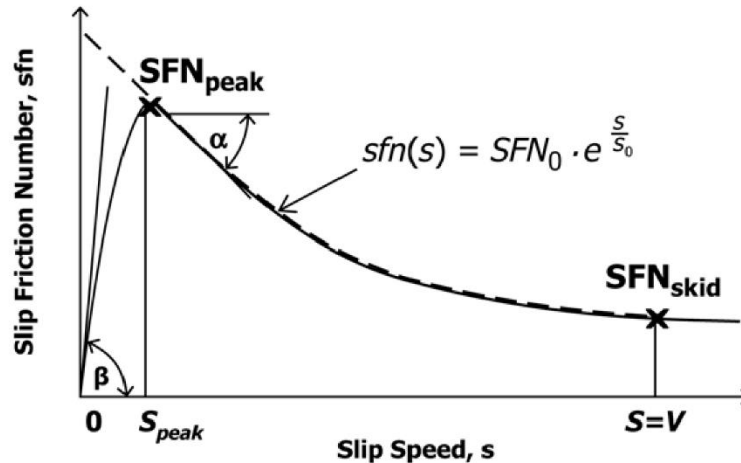
Figure A.22. Sample slip friction number trace versus slip speed (*29*).

The equation shown in the figure:

$$sfn(s) = SFN_0 \cdot e^{\frac{s}{s_0}}$$

Ribbed vs Smooth Tires

The standards for the test presented above specify that the friction can be measured either using a ribbed tire (ASTM E501) or a smooth tire (ASTM E524) as shown in Figure A.27. However, Fuentes et al. (*30*) have reported that the friction measurements obtained when using a locked wheel tester with ribbed and smooth tires resulted in different friction–speed curves for the same pavement surface, contrary to the stated ASTM assumption that the friction–speed curve depends only on the characteristics (macrotexture) of the pavement surface. Moreover, skid measurements obtained at different speeds using ribbed tires were insensitive to pavement macrotexture. This supports the benefits of using smooth tires, which are sensitive to the drainage capacity of pavement surfaces.

Figure A.23. Smooth vs ribbed tire (*30*).

A similar finding was reported in the North Carolina DOT 2017 research project (*28*), where the authors evaluated pavements with different macrotexture levels and found that the friction values recorded with a smooth tire reflected the variation of the macrotexture values, while the friction values recorded using a ribbed tire were insensitive to macrotexture variations.

Equipment for Measuring Friction

There are several different types of equipment available for measuring friction, some are capable of measuring friction by different methods, and some are capable of recording friction in a continuous base. Table A.2 and Table A.3 provide an overview summary of these equipment.

Table A.2. Summary of skid resistance measuring devices (*6*).

Title	Measurement Principle[a]	Main Parameters[b]	Tire and Wheel Load	Measurement Location
ADHERA	LFC	Water film thickness: 1 mm; Measures macrotexture; Speed: 40, 60, 90, 120 km/h; Interval: 20 m.	PIARC smooth profile tire 165R15 (180 kPa); Wheel load: 2500 N	Nearside right wheel path
BV-11	LFC	Slip ratio: 0.17 or 17%; Water film thickness: 0.5 to 1.0 mm; Speed: 70 km/h; Interval: 20 m.	Trelleborg type T49 tire (140 kPa); Wheel load: 1000 N	Right or left wheel path
GripTester	LFC	Slip ratio: 0.15 or 15%; Water film thickness: 0.5 mm; Speed: 5–100 km/h; Interval: 10–20 m or other.	254 mm diameter smooth profile ASTM-tire (140 kPa); Wheel load: 250 N	Normally nearside right or left wheel path, or as required
RoadSTAR	LFC	Slip ratio: 0.18 or 18%; Water film thickness: 0.5 mm; Measures macrotexture; Speed: 30, 60 km/h Interval: 50 m.	PIARC tire with tread; Wheel load: 3500 N	Nearside the wheelpath, right or left
ROAR DK	LFC	Slip ratio: 0.2 or 20%; Water film thickness: 0.5 mm; Measures macrotexture; Speed: 60, 80 km/h; Interval: >5 m.	ASTM 1551 tire (207 kPa); Wheel load: 1200 N	Both wheel paths
ROAR NL	LFC	Slip ratio: 0.86 or 86%; Water film thickness: 0.5 mm; Measures macrotexture; Speed: 50, 70 km/h; Interval: 5–100 m.	ASTM 1551 tire (200 kPa); Wheel load: 1200 N	Nearside the wheelpath, right or left
RWS NL Skid Resistance Trailer	LFC	Slip ratio: 0.86 or 86%; Water film thickness: 0.5 mm; Speed: 50, 70 km/h; Interval: 5–100 m.	PIARC smooth profile tire 165R15 (200 kPa); Wheel load: 1962 N	In the wheel path of nearside lane
SCRIM	SFC	Slip angle: 20°; Water film thickness: 0.5 mm; Measures macrotexture; Speed: 50 km/h; Interval: >10 m.	Avon SCRIM smooth profile tire 76/ 508 (350 kPa); Wheel load: 1960 N	Normally nearside wheel path or as required
Skiddo-meter BV-8	LFC	Slip ratio: 100% or 14%; Water film thickness: 0.5 mm; Speed: 40, 60, 80 km/h; Interval: 30–50 m.	AIPCR tire with longitudinal tread 165R15; Wheel load: 3500 N	Usually in one of the wheel path
SKM	SFC	Slip angle: 20°; Water film thickness: 0.5 mm; Speed: 50 km/h; Interval: 100 m or other.	Smooth profile tire; Wheel load: 1960 N	Normally nearside the wheelpath or as required
SRM	LFC	Slip ratio: 15% or 100%; Water film thickness: 0.5 mm; Speed: 40, 60, 80 km/h; Interval: 20 m or other.	AIPCR tire with longitudinal tread 165R15; Wheel load: 3500 N	Nearside wheel path, right or left
TRT	LFC	Slip ratio: 25%; Water film thickness: 0.5 mm; Speed: 40–140 km/h;	Smooth profile ASTM tire; Wheel load: 1000 N	Left side wheel path

Title	Measurement Principle[a]	Main Parameters[b]	Tire and Wheel Load	Measurement Location
		Interval: 20 m or other.		
SRT-3	LFC	Slip ratio: 100%; Water film thickness: 0.5 mm; Speed: 60 km/h.	Tire with tread (200 kPa)	-
IMAG	LFC	Slip ratio: 100%; Water film thickness: 1.0 mm; Speed: 65 km/h.	PIARC smooth profile tire; Wheel load: 1500 N	-
iSAVE	SFC	Slip angle: 20°; Water film thickness: 0.5 mm; Measures micro and macrotexture; Speed: 15 to 50 km/h.	-	-

[a] LFC = Longitudinal Friction Coefficient, SFC = Sideways Friction Coefficient
[b] Speed = Measurement Speed, Interval = Measurement Interval

Table A.3. Pros and cons of different friction equipment (*6*).

Name	Measuring Device View	Pros	Cons
ADHERA		The system includes a laser that measures macrotexture. The tire used in the test is a Smooth PIARC tyre.	The measures are taken at a 100% slip ratio, but the device is capable to varied for reseach purposes. Is not able to measure friction continuosly. A single test wheel.
BV-11		The water control system enables the specification of a defined water film thickness.	Operates on the longitudinal friction principle. The measures are taken at a single slip ratio of 17%. A single test wheel.
GripTester		Can be configured to be pushed manually for low-speed operation in confined areas. Used both in airports and highways.	Operates on the longitudinal friction principle. The measurements are taken at a fixed slip ratio of 15%. A single test wheel.
RoadSTAR		Measuring wheel includes braking to*Rq*ue measurement. Provides a continuos friction measurement. The slip ratio can be varied. The device also measure macrotexture. In front of the test wheel. Uses a ribbed tyre.	Operates on the longitudinal friction principle. A single test wheel.
ROAR DK		Variable slip ratio. The device is fitted with a laser for macrotexture measurements. Continuous friction measurement equipment.	Operates on the longitudinal friction principle. A single test wheel.

Name	Measuring Device View	Pros	Cons
ROAR NL		Huge water tank capacity of 12000 L. The slip ratio can be specified between 5 to 95%. A laser system in fitted in the front of the vehicle for macrotexture measurement. The friction is measured continuosly.	Operates on the longitudinal friction principle. A single test wheel which can be aligned in three positions: left, center and right.
RWS NL Skid Resistance Trailer		Uses a smooth tyre according to the PIARC standards. An expert operator can measure friction in the center or in the wheel paths.	A single measuring wheel mounted in the center of the trailer. A fixed slip ratio of 86%. Longitudinal friction. A single point friction value.
SCRIM		The device operates on the transverse friction principle and uses a special narrow test wheel. The test wheel is mounted exactly between the front and rear tyre, so it runs inside the wheel path. Fitted with a laser for measuring macrotexture. Measures friction continuosly using a variable slip ratio.	It cannot measure friction in the center.
Skiddo-meter BV-8		Measures friction continuously or for a single point. The test can be made with the test wheel either fully locked or with a slip ratio of 14%.	Longitudinal friction principle. A single test wheel in the center of the trailer. Only two slip ratio options.
SKM		This device is based on the SCRIM, so it uses the transverse friction principle with a narrow test wheel. Continuous friction measuring device with a variable slip ratio.	It cannot measure friction in the center.
SRM		Uses two wheel test, located in each wheel path. Can measure friction with a variable slip ratio or with the wheels fully locked.	Longitudinal friction principle.
TRT		Continuous friction measuring equipment. Variable slip ratio.	Operates under the longitudinal friction principle. Is not manufactured under license.

Name	Measuring Device View	Pros	Cons
SRT-3		Can varied the position of the test wheel.	Use the longitudinal friction principle. Uses a single slip ratio of 25%.
IMAG		Uses the standard PIARC smooth test tyre.	Use the longitudinal friction principle. Uses a single slip ratio of 25%.
iSAVE	· Continuous friction me · 15 to 55 mph	A continuous measuring device, capable of measuring friction, macrotexture and microtexture. It uses the transverse friction principle. Measures both wheel path simultaneously.	--

Pavement Friction Modeling

As have been shown in previous sections, the skid resistance reduces with the increase of the side-slip speed, especially in wet conditions. For this reason, a single-point measurement of skid resistance is inadequate to represent the friction performance of a pavement. This limitation of a single-point skid resistance value may be overcome using a two-parameter skid resistance model. There exist two widely known two-parameter skid resistance models, namely the Penn State model and the PIARC International Friction Index model (*31*).

Both models attempt to predict the same behavior, which is shown graphically in Figure A.24. As can be seen from this figure, the friction performance with the slip-speed (*S*) can be separated into two regions, the first region, indicated with a "1" in Figure A.24, is the transition from the free rolling mode to the slip speed at which the friction number is a maximum (SN_{peak}), and the second region, indicated with a "2" in the figure, represents the exponential decay of the friction number from SN_{peak} to SN_{skid} as a function of the slip-speed. Both the Penn State and the PIARC models only describe Region 2.

The Penn State model includes two parameters, the theoretical intercept of the friction number at zero-slip (SN_0) and a constant C_1 that is obtained through a regression analysis. Is important to notice that this model is valid only for slip-speeds greater than S_{peak}. The model is shown in Equation (36).

$$SN = SN_0 e^{C_1 S} \tag{36}$$

The World Road Association Mondiale de la Route (*PIARC*) model was developed because different friction measuring equipment gives different values for the same pavement surface, see for example the results presented by Flintch et al. (*28*). Thus, harmonization is used to adjust the outputs of the different equipment so that they all report the same value for the same pavement condition. As a result of the harmonization and *PIARC*'s standing as an international agency, the *PIARC* model is also known as the International Friction Index (IFI).
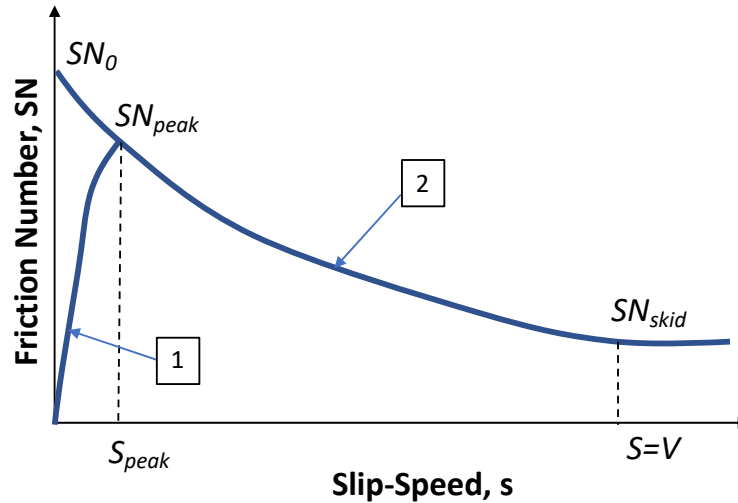
Figure A.24. Graphical representation of the two-parameter friction models.

The IFI consists of two parameters, one is the wet pavement friction (S_p) that is related with the *MPD*, and the other is the calibrated wet friction at 60 km/h (approximately 40 mph) denominated as *F60*. Normally, the friction is measured at a different speed (*V*) and is adjusted using a model similar to the one presented in Equation (36), so when the IFI is reported one have to include both the S_p and *F60*.

The calculus of the IFI consist of the following steps (ASTM E1960-07):

1. Measure and compute the *MPD*
2. Measure the friction at a given speed *V*, this will be the *FR(V)*.
3. Calculate the speed constant, S_p in km/h, using the following equation:

$$S_p = 14.2 + 89.7 \times MPD \tag{37}$$

4. Using the S_p coefficient obtained in the last step adjust the friction measurement made at the speed *V*, i.e. *FR(v)*, to obtain the friction at 60 km/h, i.e. *F(60)*, using the Equation (38).

$$F(60) = FR(v) \times e^{\frac{(v-60)}{S_p}} \tag{38}$$

5. The final step in the harmonization is the calibration of the equipment used for measurement, by regression of the adjusted measurement *FR(60)*, with the calibrated friction number *F(60)*:

$$F(60) = A + B \times FR(60) \tag{39}$$

Previous North Carolina DOT Research Efforts

The purpose of the North Carolina Highway Safety Improvement Program (HSIP) is to provide a continuous and systematic process that identifies, reviews, and addresses specific traffic safety concerns throughout the state. A system of safety warrants is developed to identify locations that are possibly deficient. Different variables are used to predict crash occurrence, like the road geometry, traffic, vehicle speed, etc. However, even though the North Carolina DOT has been measuring friction using a LWST, they have not tried to use friction as a predictor of crashes. Moreover, the North Carolina DOT has not measured and published on widespread pavement

macrotexture measurements. Some research projects that the North Carolina DOT has conducted to study the friction phenomenon of its assets are presented below.

Corley-Lay - 1998

One of the first projects in North Carolina to understand the effect of pavement surface properties on friction was made by Corley-Lay in 1998 (*32*). In her work, Corley-Lay studied 14 different pavement sections located in Greenville, North Carolina. The friction was measured for each section using three different LWSTs. The study included seven different road types: a heavy-duty surface course, polymer-modified heavy-duty surface course with carbon black, stone mastic with fibers, polymer-modified stone mastic, and large stone surface course. In addition, for each one of these surfaces, the BPN test and the sand patch test were conducted, obtaining the values presented in Table A.4.

Table A.4. Sections description, partial gradation and additive information, and average results from british pendulum and sand patch testing for test sections (*33*).

Section	Description	Sieve Size for 95% passing	% - 200	BPN (avg of 4) (Std. Dev)	Macrotexture (mm) (Std. Dev)
1	Heavy Duty Surface-Control Section	3/8	2-8	61.9 (3.29)	0.62 (0.006)
2	Polymer Modified HDS	3/8	2-8	56.6 (3.76)	0.76 (0.009)
3	Large Stone Surface & Binder	3/8	4-8	60.9 (2.04)	0.73 (0.015)
4	Carbon Black added to HDS	3/8	2-8	60.3 (1.27)	0.56 (0.006)
5	Rubber Modified HDS	3/8	2-8	60.6 (1.41)	0.78 (0.009)
6	Polymer Modified Stone Mastic	1/2	8-10	58.4 (1.58)	0.89 (0.013)
7	Stone Mastic with Fibers	1/2	8-10	60.5 (1.18)	0.89 (0.004)
8	Carbon Black added to HDS	3/8	2-8	58.1 (1.36)	0.51 (0.010)
9	Polymer Modified Stone Mastic	1/2	8-10	67.6 (0.88)	0.94 (0.011)
10	Polymer Modified HDS	3/8	2-8	65.6 (2.01)	0.82 (0.007)
11	Stone mastic with Fibers	1/2	8-10	67.8 (2.55)	1.07 (0.011)
12	Heavy Duty Surface-Control Section	3/8	2-8	64.3 (1.56)	0.78 (0.004)
13	Rubber Modified HDS	3/8	2-8	64.5 (2.58)	0.73 (0.006)
14	Large Stone Surface & Binder	3/8	4-8	62.9 (1.88)	0.822 (0.006)

In 2008, Pulugurtha et al. (*33*) presented the research report FHWA/NC/2007-12: "Relationship between Pavement Macrotexture and Crash Incidences on North Carolina Roads", which evaluated the role of pavement macrotexture in crashes on selected roads in the state of North Carolina. Scatter plots, bivariate analysis and multivariate analysis showed that a strong relationship exist between pavement macrotexture and crash incidences on NC roads. Pavement macrotexture greater than or equal to 0.06 in. (1.524 mm, but typically less than 3.048 mm) would be more appropriate to provide safe and efficient transportation to road users.

In their study, Pulugartha et al. has collected pavement profiles using Roadware ARAN Model 4100 until the fall of 2003, after that year the North Carolina DOT started using the ICC Profiler Model MDR 4085. The first profiler collected elevations in millimeters, approximately every 8 in. (0.2 m), the second profiler could collect elevations every 1.242 in. (0.032 m) and the elevations reading were in inches. Although the profile data were collected to measure roughness and rutting rather than pavement macrotexture, a procedure for calculating the *MPD* with these profiles were used.

Finally, one of the main contributions to the state of the art for implementing a Pavement Friction Management (PFM) program in North Carolina was made by Flintsch et al. (*28*) as a result of the project FHWA/NC/2017-02 "Evaluation of Methods for Pavement Surface Friction, Testing on Non-Tangent Roadways and Segments". The results of this this study included:

1. A comparison of friction measurements obtained with three different devices and methodologies, including the Loch-Wheel Skid Tester (LWST – ASTM E274), and continuous average friction measurement equipment like the Grid Tester, and the SCRIM (Side-Force Coefficient Routine Investigation Machine).

2. Recommendations and guidance with regard to the feasibility of collecting continuous friction and macrotexture data to define investigatory friction and macrotexture levels to support the state's pavement friction management program.

To meet these objectives the author's included 17 different roadways loops for measuring friction using the Grid Tester and the SCRIM, including different geometries (curves, intersections, ramps, and super-elevation) and four different surface types: i) dense graded asphalt concrete (DGAC), ii) open graded friction coarse (OGFC), iii) Bituminous surface treatment (chip seal), and iv) portland cement concrete pavements (PCCP). Additionally, the North Carolina DOT measured friction using its current state of practice, i.e., the LWST with either a ribbed (15 of the 17 loops) or smooth (2 of the 17 loops) tire. Table A.5 summarizes the test configuration used by each one of the devices.

Table A.5. Friction measurement setup.

	LWST	Grid Tester	SCRIM
Tire Configuration	Ribbed and Smooth	Smooth Tread	Smooth
Slip-Ratio	Fully-Lock	16%	34%
Tire Alignment	Longitudinal Oriented with the Vehicle movement direction	Longitudinal Oriented with the Vehicle movement direction	Free rolling test wheel, oriented with a yaw angle of 20° with respect the movement direction
Measurement Interval	Every 0.5 miles (805 m)	Every 3 feet (0.914 m)	Every 100 mm and then average every 10 m.
Outputs	Skid Number (SN)	Grid Number (GN)	Scrim Reading (SR)
Standardized Speed	40 mph	40 mph	30 mph

To compare the GN and the SR with the SN, each one of the measures were geo-referenced and the GN and the SR values were averaged over a 30-meter footprint around the SN readings (15 meters before and 15 meters after the SN measurement location). After a first inspection of the data, the research team identified two main issues with the LWST readings:

1) A high percent of the readings used a water dispense outside the allowable range (±10%)

2) The speed corrections made by the skid-tester system were not apply properly, because the software was out of date.

As a solution, those readings that used a water dispense outside the range were discarded, and the remaining data were processed using a speed correction factor developed by the authors from a locked-wheel test at the Virginia Smart Roads in Blacksburg.

Two different types of regression models were developed, an ordinary Linear Regression Model, and an Orthogonal Linear Regression (blue line and red line in Figure A.25, respectively). In the former type of model only one of the variables is assumed to have a random error term, and the model is obtained minimizing the sum of the square of the vertical distance between the data and the fitted line. In the second type of model, both the predictor and the response are assumed to have an error term associated, so instead of minimizing the sum of the square of the vertical distance between the data and the fitted line, the coefficients are obtained minimizing the sum of the square perpendicular distance between the data and the fitted line.

For comparing the outputs of each device at the same level basis, the friction values were averaged at 10 m and 100 m and were compared at their own reference speed (see Table A.5) as indicated in Figure A.25 (a) and (b), also the values were harmonized using the *PIARC* model (see section 0) and the results are presented in Figure A.25 (c) and (d). The results are presented in Figure A.25. As can be seen, a better correlation was obtained when both friction outputs were standardized using the *PIARC* model.

Then, to compare the SN (measured by the LWST) with the GN and the SR, the authors divided the analysis by the type of wheel used in the LWST device, i.e. ribbed and smooth. The results are presented in Figure A.26 and Figure A.27, as can be seen, SN-ribbed better relates with the SCRIM reading, while the SN-smooth correlates more with the GN.

According to the authors, this finding is congruent with the finding presented by other researchers, for example Fuentes et al. (2014) (*30*) realizes that the SN obtained with a ribbed tire seems to be insensitive to changes in the *MPD*, while the SN obtained with a smooth tire is somewhat sensible to a variation in the *MPD*.

Based on the results, one can infer that the SR are less sensitive to the *MPD* than the GN.

To bring recommendations and guidance to establish a PMF program in North Carolina, the authors of this study presented a detailed literature review of the current state of the art. Based on this review was recommend the following:

- It is important to develop a PMF program, in which both the friction and macrotexture are monitored together. Based on the operation cost and the amount of data collected, it was recommended to use a CFME that will be capable of measuring friction and macrotexture.
- Several studies have been successful in correlating *MPD* with crashes. Results conflict somewhat regarding macrotexture's impact on wet-weather crashes, but there is more consensus on its impact on total crashes.
- The researchers recommended that for speeds greater than 50 mph, the as constructed macrotexture of the pavement *MPD* should be greater than 0.8 mm, and for speeds greater than 70 mph, the as constructed macrotexture of the pavement *MPD* should be greater than 1.0 mm.
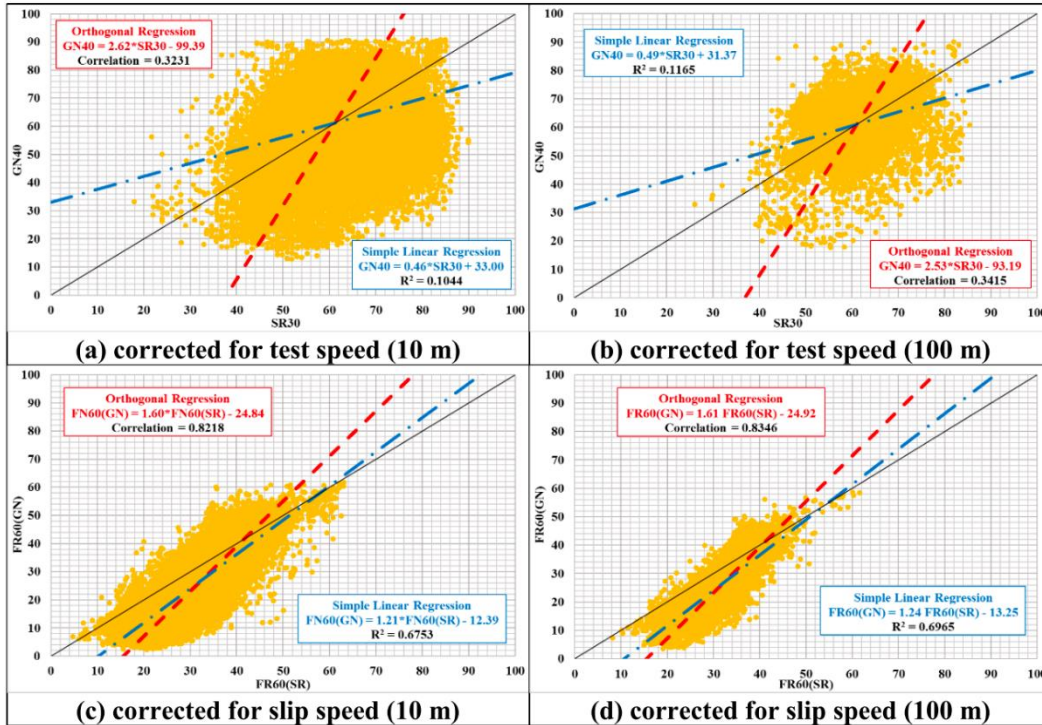
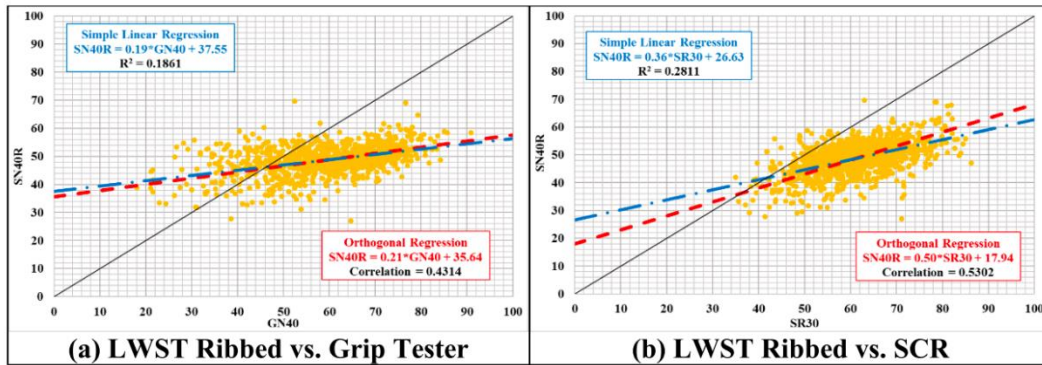**Figure A.25. Comparison of grip tester and SCRIM (*28*).**

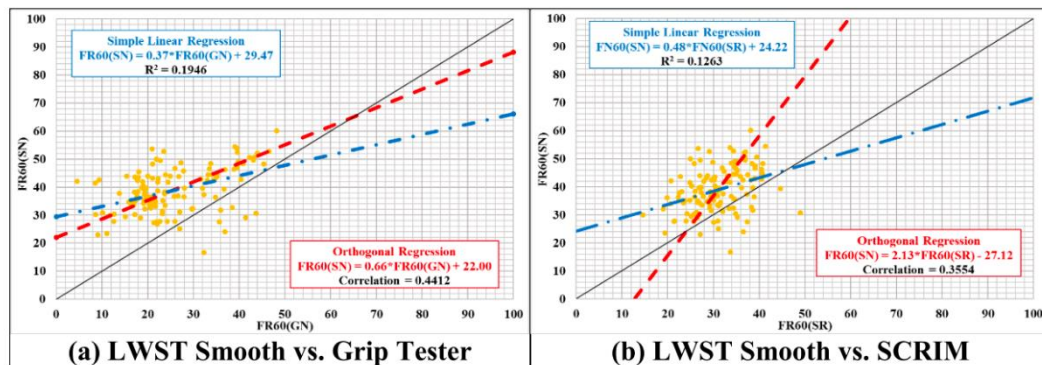**Figure A.26. Comparison with LWST ribbed tire (*28*).**

Figure A.27. Comparison with LWST with smooth Tire (*28*).

Friction Treatments

The pavement surface characteristics like the aggregate quality, gradation and binder content are controlled during the mix design. According to Kogbara et al. (*6*), the aggregate gradation and the finish quality of the surface mix determines the surface macrotexture, which affects the surface drainage, but has a minor effect in the microtexture. Typically, there are three mix design methods: Hveem, Marshall and Superpave Mix design, all three are based on volumetric analysis, but only the Superpave Mix design considers pavement performance during the design. Table A.6 presents the main texture characteristics obtained by the most common mix types.

In 2015 Merritt et al. (*40*) conducted a study to isolate the effects of various low-cost pavement treatments on roadway safety. This study was retrospective of pavement safety performance, looking back at crash data before and after treatments were installed. Both flexible and rigid pavement treatments were analyzed, with the majority typically used for pavement preservation or minor rehabilitation purposes. In this study a detailed description of the different treatments available to restore and to improve the safety performance were presented, the treatments may be grouped into three main categories overlay treatments, roughening treatments and seal treatments. The information presented in the next sub-sections are based mostly on the work of Merritt et al.

Overlay Treatments

This type of treatment involves the removal of a thin layer of asphalt concrete, typically 1 in. to 2 in., and replace it by a new layer of the same thickness. The main purpose is to provide a new surface, remove cracks and restore the friction properties of the pavement.

Thin Hot Mix Asphalt Overlay

Thin *HMA* overlays are commonly used to correct minor to moderate pavement surface defects to restore ride quality and improve friction while protecting the underlying pavement structure. The overlay typically is preceded by a milling of the existing surface of 1 in. to 2 in., and they are not considered as a new layer.

Open Graded Friction Course (OGFC)

This treatment is used in areas with high rainfall intensity but is not recommended for colder climates because of their poor performance during the freezing-thaw cycles. Similar to the *HMA* thin overlay, an *OGFC* is not considered a separate structural layer and can be placed on surfaces with low to moderate surface damage (with not damage coming from the bottom layers) and are typically used to increase the surface drainage, to renew the functional performance of a pavement, including ride quality, friction, and tire–pavement noise.

Ultra-Thin Bonded Wearing Course (UTBWC)

This is a special ultra-thin asphalt overlay used to restore ride quality while sealing and protecting the underlying pavement. Is a non-structural layer, typically of 0.5 in. to 0.75 in. thick and generally uses a gap-graded aggregate and polymer modified asphalt, it can be used on surface with low to minor rutting and cracking, and low to minor raveling and bleeding.

Table A.6. Frictional properties of asphalt mix classifications (6).

Mix Type	Texture-Based Mix Category	Description and Salient Details (3, 34, 35)	Comments on Frictional Properties
Hot Mix Asphalt (*HMA*)	Dense-Graded HMA	Well- or continuously graded mixture of coarse and fine aggregates, mineral filler and 5-6% asphalt binder. Categorized by nominal maximum aggregate size (ranging from 9.5 mm to 19 mm) into fine-graded and coarse-graded. Proper design and placement lead to relatively impermeable mixes. Mixes are suitable for all pavement layers and traffic conditions.	Has similar microtexture values to gap - and open-graded mixes. Shows lower macrotexture depths (typically 0.4-0.6 mm for fine-graded and 0.6-1.2 mm for coarse-graded) than gap- and open-graded mixes (*3, 36*).
	Gap-Graded HMA or Stone Matrix Asphalt (SMA)	Aimed at creating stone-on-stone contact within mixture to improve the tire grip and rutting (deformation) resistance. Contains more durable aggregates, higher (polymer-modified) asphalt content (6-9%), fillers and fibers. Provides benefits of wet weather friction and lower tire noise due to its coarser surface texture.	Shows macrotexture depths typically exceeding 1 mm but higher than those of dense graded mixes (*3, 36*). Larger coarse aggregate sizes in the mix gives better performance and rut resistance (*37*).
	Open-Graded Friction Course (OGFC)	Designed to be water permeable. Hence, uses mostly coarse aggregates, small percentage of sand/mineral filler and 3-6% asphalt binder. Must contain >15% air voids.	Shows similar microtexture values to other mixture types but larger macrotexture (typically of 1.5-3 mm depth). Observed to show higher friction values than gap- and dense-graded mixes (*3, 36, 38*).
Warm Mix Asphalt (WMA)	-	Manufactured with less fossil fuels and includes binding materials and additives such as wax, emulsions and zeolites for easy pouring (reduced viscosity) and spreading at low temperature.	Showed no significant difference in early age skid resistance compared to HMA pavements. Has comparable or superior rutting resistance to HMA mixes (*39*).

Roughening Treatments

This type of treatment is used for friction restoration or to increase the friction levels on high-friction demand locations.

High Friction Surfacing

High Friction Surfacing (*HFS*) involves the application of very high-quality aggregate (resistant to polishing and abrasion) to the pavement using a polymer binder to restore and/or maintain pavement friction at existing or potentially high crash areas. The higher pavement friction helps motorists maintain better control in both dry and wet driving conditions. This treatment is used

mainly as a safety improvement and allows enhancing or providing friction for those network spots where the friction is high. The treatment consists in applying the binder resin to the pavement surface and then dropping the aggregate.

Micro-Milling

Whereas milling is typically used to remove pavement in preparation for an overlay, micro-milling leaves a much less aggressive surface texture that can be opened to traffic as a final surface. Micro-milling removes old, oxidized pavement and previous surface treatments thus providing a surface which is more receptive to bonding to the new surface treatment.

Shotblasting/Abrading

This is a surface treatment in which steel pellets or "shot" are fired at the pavement surface at high velocity to pit or abrade away a superficial layer of the pavement surface. Shotblasting removes any loose material from the surface and also pits the surface of the aggregates to improve microtexture. It is frequently used to remove rubber or oil deposits on the pavement surface. For example, this treatment is commonly used by airports to remove rubber deposits on runways. For roadways, this treatment is more commonly used for surface preparation prior to applying another surface treatment.

Seal Treatments

Slurry Seal

This treatment is used for improving appearance, restoring, or enhancing friction, and to seal the pavement surface to avoid water infiltration to the underlaying structure. The slurry seal is a mixture of emulsified asphalt, water, fine aggregate, and mineral filler that is mixed into a slurry and applied onto the pavement surface in a thin layer using squeegees or a spreader box.

Microsurfacing

Microsurfacing is pretty like the slurry seal, however, is typically more durable and can be used for higher volume roads. The main difference between a microsurfacing and a slurry seal is that the former uses a polymer-modified asphalt emulsion. Microsurfacing is primarily used to mitigate raveling and oxidation of asphalt pavement surfaces, but also improves friction and appearance of both asphalt and concrete surfaces.

Chip Seal (Seal Coat)

The chip seal is a common bituminous pavement preservation treatment used to seal fine cracks in the pavement surface and prevent water intrusion into the underlying pavement structure, while sustaining or improving pavement friction. Chip seals are constructed by first applying a bituminous membrane (typically a polymer modified asphalt emulsion) onto the existing pavement followed by a layer of aggregate or "chips," which are dropped onto the surface then rolled to embed them in the binder. As a disadvantage chip seal is susceptible to chip loss, which can result in flying chips and broken windshields, and are therefore not commonly used on heavily traveled urban roadways. Also, there may be a period of time right after the seal application where the friction may be lower because of the loose chips and because the chips are covered by bitumen. After a certain wearing period, where the aggregates get exposed, the friction increases due to an increase in macrotexture.

Cape Seal

Cape seal is a surface treatment consisting of a chip seal followed by a slurry seal. After the chip seal is applied and cured, the slurry seal is used to cover the chip seal. The advantage of this treatment is that the chip seal seals and protects the underlying pavement, while the slurry seal helps to protect the chip seal, locking the chip seal aggregate in place to minimize chip/aggregate loss and providing a smoother final surface.

Scrub Seal

This is a treatment in which a bituminous material (emulsion or asphalt binder) is scrubbed into the surface of a heavily cracked asphalt pavement using brushes, after this a cover of aggregates is spread over the emulsion, like a chip seal. The scrubbing action helps the emulsion to penetrate the crack depths and sealing the surface, stopping the water for infiltrating the underlying structure. This treatment is suitable if the underlying layers are in good condition.

Table A.7. Typical macrotexture depth for various pavement treatments (*40*).

Type of Treatment	Pavement Treatment	Typical Macrotexture Depth
Overlay	Thin Hot Mix Asphalt Overlay	0.4 to 0.6 mm (Dense Graded) > 1.0 mm (Stone Matrix Asphalt)
	Open Graded Friction Course (OGFC)	1.5 to 3.0 mm
	Ultra-Thin Bonded Wearing Course (UTBWC)	> 1.0 mm
Roughening	High Friction Surfacing (HFS)	> 1.5 mm
	Micro-Milling	Typically exceeds 1 mm
	Shotblasting/abrading	0.6 to 1.2 mm
Seal	Slurry Seal	0.3 to 0.6 mm
	Microsurfacing	0.5 to 1.0 mm
	Chip Seal (Various binder type)	> 1.0 mm

Pavement Friction and Surface Analysis

In previous sections a summary with the main techniques for measuring pavement surface texture and friction was presented, now in this section a compendium of the work that have been done to evaluate the different variables that affect friction over time is analyzed.

Friction Performance

Although pavement friction is one of the main factors to control for reducing wet-pavement crashes, the current asphalt mix design does not directly included friction as a variable in the design. Bu and Abadie (2018) (*41*) developed a surface friction prediction model that can be used during a wearing course mixture design. In their study, they used twelve wearing course mixtures typically used in Louisiana, including dense-graded and open-graded mixes with different aggregate sources. Each one of these mixtures were evaluated in the lab using an accelerated polishing procedure. Then, friction and macrotexture were measured in the field in a total of 22 projects. The in-situ measurements were collected using a DFT, a CTM and a LWST. According to Bu and Abadie, designing a coarse mixture so that the pavement surface will have adequate friction over its life involves identifying an appropriate combination of micro and macrotextures

and also requires a balanced understanding between economic and engineering tradeoffs associated with selecting different mixes and aggregate material types.

Since current HMA specifications do not provide any standard friction test procedure during mix design, a polishing and friction testing procedure developed at the NCAT for rapidly evaluating the frictional performance of HMA mixtures was applied. The NCAT procedure may be summarized as follows:

- The Polished Stone Value (PSV) Test is conducted for each aggregate type.
- The British Pendulum Number is obtained (*BPN*) for the embedded aggregate samples.
- Using an accelerated polishing machine, called the Three Wheel Polishing Device (TWPD), to simulate surface wear, see Figure A.28 (a). The normal load during the test is 468 N (105 lb.) with tire pressure of pneumatic tires maintained at 2.9 MPa (50 psi).
- Evaluate the friction performance using the DFT after 5000, 10000, 30000, 50000, and 100000 cycles with the TWPD, see Figure A.28 (b). During the polishing cycles water is continuously sprayed to simulate a wet polishing in the field.
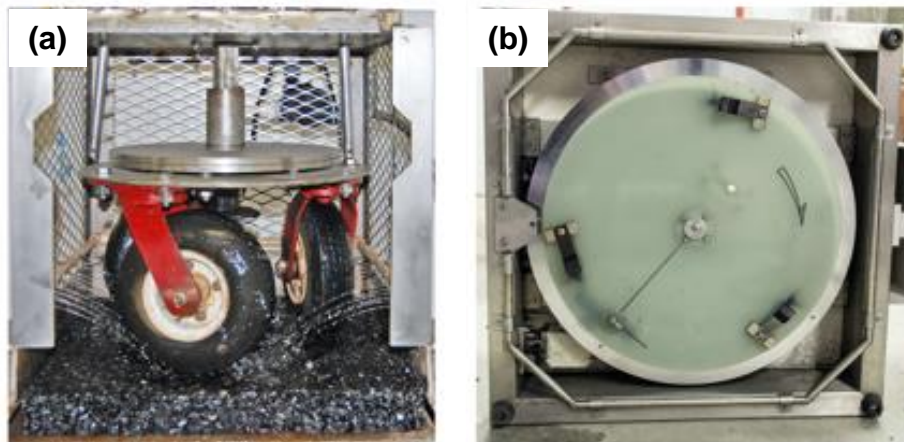

Figure A.28. NCAT accelerated polishing and testing devices; (Left) three wheeled polishing device and (Right) dynamic friction tester (*41*).

The main conclusions derived from the lab work conducted by Wu and Abadie, is that there is a peak value that typically occurs at 5000 to 10000 polishing cycles, primarily due to the development of an early surface roughness or texture on the coated aggregate particles (e.g., remove the excess binder from the surface and expose the aggregate). Also, they observed that the *MPD* has an initial peak value that later decreases to an asymptotic lower limit, typically after the first 5000 polishing cycles.

Using the lab results and the field measurements, the authors of this study proposed the friction prediction procedure shown in Figure A.29. This can be resume in two main parts, first determining the microtexture and second determining the macrotexture.
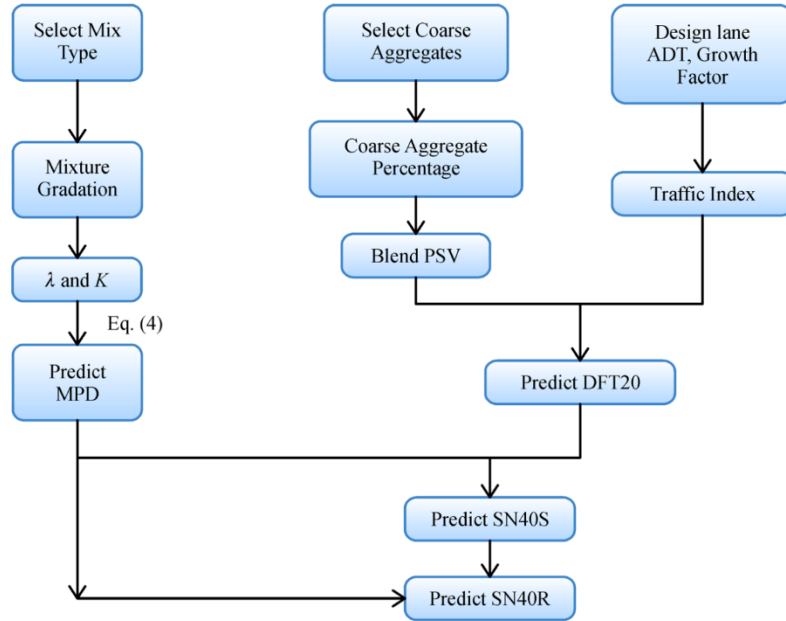
Figure A.29. Skid resistance prediction procedure (*41*).

According to the framework proposed by Wu and Abadie in Figure A.29 the microtexture friction contribution is determined by the Equation (40):

$$DFT20 = 0.13 \times e^{(-0.056 \times T.I.)} + 2.6 \times PSV \tag{40}$$

where *T.I.* is the traffic index (cumulative traffic expressed in millions of *ESALs*), the *PSV* is the polished stone value take as the weighted average of the aggregates used in the blend, and the *DFT20* is the friction number measured with the Direct Friction Tester at 20 km/h.

The macrotexture friction contribution is represented by the *MPD* which is determined as a function of the gradation curve, represented by the parameter λ and *K* (obtained from a Weibull distribution, see the Equation(41)). The *MPD* is predicted using the Equation (42).

$$F(x:K,\lambda) = 1 - e^{\left(-\frac{x}{\lambda}\right)^K} \tag{41}$$

$$MPD = 0.14 \times \lambda + 0.09 \times K - \frac{0.041}{K^4} \tag{42}$$

Finally, the expected friction value at 40 mph is calculated using Equation (43), for a smooth tire, and Equation (44) for a ribbed tire.

$$SN40S = 2.15 \times DFT20 \times e^{\left(\frac{0.54}{MPD}\right)} \tag{43}$$

$$SN40R = 0.93 \times SN40S - 0.16 \times MPD + 0.26 \tag{44}$$

These set of equations and the procedure presented in Figure A.29 can be used either to predict the friction based on aggregate PSV, gradation and traffic or may also be used to evaluate if a specific blend meets a minimum friction criterion.

Heitzman and Moore (*42*) evaluated the friction performance of eleven aggregates typically used in a *HSF* treatment, to do this the authors applied the same *NCAT* procedure used by Bu and Abadie (the accelerated polishing procedure of the *TWPD* and the *DFT*). Among the aggregates the authors evaluated were a calcinated bauxite, basalt, sand, two types of calcined kaolin (47-4x20 and 47-4x60) and different control samples.

The main results obtained by Heitzman and Moore are presented in Figure A.30, as shown the calcinate bauxite (RK bauxite) has the highest friction value, which explains why the FHWA has recommend its use in HFS treatment. Also, the highest macrotexture is obtained when the 47-4x20 (one of the calcinate kaolin sample) aggregate is used.
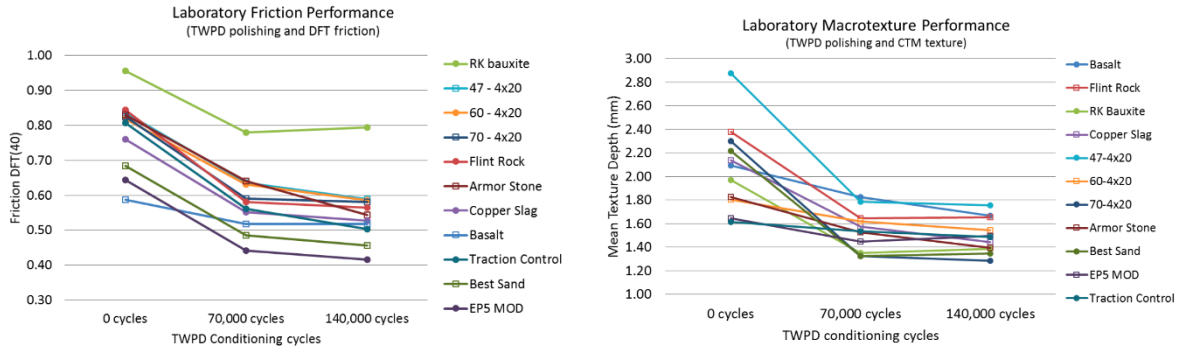

Figure A.30. Results obtained by Heitzman and Moore; (left) friction comparison and (right) macrotexture comparison (*42*).

Water-Film Thickness Effect

Cerezo et al. (*43*) studied the relation between water-film thickness and friction, the friction forces were measured with a locked-wheel tester coupled with an on-board wetting system that provides water depths varying from 0.1 mm to 1.50 mm. The authors found that the skid resistance is essentially independent of water film thickness at low speeds (30–50 km/h). However, it decreases with water depth at higher speeds. This effect is negligible for surfaces with high macrotexture, but considerably for surfaces with low macrotexture. Kogbara et al. (*6*) elaborated the graph presented in Figure A.31, comparing the results obtained by three different researchers.
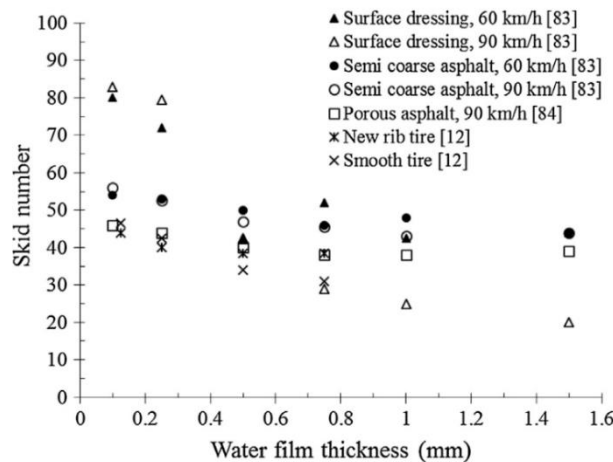

Figure A.31. Effects of water film thickness (*6*).

103

Kulawoski and Harwood (*44*) using a dedicated laboratory device performed friction tests at different water depths and found that the relationship between the friction coefficient and the water depth can be approximated by an exponential function, like the one shown in Figure A.32.
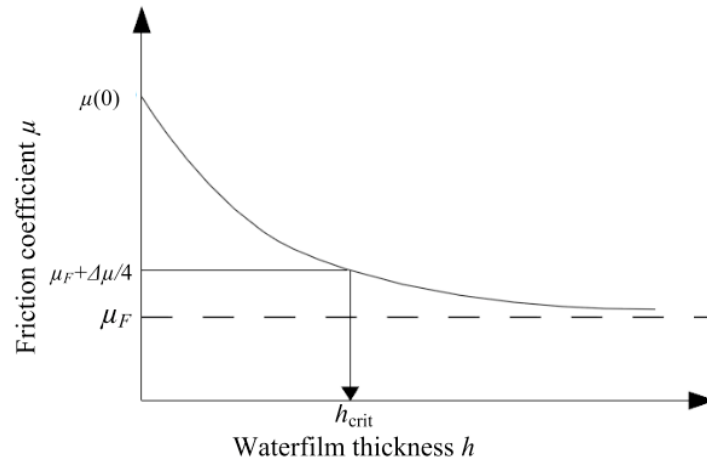

Figure A.32. Relationship between tire-pavement friction and water-film thickness (*44*).

Kulakowski and Harwood (*44*) supposed that the friction coefficient reaches a level, that is μ_F, at which there is no more variation by increasing water depths. These authors defined a critical water depth (h_{crit}) as the depth at which the dry friction $\mu(0)$ has lost an equivalent of 75% of $\Delta\mu$. The 75% threshold was chosen arbitrarily.
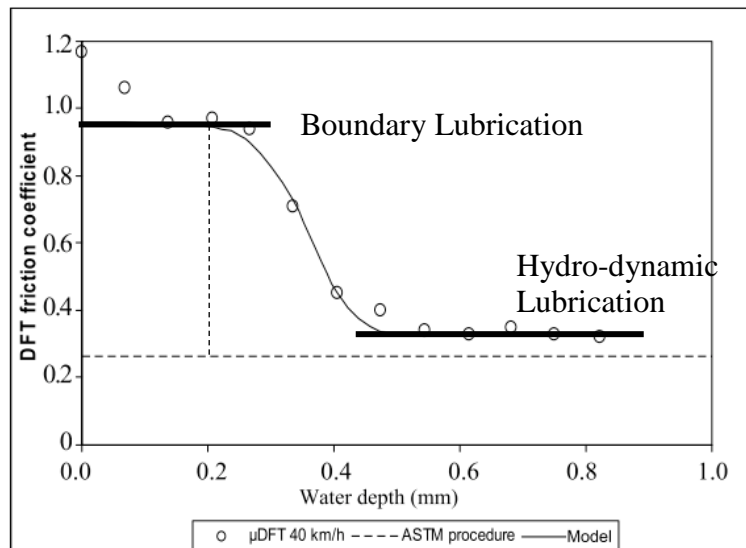
Figure A.33. Example of the variation of friction coefficient versus water-film depth (*45*).

Minh-Tan et al. (*45*) used a DFT to measure the effect of water film thickness in the samples prepared in the lab. These authors proposed a theoretical and experimental assessment of the friction-water depth relationship. The main objective was to estimate local water depths trapped between the tire and the road asperities and to define a so-called "critical" water depth, which can be used to detect risky situations for road users. It was found that the friction-water depth curves have an inverse-S shape and present an initial constant-friction part before decreasing to a minimum value. The specimens used in this study were 520 mm × 375 mm × 30 mm slabs. Four

104

slabs were produced in laboratory: a *VTAC* (very thin asphalt concrete) 0/6 (the numbers indicate the size range, in mm, of coarse aggregates); a *SCAC* (semi-coarse asphalt concrete) 0/6; a sand-asphalt and a mosaic composed of river coarse aggregates. The aggregate mosaic was sandblasted using 590 µm corundum particles to simulate a microtextured surface. An example of the results found by these authors is presented in Figure A.33.

Also, used a graph like the one shown in Figure A.33, Minh-Tan et al. (*45*) were able to identify a critical water-film thickness, defined as the point at which the friction starts changing from the boundary lubrication level to the hydro-dynamic lubrication level. In their experiments they found that the critical water depth varies with speed and may be as low as 0.15 mm when the vehicle speed is 60 km/h or as high as 0.35 mm when the vehicle speed is 20 km/h.

Finally, all the test methods presented in Section 0 specify that the test must be made using a constant flow of water, and according to the Table A.2 the water-film typically applied varies from 0.5 mm to up to 1 mm, meaning that most of the measurement are made at the worst condition when the friction values are lower, as shown in Figure A.31 and Figure A.33. However, because of the variation of the friction coefficients both with vehicle speed and water-film is necessary to conduct the friction measurement at different water-film thickness.

Influence of Environmental Factors

<u>*Influence of Temperature*</u>

The skid resistance of a wet road surface is greater in winter than in summer (*46*). Hence, the usual practice of measuring skid resistance during summer, when the lowest values are obtainable, and therefore critical for design (*6*). Different hypothesis has been made for explaining the seasonal variation of the skid resistance, one is that the stiffness of the tire rubber and the asphalt binder increase at colder temperatures, hence the hysteresis mechanism reduces. Also, in winter conditions maintenance operations tends to increase the microtexture of the aggregates, some photomicrographs of in-service pavements have shown that surface micro-roughness increases to a maximum during winter, and reaches is minimum during the summer (*47*).

An interesting work was presented by Ahammed and Tighe (2009), were they used the Long Term Pavement Performance Database (LTPP) in conjunction with a series of BPN measurements, obtaining the seasonal variation presented in Figure A.34 and in Equation (45).
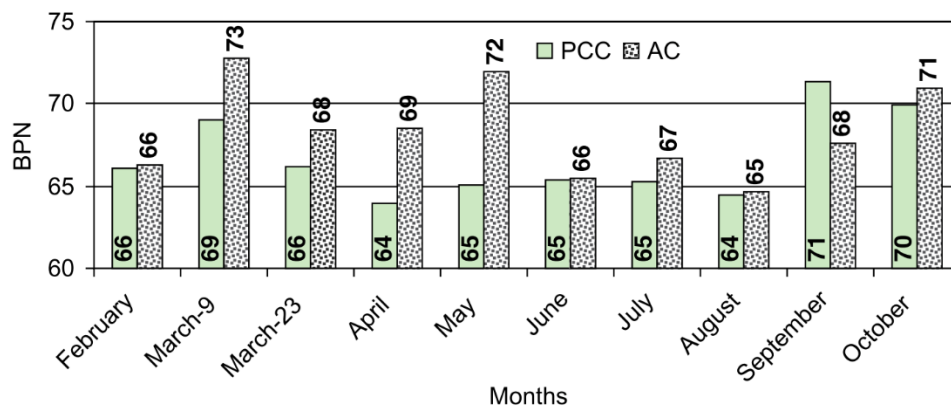

Figure A.34. Month to month variation of pavement surface friction (*46*).

$$BPN_T = 75.181 - 0.35 \times T \tag{45}$$

105

where T is the temperature at °C and BPN_T is the BPN at the temperature T.

Influence of Rainfall

Rainfall also causes a short-term variation in skid resistance. Water applied in skid tests done during the dry period mixes with the dust, detritus and oil thus reducing friction. In contrast, measurements made right after a rainfall will result in higher friction values because the surface is clean, and the water will be less viscous. It has also been shown that skid numbers decrease and reach a minimum value after 7 days of no rainfall. The lowest value is then maintained until the next significant rainfall after which it increases (*2*, *3*, *46*).

Useful Correlations

This research topic has attracted a substantial amount of interest from researchers who have subsequently developed some useful correlations for relating one or more measures of friction or friction related quantities to one another. The *IFI* standard provides the expression presented in Equation (46) and Equation (47) for converting the lock-wheel measurements to *BPN* and *MTD*, respectively.

$$BPN = 20 + 0.405 \times FN40R + 0.039 \times FN40S \tag{46}$$

$$MTD = 0.039 - 0.0029 \times FN40R + 0.0035 \times FN40S \tag{47}$$

where, *BPN* is the British Pendulum Number, *FN40R* is the friction number using a ribbed tire at 40 mi/h, *FN40S* is the friction number using a smooth tire at 40 mi/h, and *MTD* is the mean texture depth in inches.

Ong and Fwa (*48*) proposed the following expression to calculate the critical hydroplaning speed (HPS in miles per hour) as a function of the tire pressure in psi.

$$HPS = 10.35\sqrt{tire\ pressure} \tag{48}$$

The *NCHRP* 441 project (*49*) produced an equation to predict the *EMTD* as a function of the mix volumetric properties:

$$EMTD = 0.0198 \times MS - 0.004984 \times P_{200} + 0.1038 \times C_C + 0.004861 \times C_U \tag{49}$$

where, *EMTD* is the estimated mean texture depth (computed by laser measurements), *MS* is the maximum aggregate size in mm calculated as the smallest sieve size with 100 percent passing, P_{200} is the percentage passing the No. 200 (4.75 mm) sieve, C_C and C_U are given by Equations (50) and (51) respectively, and $D_{10\text{-}60}$ are the sieve sizes associated with 10%, 30% and 60% passing respectively, mm.

$$C_C = \frac{D_{30}^2}{D_{10} \times D_{60}} \tag{50}$$

$$C_U = \frac{D_{60}}{D_{10}} \tag{51}$$

Using a database of North Carolina DOT mix design characteristics compiled at NCSU, it was possible to apply the Equation 32 for different mixes used in North Carolina, as shown in Figure A.35. As shown the highest EMTD are obtained by mixes with a nominal aggregate size of 12.5 mm.
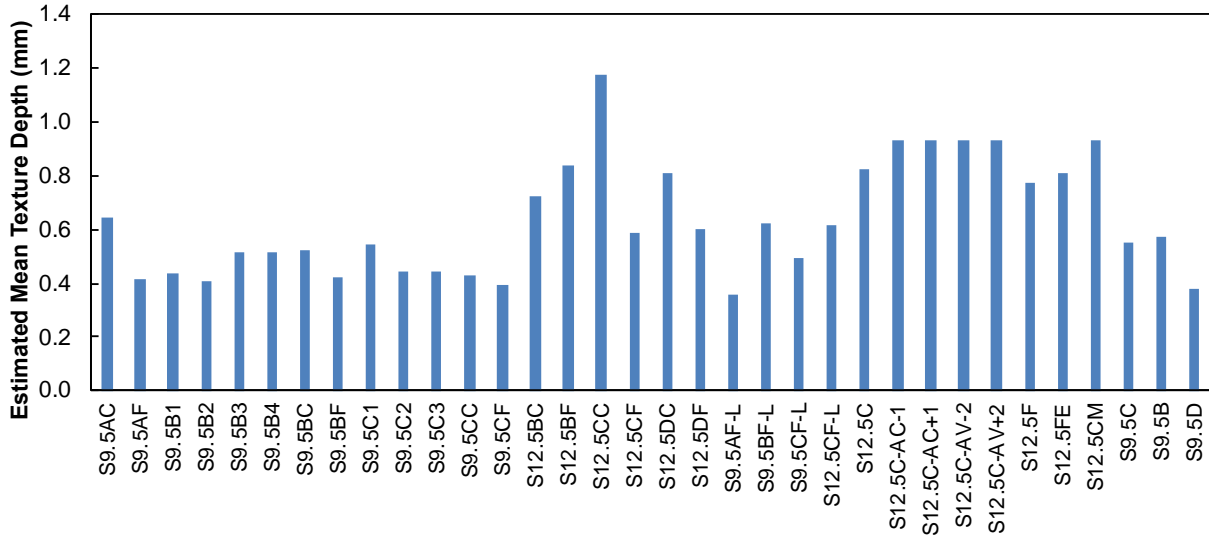
Figure A.35. EMTD for North Carolina mixes calculated using Equation 52.

Davis (*50*) presented a similar expression for calculating the *MPD*:

$$MPD = -3.596 + 0.1796 \times NMS + 0.0913 \times P_{200} - 0.0294 \times VTM + 0.1503 \times VMA \qquad (52)$$

Where, *MPD* is the mean profile depth, *NMS* is the nominal maximum aggregate size, P_{200} is the percentage passing the No. 200 (4.75 mm) sieve, *VTM* is the total voids in the mixture, and *VMA* is the voids in mineral aggregate. Similarly, using the NCDOT mix design database was possible to apply the Equation 52 for different mixes used in North Carolina, as presented in Figure A.35. As shown this equation produce higher variability in the resulting *MPD*, again some of the highest values are obtained for mixes with a maximum nominal aggregate size of 12.5 mm but there are some cases were mixes with a maximum nominal aggregate size of 9.5 mm have similar values.
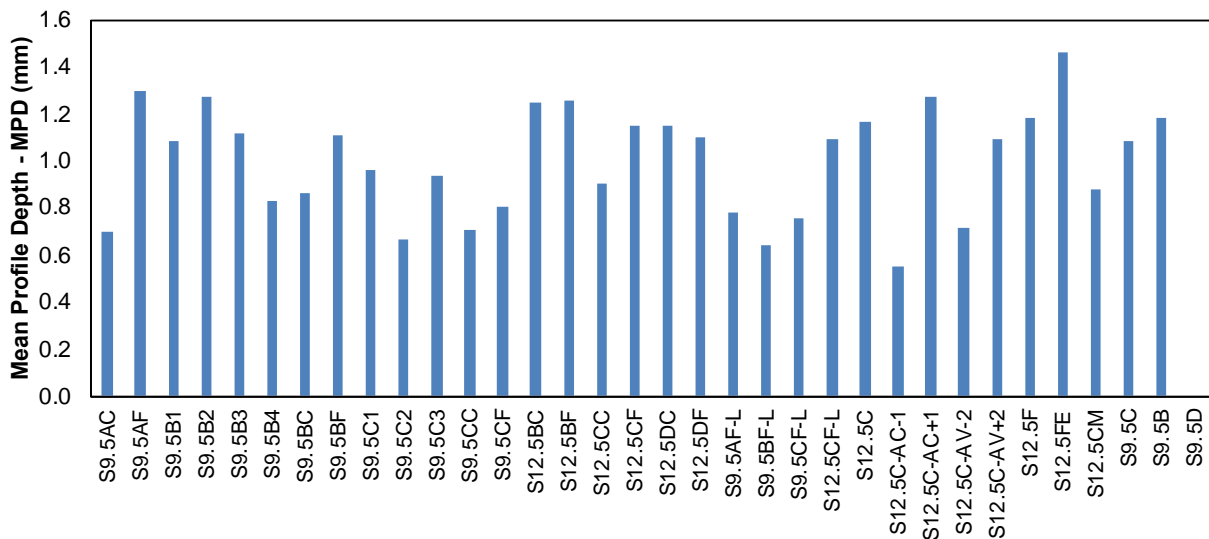

Figure A.36. *MPD* for North Carolina mixes calculated using Equation 53.

The *NCAT* derived model, presented by Sullivan (*51*) estimates the *MPD* using Equations (53) and (54).

107

$$\Omega = \sum_{i=1}^{N} \left[\left\{ \left(\frac{SivS_i}{MaxAgg} \right)^{0.45} \times 100 - \% \, pass_i \right\} \times SivS_i \right] \qquad (53)$$

$$MPD = 0.025 \times \Omega^2 + 0.037 \times \Omega - 0.0265 \times P_b + 0.052 \qquad (54)$$

Where, Ω is the gradation weighted mean distance from maximum density line, $SivS_i$ is the sieve size i in the gradation curve in mm, $MaxAgg$ is the maximum aggregate size of the mix, $\%Pass_i$ is the percent of mix passing the sieve size i, N is the number of sieves used in the gradation, and Pb is the percent binder by weight. It was not possible to apply Equation 54 to the North Carolina mix database, because after calculations the results obtained were not congruent with the previous correlations (Equation 49 and 52).

The FHWA/NC 2010-02 project included the following correlation between the Skid Number (*SN*) and the British Pendulum Number (*BPN*).

$$SN = 0.5986 \times BPN + 7.7002 \qquad (55)$$

Pavement Friction Management

Background

According to the Federal Highway Association (*FHWA*), the main purpose of a Pavement Friction Management (*PFM*) program is to minimize friction-related vehicle crashes by (*52*):

- Ensuring that new pavement surfaces are designed, constructed, and maintained to provide adequate and durable friction properties;
- Identifying and correcting sections of roadway that have elevated friction-related crash rates;
- Prioritizing the use of resources to reduce friction-related vehicle crashes in a cost-effective manner; and
- Effectively collecting and analyzing pavement friction, crash, and traffic data to reduce friction-related crashes.

To achieve these goals, State Highway Agencies (SHAs) are enforced by federal mandates and directives to develop and to implement a *PFM* program. Over the years three elements are considered basic and fundamental in any *PFM* program (*2, 3*):

i) System for evaluating in-service pavements for friction
ii) System for correlating available friction with wet-weather crashes
iii) Guidance on the design, construction, and maintenance of pavement surfaces with adequate surface friction throughout the pavement design life

In other words, it is necessary to measure friction within a network to quantify the friction demand of each of the roads to understand the effectiveness of a pavement design and for improving construction practices. Then, it is necessary to develop models that correlate observed crash rates with available friction values, to generate a warning flag for triggering a maintenance or rehabilitation action.

Agencies may vary in the emphasis placed on each of the basic elements of the programs, depending on their current level of understanding of their pavement properties, their access to

complete and timely crash data, their ability to collect network friction data, and considerations of the best use of available funds to meet the safety objective.

Elements in a Pavement Friction Management Program

In a Pavement Management System (PMS) the roads in a network are divided into sections, each section is defined based on the structural composition (number of layers, thicknesses, etc.), the construction history (age of construction and maintenance activities), and traffic (volume and composition). Sample units within a section are then identified for the purpose of field testing and evaluation.

Similarly, in a PFM program, the network is divided into sections, the only difference is that each section is defined based only on the friction demand (*3*). The friction demand for a given road depends on many factors, the more important are:

i) **Safety Measures**. Typically, the safety performance of a given site (segment of road or intersection) is expressed by the number of crashes, crash rate or crash severity (or a combination of these).
ii) **Traffic Levels**. Traffic volume and composition in the passing lane and in the outer lane.
iii) **Highway Function Class**. Interstates, primary routes, etc.
iv) **Climatic Zones**. Sites with similar rainfall intensities may be grouped for the analysis.
v) **High Risk Locations**. The friction demand depends on the geometry of the road, e.g., the friction demand in a curve will be higher than in a tangent.
vi) **Age of surfacing**. Is important to track the construction and maintenance history.

Like in a *PMS*, a section in a *PFM* program is identified using the route number, the county, the milepost or any permanent reference (like a bridge, a ramp or an exit). Because the criteria for defining the sections in a *PMS* and in a *PFM* is not the same, overlapping both systems may be problematic. Therefore it is important to reference the *PFM* sections with respect the *PMS* system. Matching these sections not only makes data storage and retrieval less confusing, but also makes it easier to coordinate field inspection/testing needs for both programs.

Establishing Friction Demand Categories

Identifying the level of friction needed by the driving public is the important first step in a *PFM* program. However, because of the great number of factors that may affect the friction developed in the tire-pavement interface, there is not a universal criterion for defining the existing friction demand levels, nevertheless there is a consensus that a rational estimate can be developed by evaluating the array of factors comprising by four broad categories (*2*, *3*, *6*):

- Highway alignment
- Highway features/environment,
- Highway traffic characteristics, and
- Driver/vehicle characteristics

However, because the driver/vehicle characteristics such as driver skills and age, vehicle tire characteristics, and vehicle steering capabilities, are difficult to assess in terms of friction demand, they are rarely included in a *PFM* program.

Highway Alignment

Friction demand is highly influenced by the highway geometry, dictated by its horizontal and vertical alignment. The amount of friction required increases with increasing complexity of the highway horizontal alignment, the grade of the vertical alignment, and the stopping sight distance. The relationship between side-force friction for horizontal curves (the most critical horizontal alignment), vehicle speed, radius of curvature, and highway cross-section (super-elevation) is defined using the following AASHTO Green Book equation (*53*):

$$F_s = \frac{V^2}{15 \times R} - e \qquad (56)$$

where F_s is the side-force friction demand in lb., e is the super-elevation rate, ft/ft, V is the speed, mi/hr, and R is the radius, ft. As the speed increases, the force required to maintain a circular path eventually exceeds the force that can be developed at the pavement-tire interface and super-elevation. At this point, the vehicle begins to slide in a straight line tangential to the highway alignment. In addition to the vehicle speed, the curve radius and the super-elevation, F_s is a function of climate, tire condition, and driver comfort while performing maneuvers (e.g., braking, making sudden lane changes, and making lateral movements within a lane).

For the vertical alignment, the *AASHTO* green book defines the Stopping Sight Distance (*SSD*) as the distance required for a driver (with a 1 m eye height) to clearly see an object of 0.15 m (0.5 ft) or more in height on the highway with enough distance to perceive, react and brake the car to a stop on a poor wet pavement. The *SSD* distance is calculated using the Equation (57), as shown this distance is the arithmetic sum of two distances, the distance traveled while the driver perceive the obstacle in the road, and the distance required to brake the car to a stop once he starts braking (*53*).

$$SSD = (1.47 \times v \times t) + \frac{v^2}{30(\mu \pm G)} \qquad (57)$$

where *SSD* is the side-force friction demand, t is the driver reaction time, s, G is the longitudinal grade, percent, and V is the speed, mi/hr.

Highway features/environment

Highway features/environment is an important but hard-to-measure characteristic of traffic flow that can significantly influence pavement friction. These characteristics of traffic flow depends on the presence and type of median barriers, the presence or absence of specially designed lanes (e.g., left or right turn lanes), number of conflict situations (e.g. intersections, ramps, exits/access), and more important depends on the setting (urban or rural) (*3*). In general, as the highway environment becomes more difficult and complex, significantly higher levels of friction are required to help drivers perform the necessary maneuvers (e.g., is expected higher friction demand in urban areas).

Highway traffic characteristics

Traffic characteristics that influence friction demand are traffic volume, composition, and speed. As traffic volume increases the number of conflicts also increase. The risk associated with this maneuver is elevated especially in high-speed areas. Also, for the same traffic levels, traffic composition may significantly affect the friction demand, mainly because in comparison to passenger cars, the trucks have worse steering capabilities, require longer distances to stop, and their tires produce less friction (*3*). Finally, vehicle speed is the most important variable

influencing friction demand. As can be seen in Figure A.37, the friction developed at the tire-pavement interface reduces as the vehicle speed increases (this phenomenon is aggravated in wet conditions). The speed at which the friction demand is exactly equal to the available friction is known as the Skid Limit, or Speed of Impending Skid. Finally, increasing speed (above 60 km/h [38 mph]) increases the likelihood of hydroplaning, which is a major cause of wet-weather crashes. Besides, higher the speed higher the severity in a collision.
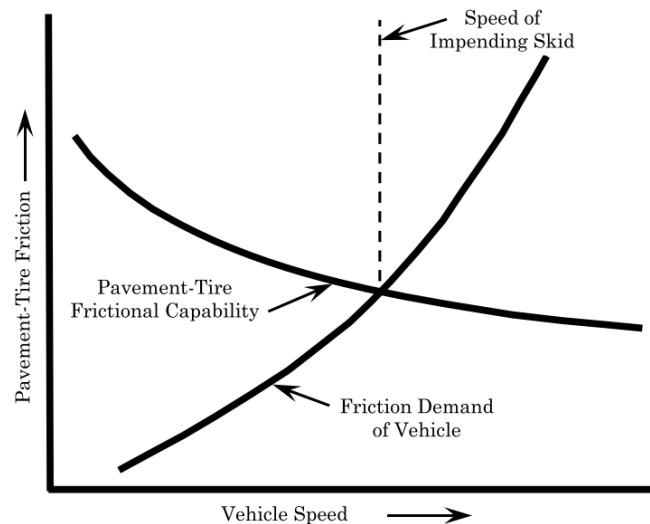

Figure A.37. Conceptual relationship between friction demand, speed, and friction availability (*3*).

Data Collection

Three key data inputs are required for an effective *PFM* program: pavement friction, pavement texture, and crash rates (*52*). Because the friction values vary depending the method used for its measurement, i.e. lock-wheel, side-skid, variable slip, etc. (see Section 0), is important to use an equipment that may be versatile to shift the test conditions depending on the friction value of interest, for example in a curve the lateral friction coefficient is more relevant than the longitudinal one. The microtexture can be measured directly in field if the equipment is capable of varying the slip ratio, friction values obtained at low slip ratios reflects the microtexture friction contribution. In case the equipment cannot adjust the slip ratio the microtexture values must be obtained with static devices, like the Dynamic Friction Tester (*DFT*) or the British Pendulum Tester (*BPT*). In addition, the macrotexture must be measured in conjunction with the friction.

Data Analysis

Because conditions and circumstances along a highway change, there is not one friction level that defines the threshold between "safe" and "potentially unsafe". Although, the ideal situation is that the available friction will be higher than the demand all the time. As mentioned in Section 3, the main road safety concern is the significantly reduced skid resistance during wet weather when there is a layer of water film on the pavement surface, for this reason it is common that agencies monitor the skid resistance at wet conditions. For this reason, the concept of minimum skid resistance has become popular as a criterion for a *PFM* program.

Two fo*RMS* of minimum skid resistance thresholds are commonly used by highway agencies for pavement friction management, namely the Investigatory Level and the Intervention Level. When

111

the investigatory level threshold is reach, the agency will start monitoring the evolution of pavement friction and crash rate (or number of crashes) and start evaluating the need of some preventive or restoration action. In contrast, the intervention level is the skid resistance at which an agency takes immediate corrective action, such as a maintenance or restorative treatment. Because at this point the skid resistance is too low and the driving safety risk becomes unacceptable (*31*).

However, because of the lack of prediction capability of pavement skid resistance under various rainfall intensities, the minimum skid resistance threshold for safe wet-weather driving has been specified by highway agencies based on either engineering judgement or past experience. Typically, the common criteria's for establishing the skid resistance thresholds are (*2*, *3*, *31*):

- Engineering judgment
- Deterioration trend of the skid resistance
- Crash history
- Other agencies practices for similar site characteristics.

Establishing Investigatory and Intervention Friction Threshold Levels

Hall et al. (*3*) recommended the following three methods for establishing skid resistance thresholds:

Method 1: Historical Skid Resistance Data Trend.

The investigatory level is defined when the skid resistance deterioration rate is higher than certain predefined threshold. The intervention level is defined as an independent threshold (a given minimum skid resistance value) or as a percentage below of the investigatory level (*3*, *31*)
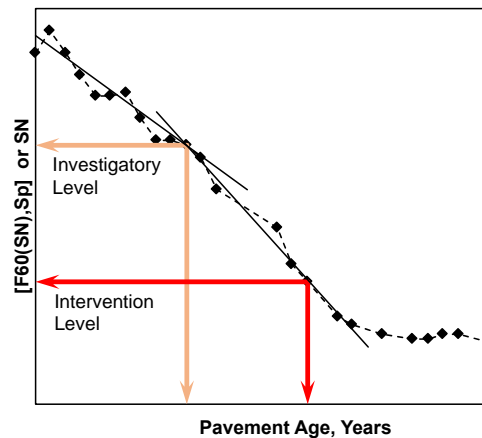

Method 2: Historical Skid Resistance and Crash Data.

The investigatory level is defined as in method 1, but the intervention level is defined as the skid resistance value at which there is a significant increase in the crash rate (*3*, *31*).
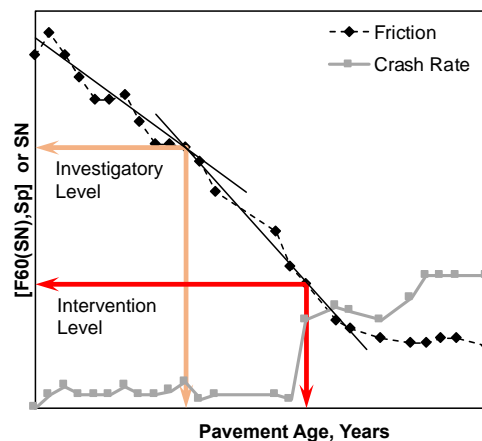
Method 3: Skid Resistance Probability Mass Function and Crash Trend.

For a given road class, calculate the friction mean and the standard deviation (σ), the investigatory level is the *mean - kσ,* where *k* is a multiplication factor of the standard deviation, and should be chosen based in the trend of the crashes (the value of skid resistance at which the crash rate starts increasing considerably). The Investigatory level is defined as the minimum desired level of skid resistance, or the *mean - 2σ* (*3*, *31*).
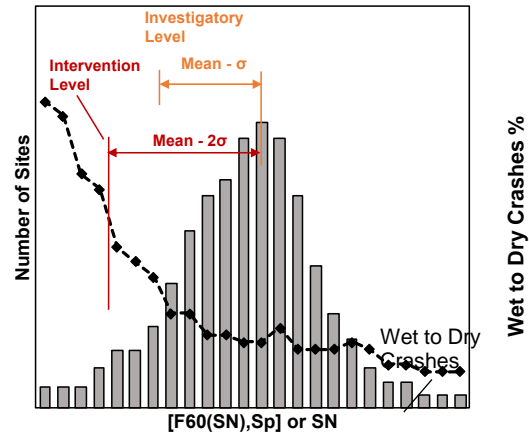
As in any engineering decision, one must weigh the financial implications of maintaining highway safety through managing pavement friction levels. Thus, an agency should examine the effects of using different investigatory and intervention levels in terms of the improvement in safety and the cost to achieve the level, which can then be adjusted to optimize the increase in safety to the agency's budget.

In the study that Flintsch et al. (*28*) presented to the North Carolina DOT was included a detailed literature review whit a summary of the more important work that have been done to correlate pavement friction and surface characteristics with crash rates (or other safety measurement, like total crash number or wet/dry crash ratio). One of their conclusions was that past studies on the relationship between friction and crashes found no device with a superior ability to predict friction-related crashes, largely because poor friction is seldom the lead cause of a crash. However, a CFME (like the SCRIM) provide a better chance of achieving a good correlation than the Locked-Wheel Tester.

An evaluation of the method proposed by Hall et al. (*3*) was conducted by Najafi et al (*54*). In this paper, the authors aimed to predict the rate of wet and dry vehicle crashes based on surface friction (measured with a LWST), traffic level, and speed limit using an artificial neural network (ANN). Crash rates were calculated using Equation (58). Najafi et al. (*54*) evaluated three learning algorithms to train the network, Levenberg–Marquardt, conjugate gradient, and resilient backpropagation. Levenberg–Marquardt produced the best precision and was used to develop the model. The results of the study suggest that the ANN model can reliably predict the rate of crashes. The prediction model can be used as a scale to prioritize safety improvement projects based on the rate of fatal and injury causing crashes.

$$\text{Crash Rate} = \frac{\text{Number of crashes} \times 1,000,000}{AADT \times n \times Y \times L} \tag{58}$$

where;

Crash Rate   = crash rate calculated using either wet or dry crashes,
AADT   = total *AADT* average for each bin defined using Method 3 of Hall et al. (*3*),
n   = wet or dry time exposure,
Y   = study duration in years, and
L   = length of the roadway segments (miles).

The authors found that applying Hall et al. methodologies is challenging, because the first two methods require a considerable number of historical observations to observe a relationship between friction and crashes. The difficulty in applying the third method was the sample size of roads with low friction values. Defining friction threshold based on a small sample size may not be appropriate. This makes the AASHTO method rather limited for project-level applications or for local and state government agencies.

Table A.8. Examples current state of practice.

State	Intervention Skid Resistance Level	Frequency of Measurements	Device Used
Idaho	SN40S = 30	Every other year in state roads and annually on interstates	LWT
Pennsylvania	-	2000 to 3000 miles annually. The test is made during the summer.	LWT with a ribbed or smooth tire
Washington	SN40R = 30	Every two years on all state-maintained roads at one-mile interval. - Undivided roads are tested only in one direction. - Divided roads with fewer than three lanes are tested in both directions in the outer lane. - Divided roads with three or more lanes are tested in both directions in the second lane from the outside.	LWT with a ribbed tire
Iowa	-	Five-year cycle	LWT
Ohio	SN40S = 32 SN40R = 23	-	LWT
Kentucky	$27 \leq SN40 \leq 38$: Investigatory $SN40 \leq 26 =$ Intervention	Test are made in the left-wheel path of each lane of interest at 0.5 miles interval. All other causatives effects should be rule out, only when the friction is considered the main safety hazard the test is scheduled.	LWT
Texas	SN40R = 30 for intestates and motorway SN40R = 26 for primary roads SN40R = 22 for secondary roads	-	Modified LWT
Maryland	SN40R = 30 for undivided highways SN40R = 25 for divided highways	-	LWT with a ribbed tire

In all cases except for urban freeway expressway, the crash rate decreased as the friction increased to average level. For urban principal arterials, an approximately 40% reduction was observed in the rate of wet crashes as friction increased from 32 to 45. Similarly, a 15% reduction was observed

in the rate of dry crashes by increasing the friction number from 32 to 45. Using this methodology, it is possible to set the wet crash value at which a section will be flag as high risk, in the case of this study if a wet crash rate of 0.6 is select, the investigatory threshold is equal to 32. Table A.8 summarizes the current state of practice of some selected state highway agencies. As can be noticed, all of them used a locked-wheel tester for conducting the measurements, and the frequency of test varies from annually to every five years, or upon request.

Similarly, Table A.9 shows the skid resistance investigatory levels used in the United Kingdom to evaluate a network performance. Is important to point out that the U.K. uses a SCRIM machine for measuring friction. The data collection is typically done in summer periods when the friction reaches its lower values. The friction is measured annually in the whole primary network.

Table A.9. Friction demand categories and friction investigatory levels in the U.K. (55).

Road Classification Definitions		Investigatory Level at 30 mph (50 km/h)							
		0.30	0.35	0.40	0.45	0.50	0.55	0.60	0.65
A	Motorways (Interstate highways)	pink	red						
B	Dual carriageways non-event (Divided highways non-event)	pink	red	red					
C	Single carriageways non-event (Two-lane roads non event)		pink	red	red				
Q	Dual carriageways (all purpose)—minor junctions (Divided highways—intersection/roundabout approaches)				red	red	red		
K	Approaches to pedestrian crossings and other high-risk situations					red	red		
R	Roundabouts				red	red			
G1	Gradients 5-10%, longer than 50 m (Slopes 5-10%, longer than 160 ft)				red	red			
G2	Gradients ≥ 10%, longer than 50 m (Slopes ≥ 10%, longer than 160 ft)				pink	red	red		
S1	Bend radius <500 m—dual carriageway (Curve radius <1,600 ft—divided highways)				red	red			
S2	Bend radius <500 m—single carriageway (Curve radius <1,600 ft—two-lane highways)				pink	red	red		

Notes: No events are tangent segments (no intersections, curves with radius > 1600 feet and slopes < 5%).
A reduction of 0.05 is allowed for categories A, B, C, G2 and S2 in low risk situations such as low traffic levels or where risk is well mitigated and a low incidence of accidents has been observed (pink).

Table A.10. T10:2002 skid resistance investigatory levels in New Zealand (56).

Site Category	Description	Notes				Investigatory Level (ESC)			Skid assessment Length (m)
5	Divided carriageway	Event free				0.35			100
4	Normal roads	Undivided carriageways only (event free)				0.40			100
3d	Roundabouts, circle only	Circular section only							60
3b and 3c	Down Gradients 5% -10%	Includes motorway on/off ramps				0.45			50
3a	Approaches to junctions								60
2	Urban curves R < 250m	All risks				0.50			50
	Rural curves R < 250m	Low risk	Med risk	High risk		0.45	0.50	0.55	
	Rural curves, 250 <R < 400m	Low risk	Med risk	High risk		0.40	0.50	0.55	
	Down Gradients > 10%	Includes on ramps with ramp metering				0.50			
1	Highest priority	Railway level crossing, approaches to roundabouts, traffic lights, Pedestrian crossings and similar Hazards				0.55			60

In New Zealand, the T10 pavement specification established that the SCRIM must be used for measuring friction. The measurements must be conducted in the whole primary network during the summer months. Table A.10 summarized the skid resistance investigatory levels used in New Zealand. Finally, using a series of historical values collected in the state of Washington using the SCRIM machine, Flintsch et al. (28) proposed the limits shown in Table A.11 for skid resistance investigatory levels.

Table A.11. SCRIM friction thresholds using GPF Method 3 (28).

Type of Roadway	SR Investigatory Level
Divided	30-35
Undivided	50-55
Curves	50-55
Intersections	55-60

As noted, all the reference presented above have tried to establish an investigatory threshold that can be used to flag locations for further evaluation. References indicating an intervention level are scarce, and because the high complexity associated to a crash event, is better to identify sites that may represent a hazard in terms of friction and start monitoring them.

In addition, it was found that none of the state agencies in the United States is using a surface texture characteristic for evaluating safety performance. Despite of this, a lot of work has been done trying to relate both friction and macrotexture with crash rates or total number of crashes, and it has been found that the macrotexture is a better predictor than the friction.

Similar to friction, defining a threshold for macrotexture that represents a safe condition is a difficult task, however some studies have brought some ideas about this, for example the work of Pulugartha (33) established that the *MPD* must be greater than 1.524 mm but less than 3.048 mm, in order to reduce the number of crashes. Similarly, the work of Flinstch et al. (28) recommended that the *MPD* must be greater than 0.8 mm for roads with a speed limit of 50 mph, and 1.0 mm for roads with a speed limit of 70 mph.

Similar attempts have been made in the Unit Kingdom and New Zealand as shown in Table A.12 and Table A.13, these tables shown the minimum *MPD* a new pavement surface should have to provide a safe operating condition.

Table A.12. Requirements for initial texture depth for trunk roads including motorways, U.K. (*28*).

Road type	Surfacing type	Average / 1,000 m	Average / 10 measures
High Speed roads >50 mph	Thin surface overlay Aggr. size<14mm	MTD > 1.3 mm (MPD 1.4)	MTD > 1.0 mm (MPD 1.0)
	Surface treatments	MTD > 1.5 mm (MPD 1.6)	MTD > 1.2 mm (MPD 1.25)
Lower Speed roads <40 mph	Thin surface overlay Aggr. size<14mm	MTD > 1.0 mm (MPD 1.4)	MTD > 0.9 mm (MPD 0.9)
	Surface treatments	MTD > 1.2 mm (MPD 1.25)	MTD > 1.0 mm (MPD 1.0)
Roundabout, high speed >50 mph	All surfaces	MTD > 1.2 mm (MPD 1.25)	MTD > 1.0 mm (MPD 1.0)
Roundabout, low speed <40 mph	All surfaces	MTD > 1.0 mm (MPD 1.0)	MTD > 0.9 mm (MPD 0.9)

Table A.13. Minimum macrotexture requirements for New Zealand (*56*).

Permanent speed limit PSL (km/h)	Minimum macrotexture – Mean Profile Depth (MPD in mm)					
	Chip Seal		Asphaltic concrete ESC > 0.40		Asphaltic concrete ESC < 0.40	
	ILM[1]	TLM[2]	ILM	TLM	ILM	TLM
PSL < 50	1.00	0.70	0.40	0.30	0.50	0.50
50<PSL<70	1.00	0.70	0.40	0.30	0.70	0.50
PSL > 70	1.00	0.70	0.40	0.30	0.90	0.70

[1] Investigatory level for macrotexture
[2] Threshold level for macrotexture

Knowledge Gaps

Based on the literature review presented, the research team has identified the following critical knowledge gaps, which will be the focus of the current research effort:

- There is evidence that the friction of the surface of a newly constructed pavement or an overlay is lower than the maximum value that can be achieved by the surface. An initial amount of wear is necessary to expose the aggregate surface and fully develop the friction components (micro and macro texture). Some authors have performed an initial attempt to develop functions that express friction performance as a function of cumulative traffic. However, past researchers have not attempted to quantify the initial lapse in time (or initial number of traffic volume) required to achieve the maximum friction value as a function of mixture properties.

- Previous research has not identified the mixture properties that govern the initial frictional characteristics of a pavement surface. In addition, actions or activities that may shorten the time window required to achieve the maximum friction potential have not been investigated.

- Ideally, friction performance should be considered during asphalt mixture design; however, there is not a proper methodology for evaluating friction during the mix design.

- According to the literature review, a successful model for predicting surface friction needs to incorporate the macrotexture and the microtexture of the asphalt mix and the microtexture of each aggregate component (see section 0). To include friction performance into the mix design, is necessary to develop a model that predicts surface wearing (friction variation with time/traffic) as a function of the aggregate's properties, the micro and macro texture of the mix, the initial friction measured in the lab (using a BPT or a DFT), and the expected cumulative traffic. To do so, is important that the NCDOT start collecting both friction, macrotexture, and microtexture measurements. This research effort will provide the basis for this purpose, specifying equipment, test methods, testing frequency and indices for summarizing friction and texture properties.

- The key to a successful and well implemented Friction Management Program is the definition of friction demand categories. A friction demand category must define the frequency and type of measurements required to monitor and manage friction properties in a network. It is imperative that the NCDOT defines the friction demand categories for the North Carolina highway network. However, there is not a consensus of the friction thresholds that flag a particular road for inspection or intervention. Although this research effort may not help to solve this problem directly, it may provide certain guidance for defining what can be considered as the initial friction value of a new or an overlaid road.

Appendix A References

1. Flintsch, G. W., D. Ph, and F. Street. Evaluation of Methods for Pavement Surface Friction , Testing on Non- Tangent Roadways and Segments. No. August, 2017.

2. Ueckermann, A., D. Wang, M. Oeser, and B. Steinauer. Calculation of Skid Resistance from Texture Measurements. *Journal of Traffic and Transportation Engineering (English Edition)*, Vol. 2, No. 1, 2015, pp. 3–16.

3. Flintsch, G. W., K. K. Mcghee, E. D. L. Izeppi, and S. Najafi. *The Little Book of Tire Pavement Friction*. 2012.

4. NCHRP Document 108. *Guide for Pavement Friction*. 2009.

5. Oh, Y., and H. Lee. Characteristics of a Tire Friction and Performances of a Braking in a High Speed Driving. *Advances in Mechanical Engineering*, 2015.

6. NCHRP Synthesis 291. *Evaluation of Pavement Friction Characteristics*. 2000.

7. Kogbara, R. B., E. A. Masad, E. Kassem, A. Scarpas, and K. Anupam. A State-of-the-Art Review of Parameters Influencing Measurement and Modeling of Skid Resistance of Asphalt Pavements. *Construction and Building Materials*, Vol. 114, 2016, pp. 602–617.

8. Mataei, B., H. Zakeri, M. Zahedi, and F. M. Nejad. Pavement Friction and Skid Resistance Measurement Methods : A Literature Review. *Open Journal of Civil Engineering*, Vol. 6, 2016, pp. 537–565.

9. ASTM C295/C295M. *Standard Guide for Petrographic Examination of Aggregates for Concrete*. 2018.

10. Vollor, T. W., and D. I. Hanson. *Development of Laboratory Procedure for Measuring Friction of HMA Mixtures – Phase I*. 2006.

11. ASTM D7428-15. *Standard Test Method for Resistance of Fine Aggregate to Degradation*

by Abrasion in the Micro-Deval Apparatus. 2015.

12. ASTM D 6928-10. *Standard Test Method for Resistance of Coarse Aggregate to Degradation by Abrasion in the Micro-Deval Apparatus*. 2017.

13. ASTM C131/C131M. *Standard Test Method for Resistance to Degradation of Small-Size Coarse Aggregate by Abrasion and Impact in the Los Angeles Machine*. 2006.

14. ASTM E303-93 (Reapproved). *Standard Test Method for Measuring Surface Frictional Properties Using the British Pendulum Tester*. 2018.

15. ASTM E965 (Reapproved). *Standard Test Method for Measuring Pavement Macrotexture Depth Using a Volumetric Technique*. 2006.

16. Li, L., K. C. P. Wang, and Q. J. Li. Geometric Texture Indicators for Safety on AC Pavements with 1 Mm 3D Laser Texture Data. *International Journal of Pavement Research and Technology*, Vol. 9, No. 1, 2016, pp. 49–62.

17. ASTM E965-15. *E965-15. Standard Test Method for Measuring Pavement Macrotexture Depth Using a Volumetric Technique*. 2015.

18. ASTM E1845 -01. *Standard Practice for Calculating Pavement Macrotexture Mean Profile Depth*. 2001.

19. Sun, L., and Y. Wang. Three-Dimensional Reconstruction of Macrotexture and Microtexture Morphology of Pavement Surface Using Six Light Sources–Based Photometric Stereo with Low-Rank Approximation. *Journal of Computing in Civil Engineering*, Vol. 31, No. 2, 2017, pp. 1–16.

20. Areal Function. Https://Guide.Digitalsurf.Com/En/Guide-Areal-Functional-Parameters .html.

21. Curve, A. M. R. Https://Www.Keyence.Com/Ss/Products/Microscope/Roughness/Surface /Smr-Areal-Material-Ratio.Jsp.

22. Halse, A. H., H. Samstad, M. Killi, S. Flügel, and F. Ramjerdi. Valuation of Transport Time and Reliability in Freight Transport. *Freight Transport Modelling*, Vol. 349, 2010.

23. ASTM E2380/E2380M - 15. *Standard Test Method for Measuring Pavement Texture Drainage Using an Outlow Meter*. 2015.

24. Aktaş, B., D. Gransberg, C. Riemer, and D. Pittenger. Comparative Analysis of Macrotexture Measurement Tests for Pavement Preservation Treatments. *Transportation Research Record*, No. 2209, 2011, pp. 34–40. https://doi.org/10.3141/2209-05.

25. ASTM E2157 -15. *Standard Test Method for Measuring Pavement Macrotexture Properties Using the Circular Track Meter*. 2015.

26. Bristish Pendulum Tester Image. Https://Www.Grestec.Co.Uk/Ptv-over-36-Ptv/.

27. Development of a New Accelerated Lab Friction Testing Standard. Http://Www.Eng.Auburn.Edu/Research/Centers/Ncat/Newsroom/2019-Spring/Friction.Html.

28. Jafari, K., and V. Toufigh. Interface between Tire and Pavement. *Journal of Materials in Civil Engineering*, Vol. 29, No. 9, 2017.

29. ASTM E1859/E1859M-11 (Reapproved). *Standard Test Method for Friction Coefficient Measurements Between Tire and Pavement Using a Variable Slip Technique*. 2015.

30. Fuentes, L. G., G. W. Flintsch, and E. de León Izeppi. Evaluation of the Use of Ribbed Tires for the Characterization of Skid Resistance Using Friction Models. *Journal of Testing and Evaluation*, Vol. 42, No. 6, 2014.

31. Fwa, T. F. Skid Resistance Determination for Pavement Management and Wet-Weather Road Safety. *International Journal of Transportation Science and Technology*, Vol. 6, No. 3, 2017, pp. 217–227.

32. Corley-Lay, J. B. Friction and Surface Texture Characterization of 14 Pavement Test Sections in Greenville, North Carolina. *Transportation Research Record*, No. 1639, 1998, pp. 155–161.

33. Pulugurtha, S. S., D. Ph, P. R. Kusam, and K. Patel. Relationship between Pavement Macrotexture and Crash Incidences on North Carolina Roads. *FHWA / NC / 2007-1*, 2008.

34. Pagán-Ortiz, J. E. *Full-Scale Accelerated Performance Testing for Superpave and Structural Validation*. 2012.

35. Pavement Interactive Mix Types. Article on Pavement Interactive – A site by PaviaSystems. *Https://Www.Pavementinteractive.Org/Reference-Desk/Pavement-Types-and-History/Pavement-Types/Pavement-Typesmix-Types/*.

36. Ongel, A., Q. Lu, and J. Harvey. Frictional Properties of Asphalt Concrete Mixes. *Proceedings of the Institution of Civil Engineers: Transport*, Vol. 162, No. 1, 2009, pp. 19–26.

37. Sarang, G., B. M. Lekha, J. S. Geethu, and A. U. R. Shankar. Laboratory Performance of Stone Matrix Asphalt Mixtures with Two Aggregate Gradations. *Journal of Modern Transportation*, Vol. 23, No. 2, 2015, pp. 130–136.

38. Mitchell, M. R., R. E. Link, S. Li, K. Zhu, and S. Noureldin. Evaluation of Friction Performance of Coarse Aggregates and Hot-Mix Asphalt Pavements. *Journal of Testing and Evaluation*, Vol. 35, No. 6, 2007, p. 100903.

39. Kim, Y., J. Lim, M. Lee, S. Kwon, S. Hwang, and J. Lee. Comprehensive Evaluation of Warm SMA Using Wax-Based WMA Additive in Korea. *Journal of Testing and Evaluation*, Vol. 43, No. 5, 2015, p. 20130144.

40. Merritt, D. K., C. Lyon, and B. Persaud. *Evaluation of Pavement Safety Performance*. 2015.

41. Wu, Z., and C. Abadie. Laboratory and Field Evaluation of Asphalt Pavement Surface Friction Resistance. *Frontiers of Structural and Civil Engineering*, Vol. 12, No. 3, 2018, pp. 372–381.

42. Heitzman, M., and J. Moore. *Evaluation of Laboratory Friction Performance of Aggregates for High Friction Surface Treatments*. 2017.

43. Cerezo, V., M. T. Do, D. Prevost, and M. Bouteldja. Friction/Water Depth Relationship - In Situ Observations and Its Integration in Tire/Road Friction Models. *Proceedings of the Institution of Mechanical Engineers, Part J: Journal of Engineering Tribology*, Vol. 228, No. 11, 2014, pp. 1285–1297.

44. Kulakowski, B. T., and D. W. Harwood. *Effect of Water-Film Thickness on Tire-Pavement Friction*. 1990.

45. Do, M.-T., V. Cerezo, Y. Beautru, and M. Kane. Influence of Thin Water Film on Skid Resistance. *Journal of Traffic and Transportation Engineering*, Vol. 2, No. 6, 2014, pp. 36–44.

46. Ahammed, M., and S. L. Tighe. Early-Life, Long-Term, and Seasonal Variations in Skid Resistance in Flexible and Rigid Pavements. *Transportation Research Record*, No. 2094, 2009, pp. 112–120.

47. Horigan Smith, R. *Analyzing Friction in the Design of Rubber Products*. 2008.

48. Ong, G. P., and T. F. Fwa. Wet-Pavement Hydroplaning Risk and Skid Resistance : Modeling. *Journal of Transportation Engineering*, Vol. 133, 2007, pp. 590–598.

49. Stroup-Gardiner, M., and E. R. Brown. *Segregation in Hot-Mix Asphalt Pavement (NCHRP Report 441)*. 2000.

50. Davis, R. M. *Comparison of Surface Characteristics of Hot-Mix Asphalt Pavement Surfaces at the Virginia Smart Road*. 2001.

51. Sullivan, B. . Development of a Fundamental Skid Resistance Asphalt Mix Design Procedure. 2005.

52. FHWA - Pavement Management Program. Https://Safety.Fhwa.Dot.Gov/Roadway_dept/Pavement_friction/Friction_management/.

53. AASHTO. *A Policy on Geometric Design of Highways and Streets*. 2018.

54. Viner, A. H. E., R. Sinhal, and A. R. Parry. Linking Road Traffic Accidents With Skid Resistance – Recent UK Developments, TRL Paper Reference PA/INF4520/05. *Highways*, No. August 2004, 2005, pp. 1–13.

55. Transport Agency, N. *T10:2002 New Zealand Specification for State Highway Skid Resistance Management*. 2012.

Table B.1. Friction measurement dates.

Site	Route Type	B-1	A-1	A-2	A-3	A-4	A-5	A-6	A-7
1	Interstate	-	17-Oct	21-Apr	18-Jun	-	-	-	-
2	Interstate	-	17-Oct	21-Apr	18-Jun	-	-	-	-
3	US	-	17-Oct	21-Apr	15-Oct	08-Feb	-	-	-
4.1	Interstate	-	29-Oct	01-May	22-Jul	19-Oct	-	-	-
4.2	Interstate	-	20-Apr	21-Jul	19-Oct	-	-	-	-
5	Interstate	-	28-Oct	04-May	20-Jul	19-Oct	-	-	-
6	Interstate	-	28-Oct	08-May	20-Jul	19-Oct	08-Feb	18-Jun	-
7	Interstate	-	08-Nov	24-Apr	19-Aug	20-Nov	09-Feb	15-Jul	-
8	NC	17-Oct	21-Apr	05-Aug	14-Oct	18-Jan	15-Mar	-	18-Jun
9	NC	-	11-Nov	26-Aug	20-Nov	02-Feb	15-Jul	-	-
11	NC	16-Apr	25-Aug	19-Nov	02-Feb	14-Jul	-	-	-
12	US	-	14-Oct	24-Apr	10-Aug	-	-	-	-
13	US	07-Nov	19-Nov	-	-	-	-	-	-
14	US	-	29-Oct	30-Apr	21-Jul	20-Oct	28-Jan	01-Jul	-
15	NC	-	08-Nov	22-Apr	05-Aug	18-Nov	11-Mar	14-Jul	-
16	NC	-	07-Nov	24-Apr	24-Aug	19-Nov	11-Mar	14-Jul	-
17	US	-	08-Nov	22-Apr	30-Jul	15-Oct	15-Jan	15-Mar	18-Jun
18	US	-	08-Nov	22-Apr	05-Aug	28-Nov	11-Mar	-	-
19	US	07-Nov	25-Apr	24-Aug	19-Nov	02-Feb	14-Jul	-	-
23	Interstate	-	24-Apr	19-Aug	18-Nov	09-Mar	-	-	-
24	NC	28-Apr	19-Jun	28-Jan	-	-	-	-	-
27	US	-	09-Jul	11-Aug	20-Nov	02-Feb	21-Jun	-	-
28	NC	-	05-Jun	19-Aug	20-Nov	-	-	-	-
29	NC	11-Jun	07-Aug	14-Oct	11-Jan	15-Apr	21-Jun	-	-
30	NC	11-Jun	14-Oct	11-Jan	-	-	-	-	-
33	US	05-Jun	12-Jun	05-Aug	14-Oct	15-Jan	15-Mar	21-Jun	-

B = Before construction and A = After construction

Data collected in	2019	2020	2021

Site	Route Type	B-1	A-1	A-2	A-3	A-4	A-5	A-6	A-7
1	Interstate	-	22-Oct	10-Feb	18-Jun	-	-	-	-
2	Interstate	-	22-Oct	10-Feb	18-Jun	-	-	-	-
3	US	-	22-Oct	17-Feb	15-Oct	08-Feb	-	-	-
4.1	Interstate	-	29-Oct	14-Feb	21-Jul	19-Oct	-	-	-
4.2	Interstate	-	01-May	21-Jul	19-Oct	-	-	-	-
5	Interstate	-	28-Oct	14-Feb	20-Jul	19-Oct	-	-	-
6	Interstate	-	28-Oct	14-Feb	20-Jul	19-Oct	08-Feb	18-Jun	-
7	Interstate	-	01-Nov	05-Feb	19-Aug	20-Nov	09-Feb	15-Jul	-
8	NC	22-Oct	21-Apr	05-Aug	14-Oct	15-Jan	15-Mar	-	18-Jun
9	NC	-	01-Nov	05-Feb	26-Aug	20-Nov	02-Feb	15-Jul	-
11	NC	31-Oct	25-Aug	19-Nov	02-Feb	14-Jul	-	-	-
12	US	-	14-Oct	05-Dec	10-Aug	-	-	-	-
13	US	31-Oct	19-Nov	-	-	-	-	-	-
14	US	-	29-Oct	14-Feb	21-Jul	20-Oct	28-Jan	01-Jul	-
15	NC	-	01-Nov	12-Feb	05-Aug	18-Nov	11-Mar	14-Jul	-
16	NC	-	31-Oct	05-Feb	24-Aug	19-Nov	11-Mar	14-Jul	-
17	US	-	01-Nov	12-Feb	23-Jul	15-Oct	15-Jan	15-Mar	18-Jun
18	US	-	01-Nov	12-Feb	05-Aug	28-Nov	11-Mar	-	-
19	US	31-Oct	24-Apr	24-Aug	19-Nov	02-Feb	14-Jul	-	-
23	Interstate	-	05-Dec	19-Aug	18-Nov	09-Mar	-	-	-
24	NC	06-Dec	19-Jun	28-Jan	-	-	-	-	-
27	US	-	09-Jul	11-Aug	20-Nov	02-Feb	21-Jun	-	-
28	NC	-	05-Jun	19-Aug	20-Nov	-	-	-	-
29	NC	11-Jun	07-Aug	14-Oct	11-Jan	15-Apr	21-Jun	-	-
30	NC	11-Jun	14-Oct	11-Jan	-	-	-	-	-
33	US	05-Jun	12-Jun	05-Aug	14-Oct	15-Jan	15-Mar	21-Jun	-

B = Before construction A = After construction

Data collected in   2019   2020   2021

APPENDIX C: CALIBRATED MODELS

Prediction Verification Plots of Friction Seasonal Model

RS9.5B Sites
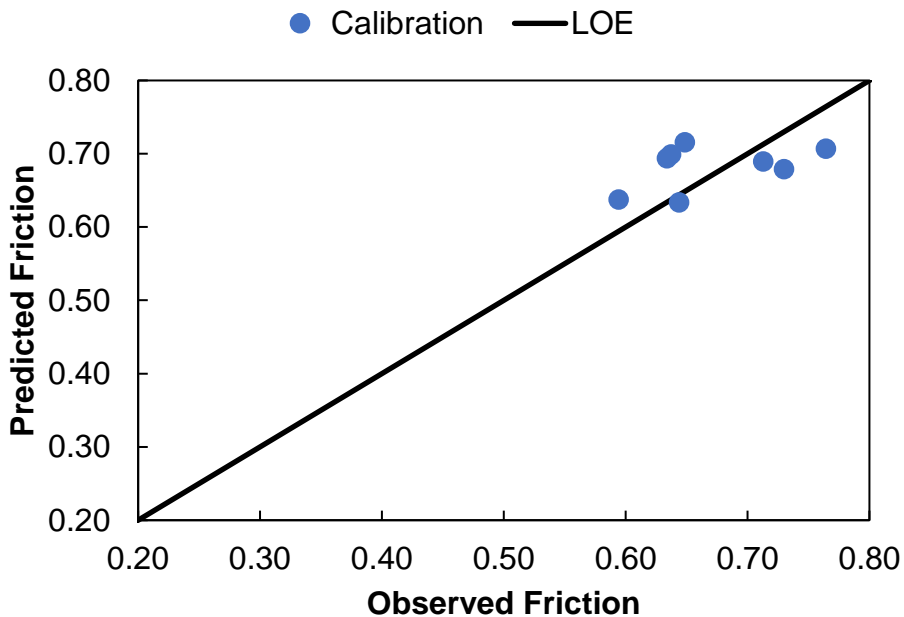
Figure C.1. Prediction verification plots of friction seasonal model for Site 3.
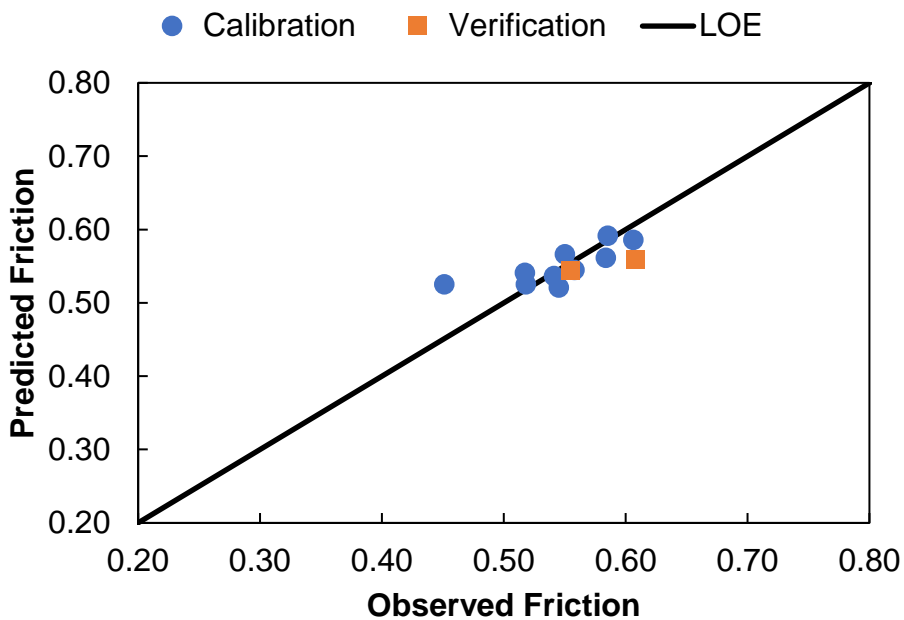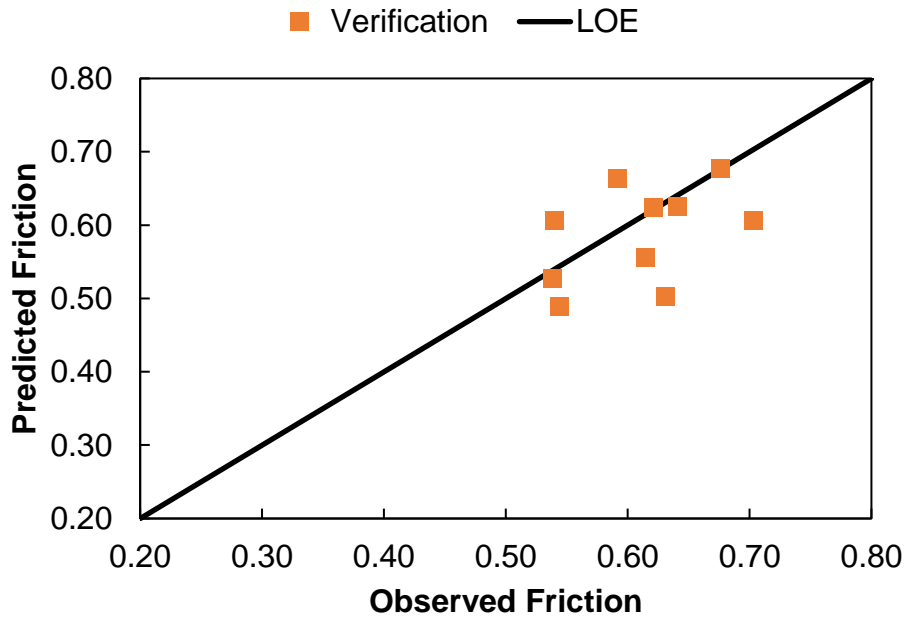

Figure C.2. Prediction verification plots of friction seasonal model for Site 15.
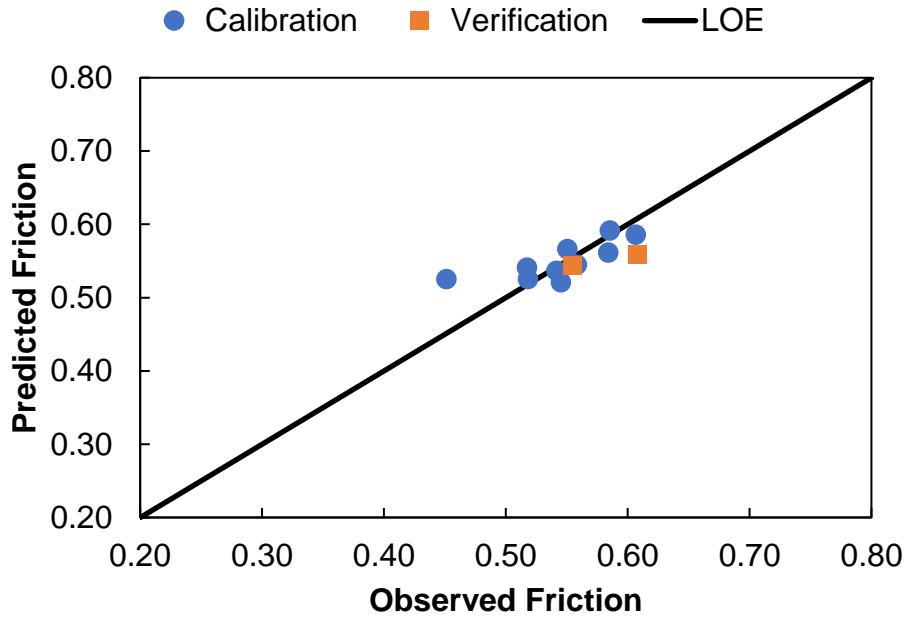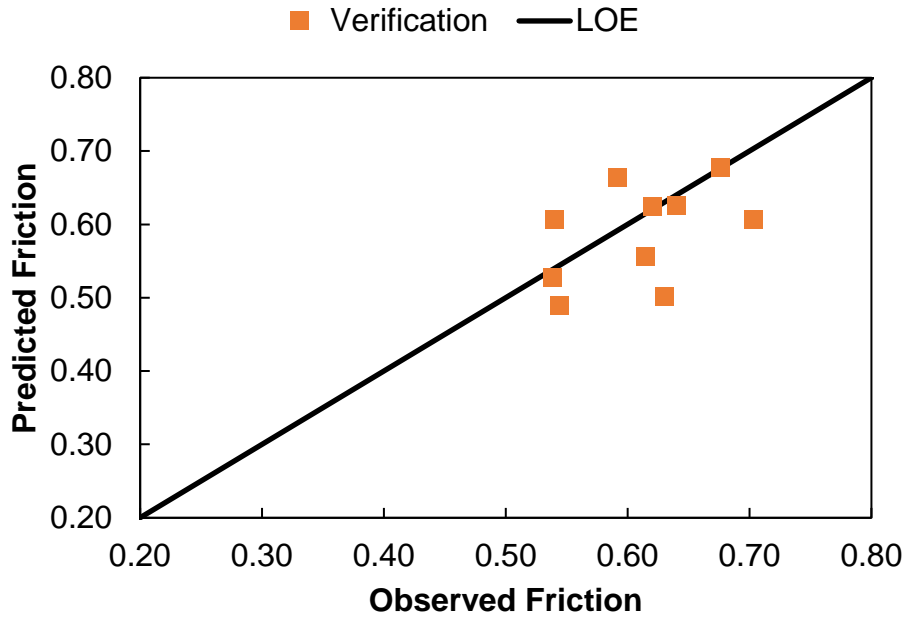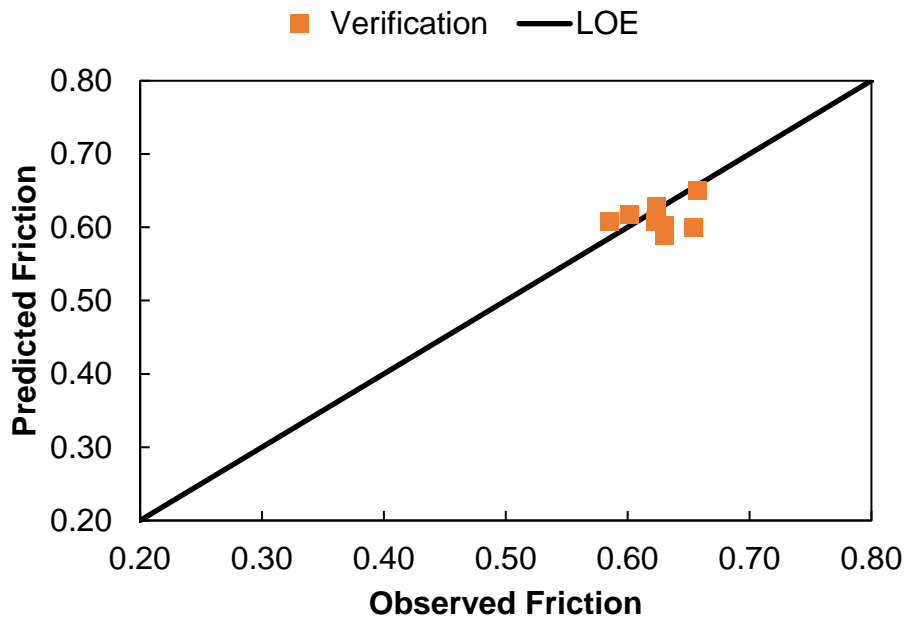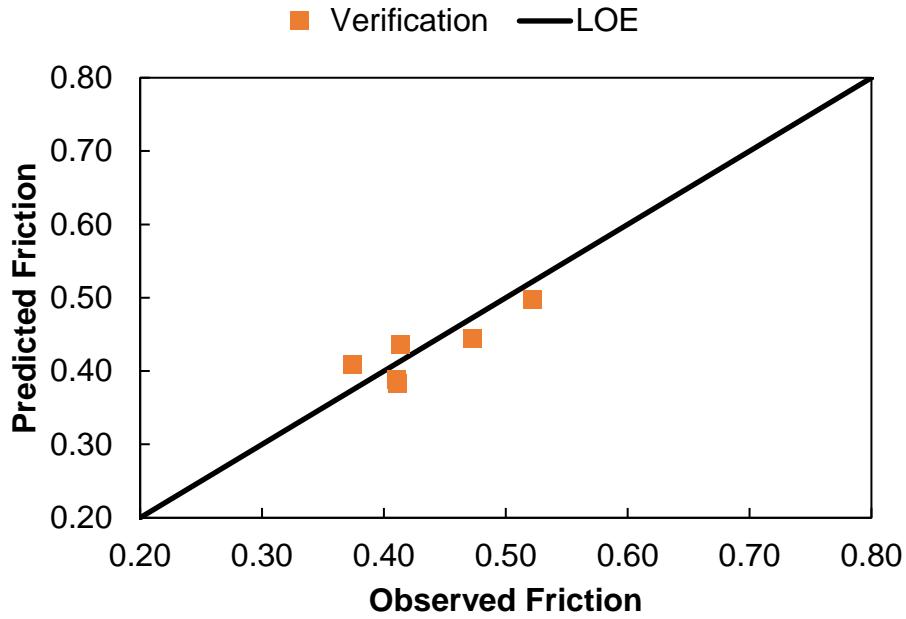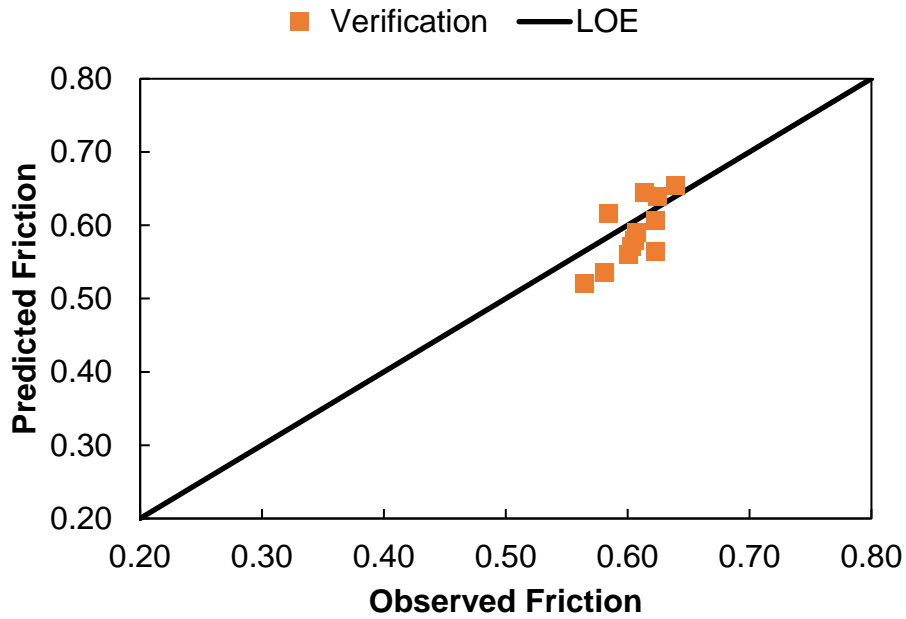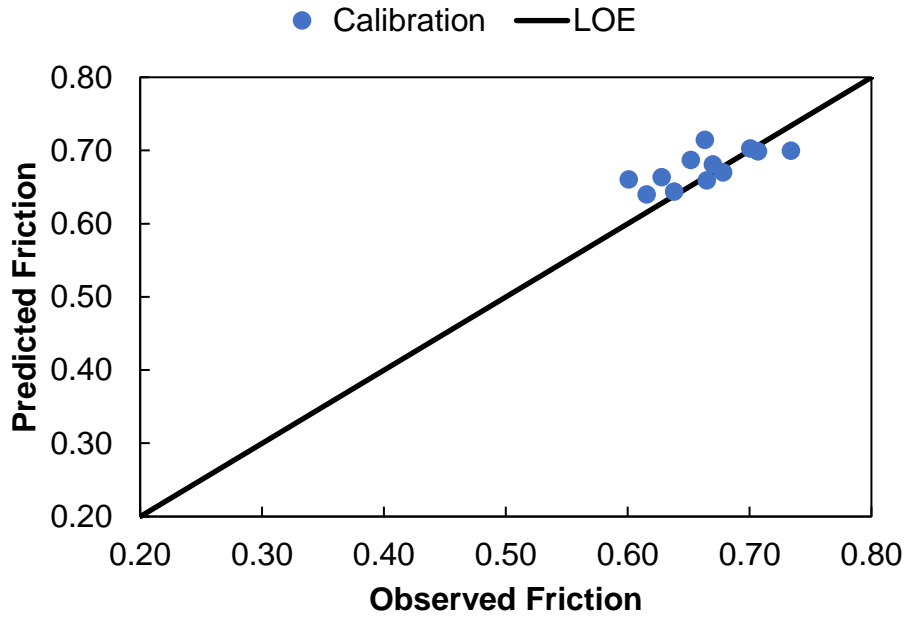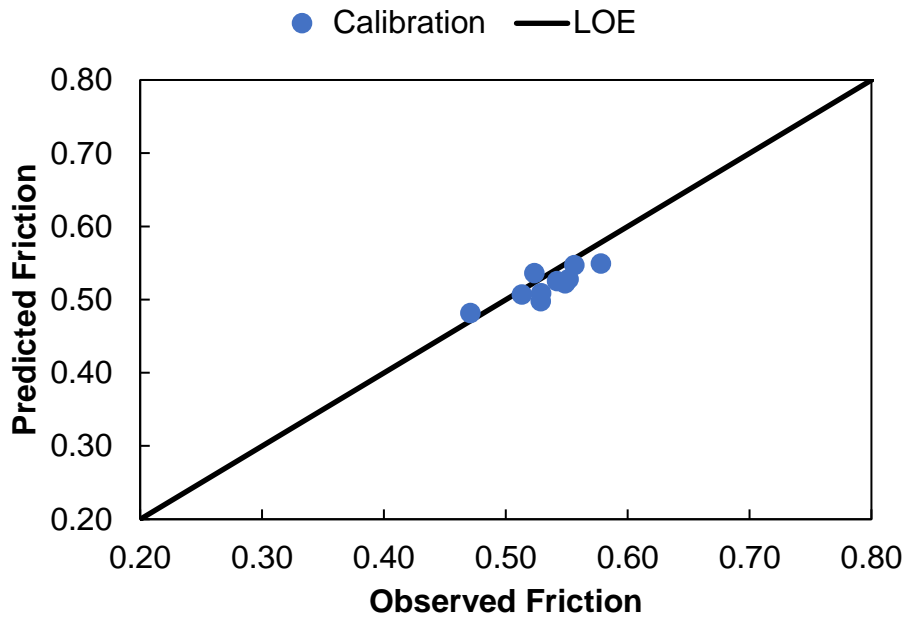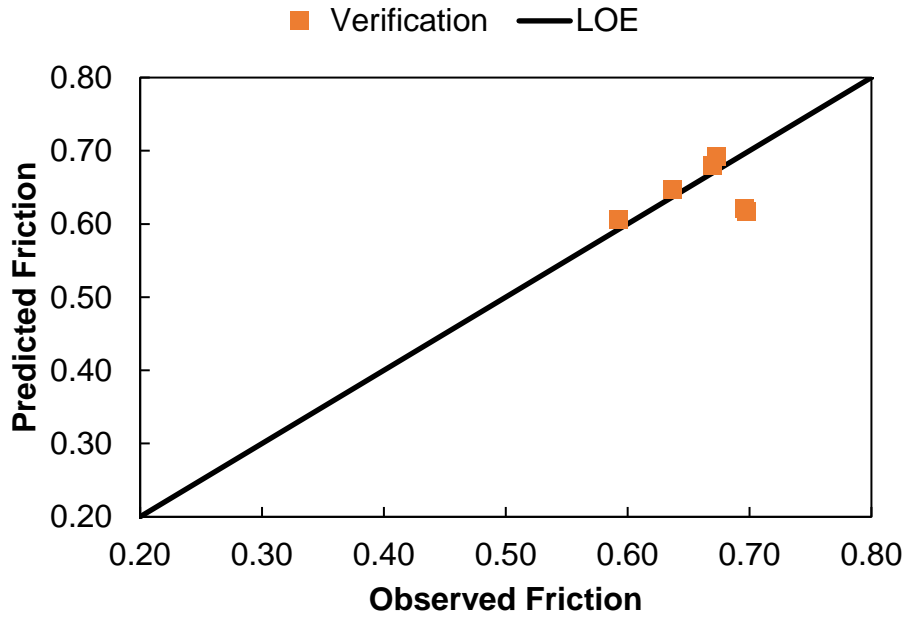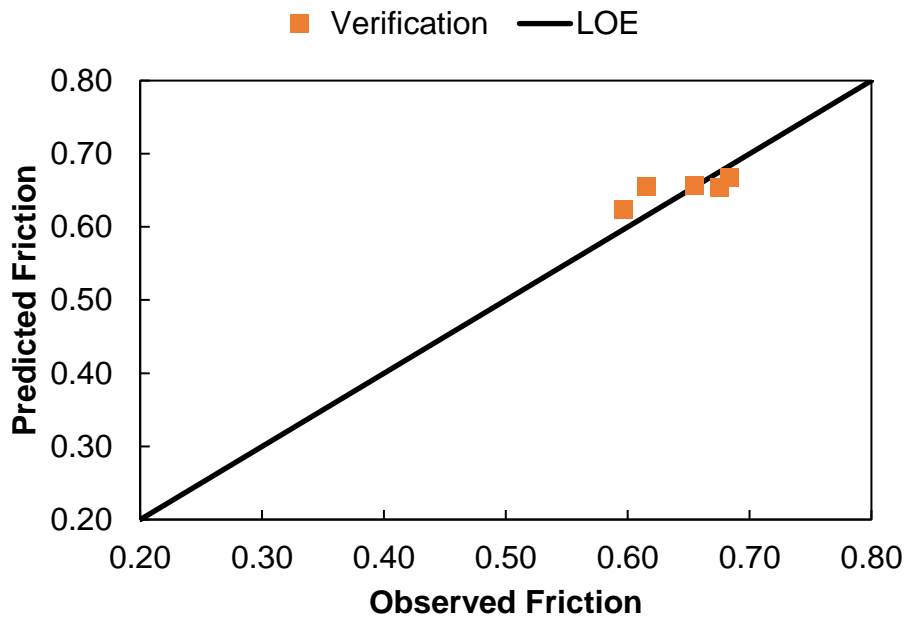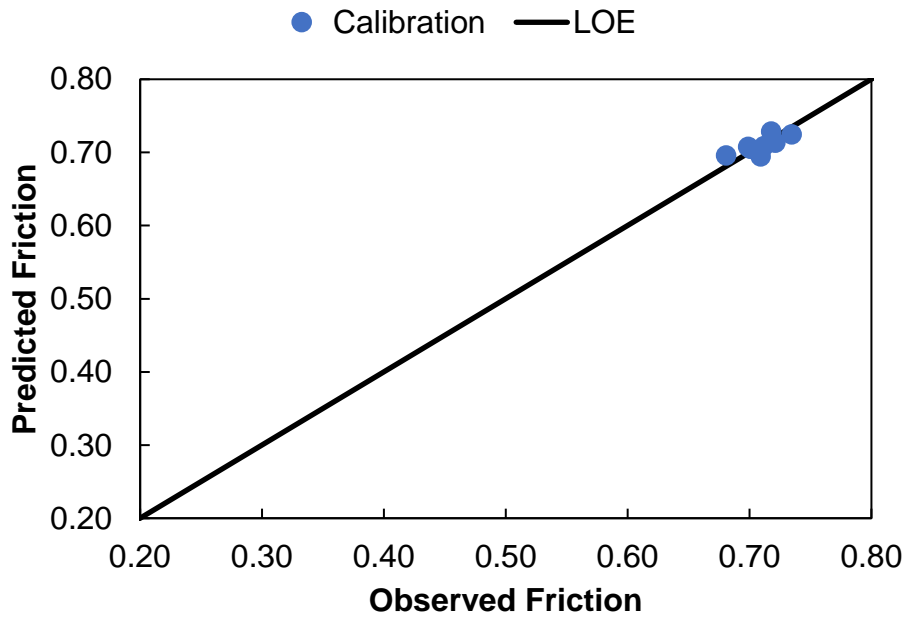
Figure C.3. Prediction verification plots of friction seasonal model for Site 16.
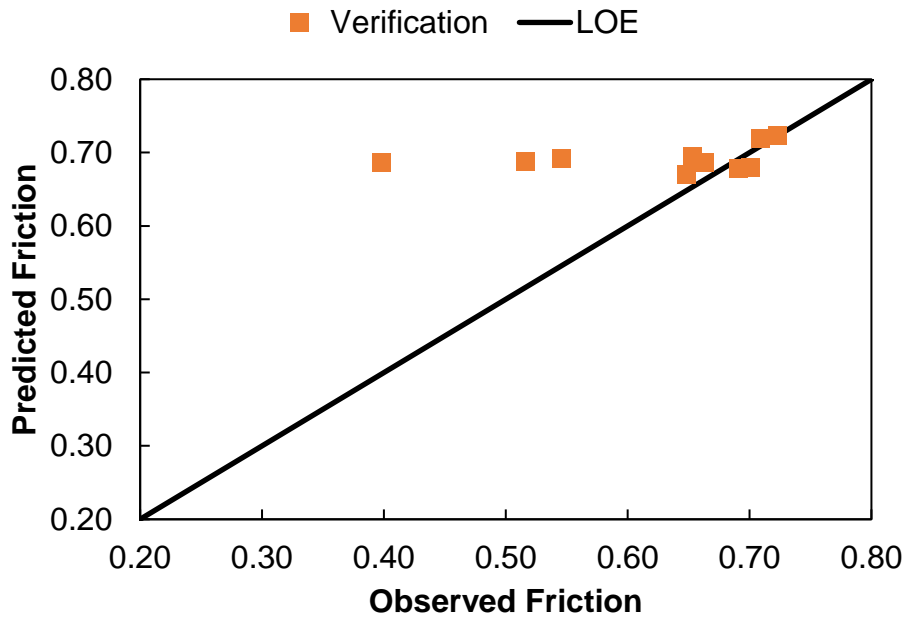
Figure C.4. Prediction verification plots of friction seasonal model for Site 29.
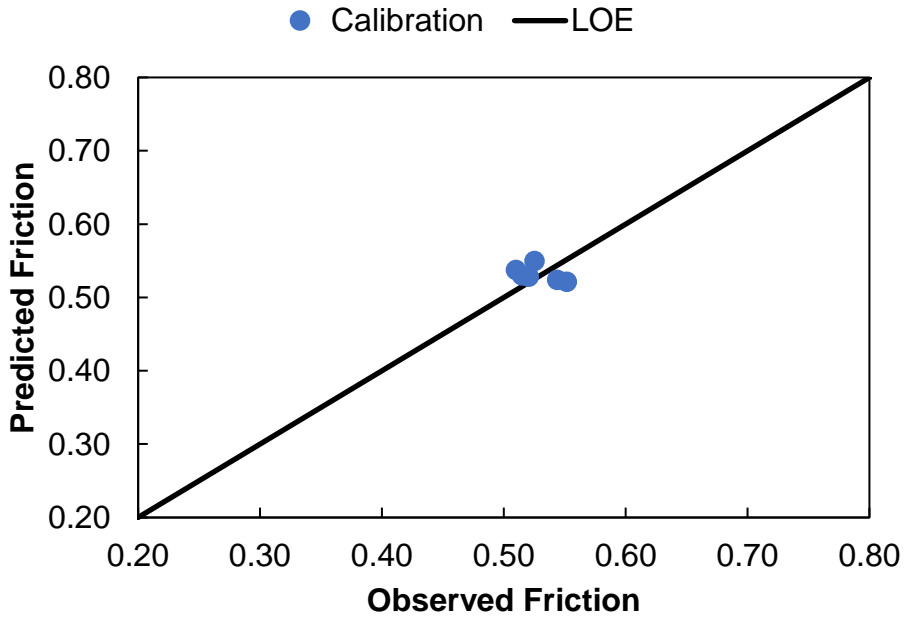
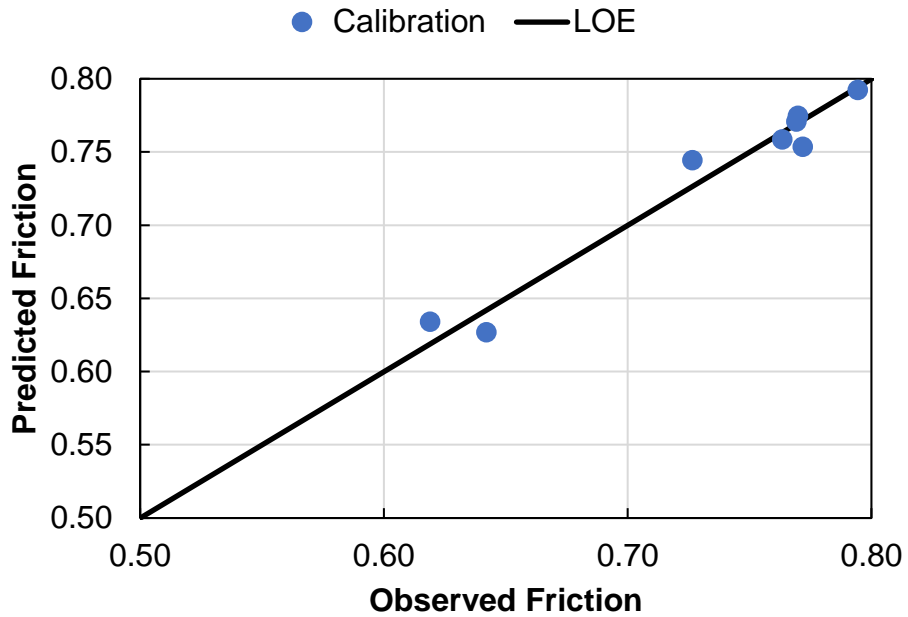**Figure C.5. Prediction verification plots of friction seasonal model for Site 1.**
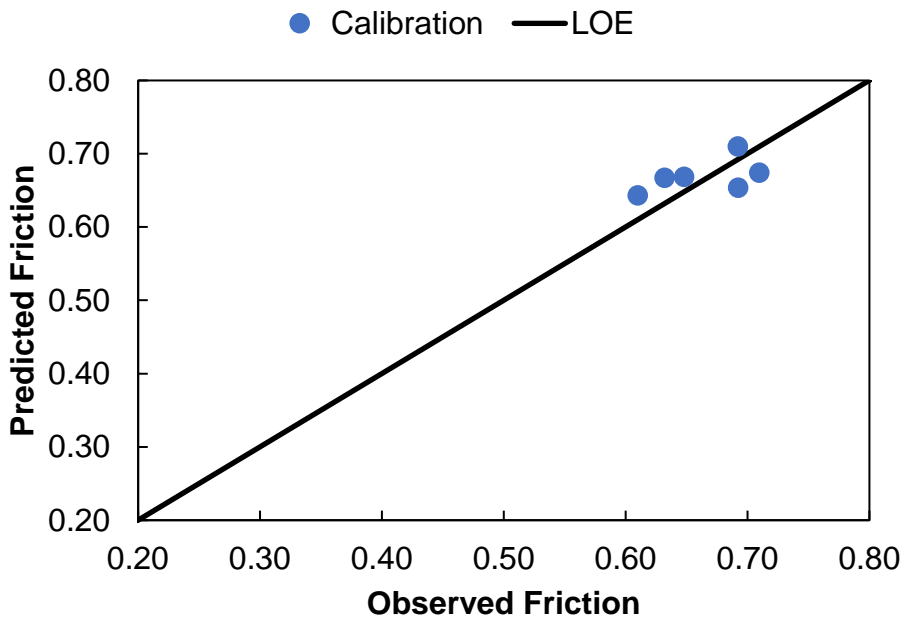
Figure C.6. Prediction verification plots of friction seasonal model for Site 2.

126
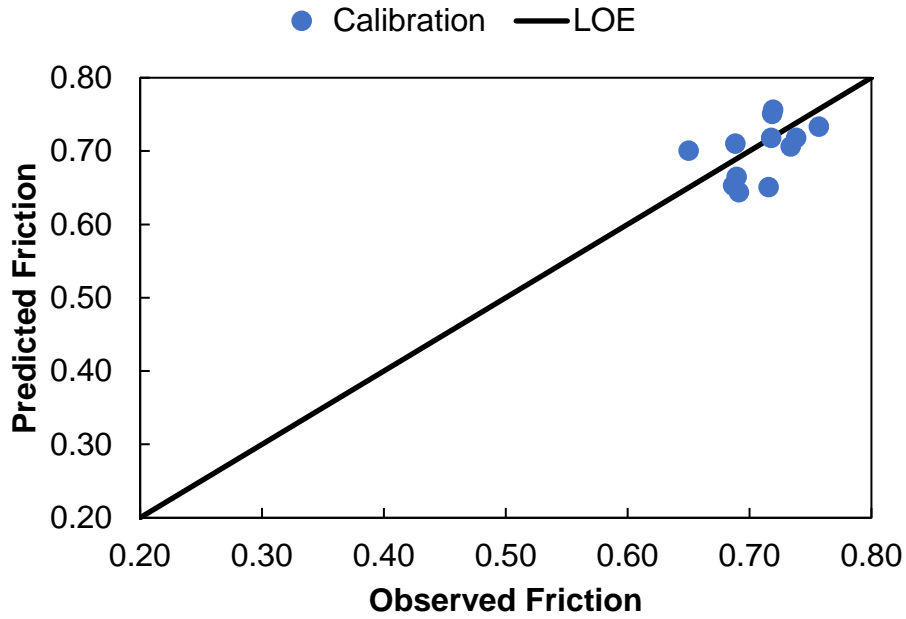
Figure C.7. Prediction verification plots of friction seasonal model for Site 8.
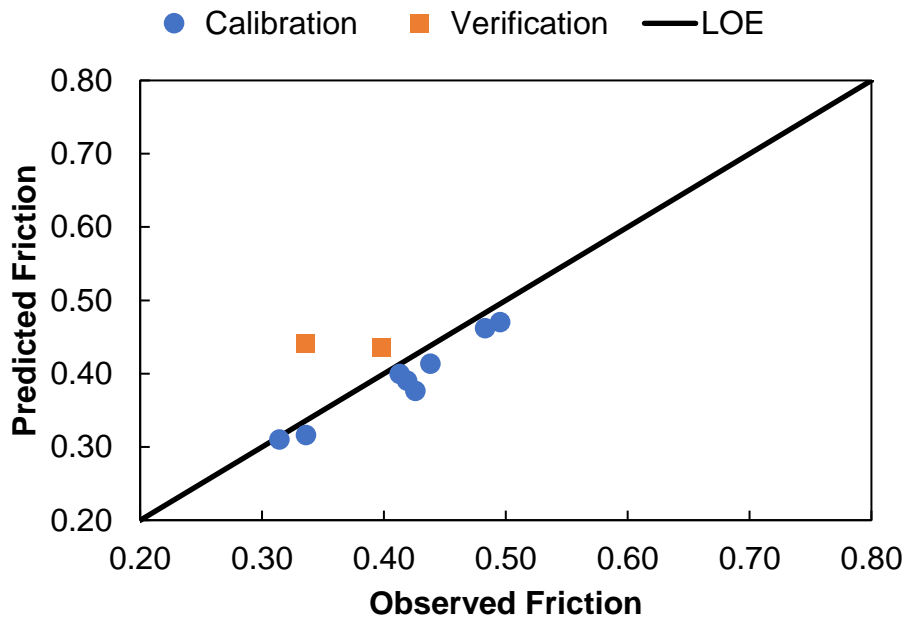
Figure C.8. Prediction verification plots of friction seasonal model for Site 9.
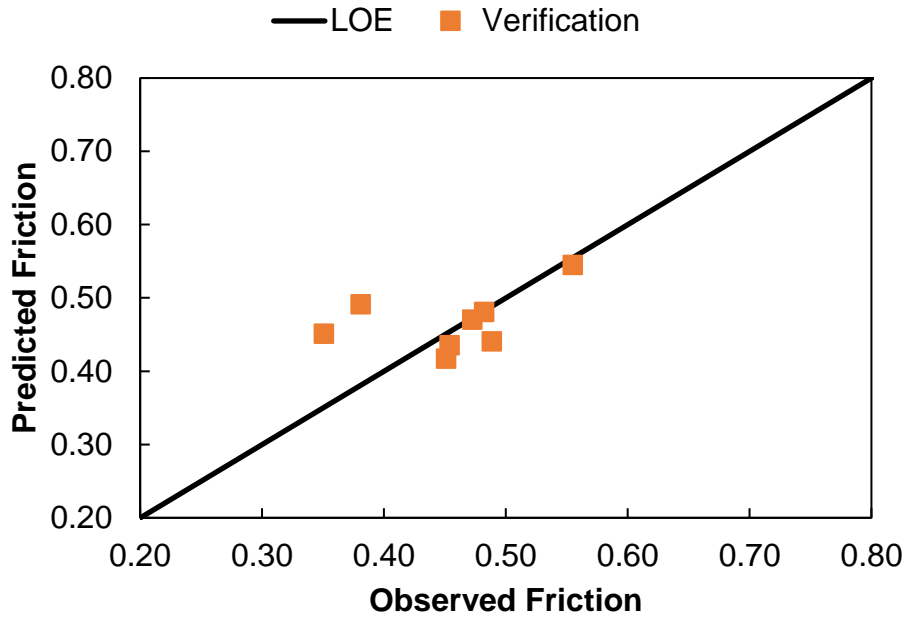
Figure C.9. Prediction verification plots of friction seasonal model for Site 11.
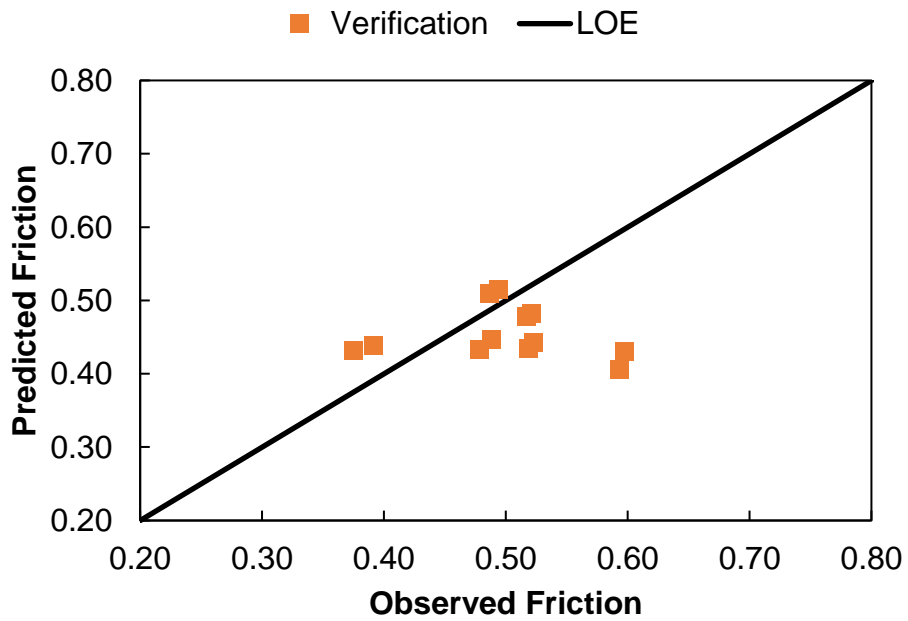
Figure C.10. Prediction verification plots of friction seasonal model for Site 14.
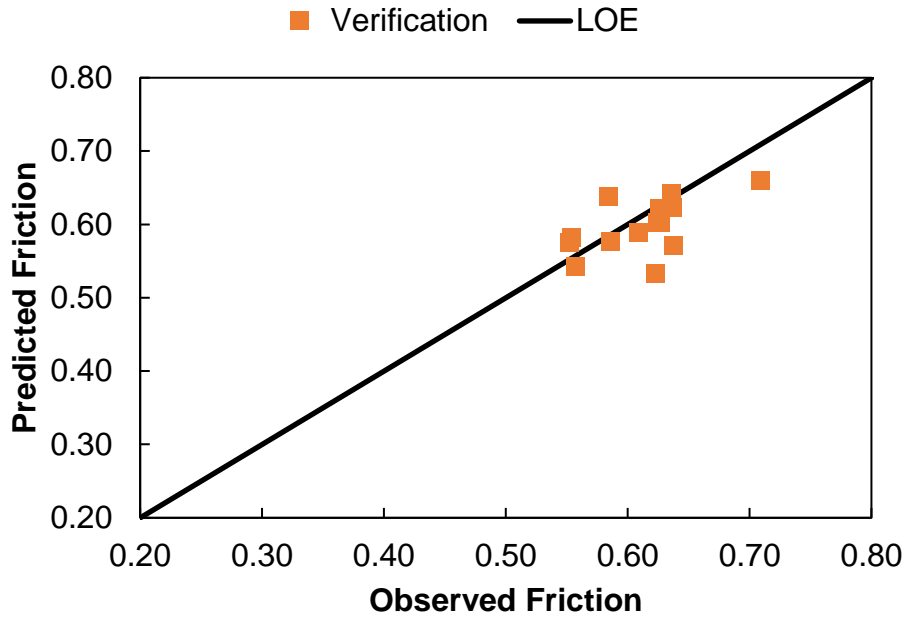
Figure C.11. Prediction verification plots of friction seasonal model for Site 17.

Figure C.12. Prediction verification plots of friction seasonal model for Site 18.

Figure C.13. Prediction verification plots of friction seasonal model for Site 19.

Figure C.14. Prediction verification plots of friction seasonal model for Site 23.

Figure C.15. Prediction verification plots of friction seasonal model for Site 28.

Figure C.16. Prediction verification plots of friction seasonal model for Site 33.

Figure C.17. Prediction verification plots of friction seasonal model for Site 6.

Figure C.18. Prediction verification plots of friction seasonal model for Site 7.

Figure C.19. Prediction verification plots of friction seasonal model for Site 12.

Figure C.20. Prediction verification plots of friction seasonal model for Site 27.

Figure C.21. Prediction verification plots of friction seasonal model for Site 4.1.

Figure C.22. Prediction verification plots of friction seasonal model for Site 5.

Friction Variation with Traffic

RS9.5B Sites
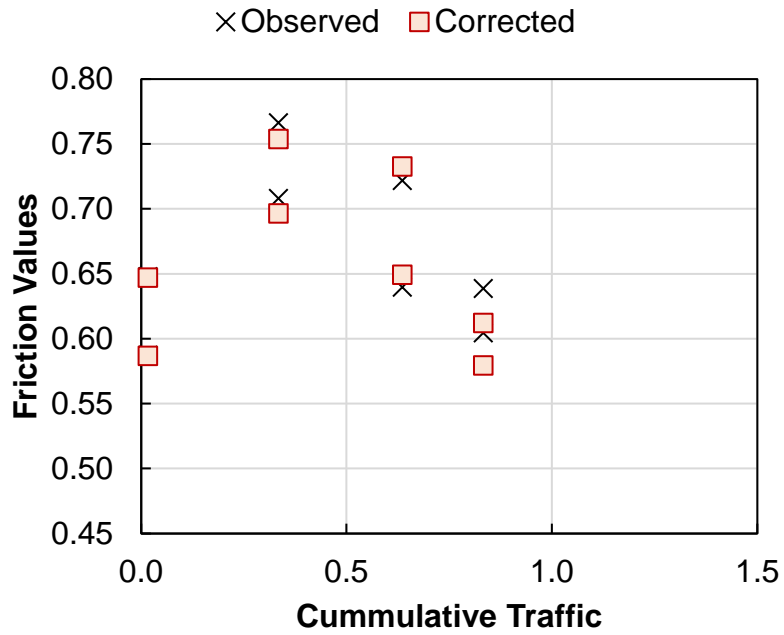
Figure C.23. Friction variation with traffic in Site 3.
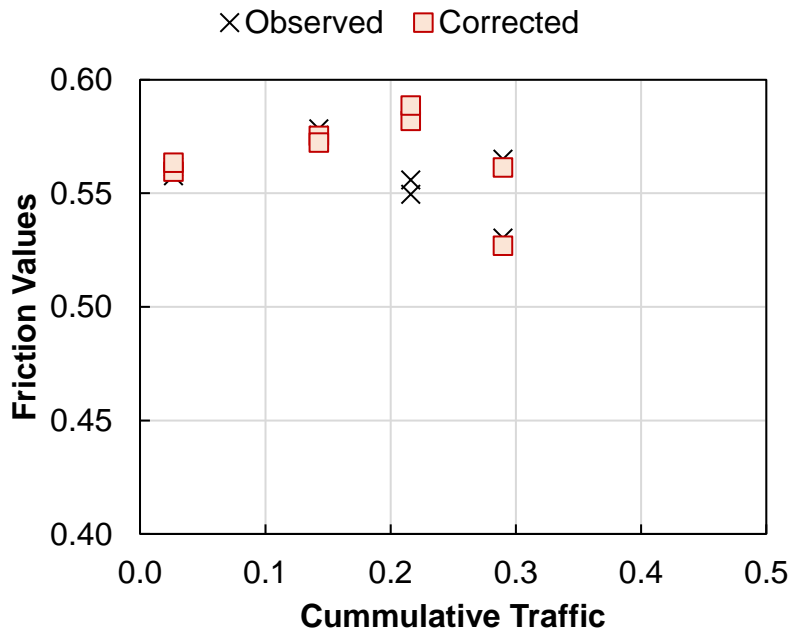
Figure C.24. Friction variation with traffic in Site 15.
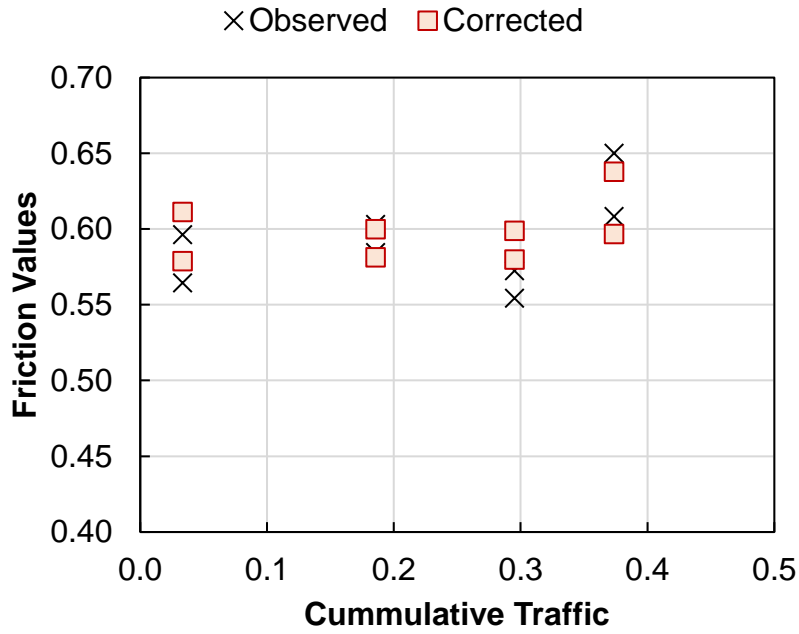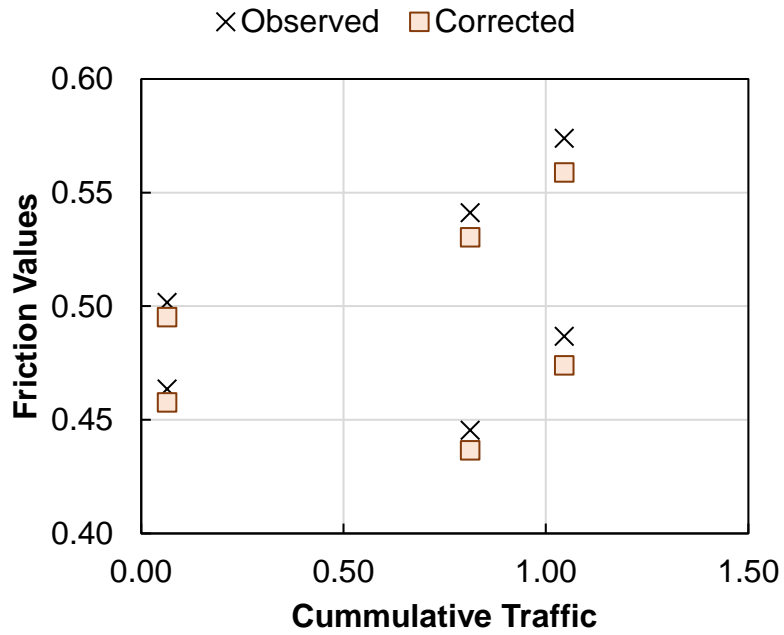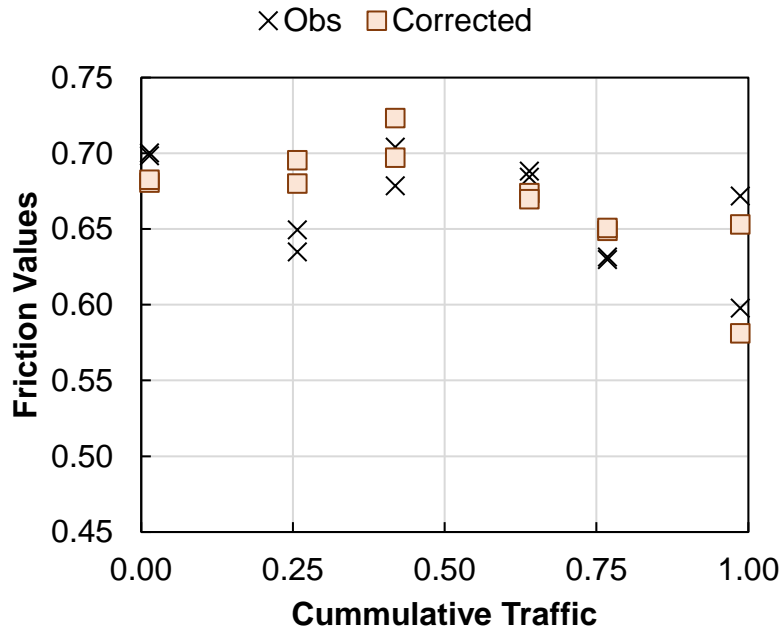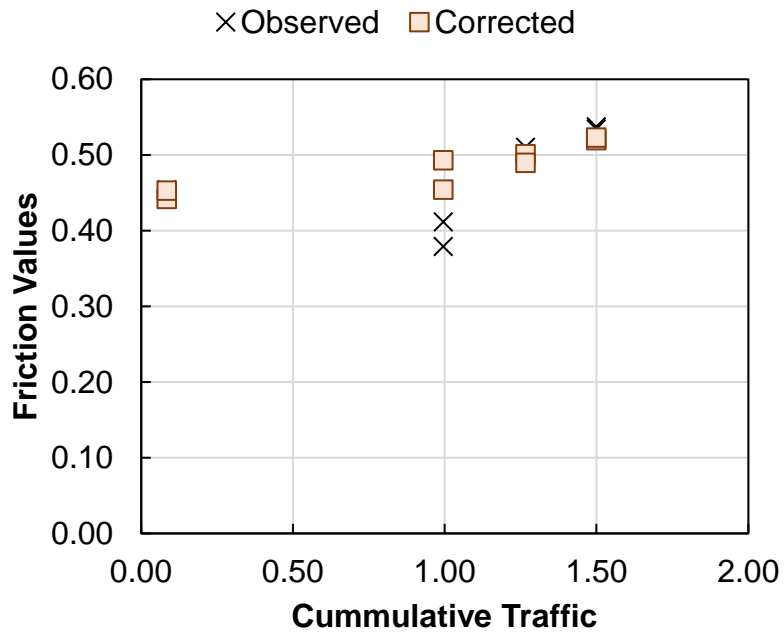
Figure C.25. Friction variation with traffic in Site 16.
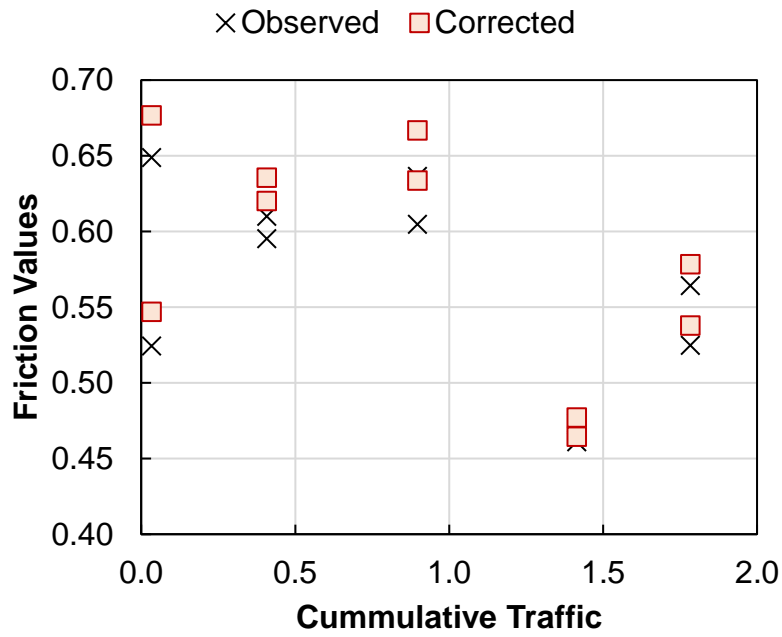
Figure C.26. Friction variation with traffic in Site 29.

136
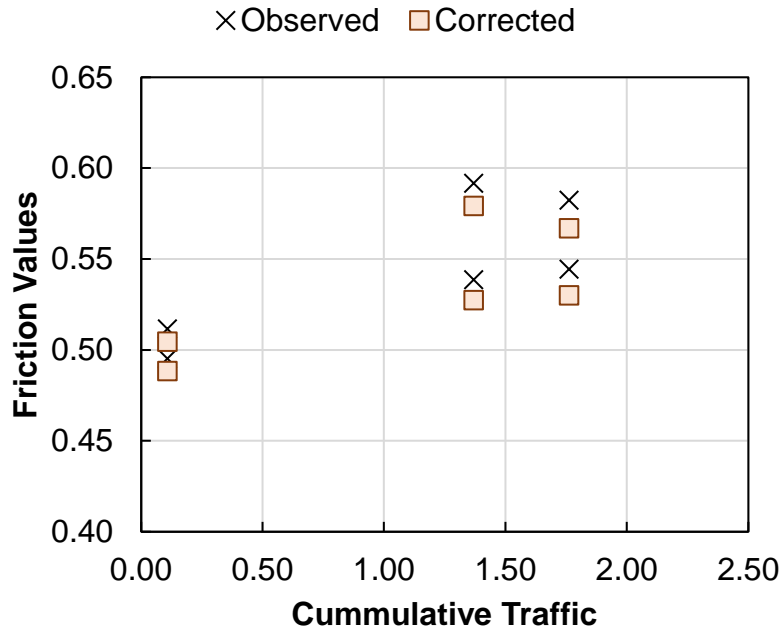
Figure C.27. Friction variation with traffic in Site 1.

Figure C.28. Friction variation with traffic in Site 2.

Figure C.29. Friction variation with traffic in Site 8.

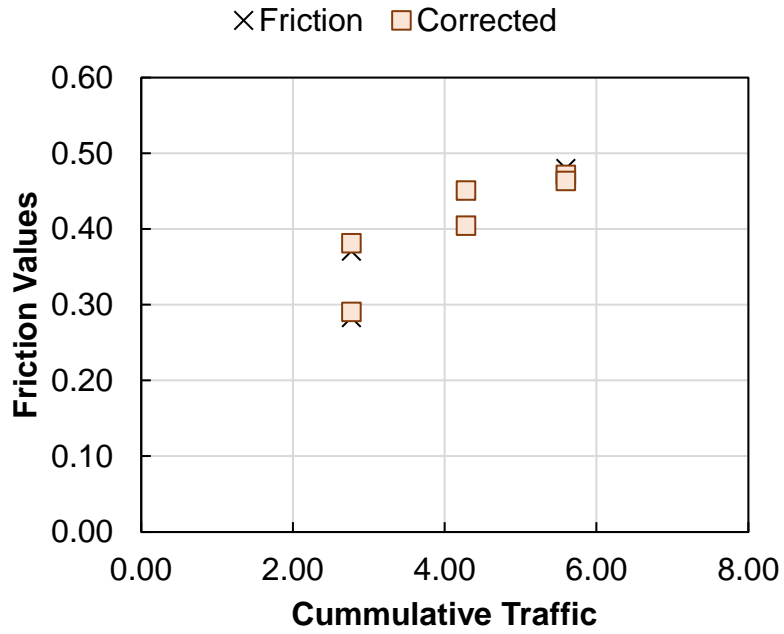**Figure C.30. Friction variation with traffic in Site 9.**

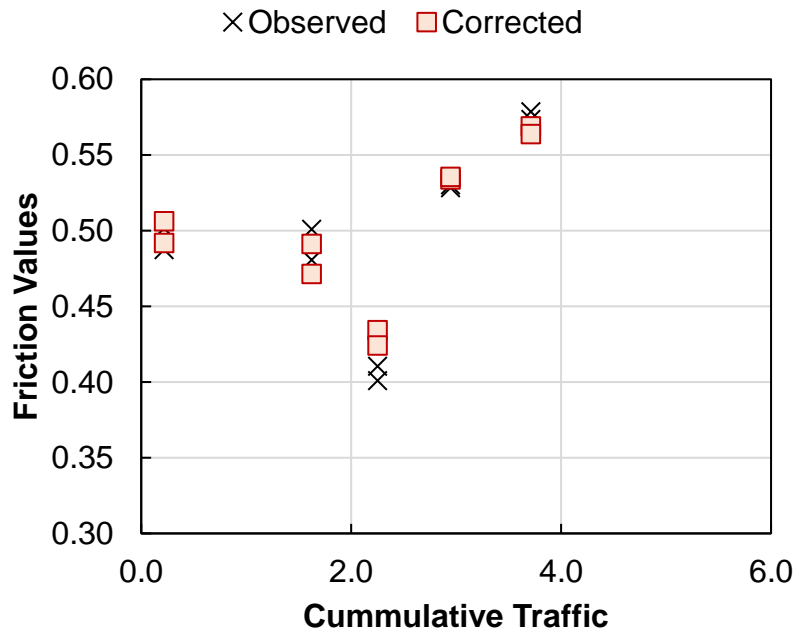**Figure C.31. Friction variation with traffic in Site 11.**

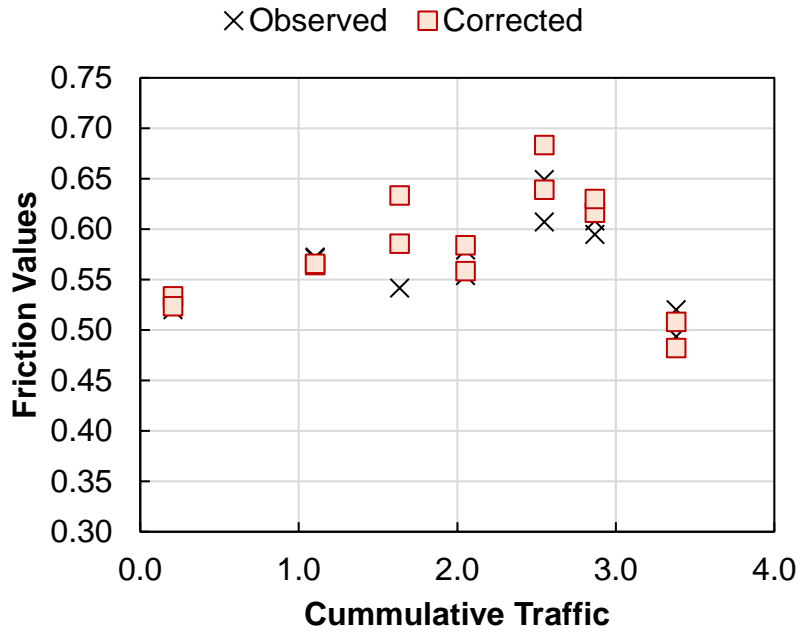**Figure C.32. Friction variation with traffic in Site 14.**

139

Figure C.33. Friction variation with traffic in Site 17.
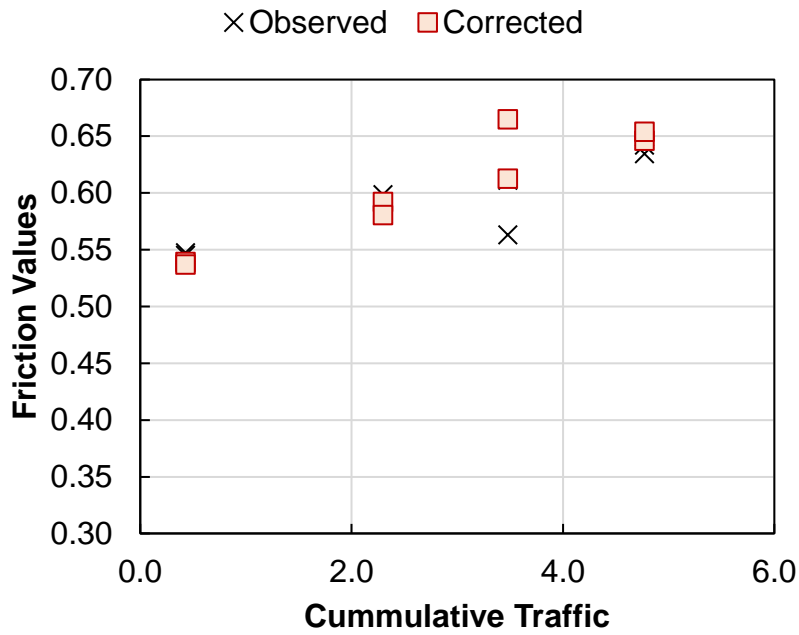

Figure C.34. Friction variation with traffic in Site 18.
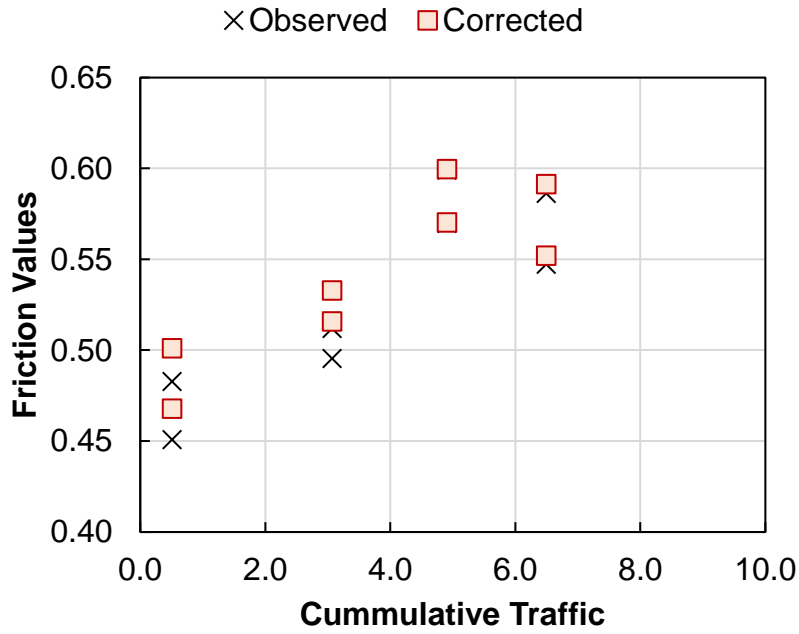
Figure C.35. Friction variation with traffic in Site 19.

Figure C.36. Friction variation with traffic in Site 23.

Figure C.37. Friction variation with traffic in Site 28.
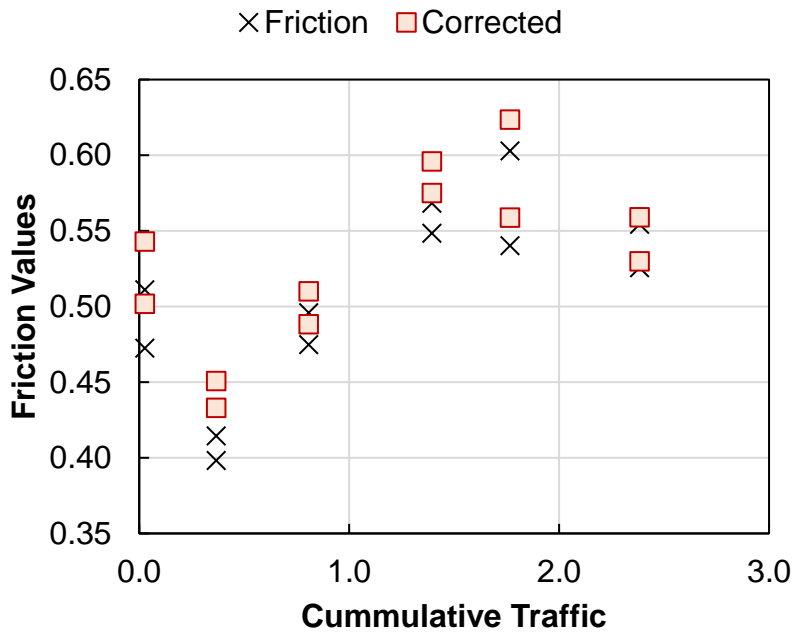
Figure C.38. Friction variation with traffic in Site 33.
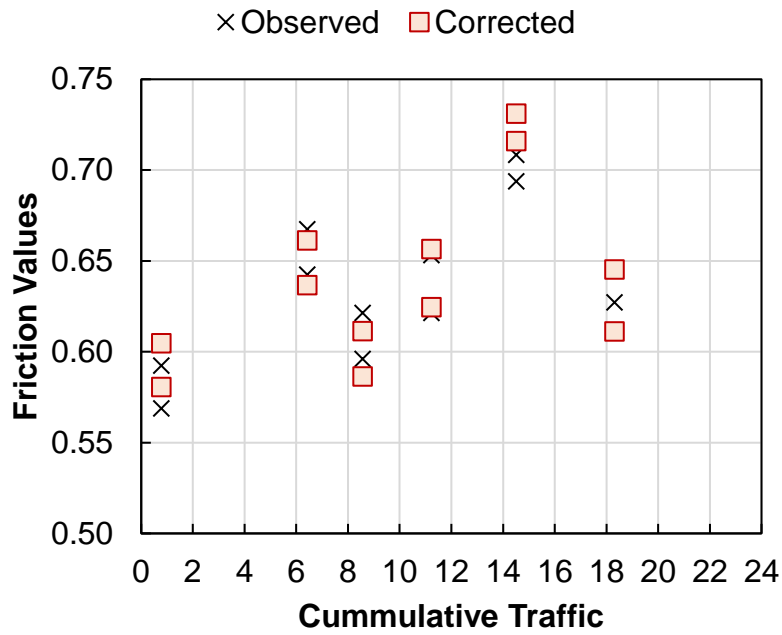
Figure C.39. Friction variation with traffic in Site 6.
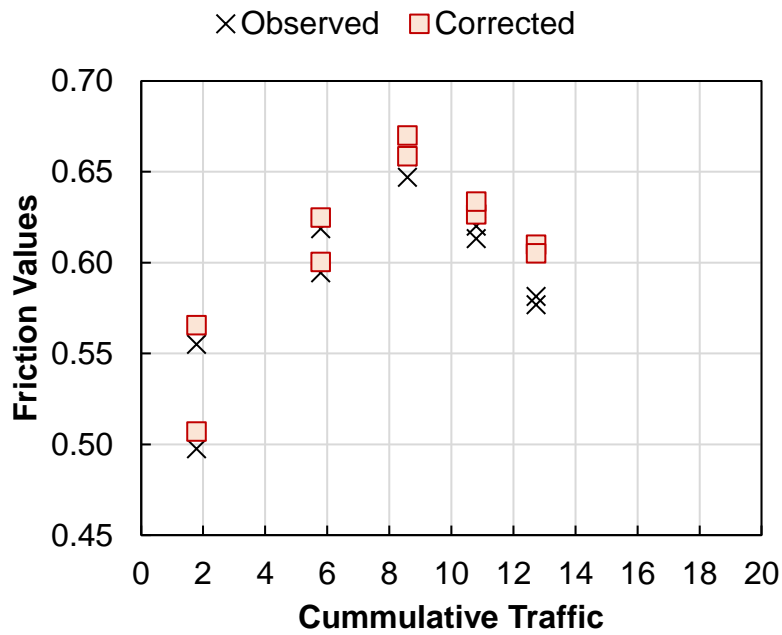
Figure C.40. Friction variation with traffic in Site 7.

143
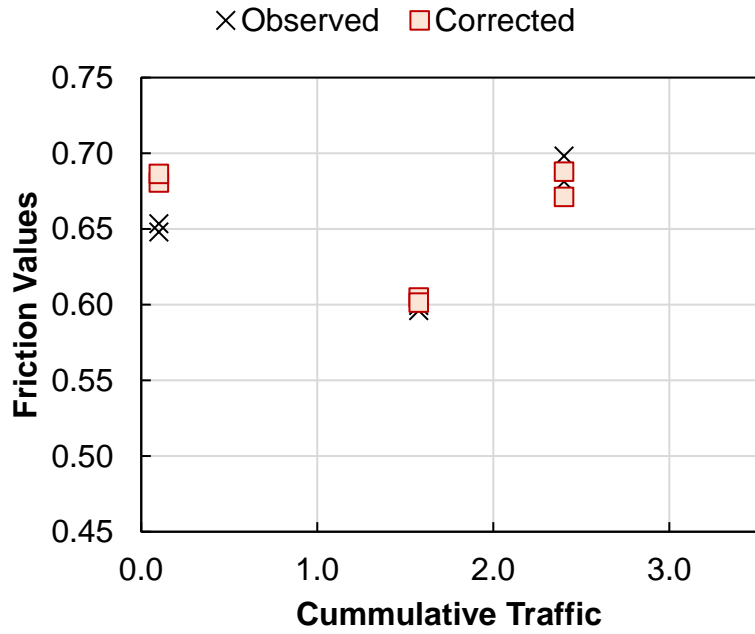
Figure C.41. Friction variation with traffic in Site 12.
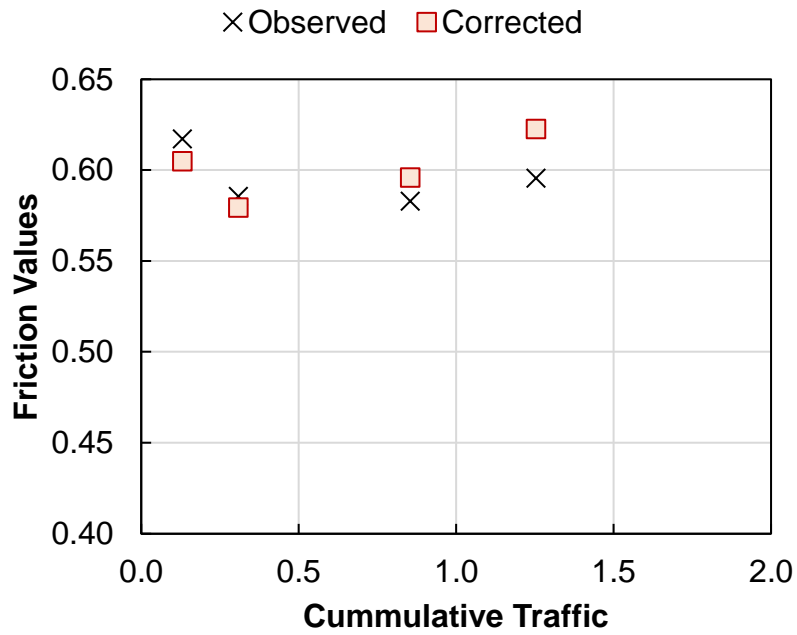
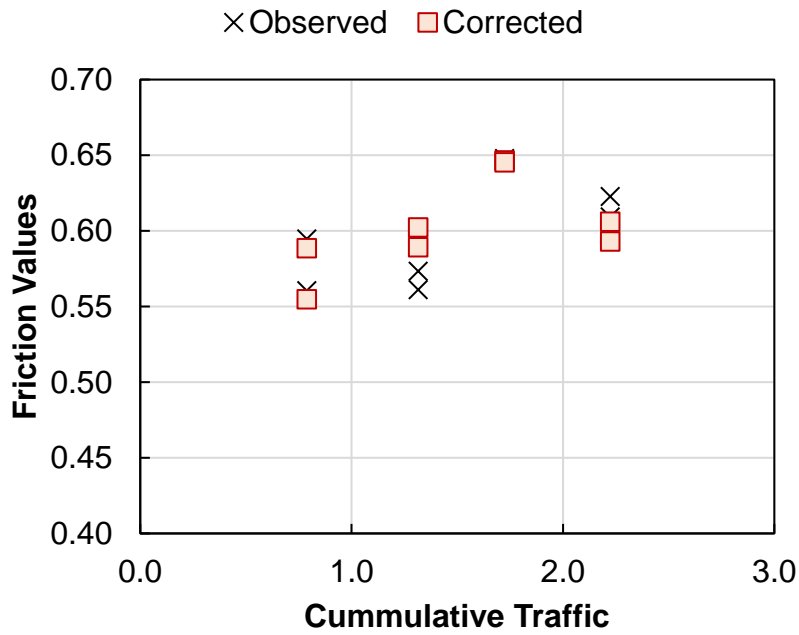**Figure C.42. Friction variation with traffic in Site 27.**

144
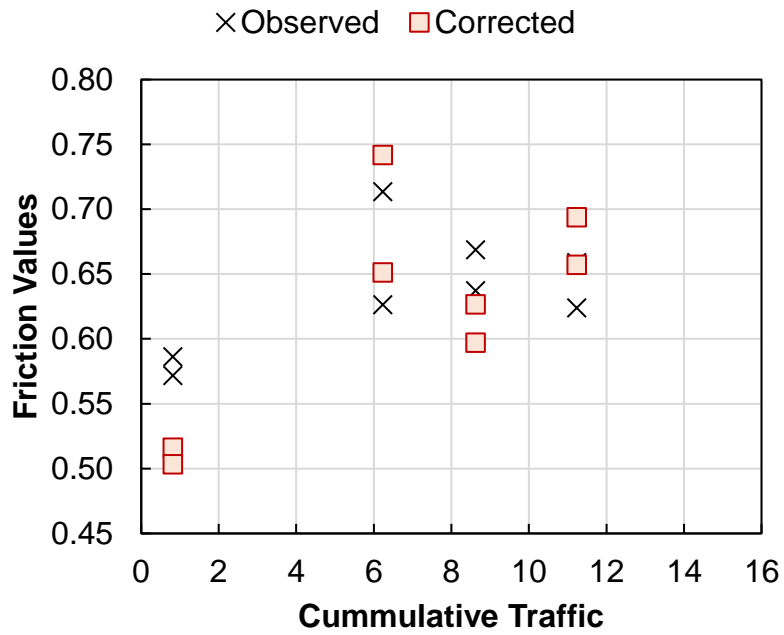
Figure C.43. Friction variation with traffic in Site 4.1.
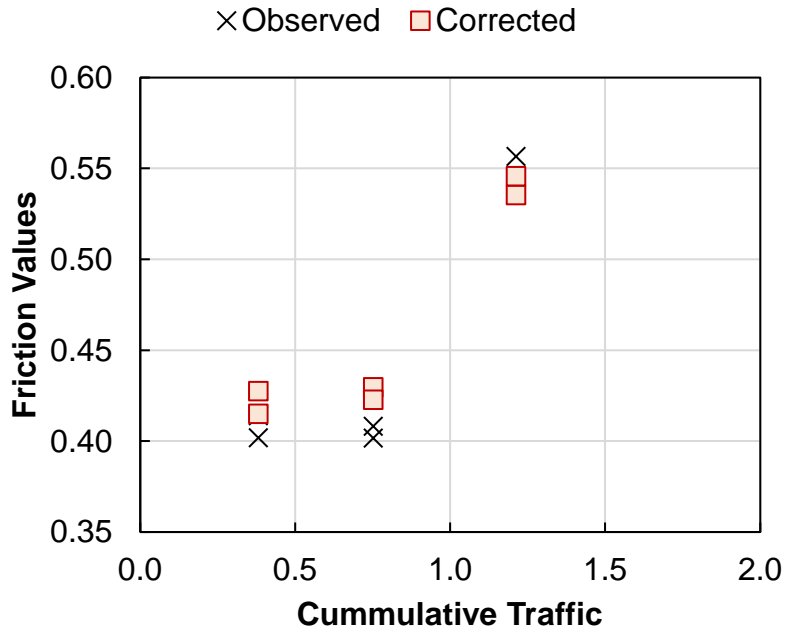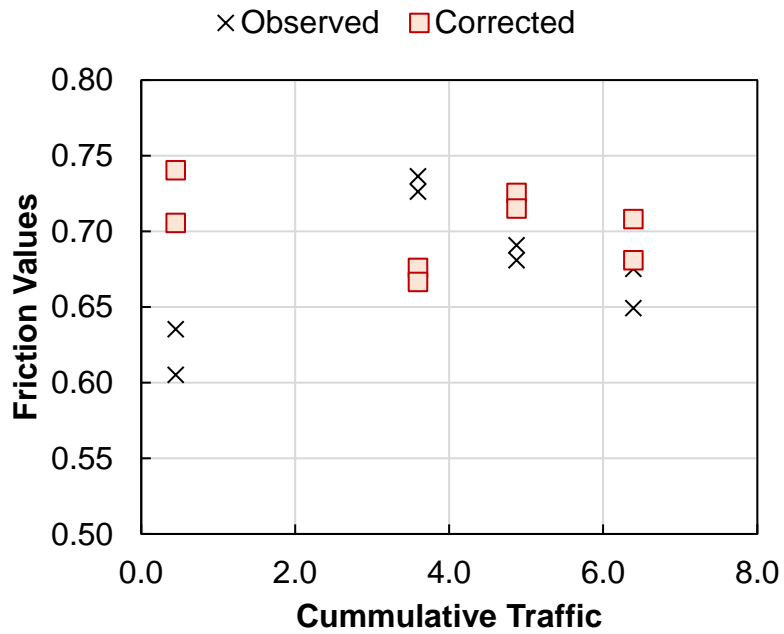

Figure C.44. Friction variation with traffic in Site 5.

***MPD* Variation with Time**

RS9.5B Sites

Figure C.45. *MPD* **variation with time in Site 3.**

Figure C.46. *MPD* **variation with time in Site 15.**

Figure C.47. *MPD* variation with time in Site 16.

Figure C.48. *MPD* variation with time in Site 29.

Figure C.49. *MPD* **variation with time in Site 1.**

Figure C.50. *MPD* **variation with time in Site 2.**

148

Figure C.51. *MPD* **variation with time in Site 8.**

Figure C.52. *MPD* **variation with time in Site 9.**

Figure C.53. *MPD* variation with time in Site 11.

Figure C.54. *MPD* variation with time in Site 14.

150

Figure C.55. *MPD* **variation with time in Site 17.**

Figure C.56. *MPD* **variation with time in Site 18.**

151

Figure C.57. *MPD* variation with time in Site 19.

Figure C.58. *MPD* variation with time in Site 23.

Figure C.59. *MPD* **variation with time in Site 28.**
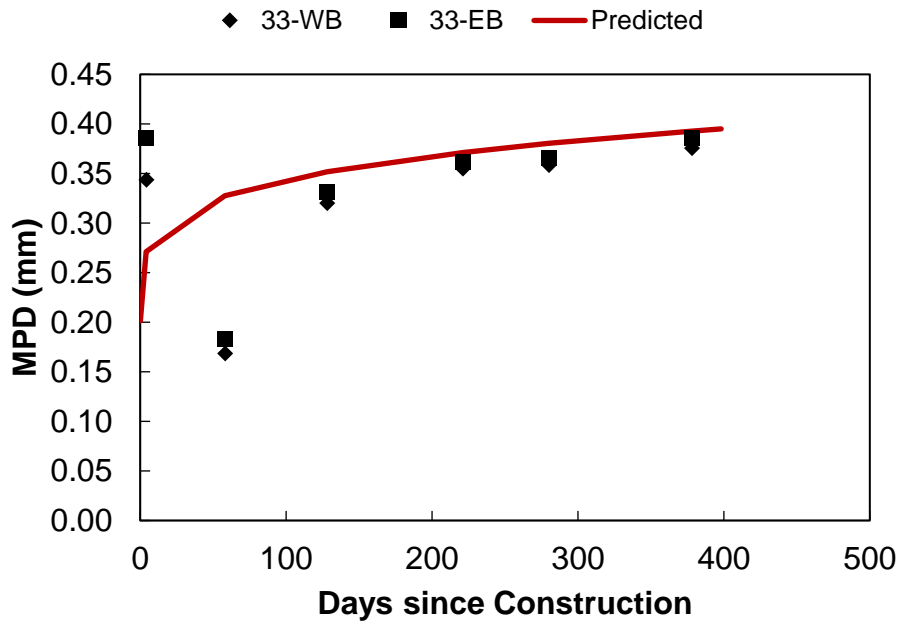
Figure C.60. *MPD* **variation with time in Site 33.**

153
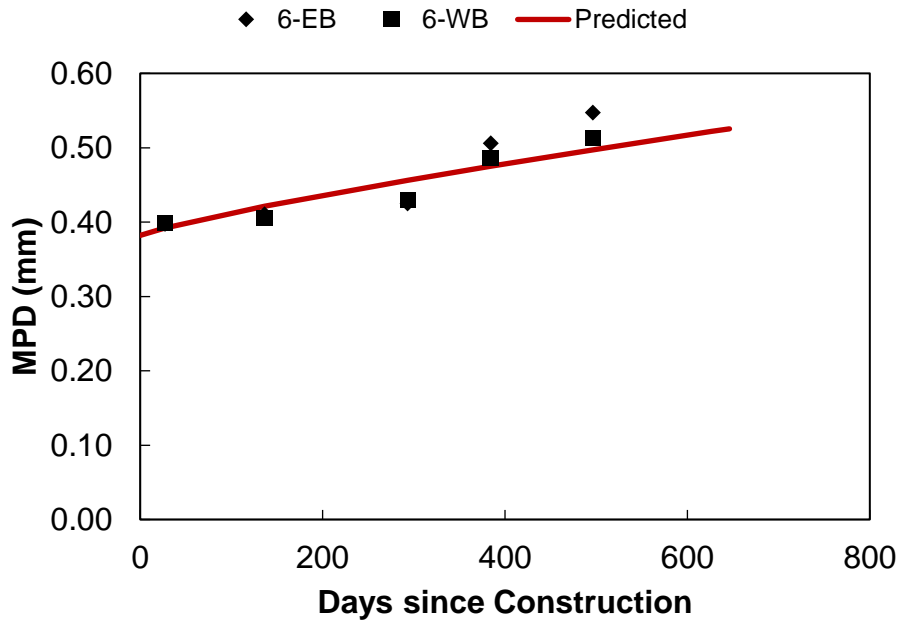
Figure C.61. *MPD* **variation with time in Site 6.**
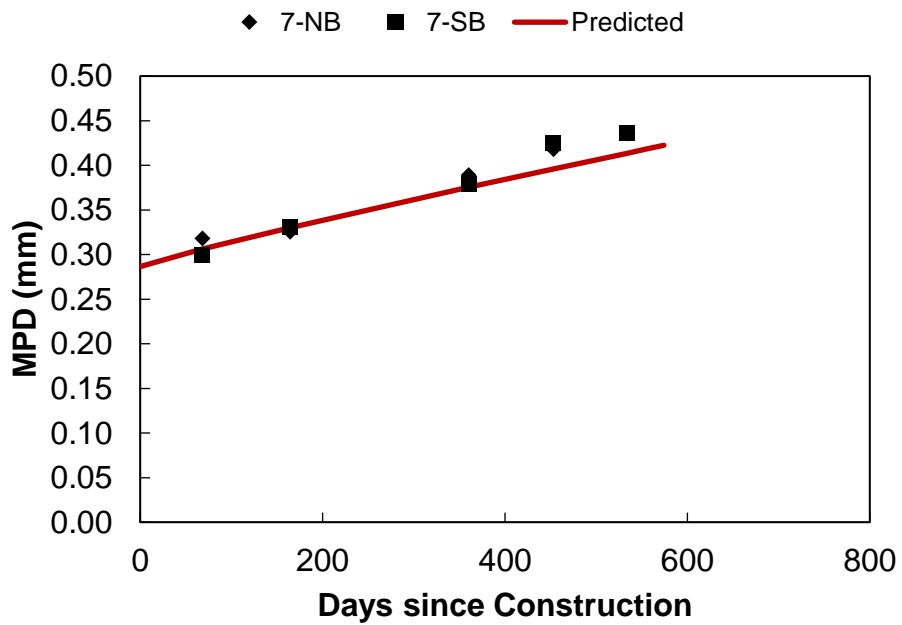
Figure C.62. *MPD* **variation with time in Site 7.**
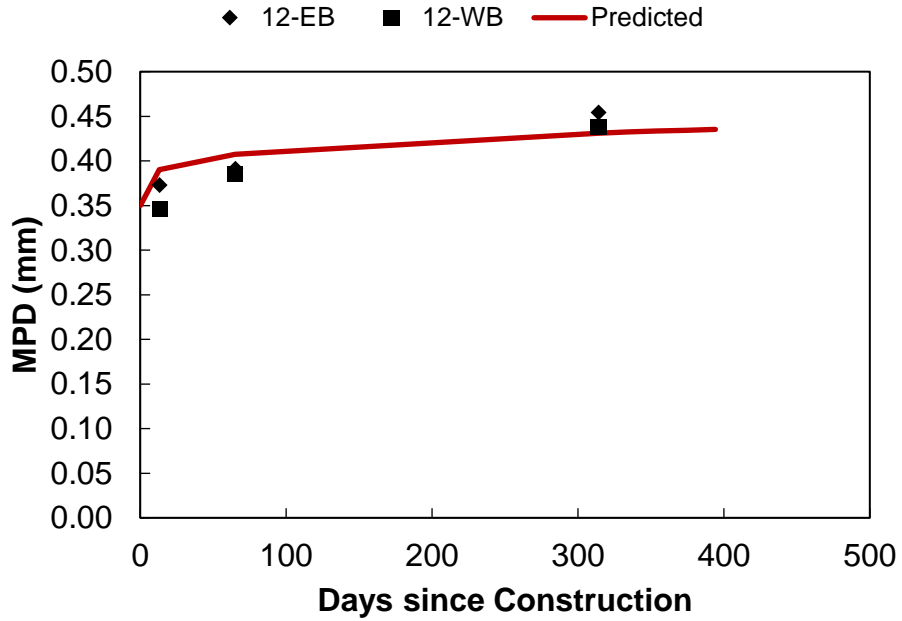
Figure C.63. *MPD* variation with time in Site 12.
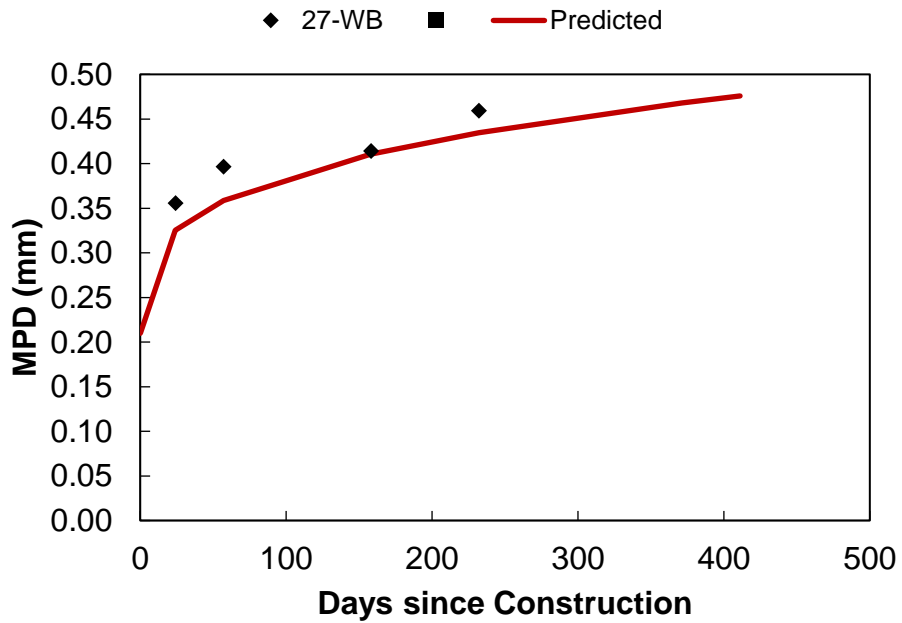
Figure C.64. *MPD* variation with time in Site 27.

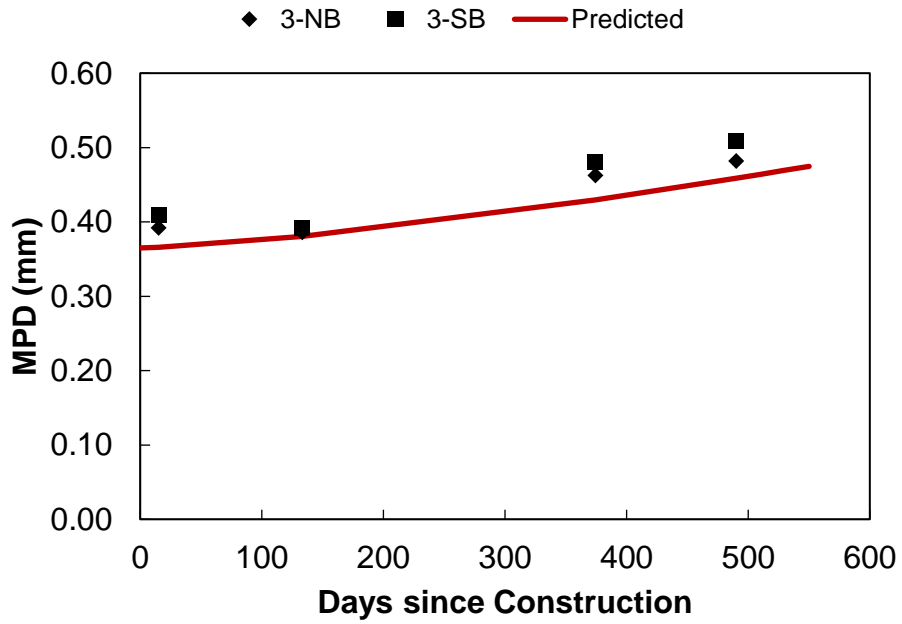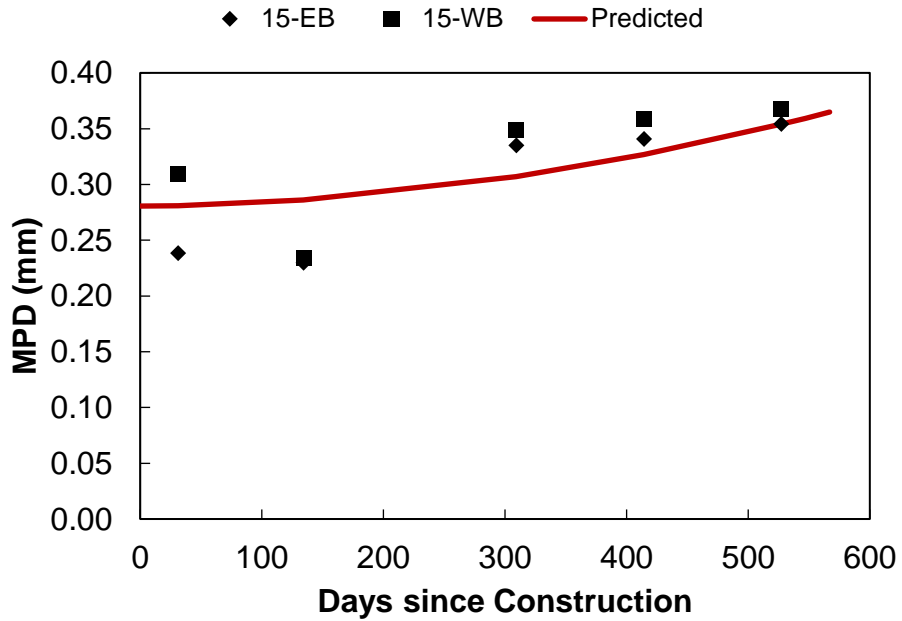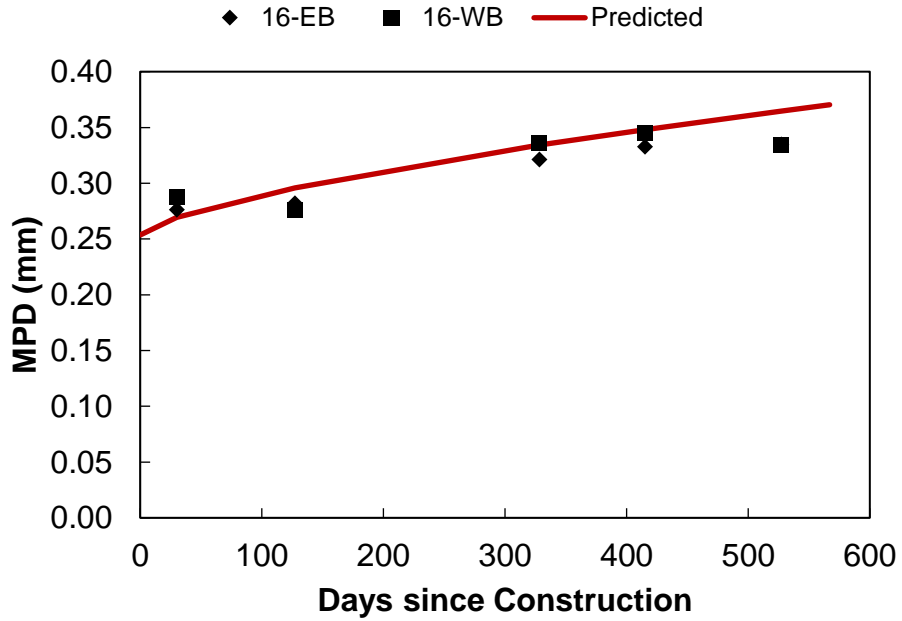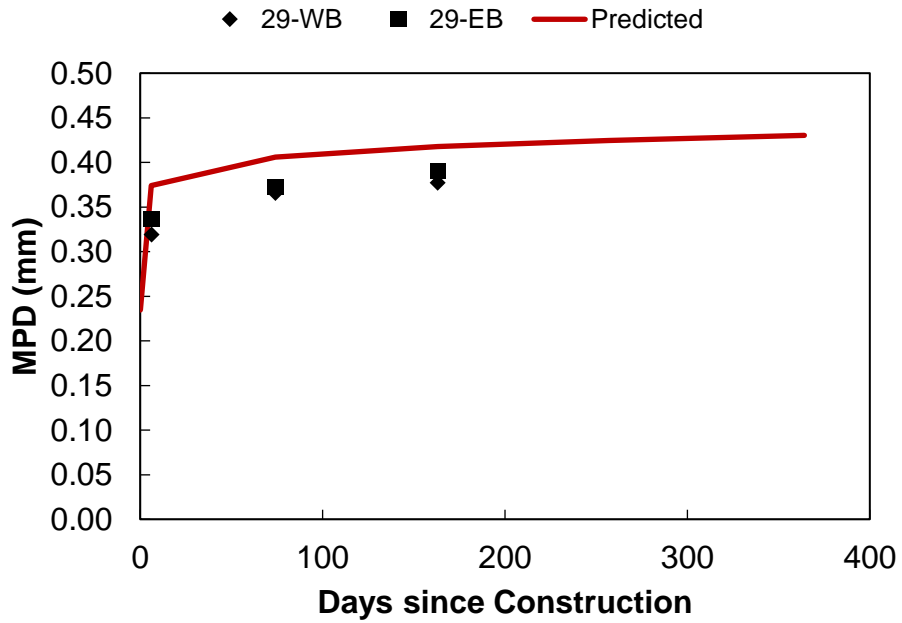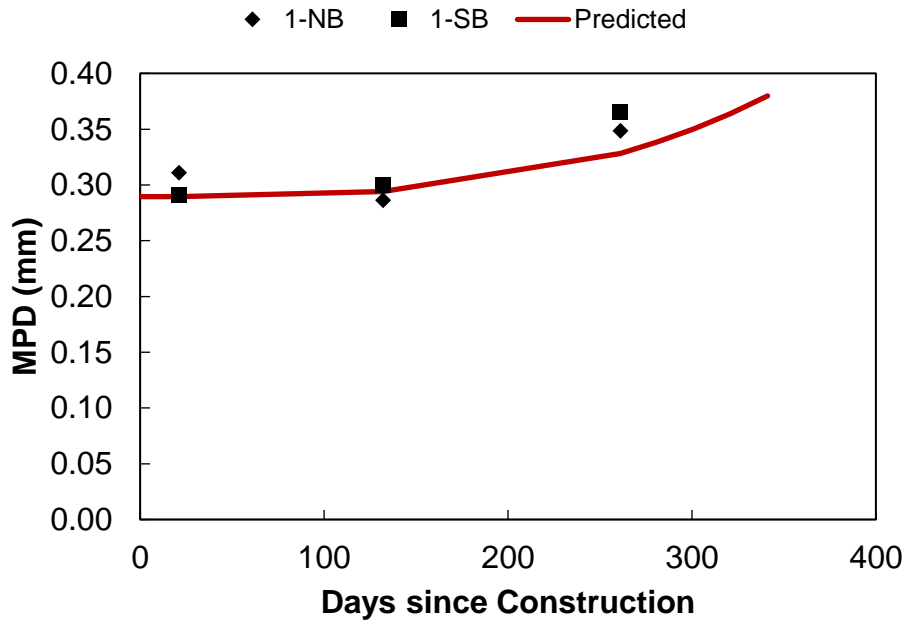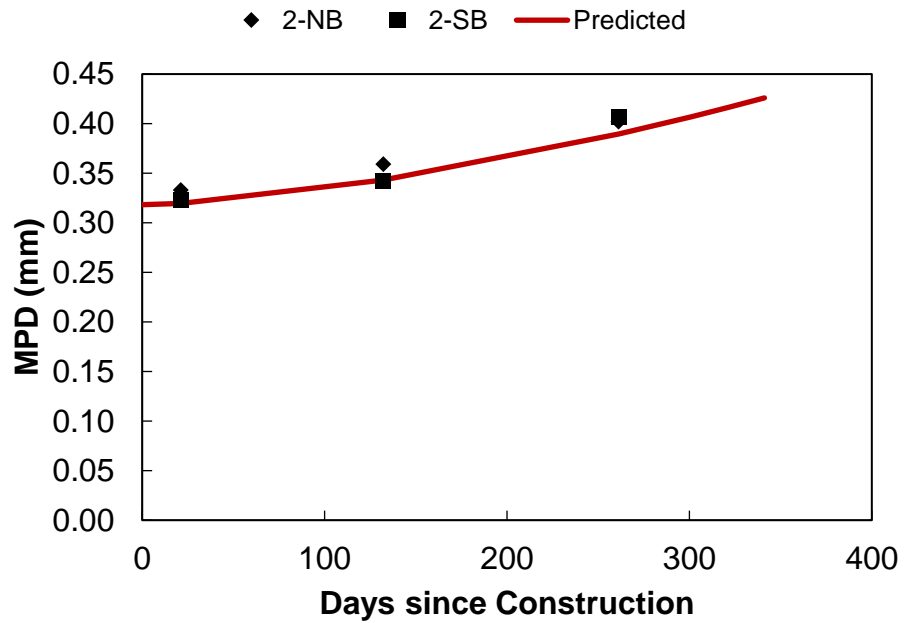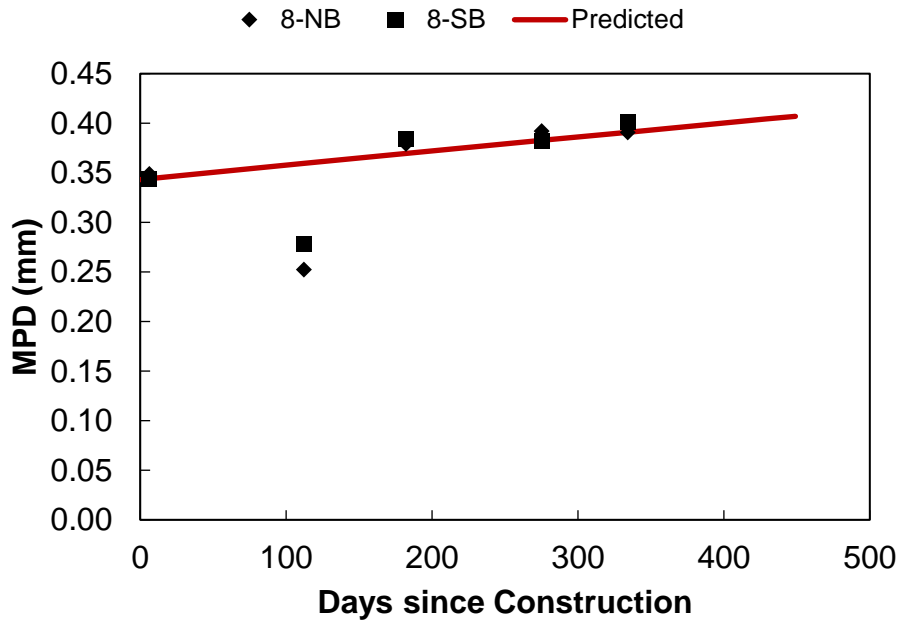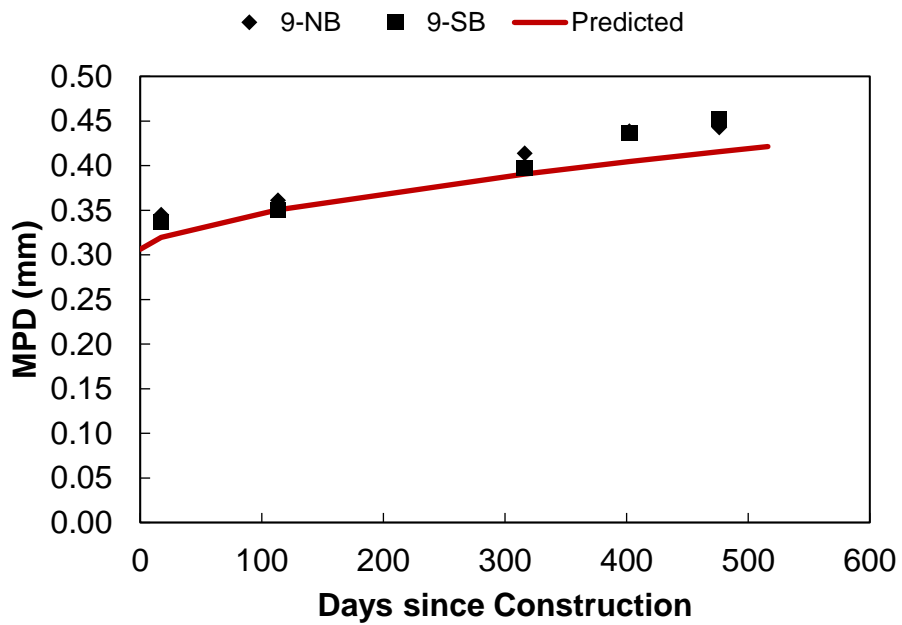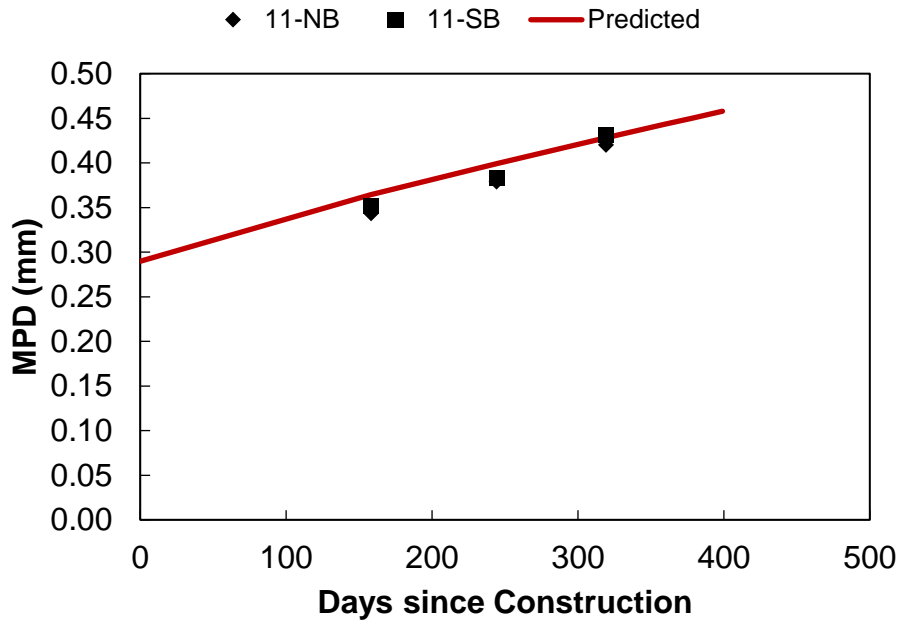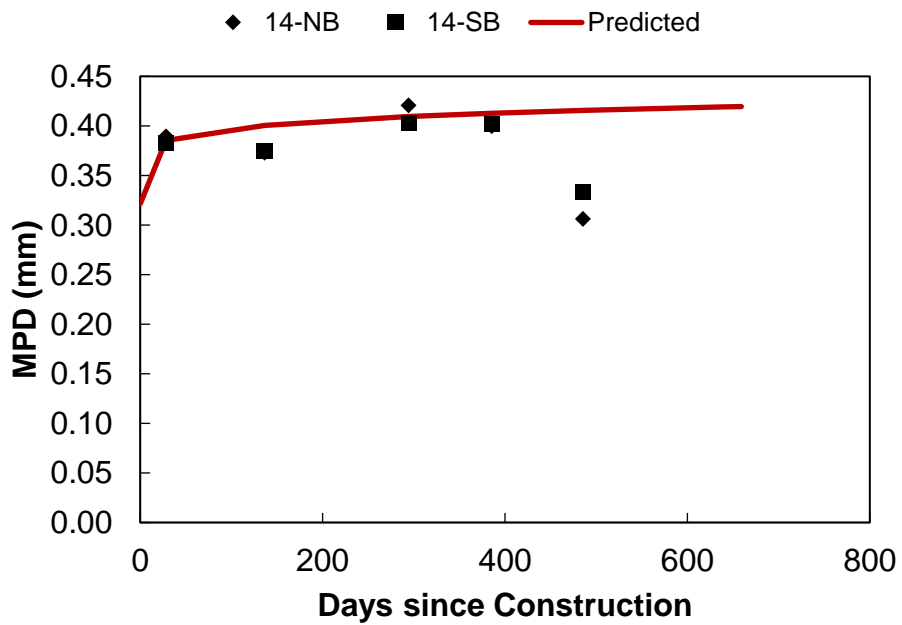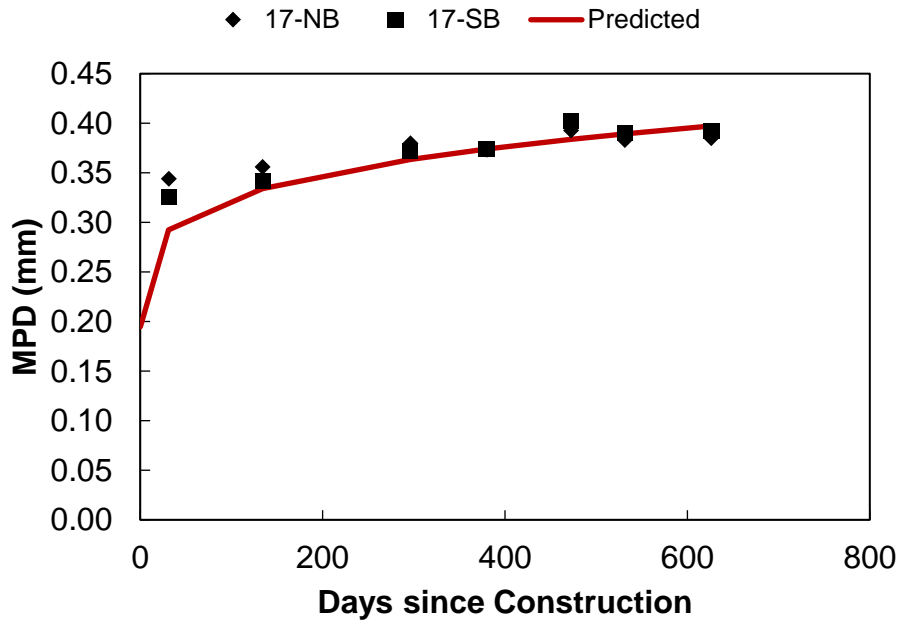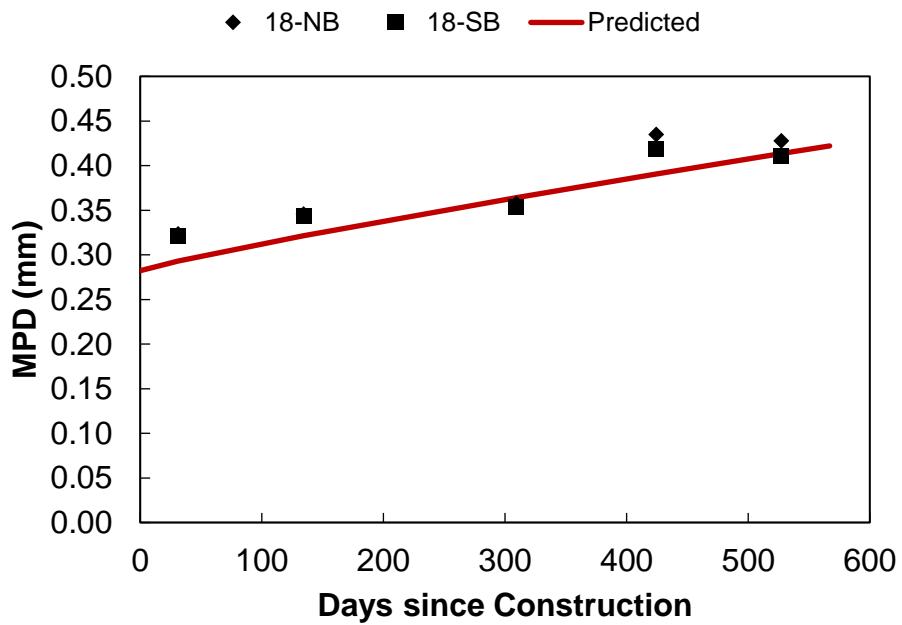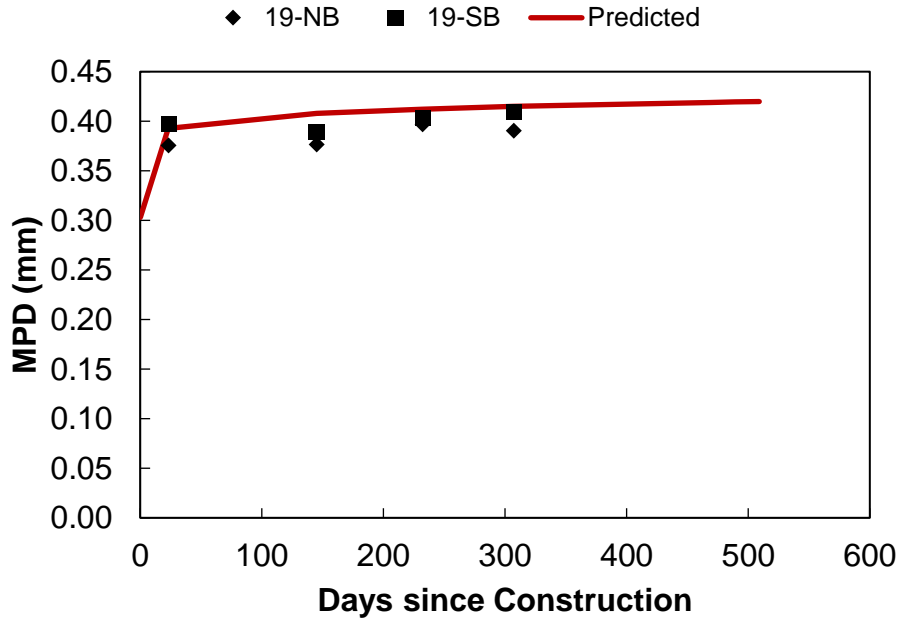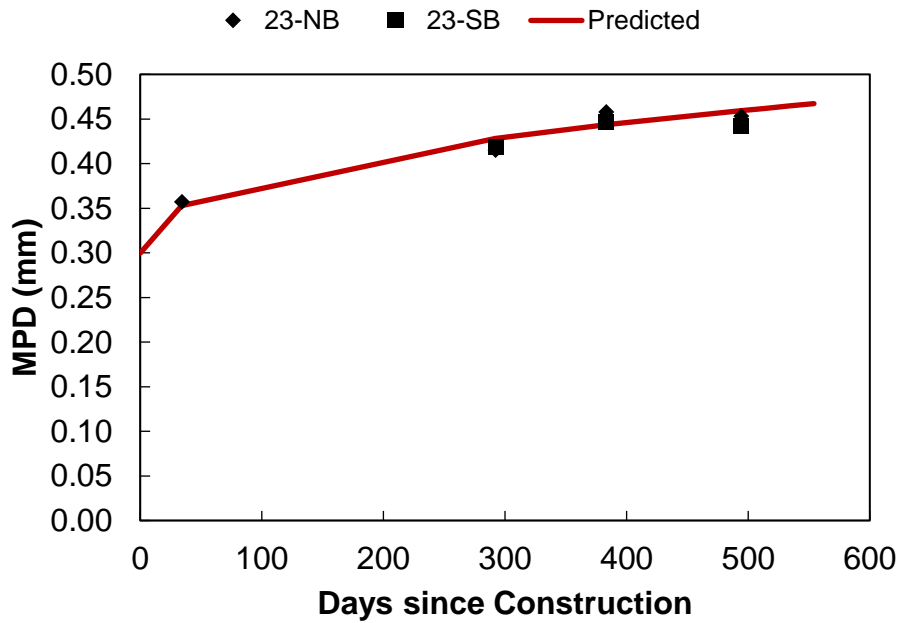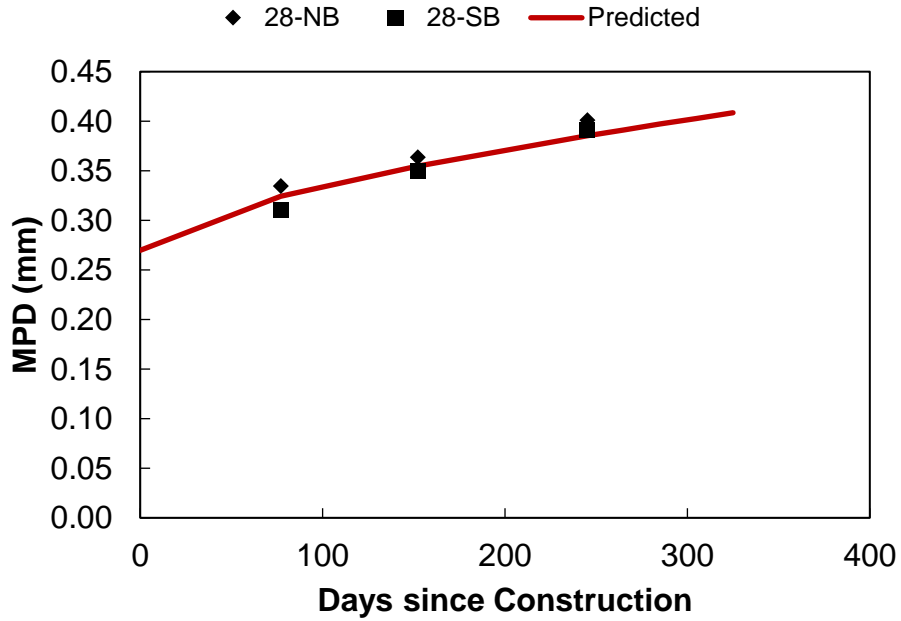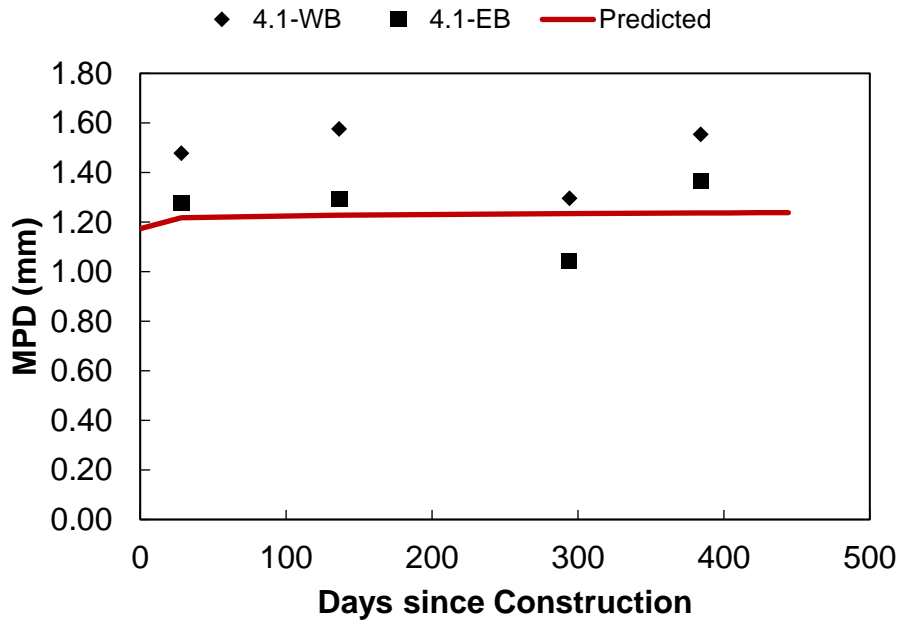**Figure C.65.** *MPD* **variation with time in Site 4.1.**
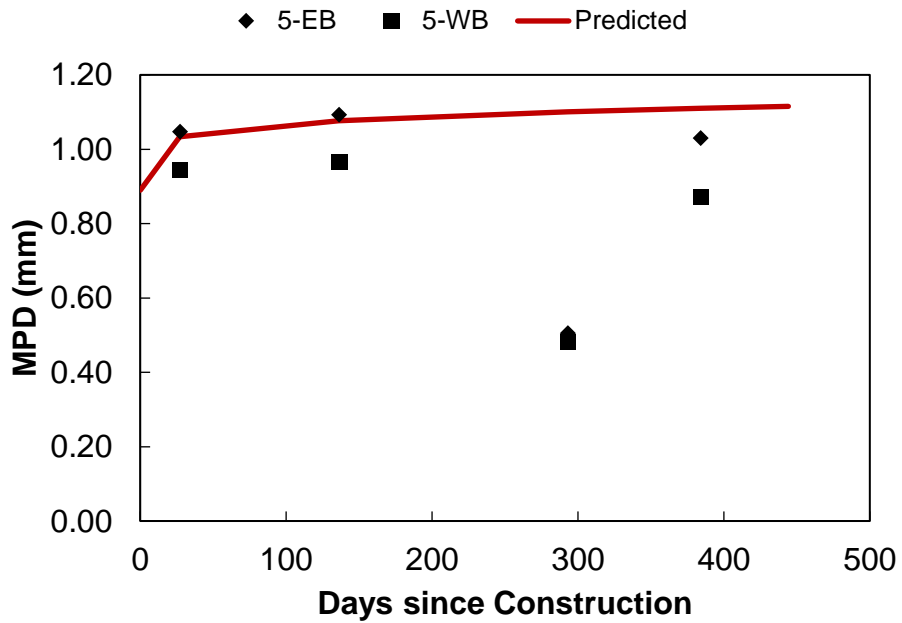
Figure C.66. *MPD* **variation with time in Site 5.**

Overview

To assess the effect of a treatment on the safety a roadway one must compare the number of crashes or the crash rates that were observed after the treatment to the estimated crash rate in the absence of that treatment. The difficulty of this process is the prediction of 'what would have been' if the treatment had not been applied. It is physically impossible to do this type of assessment with complete accuracy, but there are various ways to estimate the number of crashes that could have been expected.

The simplest approach, a so-called naïve analysis, is one where the number of crashes in the period before the treatment is compared directly with the observations after the treatment. The tacit assumption under such analysis is that the count of the number of collisions in the 'before' period is a good estimate of what would have been the number of collisions in the 'after' period. However, since traffic, weather, road condition, driver characteristics, and other important factors all change in time, this assumption might not always be correct, and naïve analyses might reflect not only the effect of the treatment but also the effect of changes in all the other factors (*30*).

The goal then is to estimate the effect of a treatment on safety. Hence, the first step is to define what safety is. According to Hauer (*30–32*) the safety of a facility should not be equated with the fluctuating accident counts; rather, one should define safety as an underlaying stable property that has the nature of a long-term average. Consequently, the safety definition proposed by Hauer is as follows: "the number of accidents (crashes) per unit of time by kind and severity, expected to occur on a facility during a specific period." Based on this definition, safety is an expected accident frequency.

In this research, the safety effect of the overlay placed in the different sites is analyzed using the aforementioned 'naïve' before-after study approach. To do so, the following quantities are defined:

σ_{before} = expected number of target accidents of a specific site in the 'before' period and

σ_{after} = expected number of target accidents of a specific site in the 'after' period if the treatment would has not applied.

The effect of the treatment on safety is judge by comparing σ_{before} to σ_{after} ; if $\sigma_{after} > \sigma_{before}$ then the treatment increased the number of crashes; if $\sigma_{after} < \sigma_{before}$ the treatment reduced the number of crashes; finally, if $\sigma_{after} = \sigma_{before}$ then the overlay has no effect on crashes. Because both σ_{before} and σ_{after} are discrete random variables, a comparison between the two needs to account for the uncertainty associated with each.

Before-After Study to Evaluate the Safety Effect of Asphalt Overlays

For this research, the NCDOT provided three related datasets to evaluate the safety effect of the asphalt overlays placed on each site. These datasets were provided for 23 of the 26 sites (Sites 2, 23, and 27 were omitted). The dataset for each site consisted of the following information:

- Database 1 - A detailed crash study that included the crash events between January 1, 2017, and March 31, 2021. The location of each crash event was verified by the NCDOT personnel; therefore, there is a good confidence about the milepost and direction of each crash. The dataset contained a detailed description of the severity of the crash, the road condition, the most harmful event, etc.

- Database 2 - Data on the average speed recorded across the whole segment of route, reported in 1-hour bins. The information corresponds to the period from January 1, 2017, through June 15, 2021.
- Database 3 - Supplementary information such as the average traffic level, surface type, posted speed limit, and the number of lanes was collected. This information is summarized in Table D.1.

Table D.1. Complementary information for the before-after study.

Site	Route Type	Layout	Speed Limit	ADT	Lane Configuration
15	NC	Rural	55	1,400	2-Lane
16	NC	Rural	55	1,800	2-Lane
3	US	Rural	55	3,400	2-Lane
29	NC	Rural	55	11,000	2-Lane
9	NC	Rural	35/45	3,150	2-Lane
8	NC	Rural	55	4,600	2-Lane
24	NC	Rural	55	7,200	2-Lane
28	NC	Rural	55	11,000	4-Lane Divided Highway
17	US	Rural	60	12,000	4-Lane Divided Highway
33	US	Rural	55	14,000	4-Lane Divided Highway
1	Interstate	Rural	70	15,000	4-Lane Freeway
14	US	Rural	35/55	17,000	4-Lane Divided Highway
18	US	Rural	65	25,000	4-Lane Freeway
13	US	Urban	55	31,050	4-Lane Freeway
11	NC	Urban	45	39,000	4-Lane Divided Highway
19	US	Rural	45/55	47,000	4-Lane Divided Highway
30	NC	Urban	70	13,000	6-Lane Freeway
12	US	Rural	55	17,000	4-Lane Divided Highway
7	Interstate	Rural	65	53,000	4-Lane Freeway
6	Interstate	Urban	65	65,000	6-Lane Freeway
5	Interstate	Rural	65	37,000	4-Lane Freeway
4.2	Interstate	Rural	65	51,000	4-Lane Freeway
4.1	Interstate	Urban	55	65,000	4-Lane Freeway

RS9.5C	RS9.5D	UTBWC

As shown, four of the sites are RS9.5B, all of these have a 2-lane configuration, and are in a rural layout. Next, there are twelve RS9.5C sites, three of them have a 2-lane configuration, three are 4-lane freeways, and the remaining six are 4-lane divided highways. Also, there are four RS9.5D and three UTBWC. All the RS9.5D sites are 6-lane freeways except by Site 12, which is a 4-lane divided highway. In the case of the UTBWC sites, of particular interest is Site 4.2 because this site was first paved with a RS9.5D and a few months later it did receive a UTBWC.

Crash Analysis

To start the analysis, the paved date of each site was pulled from HiCAMS, see Table 1. Based on this date, the 'before' period was set from January 1, 2017, to one year prior to the construction date. Likewise, the 'after' period was set to start one month after the construction date up to March 31, 2021. Based on the crash description, four categories have been established:

- Total number of crashes,
- Total number of wet crashes,

- Number of lane departure crashes,
- Number of wet lane departure crashes.

For each of these categories, crashes have been totaled by month and the records divided between the 'before' (B) and 'after' (A) period. The summary of the number of crashes in each of these categories during the 'before' and 'after' period for each of the sites is presented in Table D.2. As indicated in Table D.2, there are fewer observations in the 'after' period than in the 'before' period, especially for Sites 13 and 30, which only have three and four months in the 'after' period respectively. Because the 'after' period has a reduced number of observations, it is not statistically reliable to define the expected value and its corresponding variation for the 'after' period in most of the sites. In contrast, the number of observations in the 'before' period is more consistent with a minimum of 20 months of observations.

Nevertheless, the naïve after study is made by computing the percent increment in the number of crashes as indicated in Equation (59). An example of this calculation is described by using the observations of Site 1 (see Table D.2), in the 'before' period the number of totals, totals wet, lane departure, and lane departure wet crashes was 6, 1, 3, and 1, respectively. These crashes were observed in the lapse of 23 months; hence, the estimated crashes per month in each category in the 'before' period is; $\sigma_{before}^{total} = 6/23 = 0.261$, $\sigma_{before}^{total\ wet} = 0.043$, $\sigma_{before}^{lane\ departure} = 0.130$, and $\sigma_{before}^{lane\ departure\ wet} = 0.043$. Conversely, in the 'after' period the number of totals, totals wet, lane departure, and lane departure wet crashes was 1, 0, 1, and 0, respectively. These crashes were observed in the lapse of 16 months; in consequence, the estimated crashes per month in each category in the 'after' period is $\sigma_{after}^{total} = 1/16 = 0.062$, $\sigma_{after}^{total\ wet} = 0$, $\sigma_{after}^{lane\ departure} = 0.062$, and $\sigma_{after}^{lane\ departure\ wet} = 0$. Then, using Equation (59) the percent charge in the number of crashes per month in the 'after' period is -77.1%, -100.0%, -54.2%, and -100.0% for the totals, totals wet, lane departure, and lane departure wet crashes, respectively.

$$Crash\ \%Change = \frac{\left(\sigma_{after} - \sigma_{before}\right)}{\sigma_{before}} \times 100 \tag{59}$$

where;

σ_{after} = estimated number of crashes per month in the 'after' period, and

σ_{before} = estimated number of crashes per month in the 'before' period.

Table D.2. Number of crashes in the 'before' (B) and 'after' (A) period.

Site	Speed Limit	ADT	Number of Months		Total		Total Wet		Lane Departure		Wet Lane Departure	
			B	A	B	A	B	A	B	A	B	A
15	55	1,400	23	16	6	1	1	0	3	1	1	0
16	55	1,800	23	16	9	11	1	0	3	2	1	0
3	55	3,400	23	16	8	10	0	1	1	4	0	1
29	55	11,000	33	6	21	6	1	3	5	4	0	3
9	35/45	3,150	23	16	17	15	3	6	4	7	1	4
8	55	4,600	29	10	26	11	2	4	8	4	2	1
24	55	7,200	31	8	62	9	8	2	15	5	5	2
28	55	11,000	28	11	14	12	6	7	10	9	4	6
17	60	12,000	19	20	7	17	1	6	0	8	0	6
33	55	14,000	31	8	17	7	4	6	7	6	1	6
1	70	15,000	23	16	49	46	20	19	30	25	18	16
14	35/55	17,000	23	16	27	20	4	6	9	6	1	3
18	65	25,000	23	16	12	17	6	10	9	14	4	10
13	55	31,050	36	3	219	16	73	10	105	14	47	10
11	45	39,000	28	11	209	88	30	21	31	19	5	7
19	45/55	47,000	29	10	188	53	18	6	37	11	4	2
30	70	13,000	35	4	34	1	8	0	13	0	3	0
12	55	17,000	23	16	197	163	31	51	71	86	15	40
7	65	53,000	21	18	33	52	4	20	15	32	2	15
6	65	65,000	23	16	63	60	14	10	29	30	9	8
5	65	37,000	23	16	79	53	16	10	53	22	12	5
4.2	65	51,000	29	10	122	36	42	7	61	21	29	7
4.1	55	65,000	23	16	99	59	29	17	42	36	16	10
Surface Type		RS9.5B			RS9.5C			RS9.5D			UTBWC	

The percent increment in the number of crashes for each site is summarized in Table D.3. To facilitate the discussion of the results it was decided to color code the *Crash %Change*. In Table D.3, a *Crash %Change* less than or equal 0% is coded with black font, *a Crash %Change* greater than 0% but less than 100% is coded with pink, and a value greater than 100% is coded as red.

Assuming there is evidence of change in the crash frequencies when the *Crash %Change* is greater than or equal to 0%, more than half of the sites showed evidence of a change in the crash frequencies in the 'after' period. In the other hand, if one focus only in those sites with a *Crash %Change* greater than 100% it is evident that the greatest changes occurred in wet conditions, i.e., total wet and lane departure wet crashes. Also, the surface type with the lowest *Crash %Change* is the UTBWC, in fact all the sites showed a reduction in crashes, except for Site 4.1 in the lane departure category.

Table D.3. Summary of the *Crash %Change*.

Site No.	Lane Configuration	Surface Type	Total	Total Wet	Lane Departure	Lane Departure Wet
15	2-Lane	RS9.5B	-77.08	-100.00	-54.17	-100.00
16	2-Lane	RS9.5B	*68.06*	-100.00	-8.33	-100.00
3	2-Lane	RS9.5B	*71.88*	**-ᵃ**	**450.00**	-
29	2-Lane	RS9.5B	*57.14*	**1550.00**	**340.00**	-
9	2-Lane	RS9.5C	*21.32*	**175.00**	**140.63**	**450.00**
8	2-Lane	RS9.5C	*22.69*	**480.00**	*45.00*	*45.00*
24	2-Lane	RS9.5C	-43.75	-3.13	*29.17*	*55.00*
28	4-Lane Divided Highway	RS9.5C	**118.18**	**196.97**	**129.09**	**281.82**
17	4-Lane Divided Highway	RS9.5C	**118.57**	**440.00**	-	-
33	4-Lane Divided Highway	RS9.5C	*59.56*	**481.25**	**232.14**	**2225.00**
14	4-Lane Divided Highway	RS9.5C	5.77	**175.00**	-8.33	**312.50**
11	4-Lane Divided Highway	RS9.5C	7.18	*78.18*	*56.01*	**256.36**
19	4-Lane Divided Highway	RS9.5C	-18.24	-3.33	-13.78	*45.00*
1	4-Lane Freeway	RS9.5C	*29.08*	*30.63*	*14.58*	*22.22*
18	4-Lane Freeway	RS9.5C	**112.50**	**175.00**	**113.89**	**243.75**
13	4-Lane Freeway	RS9.5C	-12.33	*64.38*	*60.00*	**155.32**
12	4-Lane Divided Highway	RS9.5D	*13.77*	**126.21**	*66.55*	**266.67**
7	4-Lane Freeway	RS9.5D	*75.08*	**455.56**	**137.04**	**733.33**
30	6-Lane Freeway	RS9.5D	-74.26	-100.00	-100.00	-100.00
6	6-Lane Freeway	RS9.5D	*30.95*	-1.79	*42.24*	*22.22*
5	4-Lane Freeway	UTBWC	-7.75	-14.06	-42.92	-42.71
4.2	4-Lane Freeway	UTBWC	-14.43	-51.67	-0.16	-30.00
4.1	4-Lane Freeway	UTBWC	-18.06	-19.40	*17.86*	-14.06

Note: *Crash %Change* colors are **More than 100%**; *between 0% and 100%*; less than 0%.
ᵃ: zero crash count in the 'before' period.

Speed Analysis

The hourly speed variation on each site was studied using the second database. Because crashes were totaled by month, the daily speed values recorded from 6 am to 6 pm were grouped in the same unit of time and the 2.5, 50, 85, and 97.5 percentiles were calculated to describe the speed variation on each month. An example of the speed variation obtained for each site is shown in Figure D.1. Similar plots were generated for each site and are included at the end of this appendix.

To compare the speeds in the 'before' and 'after' period, the median speed observed within a month was used (blue line in Figure D.1). Three trends were observed among the sites:

- Trend 1: there were no statistically significant difference between the median speed in the 'before' and 'after' period. Three sites showed this trend.
- Trend 2: There was a statistically significant increase in the median speed in the 'after' period. Nineteen sites showed this trend.
- Trend 3: There was a reduction in the median speed during the period of analysis. One site followed this trend.
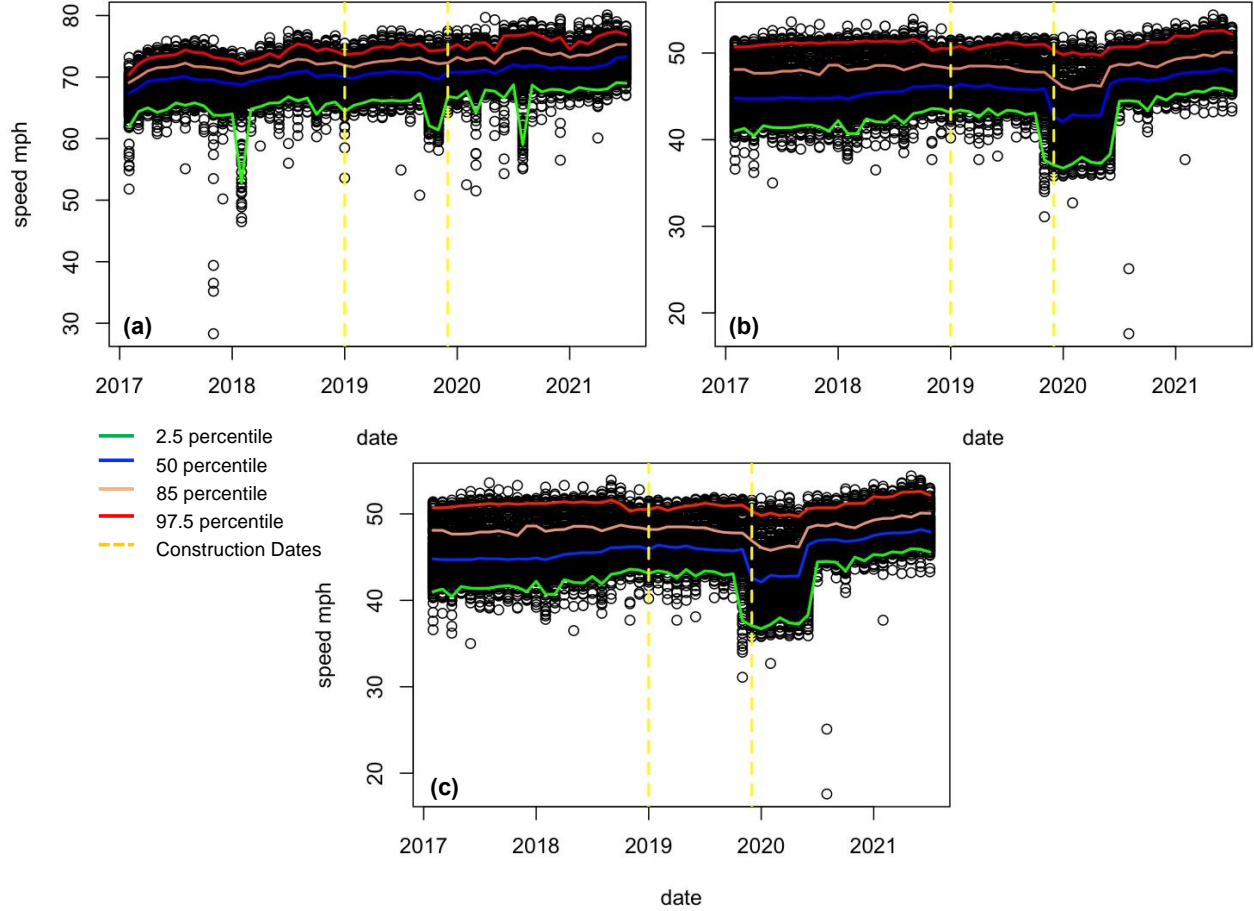
Figure D.1. Speed variation on: (a) Site 1 NB, (b) Site 3 NB, and (c) Site 29 EB.

For both the 'before' and 'after' period, the mean and standard deviation of the monthly median speed were calculated as indicated in Table D.4. The number of observations used to calculate the mean and standard deviation is also included in Table D.4. The statistical test used to compare the average median speed in both periods was the Welch's t-test; in this test, the t-statistic is computed with Equation (60), while the number of degrees of freedom required to compute the p-value is estimated with Equation (61).

$$t = \frac{\overline{X}_1 - \overline{X}_2}{\sqrt{S_{\overline{X}_1}^2 + S_{\overline{X}_2}^2}} \tag{60}$$

$$v \approx \frac{\left(\dfrac{S_1^2}{N_1} + \dfrac{S_2^2}{N_2}\right)^2}{\dfrac{S_1^4}{N_1^2(N_1 - 1)} + \dfrac{S_2^4}{N_2^2(N_2 - 1)}} \tag{61}$$

Table D.4. Statistical comparison of the 'before' and 'after' average speed.

Site No.	Before			After			Test of Difference	Difference	Percent Change	Trend
	μ_1	S_1	N_1	μ_2	S_2	N_2	p-value			
15	51.40	0.16	28	51.59	1.10	9	0.62	0.19	0.37	1
16	44.30	0.31	26	45.77	0.55	11	**0.00**	1.47	3.32	2
3	45.40	0.63	31	47.56	0.47	10	**0.00**	2.16	4.76	2
29	41.24	0.47	27	31.50	0.11	9	**0.00**	**-9.74**	-23.62	3
24	48.16	0.28	39	48.38	0.26	9	**0.05**	0.22	0.45	2
28	56.58	0.28	37	57.11	0.50	14	**0.00**	0.54	0.95	2
9	51.18	0.28	26	51.83	0.18	18	**0.00**	0.65	1.27	2
8	50.47	0.36	32	52.07	0.11	12	**0.00**	1.60	3.17	2
17	62.75	0.45	27	64.22	0.67	23	**0.00**	1.47	2.34	2
33	59.12	1.07	39	61.29	0.52	11	**0.00**	2.17	3.67	2
1	69.81	0.82	30	71.74	0.67	16	**0.00**	1.92	2.76	2
14	54.74	0.39	30	55.27	0.41	17	**0.00**	0.53	0.97	2
18	67.85	0.32	31	69.12	0.67	17	**0.00**	1.27	1.87	2
13	56.27	0.42	43	57.14	0.36	5	**0.00**	0.87	1.54	2
11	38.94	0.53	37	39.34	0.64	14	**0.05**	0.40	1.03	2
19	42.89	0.80	37	43.68	0.56	12	**0.00**	0.79	1.85	2
30	70.48	0.52	42	71.32	0.81	6	0.05	0.83	1.18	1
6	68.08	0.21	30	68.15	1.04	16	0.80	0.07	0.10	1
12	43.35	0.39	32	44.40	0.55	16	**0.00**	1.05	2.41	2
7	69.78	0.23	30	71.08	0.52	18	**0.00**	1.30	1.86	2
5	68.18	0.25	32	69.50	0.51	16	**0.00**	1.32	1.94	2
4.2	66.06	0.26	37	67.10	0.70	13	**0.00**	1.04	1.57	2
4.1	63.46	0.22	30	64.20	0.21	16	**0.00**	0.74	1.17	2

As shown in Table D.4, for those sites exhibiting Trend 2, the difference in the median speed between the 'before' and 'after' period was between 0.1 mph and 2.17 mph; in terms of percent change, the range was between 0.10% and 4.70%, respectively. Table D.5 shows similar analysis results but using the 85-percentile instead of the average. In the case of the 85-percentile, the same sites were deemed statistically significant except Site 24, which showed a non-significant change in speed in the 85-percentile case and a significant change in the case of the average. For the other sites that showed statistically insignificant differences, the p-values decreased in two and increased in one.

In conclusion, both analysis the naïve before-after study and the speed analysis indicate the overlay had an effect, this is the number of crashes per month were in general higher in the 'after' period than in the 'before' period, also the UTBWC seems to provide for better safety performance because this surface type had the lowest *Crash %Change*. More observations are required to evaluate the statistical significance of the calculated *Crash %Change*.

Finally, it is important to point out that COVID-19 related traffic impacts affected many of the 'after' periods in this database. Based on the method of calculating crash frequencies (non-adjusted for traffic volumes), not accounting for this effect may mean that the impacts of the overlays are understated.

Table D.5. Statistical comparison of the 'before' and 'after' 85-percentile speed.

Site No.	Before			After			Test of Difference	Difference	Percent Change	Trend
	μ_1	S_1	N_1	μ_2	S_2	N_2	p-value			
15	53.51	0.31	28	53.20	0.52	9	0.12	**-0.31**	-0.58	1
16	46.50	0.34	26	47.50	0.68	11	**0.00**	1.00	2.15	2
3	48.20	0.33	31	49.37	0.59	10	**0.00**	1.17	2.42	2
29	43.08	0.37	27	32.49	0.08	9	**0.00**	**-10.59**	-24.58	3
24	49.74	0.23	39	49.94	0.42	9	0.20	0.20	0.41	1
28	58.33	0.26	37	58.80	0.42	14	**0.00**	0.47	0.80	2
9	53.02	0.36	26	53.32	0.38	18	**0.01**	0.31	0.58	2
8	52.23	0.29	32	53.51	0.33	12	**0.00**	1.28	2.45	2
17	64.33	0.35	27	65.79	0.73	23	**0.00**	1.46	2.27	2
33	60.73	1.08	39	63.00	0.43	11	**0.00**	2.27	3.73	2
1	71.73	0.87	30	73.97	0.82	16	**0.00**	2.24	3.13	2
14	56.77	0.34	30	57.54	0.36	17	**0.00**	0.77	1.35	2
18	69.74	0.31	31	70.96	0.66	17	**0.00**	1.22	1.75	2
13	57.98	0.47	43	59.39	0.40	5	**0.00**	1.41	2.44	2
11	42.18	0.60	37	43.09	0.65	14	**0.00**	0.91	2.17	2
19	45.24	0.73	37	46.33	0.41	12	**0.00**	1.09	2.41	2
30	72.46	0.59	42	73.23	1.00	6	0.12	0.76	1.05	1
6	69.48	0.24	30	69.92	0.95	16	0.09	0.43	0.62	1
12	45.72	0.35	32	46.74	0.53	16	**0.00**	1.02	2.22	2
7	71.05	0.32	30	72.90	0.45	18	**0.00**	1.85	2.60	2
5	69.74	0.22	32	71.09	0.51	16	**0.00**	1.35	1.94	2
4.2	67.42	0.31	37	68.73	0.76	13	**0.00**	1.31	1.94	2
4.1	64.92	0.31	30	65.89	0.27	16	**0.00**	0.97	1.49	2

Figure D.2. Monthly variation of the one-hour vehicle speed in Site 1 – NB.
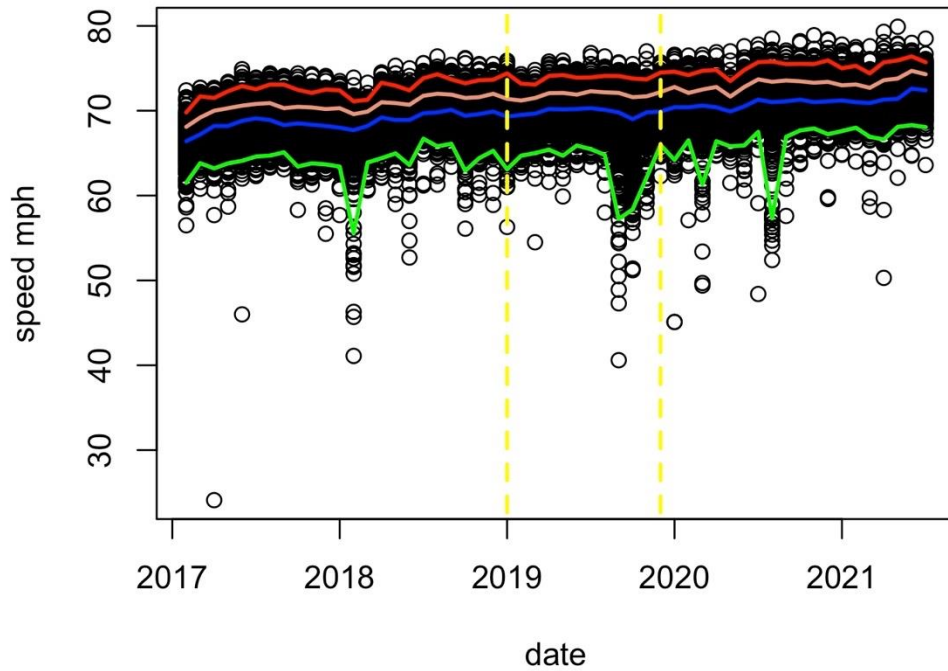
Figure D.3. Monthly variation of the one-hour vehicle speed in Site 1 – SB.

Figure D.4. Monthly variation of the one-hour vehicle speed in Site 3 – NB.
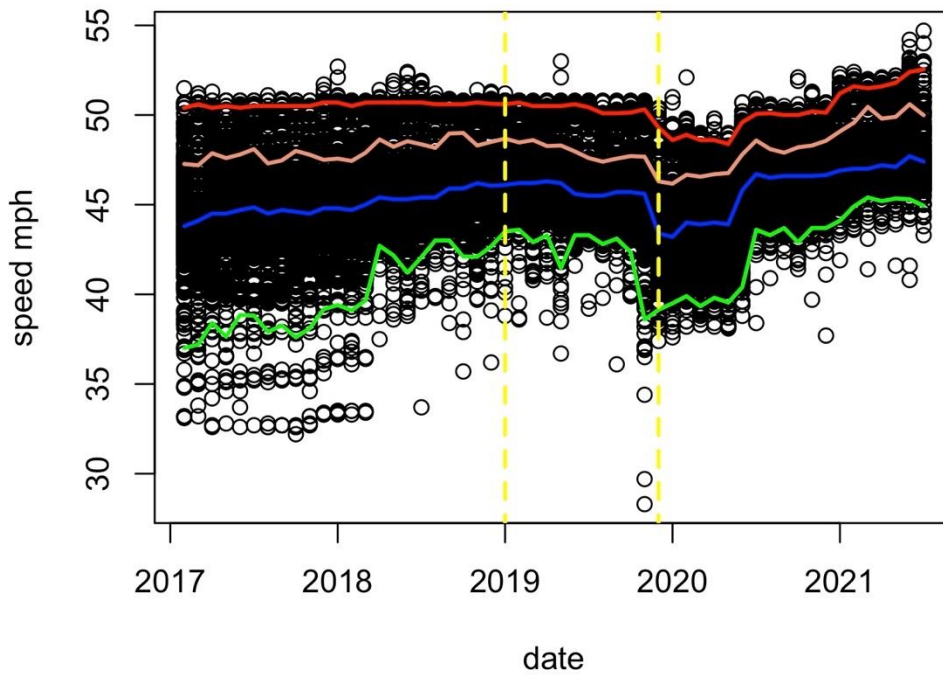
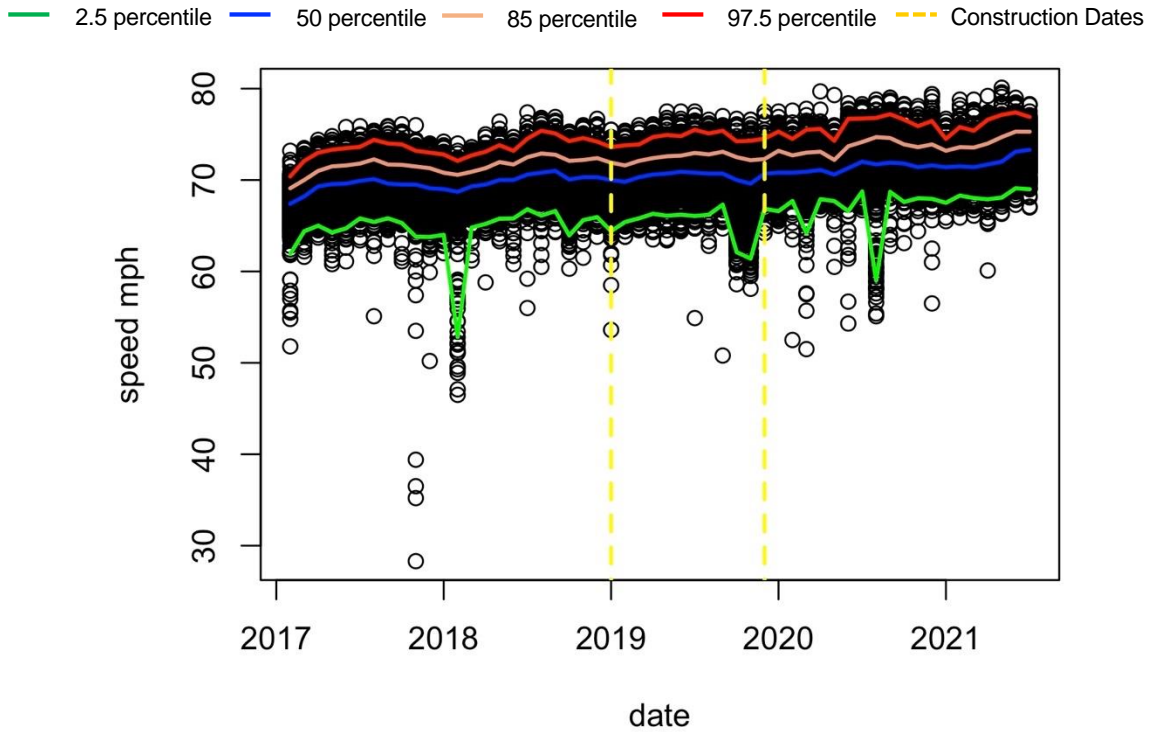**Figure D.5. Monthly variation of the one-hour vehicle speed in Site 3 – SB.**

Figure D.6. Monthly variation of the one-hour vehicle speed in Site 4.1 – EB.

Figure D.7. Monthly variation of the one-hour vehicle speed in Site 4.1 – WB.

Figure D.8. Monthly variation of the one-hour vehicle speed in Site 4.2 – EB.

Figure D.9. Monthly variation of the one-hour vehicle speed in Site 4.2 – WB.

Figure D.10. Monthly variation of the one-hour vehicle speed in Site 5 – EB.

Figure D.11. Monthly variation of the one-hour vehicle speed in Site 5 – WB.

169

Figure D.12. Monthly variation of the one-hour vehicle speed in Site 6 – EB.

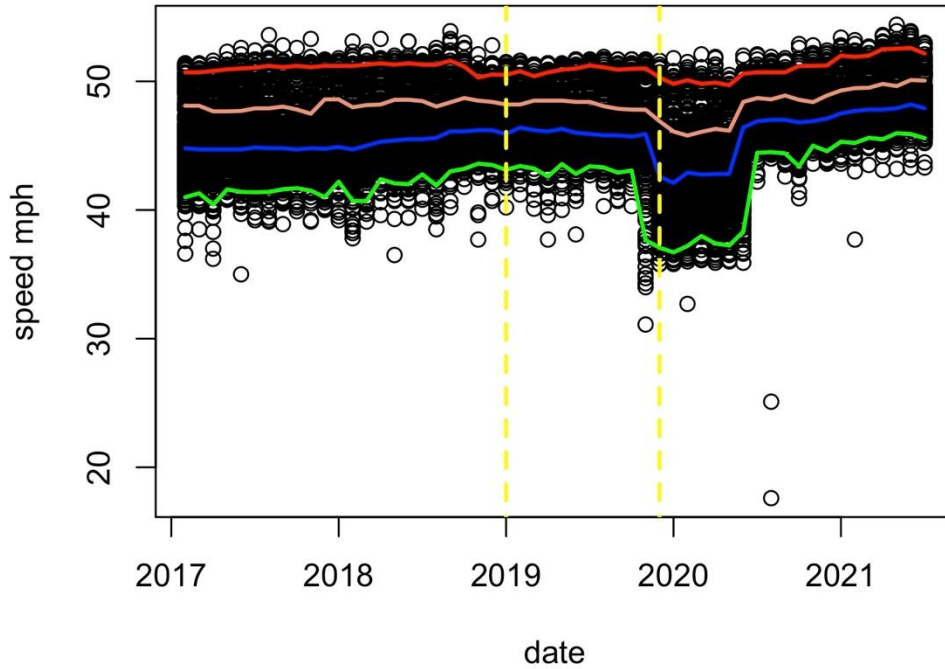**Figure D.13. Monthly variation of the one-hour vehicle speed in Site 6 – WB.**

Figure D.14. Monthly variation of the one-hour vehicle speed in Site 7 – NB.

Figure D.15. Monthly variation of the one-hour vehicle speed in Site 7 – SB.

Figure D.16. Monthly variation of the one-hour vehicle speed in Site 8 – NB.

Figure D.17. Monthly variation of the one-hour vehicle speed in Site 8 – SB.
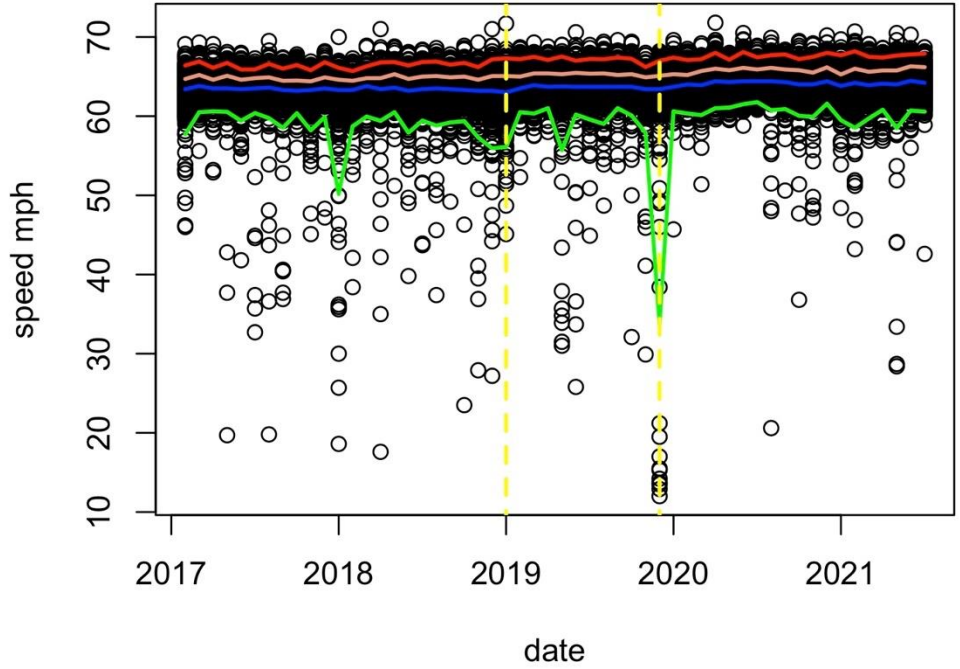
Figure D.18. Monthly variation of the one-hour vehicle speed in Site 9 – EB.

Figure D.19. Monthly variation of the one-hour vehicle speed in Site 9 – WB.
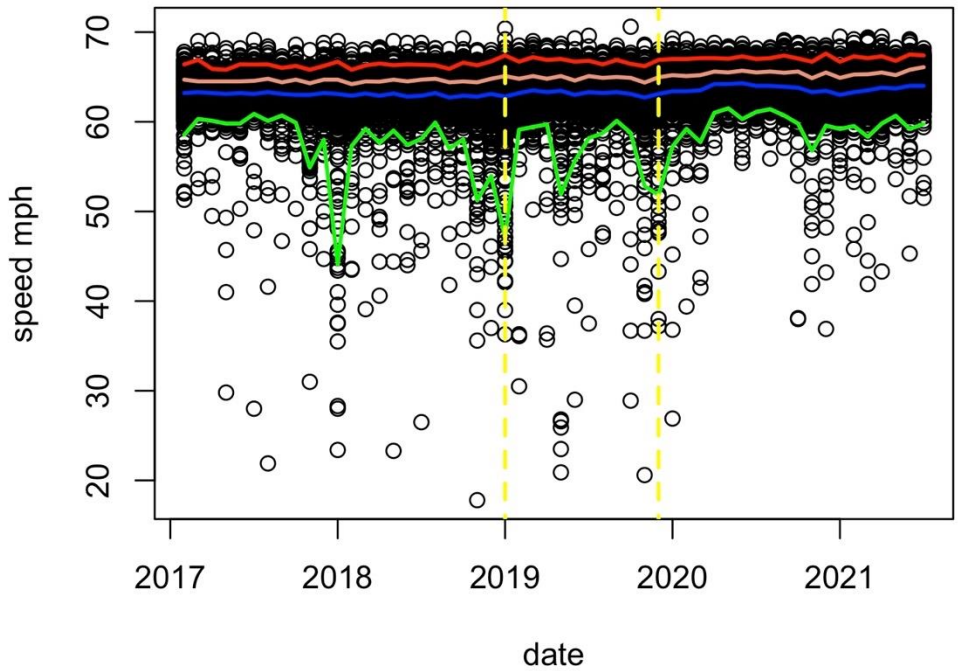
Figure D.20. Monthly variation of the one-hour vehicle speed in Site 11 – NB.

Figure D.21. Monthly variation of the one-hour vehicle speed in Site 11 – SB.

Figure D.22. Monthly variation of the one-hour vehicle speed in Site 12 – EB.

Figure D.23. Monthly variation of the one-hour vehicle speed in Site 12 – WB.

Figure D.24. Monthly variation of the one-hour vehicle speed in Site 13 – EB.
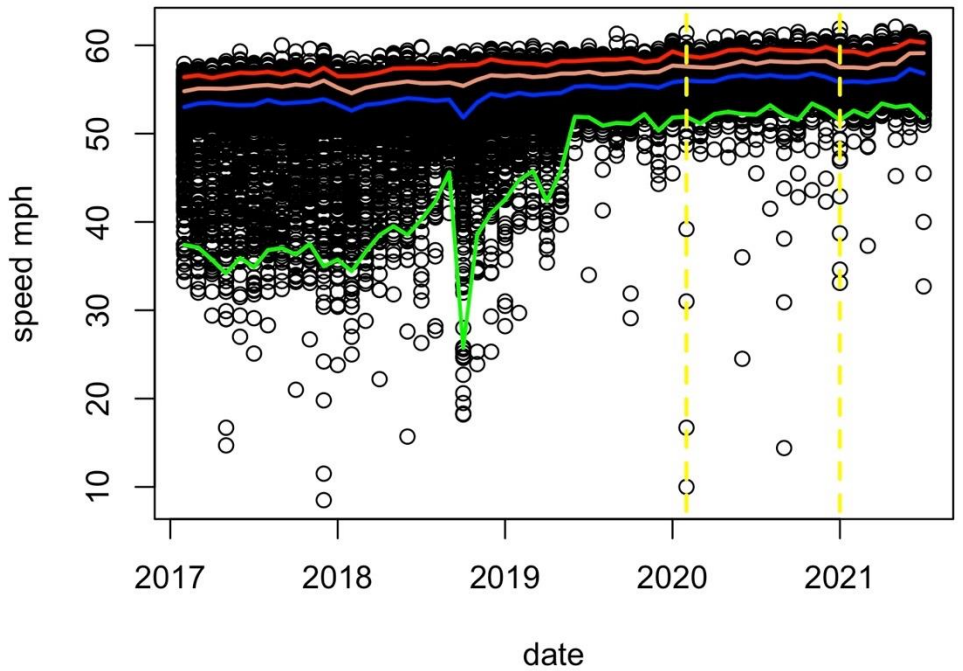
Figure D.25. Monthly variation of the one-hour vehicle speed in Site 13 – WB.

Figure D.26. Monthly variation of the one-hour vehicle speed in Site 14 – NB.
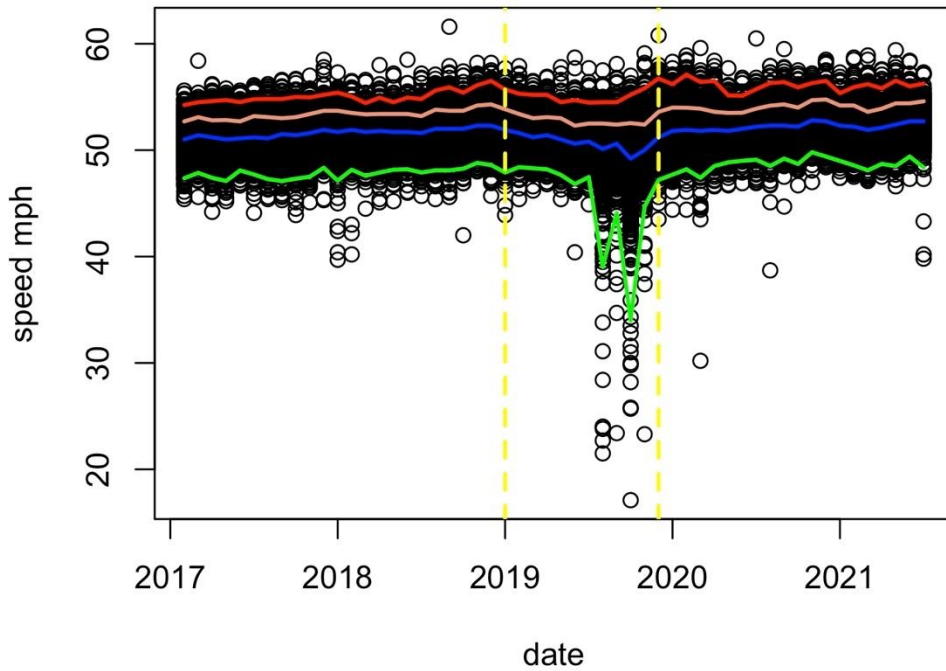
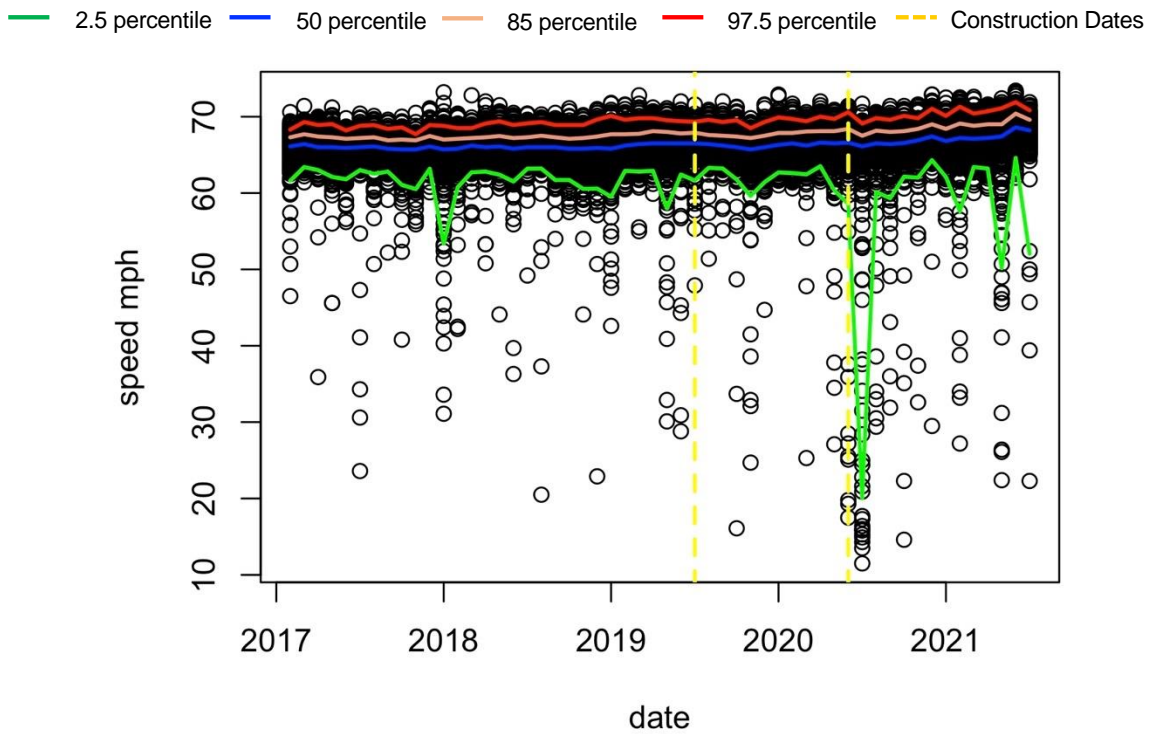**Figure D.27. Monthly variation of the one-hour vehicle speed in Site 14 – SB.**

177
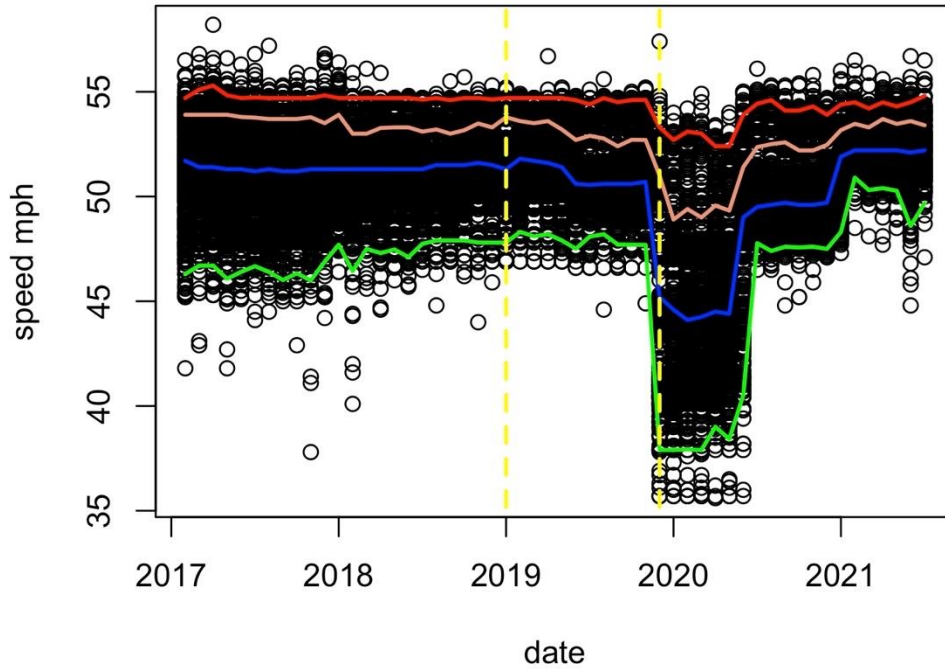
Figure D.28. Monthly variation of the one-hour vehicle speed in Site 15 – EB.
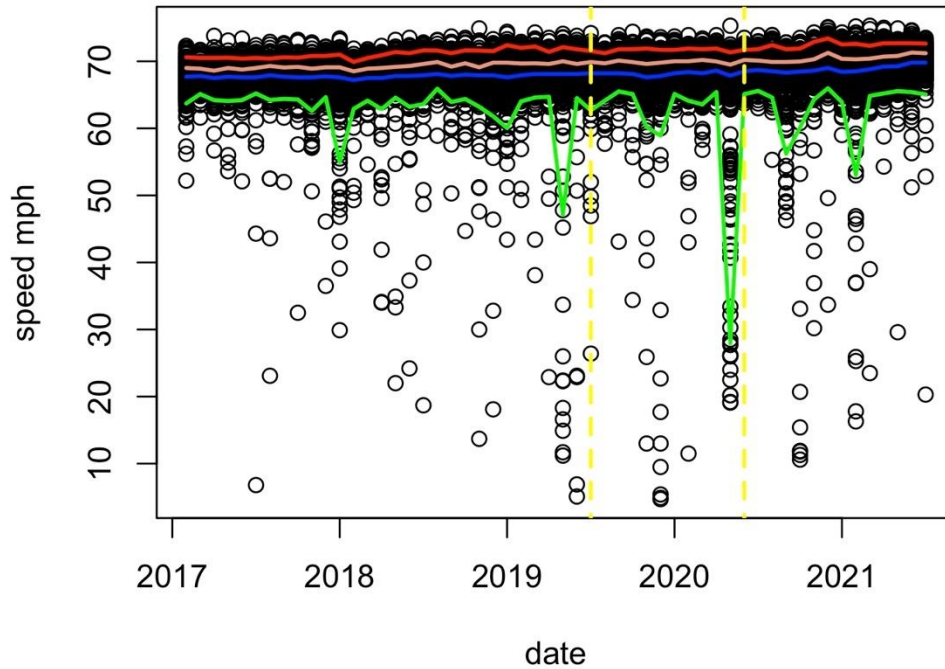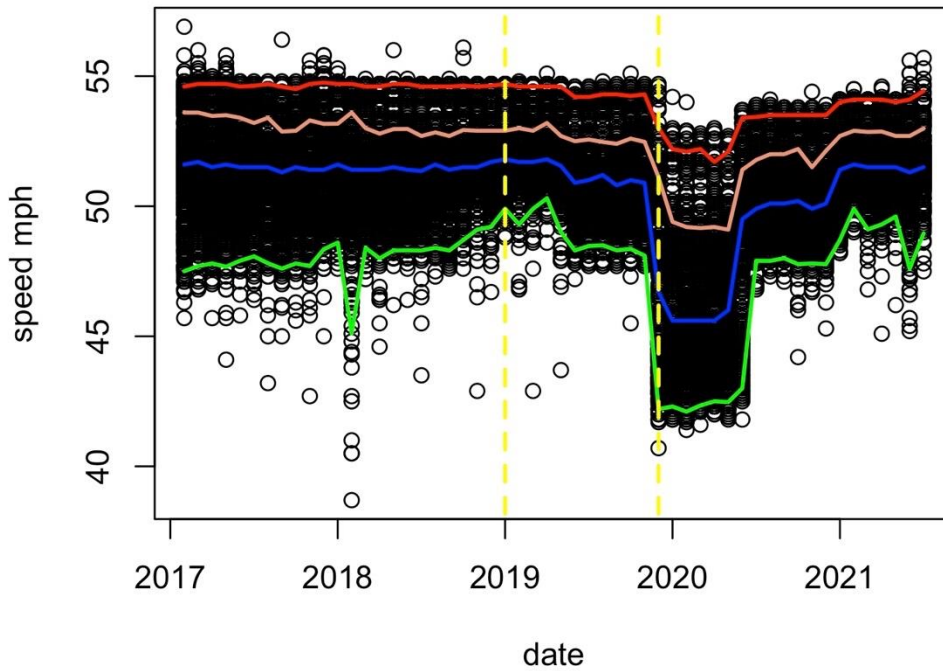

Figure D.29. Monthly variation of the one-hour vehicle speed in Site 15 – WB.

178
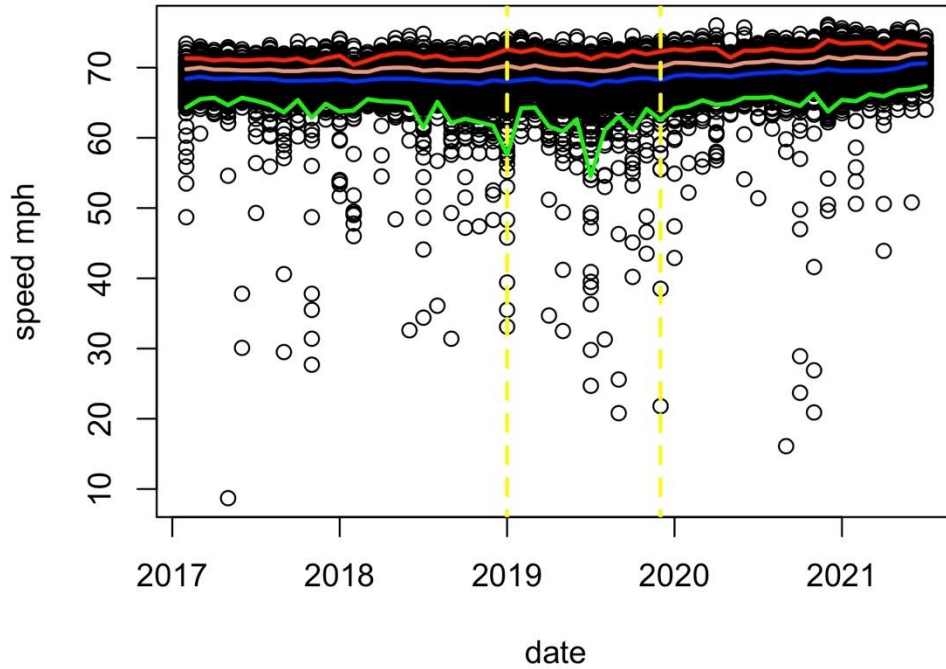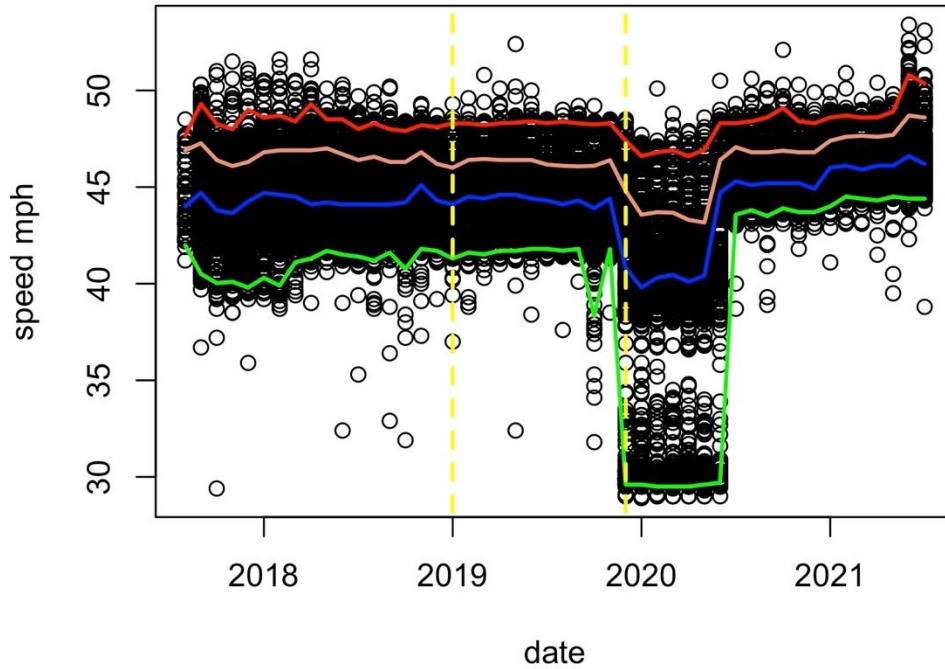
Figure D.30. Monthly variation of the one-hour vehicle speed in Site 16 – NB.
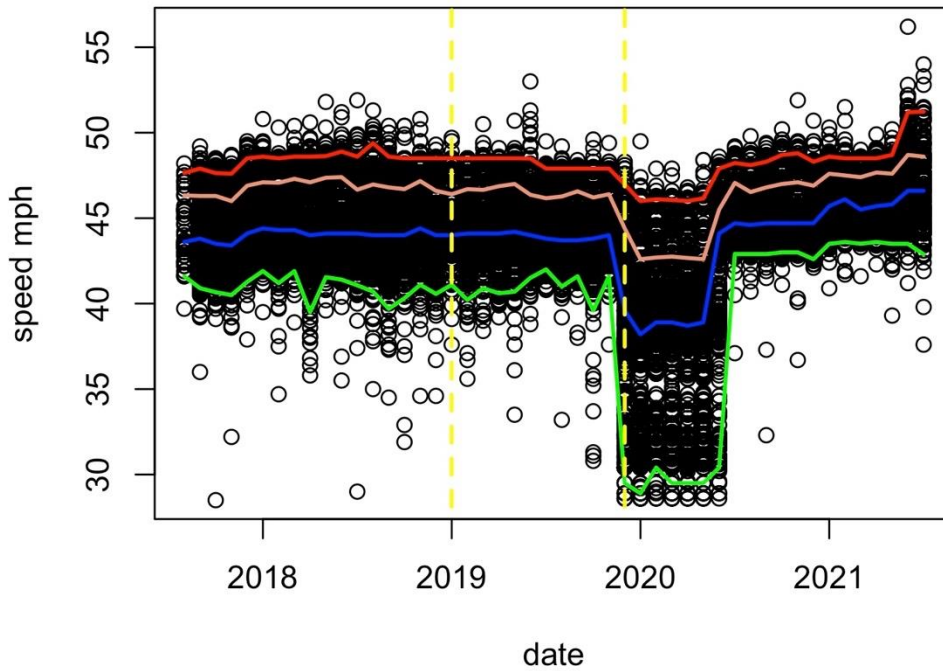
Figure D.31. Monthly variation of the one-hour vehicle speed in Site 16 – SB.
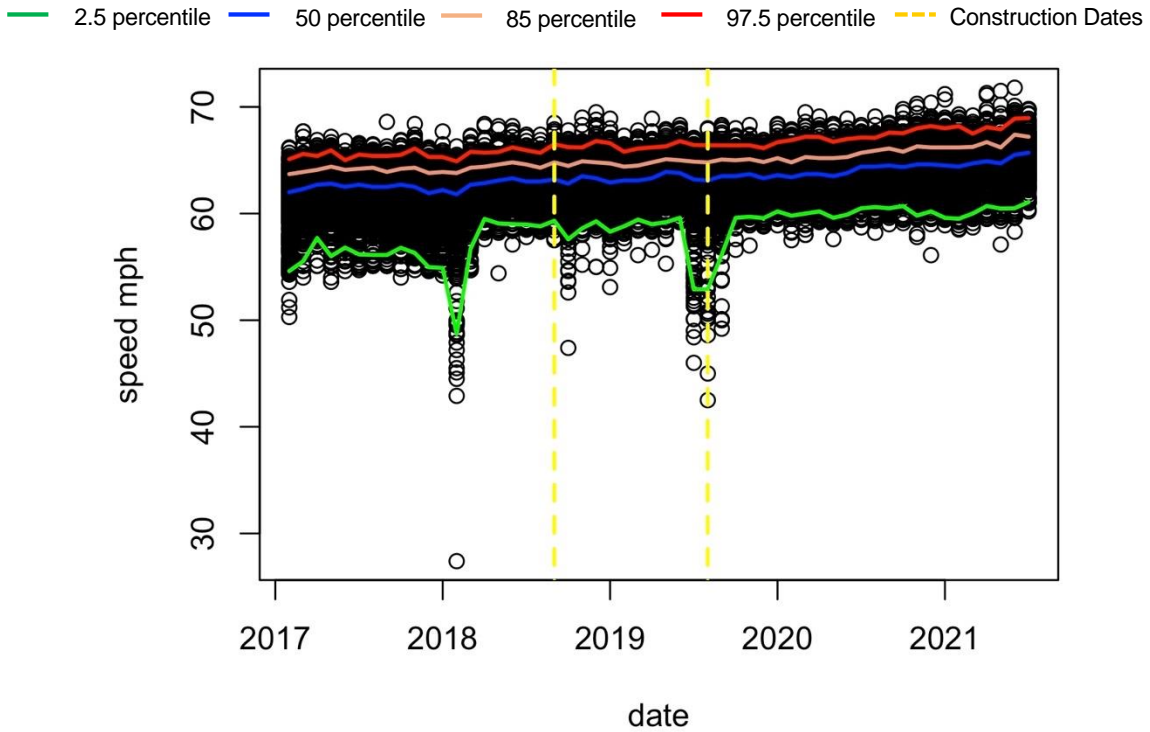
Figure D.32. Monthly variation of the one-hour vehicle speed in Site 17 – NB.
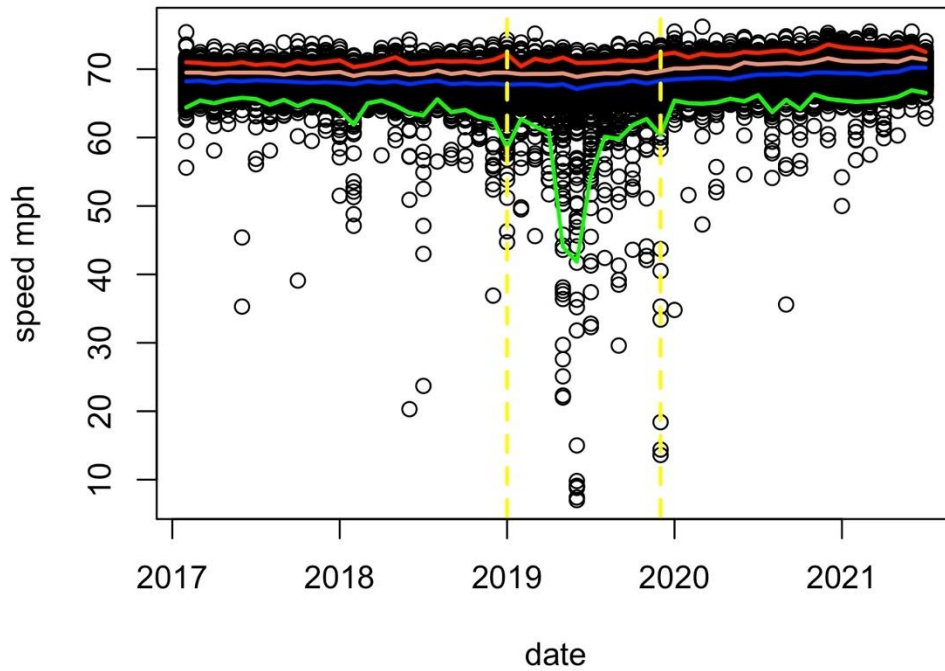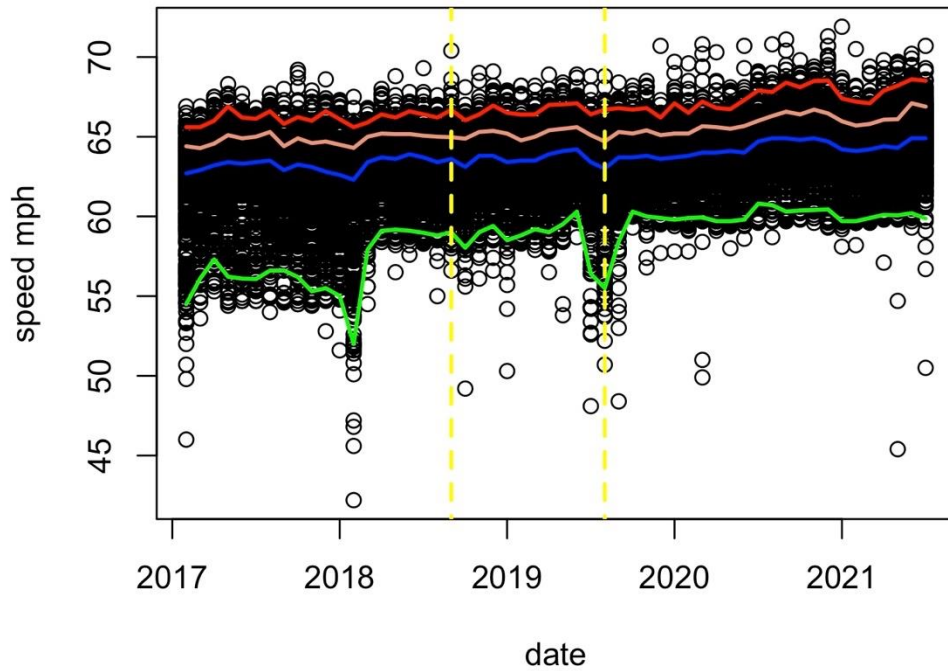

Figure D.33. Monthly variation of the one-hour vehicle speed in Site 17 – SB.
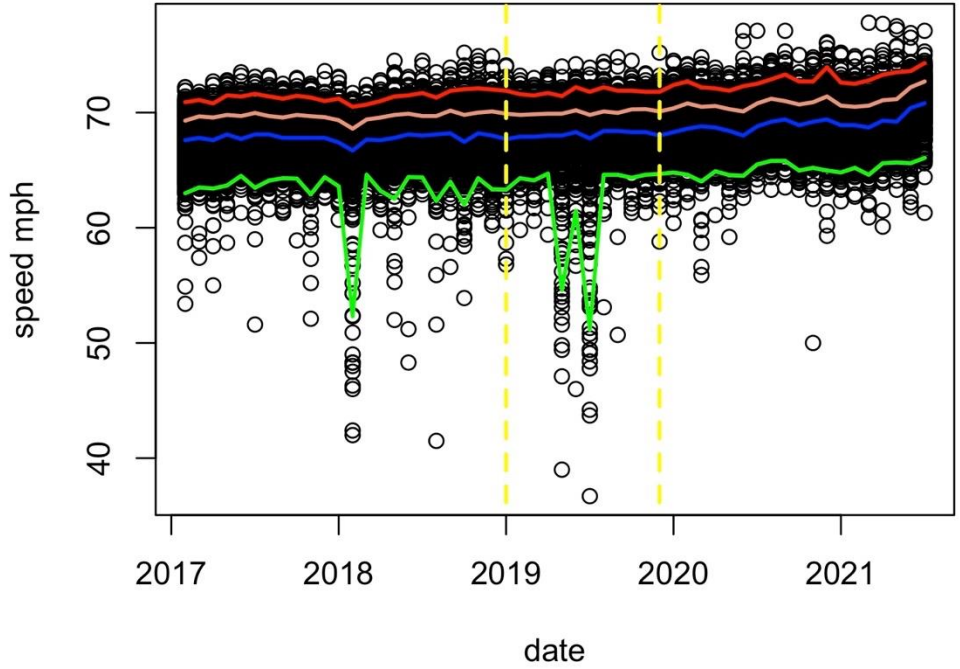
Figure D.34. Monthly variation of the one-hour vehicle speed in Site 18 – NB.
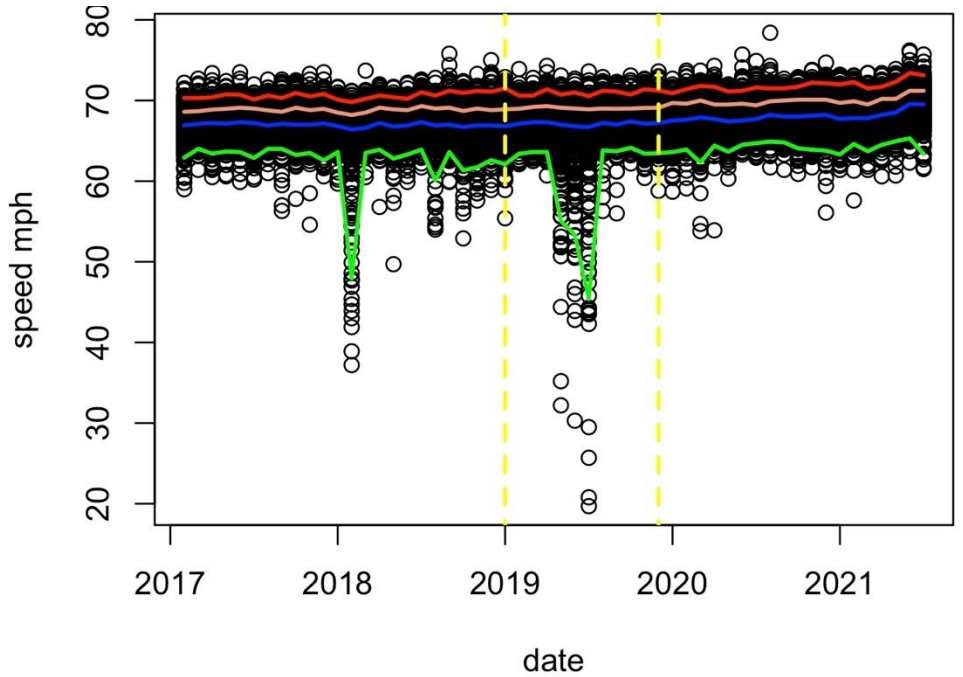
Figure D.35. Monthly variation of the one-hour vehicle speed in Site 18 – SB.
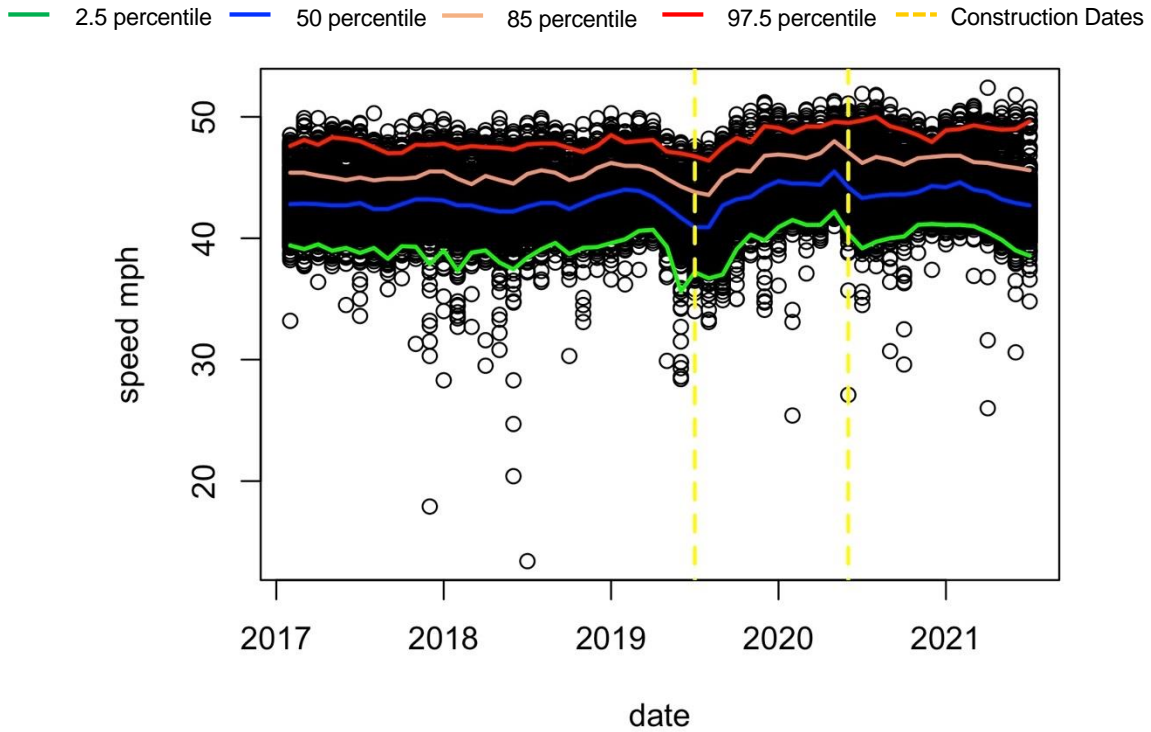
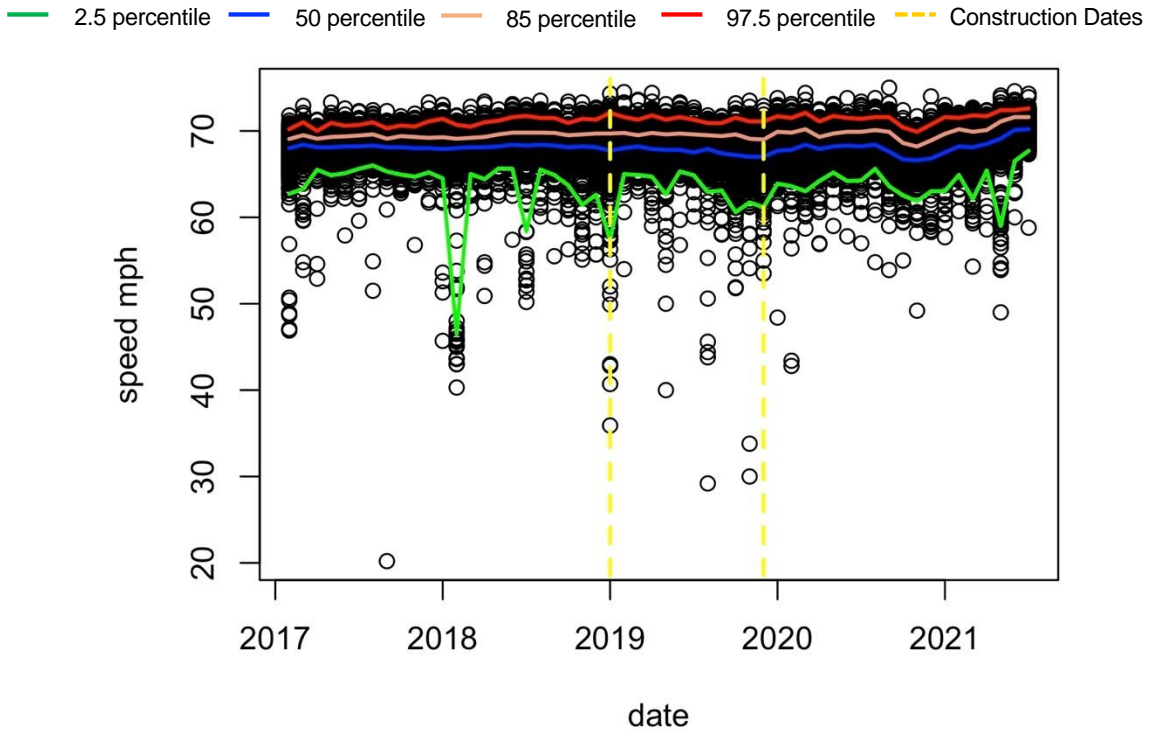**Figure D.36. Monthly variation of the one-hour vehicle speed in Site 19 – NB.**
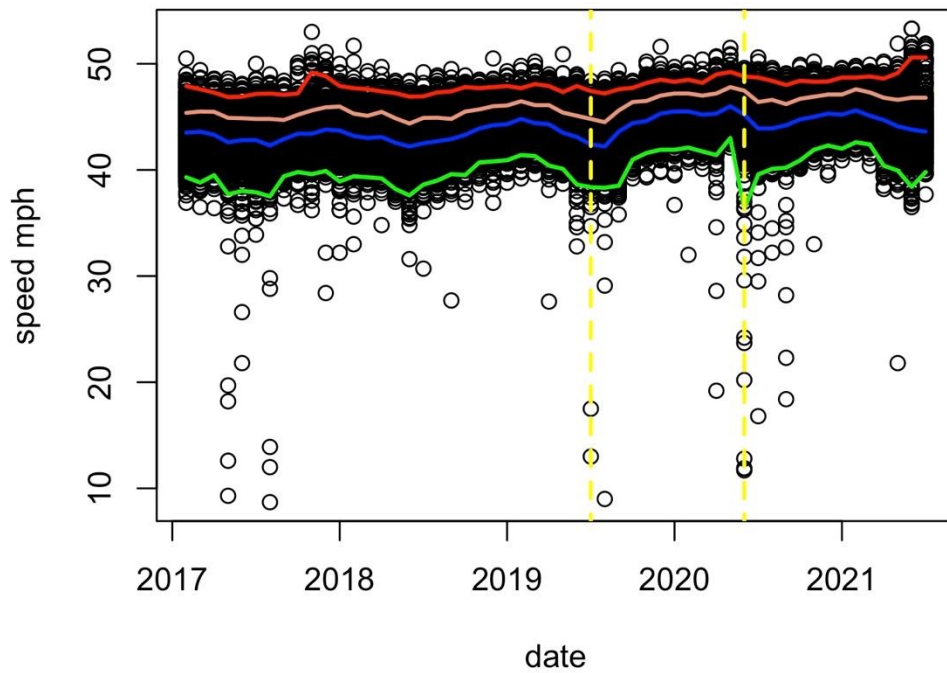
Figure D.37. Monthly variation of the one-hour vehicle speed in Site 19 – SB.
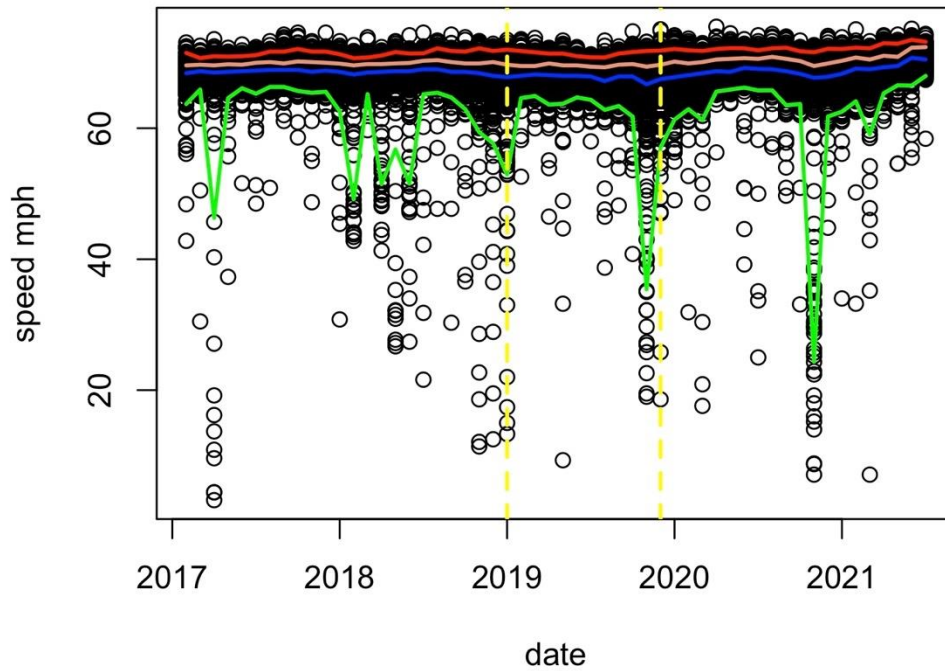
182
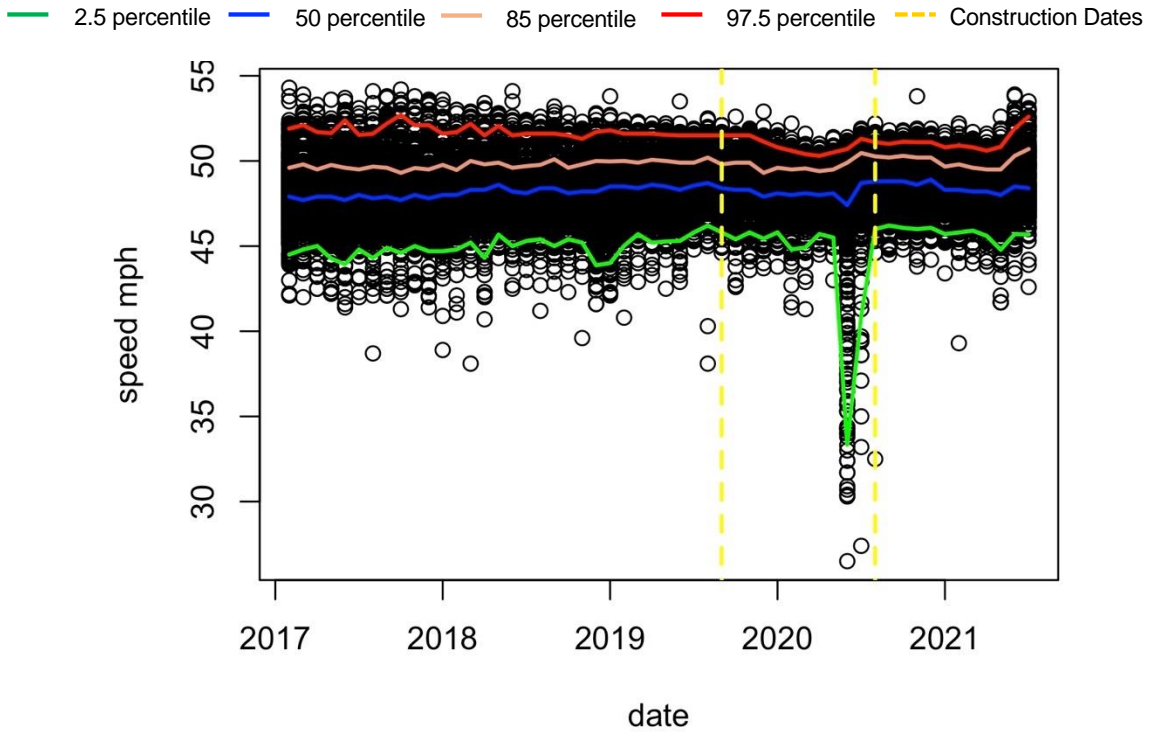
Figure D.38. Monthly variation of the one-hour vehicle speed in Site 24 – NB.
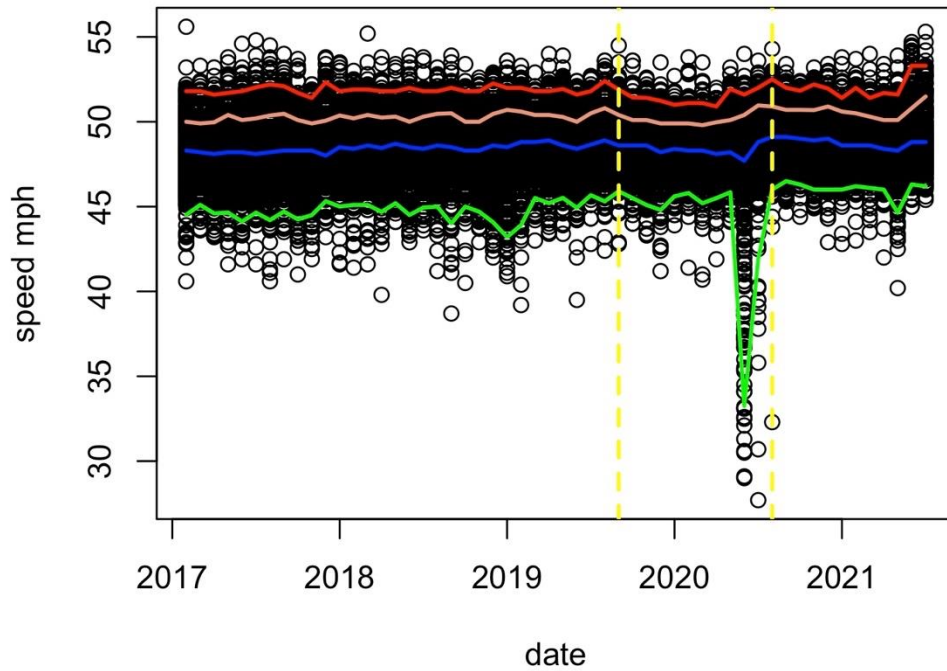
Figure D.39. Monthly variation of the one-hour vehicle speed in Site 24 – SB.
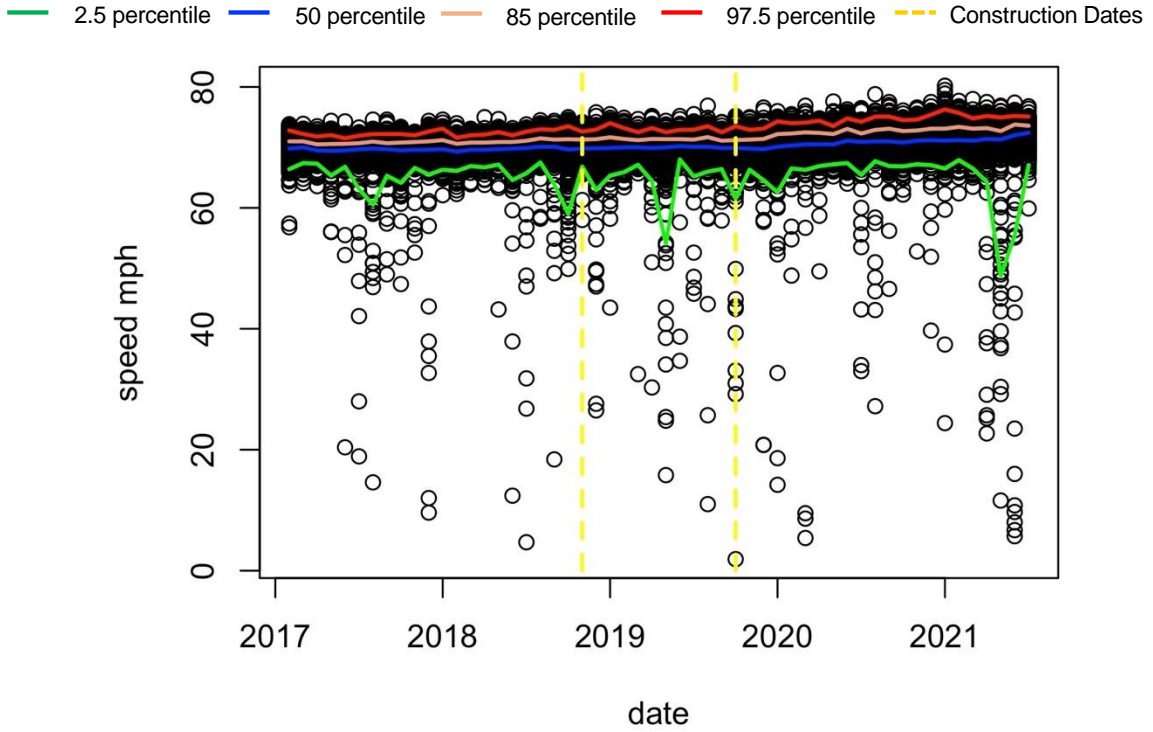
183
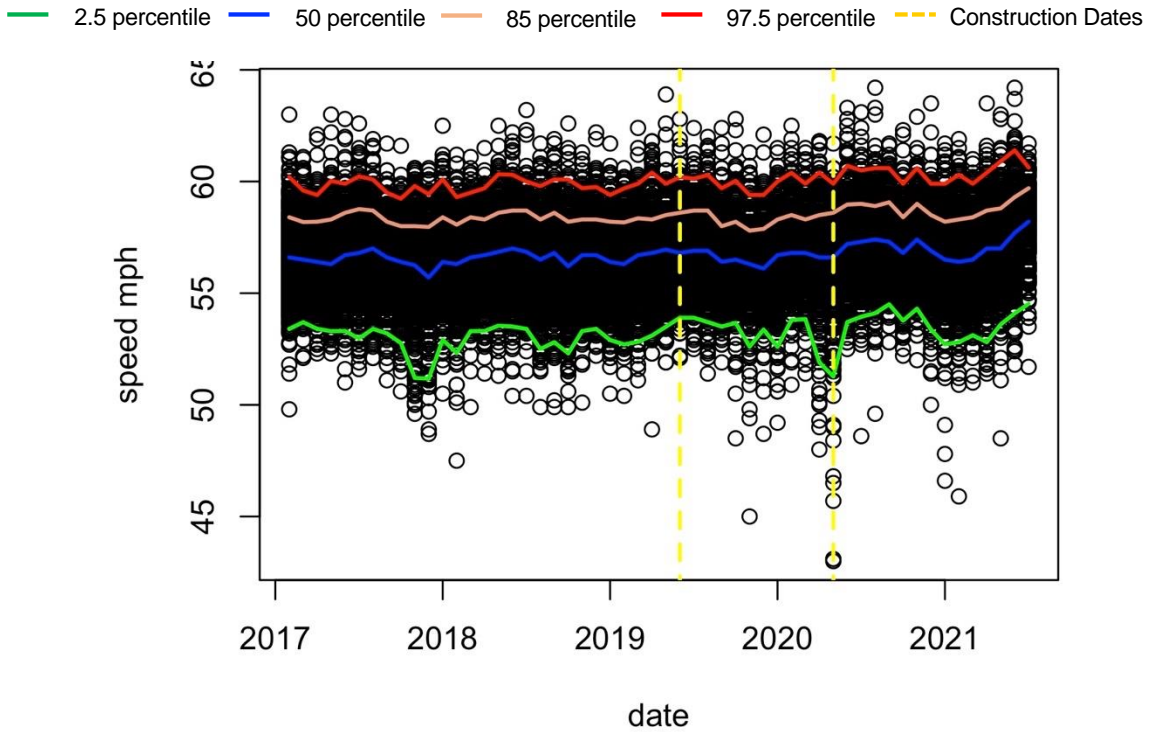
Figure D.40. Monthly variation of the one-hour vehicle speed in Site 28 – NB.
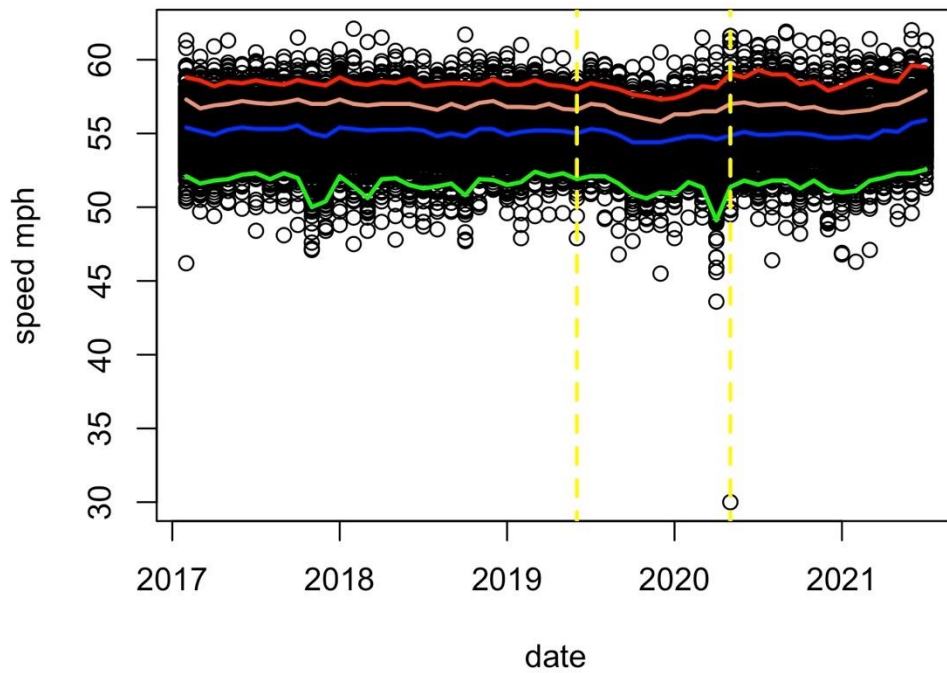
Figure D.41. Monthly variation of the one-hour vehicle speed in Site 28 – SB.
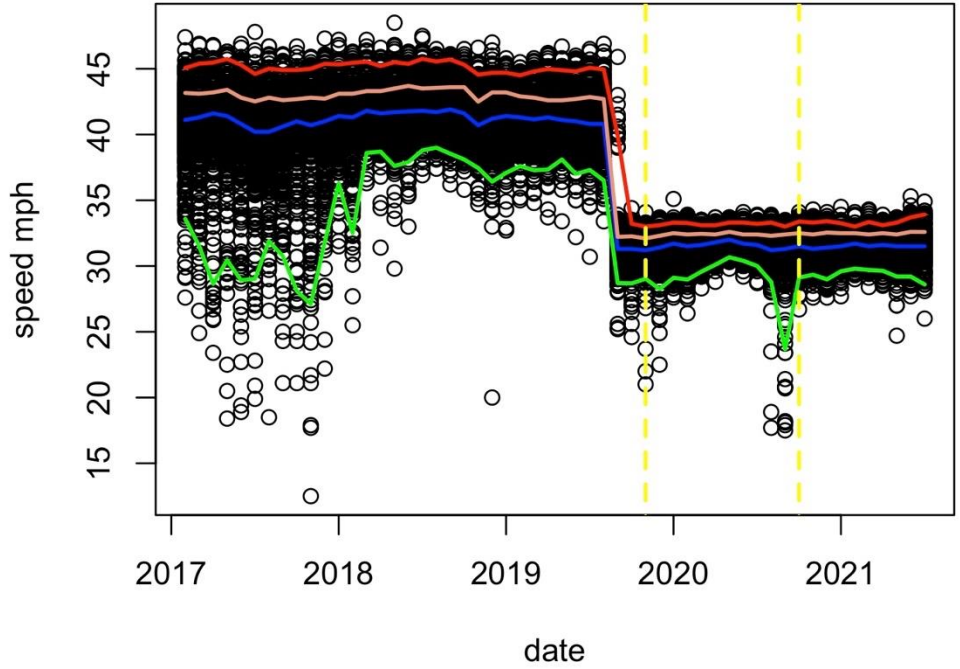
Figure D.42. Monthly variation of the one-hour vehicle speed in Site 29 – EB.
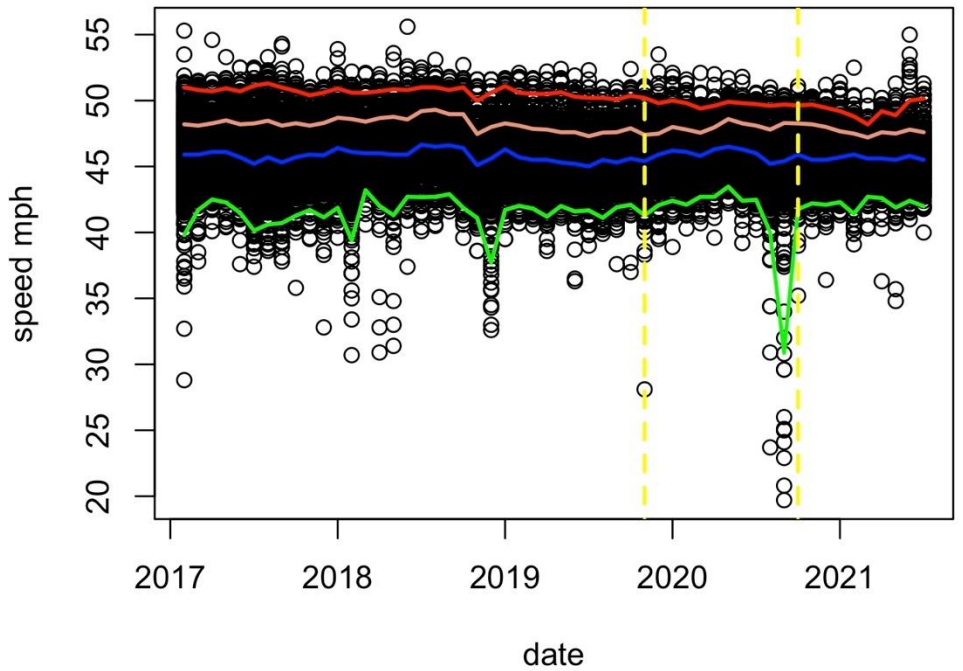
Figure D.43. Monthly variation of the one-hour vehicle speed in Site 29 – WB.
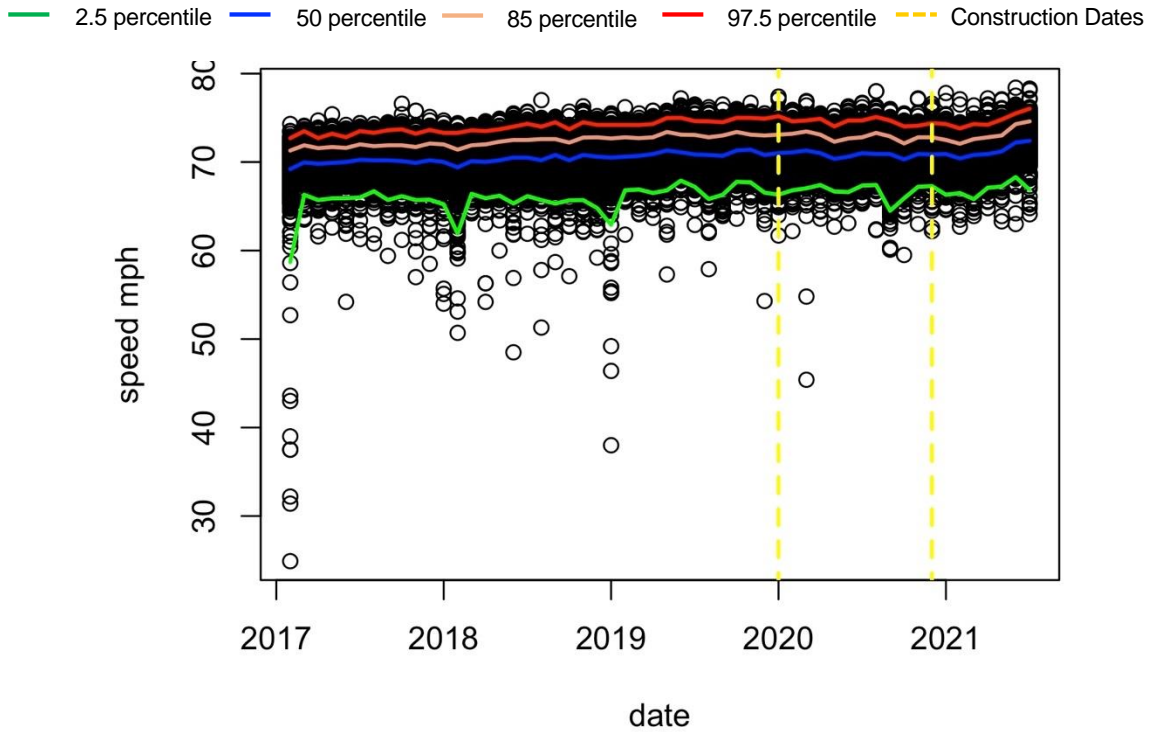
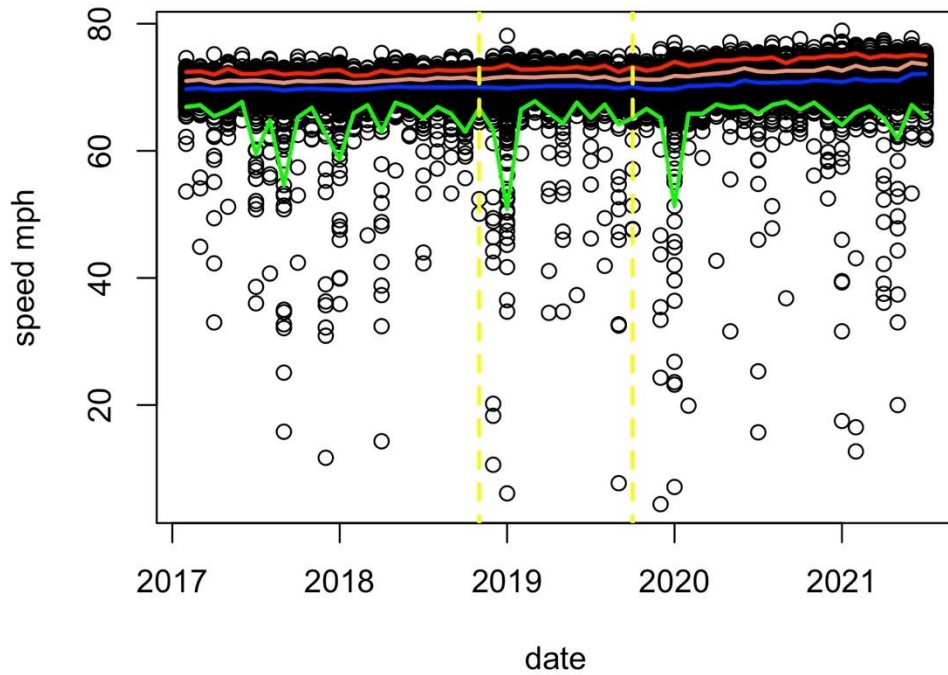**Figure D.44. Monthly variation of the one-hour vehicle speed in Site 30 – NB.**
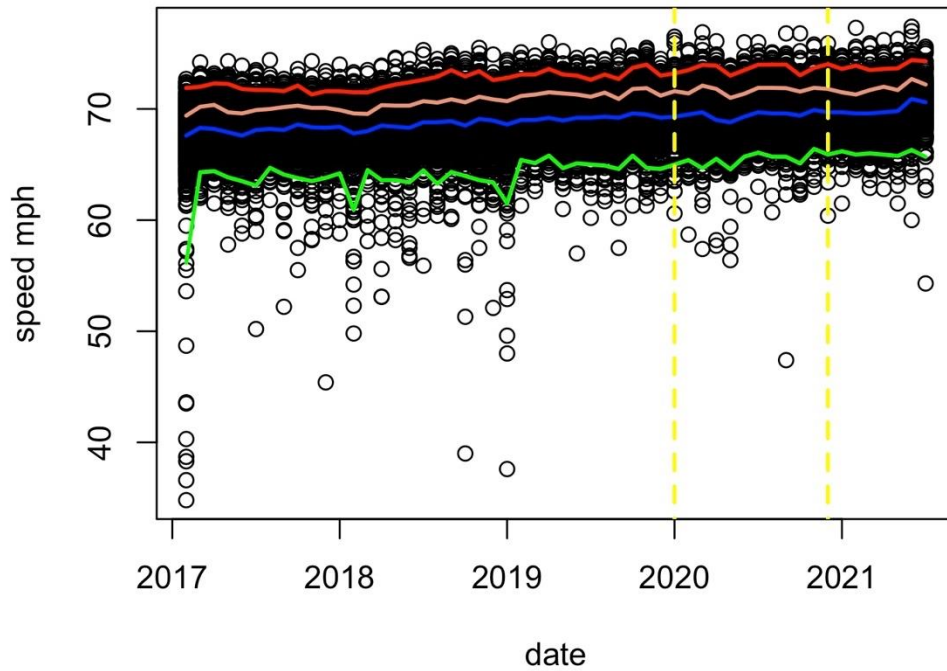
Figure D.45. Monthly variation of the one-hour vehicle speed in Site 30 – SB.
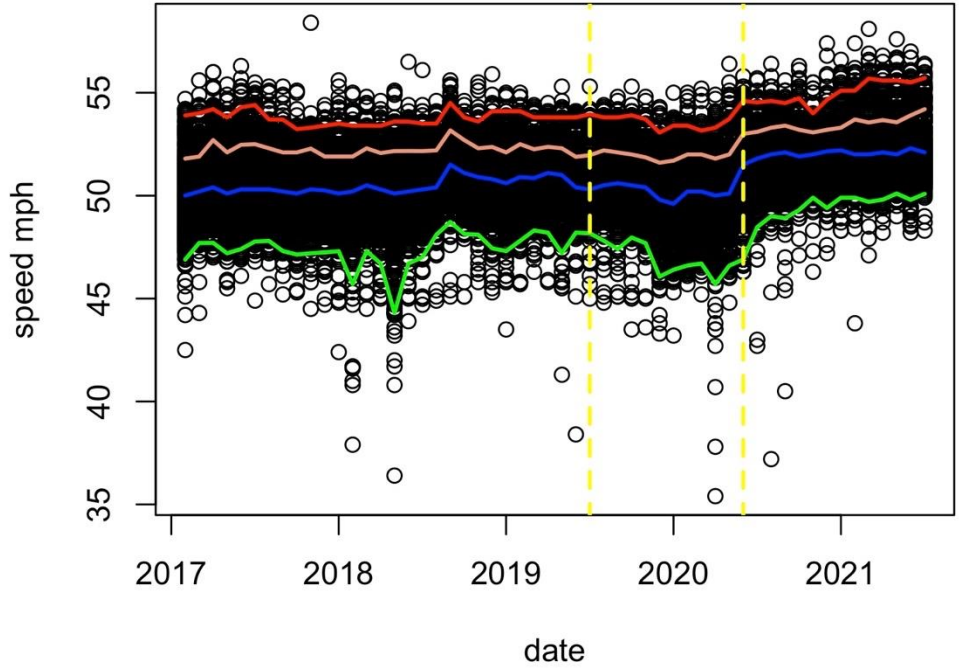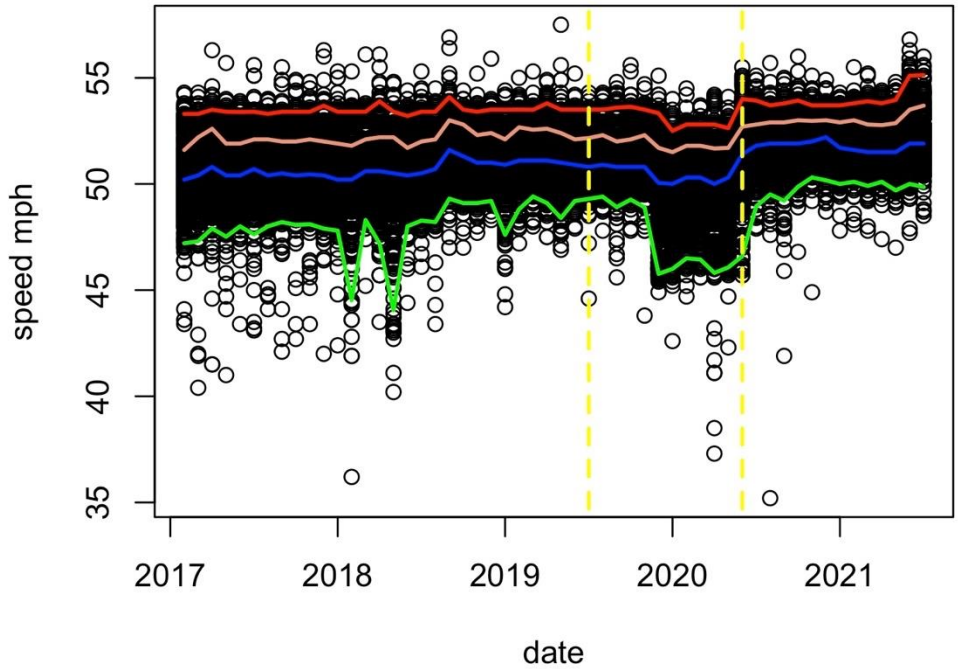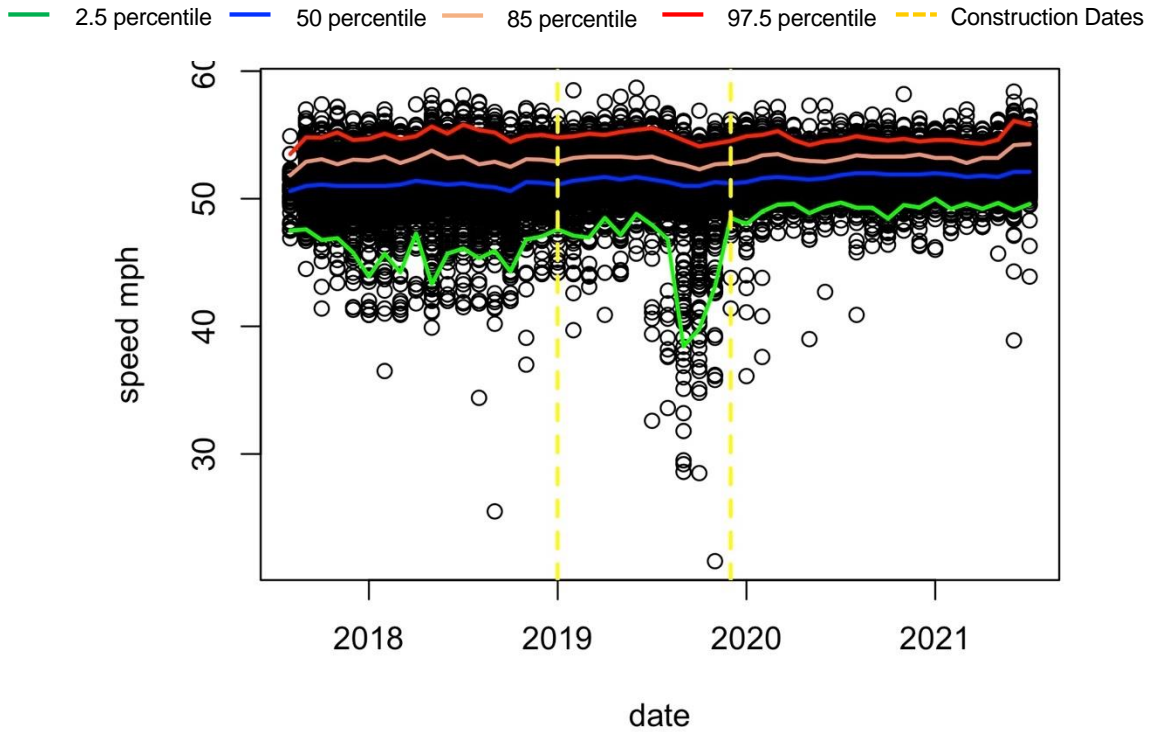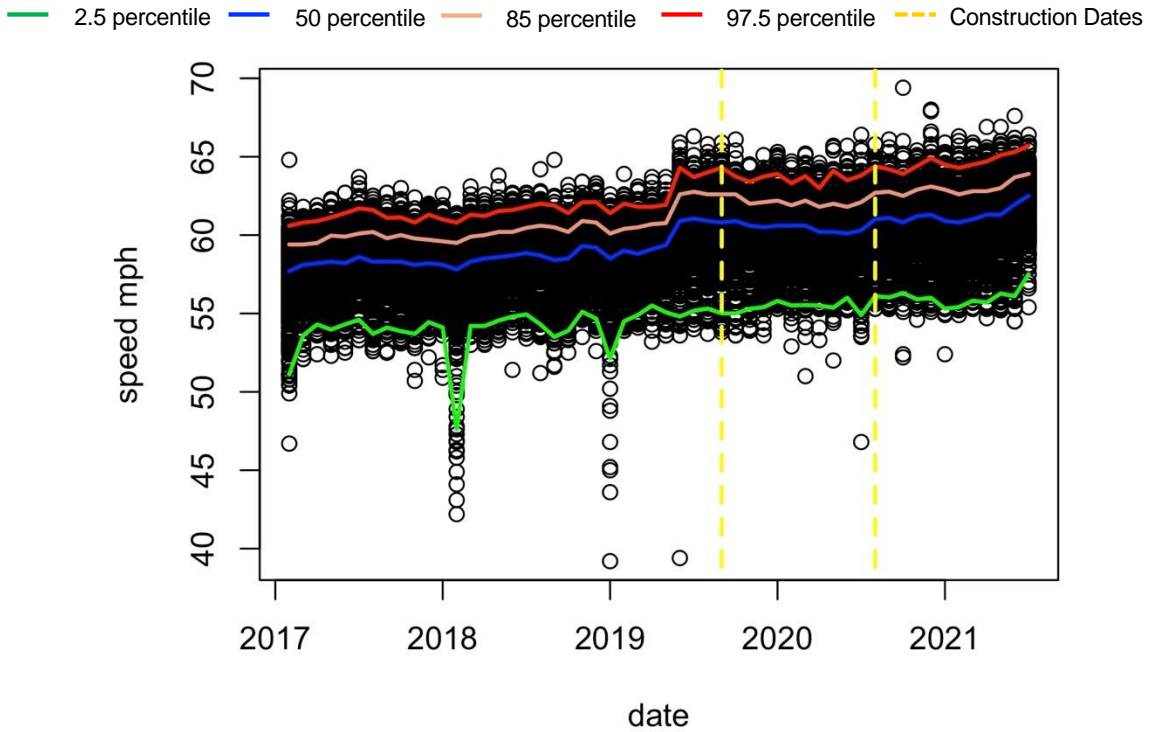
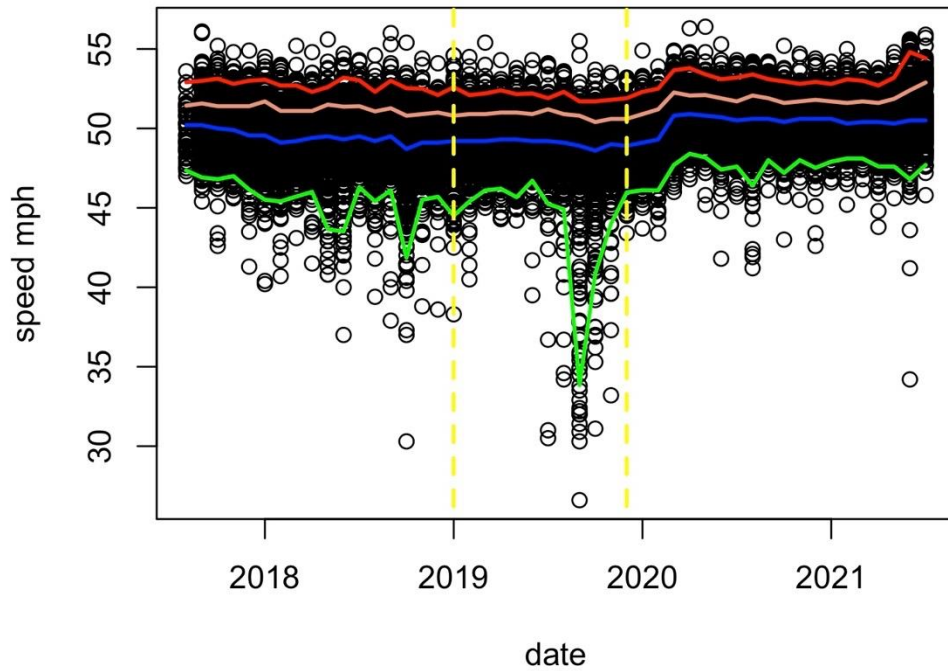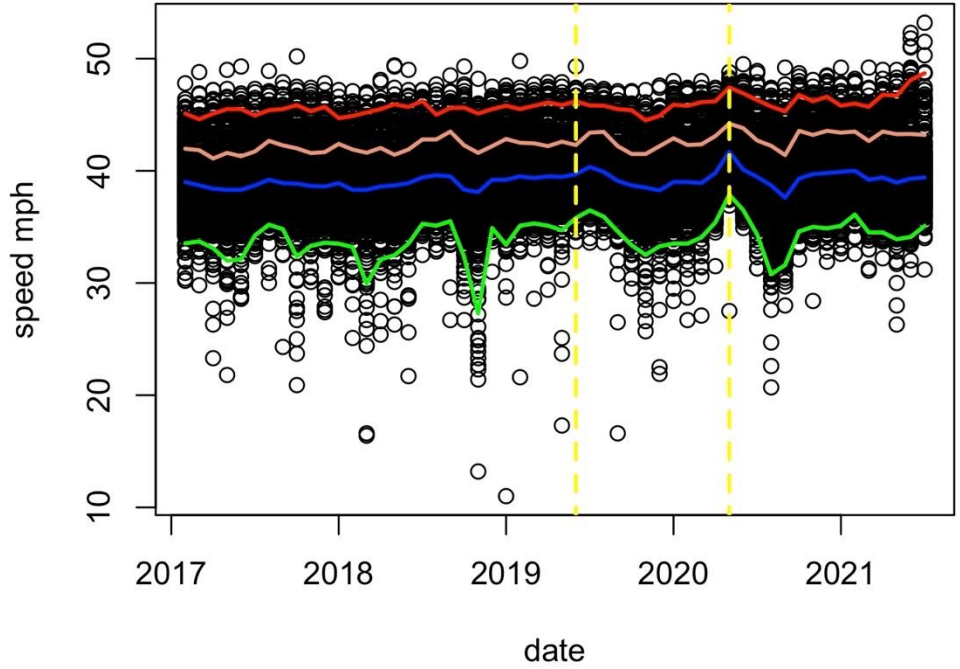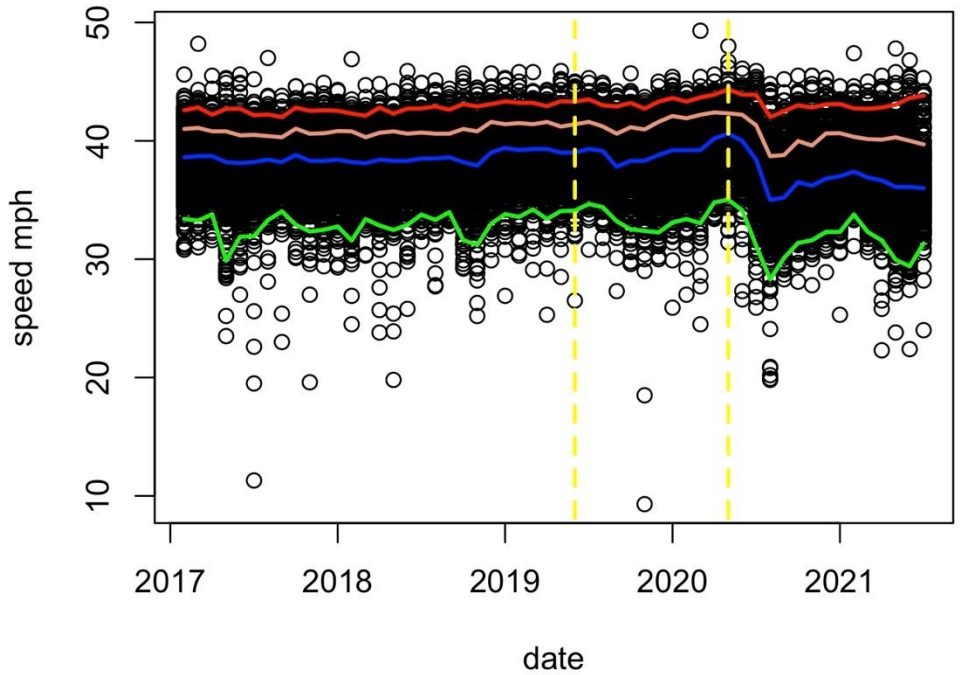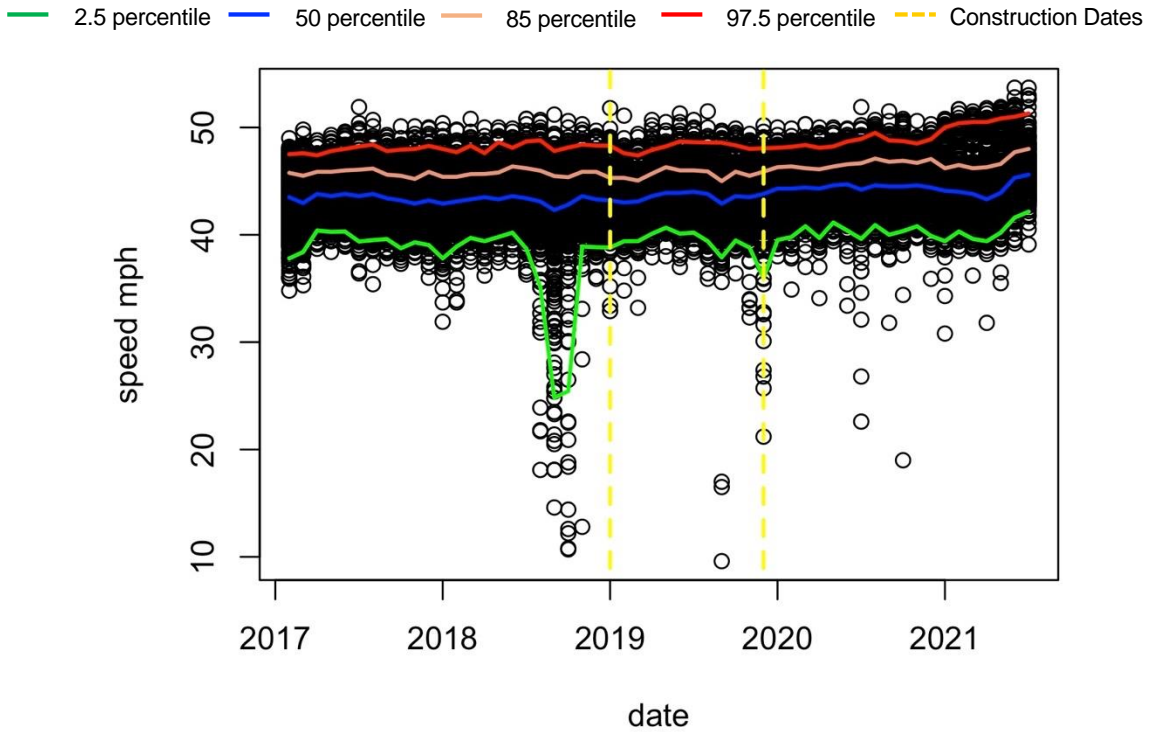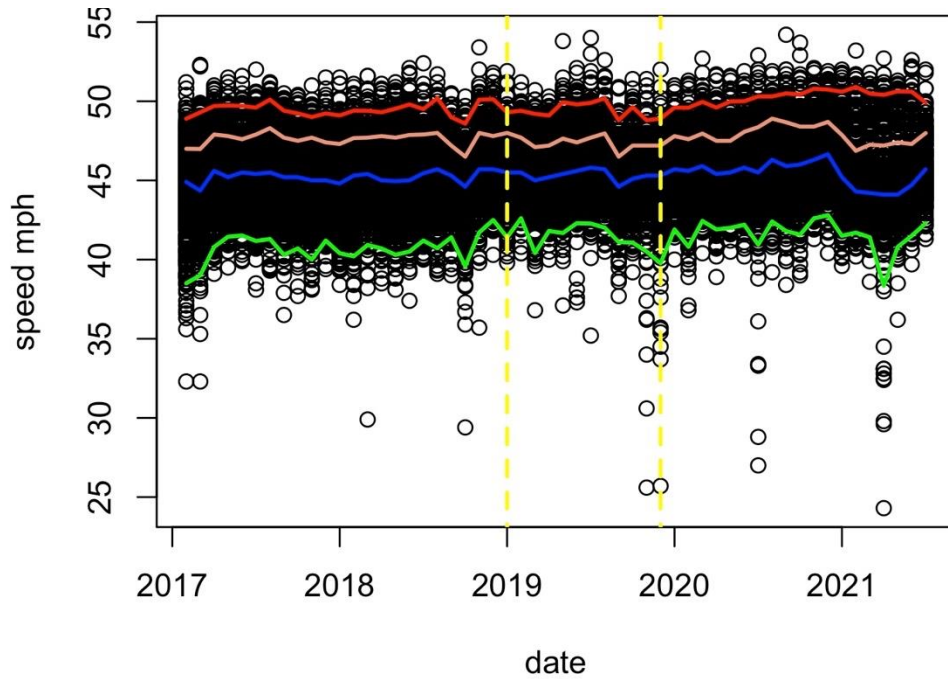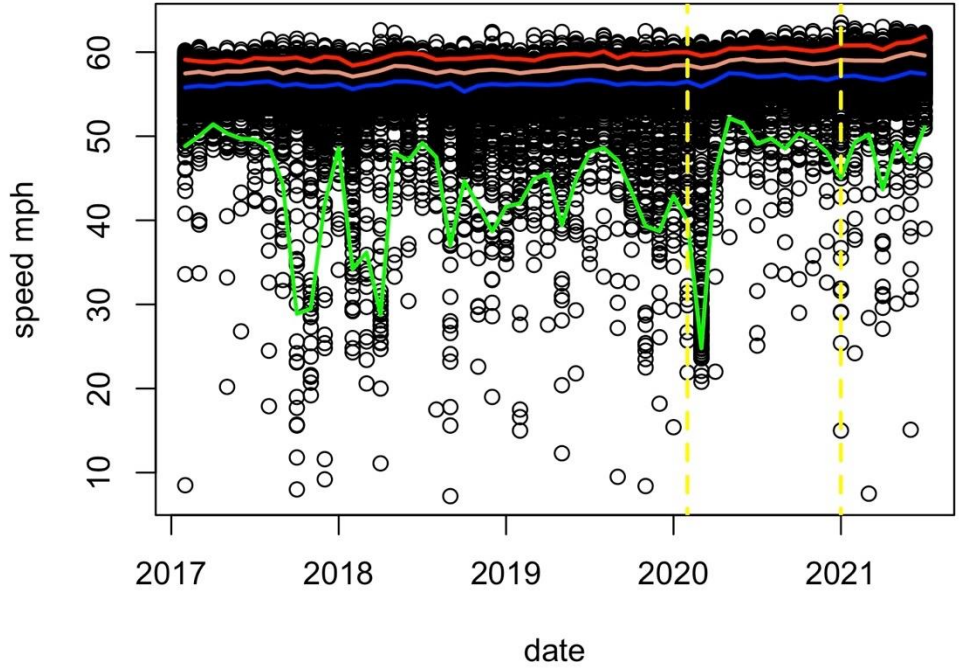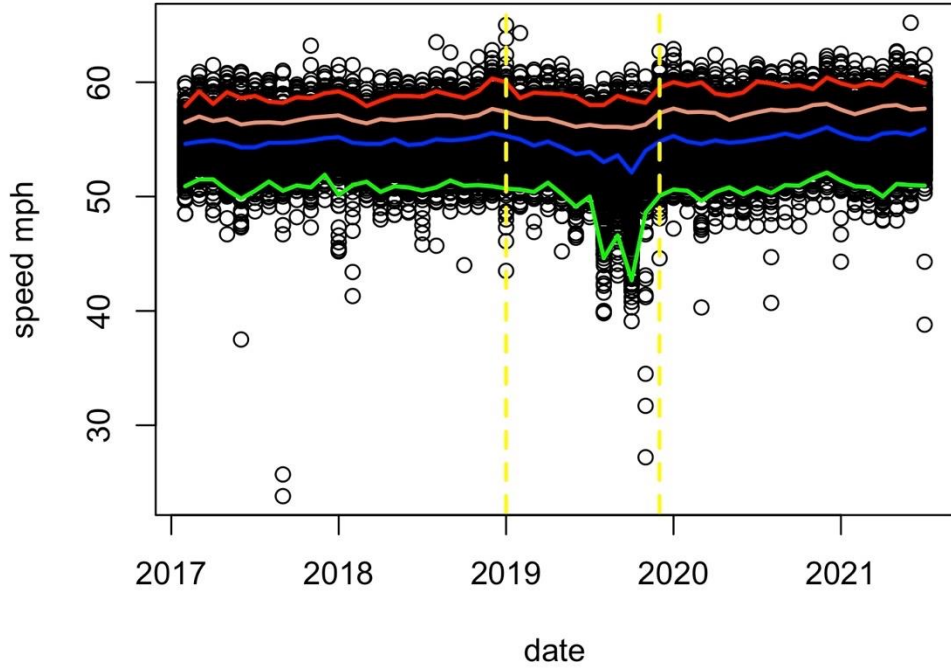**Figure D.46. Monthly variation of the one-hour vehicle speed in Site 33 – EB.**
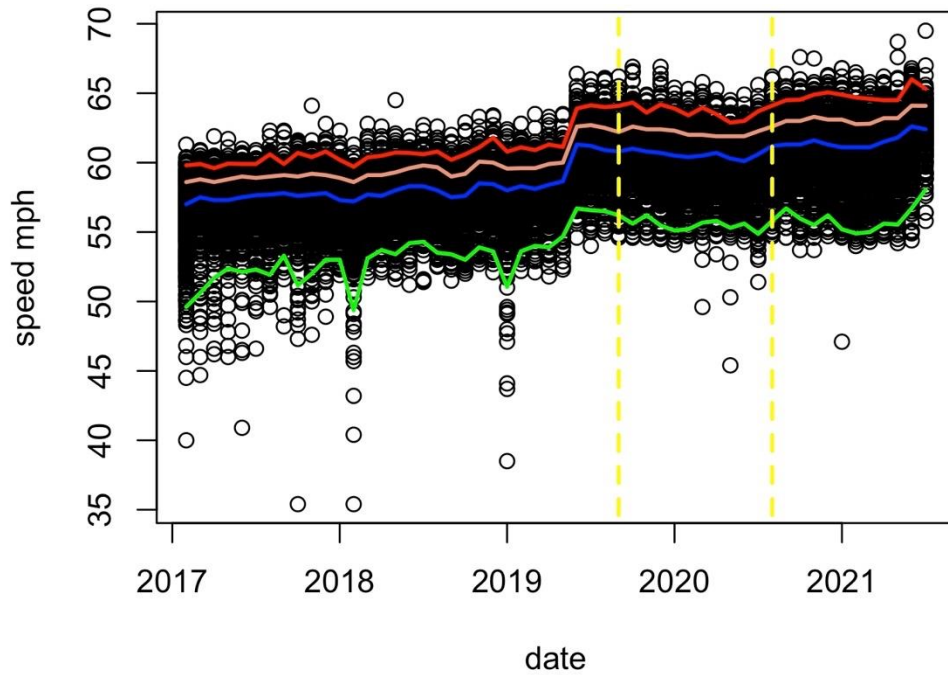
Figure D.47. Monthly variation of the one-hour vehicle speed in Site 33 – WB.

APPENDIX E: STATISTICAL COMPARISON OF THE FRICTION VALUES AT DIFFERENT SPEEDS

Table E.1. Statistical comparison of the friction values measured in the RWP at 40 mph (64 km/h) and 60 mph (97 km/h).

| Site No.	Meas.	Approach	40 mph			60 mph			p-value	Difference	Surface Type
			m40	S40	N40	m60	S60	N60			
3	4	NB	0.68	0.04	231	0.63	0.04	229	**0.00**	0.044	RS9.5B
3	4	SB	0.70	0.02	229	0.67	0.02	221	**0.00**	0.033	RS9.5B
15	6	EB	0.65	0.06	231	0.66	0.06	224	**0.00**	-0.016	RS9.5B
15	6	WB	0.54	0.05	229	0.60	0.07	228	**0.00**	-0.061	RS9.5B
15	5	EB	0.68	0.06	227	0.65	0.06	225	**0.00**	0.032	RS9.5B
15	5	WB	0.62	0.05	229	0.62	0.07	226	0.36	0.005	RS9.5B
16	6	EB	0.66	0.06	245	0.65	0.05	246	0.47	0.004	RS9.5B
16	6	WB	0.71	0.06	246	0.75	0.04	246	**0.00**	-0.037	RS9.5B
16	5	EB	0.72	0.04	246	0.71	0.03	246	**0.00**	0.014	RS9.5B
16	5	WB	0.72	0.04	244	0.68	0.03	246	**0.00**	0.038	RS9.5B
29	5	WB	0.65	0.07	120	0.59	0.06	117	**0.00**	0.060	RS9.5B
29	5	EB	0.66	0.06	119	0.62	0.06	119	**0.00**	0.038	RS9.5B
29	4	WB	0.41	0.03	118	0.52	0.03	111	**0.00**	-0.108	RS9.5B
29	4	EB	0.41	0.02	116	0.50	0.03	115	**0.00**	-0.097	RS9.5B
8	6	NB	0.69	0.06	221	0.65	0.05	221	**0.00**	0.037	RS9.5C
8	6	SB	0.71	0.05	222	0.71	0.04	218	0.67	0.002	RS9.5C
8	5	NB	0.69	0.03	219	0.66	0.04	215	**0.00**	0.030	RS9.5C
8	5	SB	0.70	0.03	221	0.66	0.03	217	**0.00**	0.044	RS9.5C
9	5	NB	0.49	0.03	246	0.50	0.05	246	0.11	-0.006	RS9.5C
9	5	SB	0.49	0.04	242	0.51	0.06	239	**0.00**	-0.014	RS9.5C
9	4	NB	0.58	0.02	244	0.55	0.03	246	**0.00**	0.026	RS9.5C
9	4	SB	0.60	0.02	244	0.56	0.02	246	**0.00**	0.039	RS9.5C
11	4	NB	0.48	0.06	274	0.45	0.03	274	**0.00**	0.030	RS9.5C
11	4	SB	0.47	0.04	240	0.46	0.04	249	**0.00**	0.011	RS9.5C
11	3	NB	0.53	0.02	264	0.51	0.03	258	**0.00**	0.018	RS9.5C
11	3	SB	0.50	0.03	245	0.51	0.03	242	**0.00**	-0.007	RS9.5C
14	6	NB	0.54	0.03	239	0.52	0.03	245	**0.00**	0.022	RS9.5C
14	6	SB	0.50	0.03	246	0.52	0.04	246	**0.00**	-0.020	RS9.5C
17	7	NB	0.55	0.04	246	0.53	0.04	246	**0.00**	0.019	RS9.5C
17	7	SB	0.59	0.04	243	0.56	0.04	246	**0.00**	0.036	RS9.5C
17	6	NB	0.67	0.03	245	0.62	0.03	246	**0.00**	0.049	RS9.5C
17	6	SB	0.70	0.03	246	0.63	0.02	246	**0.00**	0.074	RS9.5C
18	5	NB	0.68	0.04	236	0.67	0.02	232	**0.00**	0.012	RS9.5C
18	5	SB	0.62	0.02	224	0.64	0.02	222	**0.00**	-0.019	RS9.5C
19	5	NB	0.50	0.08	306	0.46	0.04	301	**0.00**	0.032	RS9.5C
19	5	SB	0.52	0.03	306	0.52	0.05	305	**0.05**	-0.007	RS9.5C
19	4	NB	0.60	0.02	293	0.57	0.02	304	**0.00**	0.025	RS9.5C
19	4	SB	0.61	0.02	570	0.61	0.02	285	**0.00**	0.006	RS9.5C
23	4	NB	0.65	0.06	305	0.64	0.05	306	0.09	0.007	RS9.5C
23	4	SB	0.61	0.05	286	0.65	0.03	280	**0.00**	-0.042	RS9.5C
24	2	NB	0.65	0.03	229	0.62	0.03	231	**0.00**	0.030	RS9.5C
24	2	SB	0.66	0.03	231	0.67	0.03	229	**0.00**	-0.009	RS9.5C

Table E.1 (continued). Statistical comparison of the friction values measured in the RWP at 40 mph (60 km/h) and 60 mph (97 km/h).

Site No.	Meas.	Approach	40 mph			60 mph			p-value	Difference	Surface Type
			m40	S40	N40	m60	S60	N60			
24	2	NB	0.65	0.03	229	0.62	0.03	231	**0.00**	0.030	RS9.5C
24	2	SB	0.66	0.03	231	0.67	0.03	229	**0.00**	-0.009	RS9.5C
33	6	WB	0.62	0.03	135	0.59	0.03	136	**0.00**	0.026	RS9.5C
33	6	EB	0.58	0.06	153	0.56	0.03	153	**0.00**	0.018	RS9.5C
33	5	WB	0.60	0.03	135	0.62	0.03	135	**0.00**	-0.018	RS9.5C
33	5	EB	0.58	0.02	153	0.56	0.02	152	**0.00**	0.020	RS9.5C
27	5	WB	0.40	0.02	298	0.67	0.04	297	**0.00**	-0.276	RS9.5D
27	5	WB	-	-	-	-	-	-	**-**	0.000	RS9.5D
27	4	WB	0.65	0.02	294	0.62	0.03	301	**0.00**	0.021	RS9.5D
27	4	WB	-	-	-	-	-	-	**-**	0.000	RS9.5D
6	6	EB	0.70	0.05	231	0.66	0.04	232	**0.00**	0.033	RS9.5D
6	6	WB	0.73	0.03	230	0.70	0.03	231	**0.00**	0.032	RS9.5D
6	5	EB	0.66	0.02	227	0.61	0.02	229	**0.00**	0.044	RS9.5D
6	5	WB	0.66	0.02	226	0.63	0.02	223	**0.00**	0.036	RS9.5D
7	6	NB	0.65	0.04	163	0.64	0.04	161	**0.00**	0.016	RS9.5D
7	6	SB	0.64	0.04	178	0.63	0.05	176	**0.04**	0.010	RS9.5D
7	5	NB	0.63	0.02	165	0.60	0.02	160	**0.00**	0.030	RS9.5D
7	5	SB	0.61	0.02	176	0.60	0.02	174	**0.00**	0.010	RS9.5D

m40: friction mean collected at 40 mph
S40: standard deviation of friction collected at 40 mph
N40: Number of friction values at 40 mph reported every 10 m (32 ft)
m60: friction mean collected at 60 mph
S60: standard deviation of friction collected at 60 mph
N60: Number of friction values at 60 mph reported every 10 m (32 ft)

Table E.2. Statistical comparison of the friction values measured in the CL at 40 mph (64 km/h) and 60 mph (97 km/h).

Site No.	Meas.	Approach	40 mph			60 mph			p-value	Difference	Surface Type
			m40	S40	N40	m60	S60	N60			
3	4	NB	0.70	0.04	231	0.68	0.04	231	0.00	0.020	RS9.5B
3	4	SB	0.73	0.02	228	0.68	0.03	226	0.00	0.047	RS9.5B
15	6	EB	0.66	0.09	224	0.69	0.08	228	0.00	-0.029	RS9.5B
15	6	WB	0.59	0.06	226	0.62	0.06	230	0.00	-0.032	RS9.5B
15	5	EB	0.65	0.07	228	0.57	0.09	227	0.00	0.076	RS9.5B
15	5	WB	0.66	0.05	229	0.60	0.06	226	0.00	0.055	RS9.5B
16	6	EB	0.72	0.05	246	0.76	0.04	246	0.00	-0.037	RS9.5B
16	6	WB	0.72	0.04	246	0.78	0.04	246	0.00	-0.060	RS9.5B
16	5	EB	0.75	0.04	245	0.72	0.04	246	0.00	0.034	RS9.5B
16	5	WB	0.77	0.03	246	0.71	0.04	243	0.00	0.061	RS9.5B
29	5	WB	0.74	0.06	120	0.71	0.05	115	0.00	0.028	RS9.5B
29	5	EB	0.76	0.06	117	0.58	0.12	118	0.00	0.174	RS9.5B
29	4	WB	0.49	0.04	117	0.61	0.05	114	0.00	-0.119	RS9.5B
29	4	EB	0.49	0.03	116	0.44	0.03	121	0.00	0.056	RS9.5B
8	6	NB	0.79	0.05	220	0.71	0.04	219	0.00	0.081	RS9.5C
8	6	SB	0.80	0.04	221	0.74	0.03	223	0.00	0.067	RS9.5C
8	5	NB	0.78	0.03	230	0.73	0.04	217	0.00	0.049	RS9.5C
8	5	SB	0.79	0.03	229	0.73	0.03	215	0.00	0.061	RS9.5C
9	5	NB	0.49	0.04	244	0.39	0.05	240	0.00	0.098	RS9.5C
9	5	SB	0.49	0.05	239	0.47	0.08	242	0.01	0.017	RS9.5C
9	4	NB	0.61	0.04	245	0.53	0.05	246	0.00	0.080	RS9.5C
9	4	SB	0.57	0.02	246	0.53	0.03	244	0.00	0.039	RS9.5C
11	4	NB	-	-	-	0.53	0.05	267	-	-0.529	RS9.5C
11	4	SB	-	-	-	0.50	0.05	246	-	-0.503	RS9.5C
11	3	NB	0.57	0.03	269	0.59	0.05	263	0.00	-0.016	RS9.5C
11	3	SB	0.56	0.03	244	0.51	0.03	242	0.00	0.051	RS9.5C
14	6	NB	0.55	0.04	241	0.56	0.09	244	0.26	-0.007	RS9.5C
14	6	SB	0.57	0.05	242	0.58	0.07	246	0.15	-0.008	RS9.5C
17	7	NB	0.62	0.07	246	0.59	0.05	246	0.00	0.036	RS9.5C
17	7	SB	0.71	0.06	246	0.68	0.05	246	0.00	0.023	RS9.5C
17	6	NB	0.69	0.03	246	0.65	0.03	246	0.00	0.040	RS9.5C
17	6	SB	0.76	0.03	246	0.67	0.04	246	0.00	0.083	RS9.5C
18	5	NB	0.72	0.02	235	0.73	0.04	232	0.01	-0.008	RS9.5C
18	5	SB	0.65	0.02	224	0.65	0.02	222	0.46	0.002	RS9.5C
19	5	NB	-	-	-	0.54	0.05	306	-	-0.542	RS9.5C
19	5	SB	-	-	-	0.54	0.05	306	-	-0.538	RS9.5C
19	4	NB	0.64	0.03	306	0.64	0.04	295	0.80	-0.001	RS9.5C
19	4	SB	0.65	0.04	285	0.65	0.04	560	0.36	0.003	RS9.5C
23	4	NB	0.67	0.06	306	0.67	0.05	306	0.51	-0.003	RS9.5C
23	4	SB	0.67	0.04	279	0.69	0.03	277	0.00	-0.010	RS9.5C
24	2	NB	0.70	0.03	228	0.72	0.02	229	0.00	-0.015	RS9.5C
24	2	SB	0.76	0.03	231	0.72	0.03	212	0.00	0.034	RS9.5C

Table E.2 (continued). Statistical comparison of the friction values measured in the CL at 40 mph (60 km/h) and 60 mph (97 km/h).

Site No.	Meas.	Approach	40 mph			60 mph			p-value	Difference	Surface Type
			m40	S40	N40	m60	S60	N60			
33	6	WB	0.73	0.04	136	0.67	0.03	135	**0.00**	0.055	RS9.5C
33	6	EB	0.75	0.06	151	0.67	0.05	153	**0.00**	0.083	RS9.5C
33	5	WB	0.71	0.03	136	0.64	0.02	136	**0.00**	0.072	RS9.5C
33	5	EB	0.69	0.03	153	0.65	0.03	151	**0.00**	0.046	RS9.5C
27	5	WB	0.54	0.03	299	0.69	0.04	298	**0.00**	-0.155	RS9.5D
27	5	WB	-	-	-	-	-	-	**-**	-	RS9.5D
27	4	WB	0.71	0.02	294	0.63	0.03	296	**0.00**	0.087	RS9.5D
27	4	WB	-	-	-	-	-	-	**-**	-	RS9.5D
6	6	EB	0.73	0.05	231	0.71	0.05	229	**0.00**	0.022	RS9.5D
6	6	WB	0.80	0.03	231	0.69	0.03	231	**0.00**	0.111	RS9.5D
6	5	EB	0.65	0.02	226	0.64	0.03	226	**0.00**	0.013	RS9.5D
6	5	WB	0.66	0.02	226	0.62	0.02	231	**0.00**	0.037	RS9.5D
7	6	NB	0.66	0.05	165	0.62	0.05	162	**0.00**	0.042	RS9.5D
7	6	SB	0.64	0.06	178	0.59	0.06	177	**0.00**	0.052	RS9.5D
7	5	NB	0.61	0.02	163	0.56	0.02	166	**0.00**	0.050	RS9.5D
7	5	SB	0.58	0.04	178	0.55	0.04	178	**0.00**	0.024	RS9.5D

m40: friction mean collected at 40 mph
S40: standard deviation of friction collected at 40 mph
N40: Number of friction values at 40 mph reported every 10 m (32 ft)
m60: friction mean collected at 60 mph
S60: standard deviation of friction collected at 60 mph
N60: Number of friction values at 60 mph reported every 10 m (32 ft)

APPENDIX F: DATABASE

Table F.1. Job mix formula information.

Site	*Pb*	VFA	VirginRatio	Virgin *Pb*	VMA	VTM	D10	D30	D60	Cc	Cu
1	6.4	75.7	85	5.6	17.3	4	0.12	0.38	2.36	0.53	20.27
1	6.4	75.7	85	5.6	17.3	4	0.12	0.38	2.36	0.53	20.27
2	6.3	77.2	67	4.2	18.2	4	0.11	0.33	1.62	0.62	14.87
2	6.3	77.2	67	4.2	18.2	4	0.11	0.33	1.62	0.62	14.87
3	6.3	78.5	70	4.9	18.3	4	0.13	0.58	2.36	1.12	18.82
3	6.3	78.5	70	4.9	18.3	4	0.13	0.58	2.36	1.12	18.82
4.1	5.2	60.1	100	5.2	17.8	7	0.27	3.20	6.37	5.95	23.57
4.1	5.2	60.1	100	5.2	17.8	7	0.27	3.20	6.37	5.95	23.57
4.2	6.0	76.5	85	5.3	17.3	4	0.13	0.60	3.79	0.75	30.16
4.2	6.0	76.5	85	5.3	17.3	4	0.13	0.60	3.79	0.75	30.16
5	5.5	34.6	100	5.5	15.4	10	0.60	2.78	6.48	1.99	10.80
5	5.5	34.6	100	5.5	15.4	10	0.60	2.78	6.48	1.99	10.80
6	5.6	76.5	80	4.6	16.7	4	0.15	0.65	3.56	0.80	23.70
6	5.6	76.5	80	4.6	16.7	4	0.15	0.65	3.56	0.80	23.70
7	5.7	76.0	80	4.7	16.7	4	0.12	0.44	2.09	0.76	17.01
7	5.7	76.0	80	4.7	16.7	4	0.12	0.44	2.09	0.76	17.01
9	6.4	77.8	72	4.6	18.4	4	0.12	0.47	1.87	0.97	15.35
9	6.4	77.8	72	4.6	18.4	4	0.12	0.47	1.87	0.97	15.35
12	5.4	75.3	80	4.5	16.2	4	0.13	0.53	2.86	0.73	21.31
12	5.4	75.3	80	4.5	16.2	4	0.13	0.53	2.86	0.73	21.31
14	6.2	76.9	85	5.4	17.3	4	0.10	0.35	1.97	0.60	19.41
14	6.2	76.9	85	5.4	17.3	4	0.10	0.35	1.97	0.60	19.41
15	6.2	78.5	70	4.7	17.9	4	0.12	0.39	2.10	0.61	17.40
15	6.2	78.5	70	4.7	17.9	4	0.12	0.39	2.10	0.61	17.40
16	6.8	78.8	71	4.6	18.9	4	0.18	0.42	1.52	0.66	8.56
16	6.8	78.8	71	4.6	18.9	4	0.18	0.42	1.52	0.66	8.56
17	5.7	74.1	70	4.2	17.4	4	0.17	0.49	2.86	0.49	16.54
17	5.7	74.1	70	4.2	17.4	4	0.17	0.49	2.86	0.49	16.54
18	5.7	75.5	60	3.9	16.5	4	0.13	0.48	2.84	0.60	21.07
18	5.7	75.5	60	3.9	16.5	4	0.13	0.48	2.84	0.60	21.07
23	6.0	76.6	82	4.2	17.1	4	0.175	0.6	2.36	0.87	13.49
23	6.0	76.6	82	4.2	17.1	4	0.175	0.6	2.36	0.87	13.49
27	5.5	73.1	80	4.5	16.0	4	0.12	0.56	2.29	1.10	18.56
27	5.5	73.1	80	4.5	16.0	4	0.12	0.56	2.29	1.10	18.56
28	6.6	77.7	66	4.4	18.7	4	0.11	0.39	1.77	0.82	16.58
28	6.6	77.7	66	4.4	18.7	4	0.11	0.39	1.77	0.82	16.58
11	6.0	76.9	70	4.5	17.3	4	0.13	0.41	1.92	0.66	14.72
11	6.0	76.9	70	4.5	17.3	4	0.13	0.41	1.92	0.66	14.72
19	6.0	76.9	70	4.5	17.3	4	0.13	0.41	1.67	0.76	12.83
19	6.0	76.9	70	4.5	17.3	4	0.13	0.41	1.67	0.76	12.83
29	6.3	79.6	70	4.7	19.5	4	0.11	0.44	2.29	0.75	20.32
29	6.3	79.6	70	4.7	19.5	4	0.11	0.44	2.29	0.75	20.32
30	5.3	75.3	85	4.6	16.2	4	0.13	0.65	3.12	1.02	23.34
30	5.3	75.3	85	4.6	16.2	4	0.13	0.65	3.12	1.02	23.34
8	5.7	77.8	75	4.5	16.9	4	0.15	0.79	3.37	1.25	22.44
8	5.7	77.8	75	4.5	16.9	4	0.15	0.79	3.37	1.25	22.44
24	5.8	76.6	80	4.6	17.5	4	0.20	0.82	2.53	1.34	12.65
24	5.8	76.6	80	4.6	17.5	4	0.20	0.82	2.53	1.34	12.65
33	5.6	75.5	60	3.6	16.6	4	0.12	0.47	2.91	0.62	23.92
33	5.6	75.5	60	3.6	16.6	4	0.12	0.47	2.91	0.62	23.92
13	6.5	77.5	60	3.6	17.9	4	0.13	0.41	1.67	0.76	12.83

Table F.2. Gradation of the mix used in each site (percent passing).

Site	Sieve Size (mm)											
	37.5	25	19	12.5	9.5	4.75	2.36	1.18	0.6	0.3	0.15	0.075
1	100	100	100	100	97	75	60	52	41	26	13	6.30
1	100	100	100	100	97	75	60	52	41	26	13	6.30
2	100	100	100	100	96	78	65	57	47	28	13	7.50
2	100	100	100	100	96	78	65	57	47	28	13	7.50
3	100	100	100	100	95	77	60	45	31	19	12	5.90
3	100	100	100	100	95	77	60	45	31	19	12	5.90
4.1	100	100	100	100	93	43	23	17	14	11	6	4.10
4.1	100	100	100	100	93	43	23	17	14	11	6	4.10
4.2	100	100	100	100	97	68	48	38	30	22	12	5.80
4.2	100	100	100	100	97	68	48	38	30	22	12	5.80
5	100	100	100	100	88	44	27	14	10	8	5	3.50
5	100	100	100	100	88	44	27	14	10	8	5	3.50
6	100	100	100	100	95	68	52	40	29	17	10	5.80
6	100	100	100	100	95	68	52	40	29	17	10	5.80
7	100	100	100	100	95	74	63	50	39	22	12	6.50
7	100	100	100	100	95	74	63	50	39	22	12	6.50
9	100	100	100	100	97	79	65	53	37	21	12	6.70
9	100	100	100	100	97	79	65	53	37	21	12	6.70
12	100	100	100	100	97	75	56	44	33	20	11	6.20
12	100	100	100	100	97	75	56	44	33	20	11	6.20
14	100	100	100	100	98	83	64	52	41	28	15	7.30
14	100	100	100	100	98	83	64	52	41	28	15	7.30
15	100	100	100	100	96	77	62	53	41	25	12	6.90
15	100	100	100	100	96	77	62	53	41	25	12	6.90
16	100	100	100	100	97	78	65	58	46	19	8	7.00
16	100	100	100	100	97	78	65	58	46	19	8	7.00
17	100	100	100	100	99	75	56	46	35	21	8	5.90
17	100	100	100	100	99	75	56	46	35	21	8	5.90
18	100	100	100	100	96	72	57	47	36	21	11	6.10
18	100	100	100	100	96	72	57	47	36	21	11	6.10
23	100	100	100	100	97	76	60	44	30	15	9	7.00
23	100	100	100	100	97	76	60	44	30	15	9	7.00
27	100	100	100	100	94	74	61	45	32	18	12	6.40
27	100	100	100	100	94	74	61	45	32	18	12	6.40
28	100	100	100	100	97	79	65	55	41	25	13	7.80
28	100	100	100	100	97	79	65	55	41	25	13	7.80
11	100	100	100	100	97	82	63	55	41	24	11	7.20
11	100	100	100	100	97	82	63	55	41	24	11	7.20
19	100	100	100	100	97	82	67	55	41	24	11	7.20
19	100	100	100	100	97	82	67	55	41	24	11	7.20
29	100	100	100	99	95	75	61	45	37	24	13	7.00
29	100	100	100	99	95	75	61	45	37	24	13	7.00
30	100	100	100	100	98	75	53	40	29	19	11	6.40
30	100	100	100	100	98	75	53	40	29	19	11	6.40
8	100	100	100	100	95	71	52	38	26	17	10	5.80
8	100	100	100	100	95	71	52	38	26	17	10	5.80
24	100	100	100	100	96	73	59	38	25	14	8	5.90
24	100	100	100	100	96	73	59	38	25	14	8	5.90
33	100	100	100	100	97	70	57	49	37	21	12	6.70
33	100	100	100	100	97	70	57	49	37	21	12	6.70
13	100	100	100	100	97	82	67	55	41	24	11	7.20